

# Analysis of extreme fire weather during catastrophic wildfires in Croatia and Australia

---

Čavlina Tomašević, Ivana

Doctoral thesis / Disertacija

2022

Degree Grantor / Ustanova koja je dodijelila akademski / stručni stupanj: **University of Zagreb, Faculty of Science / Sveučilište u Zagrebu, Prirodoslovno-matematički fakultet**

Permanent link / Trajna poveznica: <https://um.nsk.hr/um:nbn:hr:217:146249>

Rights / Prava: [In copyright](#)/[Zaštićeno autorskim pravom.](#)

Download date / Datum preuzimanja: **2025-02-20**



Repository / Repozitorij:

[Repository of the Faculty of Science - University of Zagreb](#)





University of Zagreb  
Faculty of Science



**MACQUARIE**  
University  
SYDNEY · AUSTRALIA

Faculty of Science and Engineering

Ivana Čavlina Tomašević

**ANALYSIS OF EXTREME FIRE  
WEATHER DURING CATASTROPHIC  
WILDFIRES IN CROATIA AND  
AUSTRALIA**

INTERNATIONAL DUAL DOCTORATE

Zagreb, 2022



University of Zagreb

Prirodoslovno-matematički fakultet



**MACQUARIE**  
University  
SYDNEY · AUSTRALIA

Fakultet znanosti i inženjeringa

Ivana Čavlina Tomašević

**ANALIZA EKSTREMNIH VREMENSKIH  
UVJETA TIJEKOM KATASTROFALNIH  
POŽARA U HRVATSKOJ I AUSTRALIJI**

MEĐUNARODNI DVOJNI DOKTORAT ZNANOSTI

Izv. Prof. Dr. Sc. Maja Telišman Prtenjak

Izv. Prof. Dr. Sc. Paul Beggs

Zagreb, 2022

## ABSTRACT

The main focus of this study was to investigate fire weather of two catastrophic wildfires, one from Croatia, which is a part of one of the world's most fire prone areas – the Mediterranean basin and other from Tasmania, a part of well-known fire continent – Australia. The Croatian case study included the Split wildfire in July 2017, the most severe wildfire in history given the size and unexpected fire behavior, which produced the downslope fire runs into the densely populated area while the Australian case study included the Forcett-Dunalley wildfire in January 2013, which caused vast destruction, rapid fire spread and generated firestorm in form of pyroCb, the first on record in Tasmania. Meteorological analyses of wildfires were preceded by their reconstruction and definition of the most severe burn periods in order to associate atmospheric conditions and fire behavior in detail. The study draws similarities between dynamic atmospheric processes and mechanisms that occurred in chosen wildfire cases and implemented a coupled fire-atmosphere model for the first time in Croatia. The study also contains comprehensive literature review of fire weather meteorology together with past and future climate influencing fire risk at the Adriatic coast in Croatia and in southeast Australia, including Tasmania.

The research has showed that both wildfires were wind driven from the ignition due to wildfires' locations situated in the area of tight pressure gradient which resulted in strong gusty surface wind. In the case of Split, the ignition of the wildfire coincided with an episode of strong downslope *bura* windstorm, while in Dunalley case wildfire occurred at the peak of the heatwave and right before the cold front passage. The antecedent conditions in both cases included the drier and warmer-than-average periods in months' prior the wildfires, which contributed to continued drying out fuels in the area and had an impact on fire danger rating. In particular, the FWI reached its annual maximum exactly on the day of the Split wildfire, while in the case of Dunalley FFDI reached 'catastrophic' category and got close to the all-time state record.

Important findings on atmospheric dynamics in the Split case of included long amplitude and shortwave upper-level trough, which caused the cool and dry air outbreak and produced a deep northeasterly *bura* flow. Upper-level features of the deep *bura* flow included hydraulic jump, dry air subsidence and low-level jet (LLJ). This research is the first known to present spatial distribution of LLJ.

The explosive pyroCb development in the case of the Dunalley was triggered by the highly unstable atmosphere and the line of convergence over the wildfire's area in the hours

prior to the cold front passage. Also, combustion processes within the escalated wildfire further enhanced instability and contributed to the blow-up up to 12 km height, in spite of the strong jet stream at the tropopause. Enhanced fuel consumption in combination with complex local topography is found to play an important role in the total fire escalation in the Split case as well.

#### **KEY WORDS**

Meteorology; Fire weather; wildfires; meteorological analysis; comparison study; numerical weather prediction model; coupled fire-atmosphere model

## LIST OF ABBREVIATIONS

ACT	Australian Capitol Territory
AEDT	Australian Eastern Daylight Time
ALADIN	Aire Limitee Adaptation Dynamique Developpement InterNational
ALADIN/HR	ALADIN Croatian domain
ALADIN-HR44	ALADIN Croatian domain with 4 km horizontal resolution
ALADIN-HRDA	ALADIN dynamical adaptation
AWS	Automatic weather stations
BARRA	Bureau of Meteorology Atmospheric Regional Reanalysis for Australia
BARRA-R	BARRA Regional
BARRA-TA	BARRA Tasmania
BoM	Bureau of Meteorology
BUI	Buildup Index
CEST	Central European Summer Time
CFFDRS	Canadian Forest Fire Danger Rating System
CFFWIS	Canadian Forest Fire Weather Index System
CLC	CORINE Land Cover
CORINE	Coordination of Information on the Environment Land Cover
DC	Drought Code
DF	Drought factor
DHMZ	Croatian Meteorological and Hydrological Service
DMC	Duff Moisture Code
DSR	Daily Severity Rating
DWD	Deutscher Wetterdienst
ECMWF	European Center for Medium-Range Weather Forecasts
ERA-Interim	ECMWF Re-Analysis
FFDI	Forest Fire Danger Index
FFDR	Forest Fire Danger Rating
FFMC	Fine Fuel Moisture Code
GADM	Database of Global Administrative Areas
GCM	General circulation model
GFDI	Grassland Fire Danger Index
HDR	Higher degree research

HI	Heines Index
ISI	Initial Spread Index
LLJ	Low-level jet
NASA	National Aeronautics and Space Administration
NCAR	National Center for Atmospheric Research
NFFL	Northern Forest Fire Laboratory
NMOC	National Meteorological and Oceanographic Centre
NWP	Numerical weather prediction
MODIS	Moderate Resolution Imaging Spectroradiometer
MORR	Morrison double-moment scheme
MSLP	Mean sea level pressure
MSR	Monthly Severity Rating
MYNN2.5	Mellor-Yamada-Nakanishi-Niino boundary layer
PBL	Planetary boundary layer
PFT	Firepower threshold
pyroCb	Pyrocumulonimbus
pyroCu	Pyrocumulus
RRTM	Rapid radiative transfer model scheme
SFB	Split Firefighting Brigade
SSR	Season Severity Rating
SRTM	Shuttle Radar Topographic Mission
TFS	Tasmania Fire Service
UTC	Universal Coordinated Time
WRF	Weather Research and Forecasting
WRF SFIRE	Weather Research and Forecasting Spread FIRE model
WUI	Wildland-urban interface

## **STATEMENT OF ORIGINALITY**

*This thesis is being submitted to Macquarie University and University of Zagreb in accordance with the Cotutelle agreement dated 29 September 2017.*

*To the best of my knowledge and belief, the thesis contains no material previously published or written by another person except where due reference is made in the thesis itself.*

Date: 27 July 2022

---

Ivana Čavlina Tomašević



## ACKNOWLEDGMENTS

This Cotutelle PhD has been conducted in both Sydney, Australia and Zagreb, Croatia. I wish to want thank the institutions whose scholarship, data and tools made this research possible:

- Macquarie University in Sydney, Australia for providing me with the scholarship for this Cotutelle PhD.
- University of Rijeka, Centre for Advanced Computing and Modelling for providing high performance computing infrastructure.
- Croatian Meteorological and Hydrological Service (DHMZ) for providing meteorological data and operational model simulation.
- Bureau of Meteorology (BoM) for providing meteorological and reanalysis data and reports on the Forcett-Dunalley wildfire.
- Split Firefighting Brigade for providing a map of the final fire perimeter and emergency calls and radio logs.

I am grateful for a number of colleagues, friends and family members for encouraging me to start the PhD, persevere with it, and finally to finish it.

First and foremost, I would like to thank two fantastic fire weather researchers – Dr Višnjica Vučetić from Croatia and Dr Paul Fox-Hughes from Australia. Dr Vučetić, who introduced me to fire weather research while preparing me for my Master Thesis. Her guidance, passion and love for agrometeorology and forest meteorology kept me wanting to learn more. I am so happy and proud that I have managed to finish this fantastic research that we have been talking about for years. I am forever grateful to have such a role model to guide me in my professional and personal development. Thank you for all conversations and advice. I am forever grateful for our time together in and outside the office at the DHMZ. I feel blessed that during my time in Australia I received the invitation from Dr Paul Fox-Hughes to come to Hobart. During the visit he introduced me to a fantastic group of people working at the BoM's Hobart office, Tasmania Fire Service (TFS) and University of Tasmania. His dedication and keen interest to help me and support me was crucial for me completing this research. Thank you for introducing me to the Forcett-Dunalley wildfire case and providing me with all meteorological and wildfire reconstruction data. Thank you for always updating me on the newest research and giving me more ideas for my research. Thank you for believing me and my work, it kept me motivated to go forward and believe in myself. Thank you both for reading and commenting on the thesis and being there for me at every stage of my research. Watching

your passion for fire weather research truly inspired me and gave me purpose for my life. I am forever in your debt.

I want to thank my supervisors Assoc. Prof. Maja Telišman Prtenjak from the University of Zagreb and Assoc. Prof. Paul Beggs from Macquarie University in Sydney. Thank you both for all your help, patience, management, guidance and encouragement. Thank you both for trusting me and accepting my ideas and being there for me for any question I had at any time. I am very grateful to have you as my supervisors. I also want to thank Dr Kevin Cheung, my former supervisor. I am very happy that we have continued to work together in spite of circumstances beyond our control that ended our official collaboration. Thank you for your support, believing in me, helping me to develop my ideas and willing to help me every step of the way.

I want to thank a fantastic group of researchers from Australia who imparted to me their incredible knowledge they are doing regarding fire weather and meteorology in general. Thanks to Dr Jeff Kepert for inviting me to Melbourne and suggesting fire cases for my research. Thanks to Dr Kevin Tory for introducing me to pyroconvection and pyrocumulonimbus and sharing his knowledge on the topic. I also want to thank Monica Long for inspirational talks and introducing me to fire weather training program she provided at the BoM. From the Hobart office of the BoM I want to say special thanks to David James for sharing reports and all available data on Forcett-Dunalley wildfire. I enjoyed our talks about the wildfire and agrometeorology in general. Thank you for sharing the insights on agrometeorology in Tasmania with me. A special word of gratitude goes to Samuel Sauvage who provided me with the BARRA reanalysis data. I will never forget the Great Circle of Good. I want to thank John Bally from the BoM and Mark Chladil from TFS for inspirational talks, information and knowledge regarding fire weather and firefighting operations. I am honoured to have met you and I wish you a peaceful retirement. A special thanks goes to Alen Slijepčević, Deputy Chief Officer from the Country Fire Authority in Victoria. Thank you for being my Croatian ally in Australia. Thank you for all the support, conversations, motivation and belief in me. It means a lot.

Thanks to all other fantastic researchers in fire and fire weather I met in Sydney, Melbourne and Hobart. Special thanks to Dr Andrew Dowdy, Dr Dragana Zovko Rajak and Musa Kilinc for reading and commenting on several chapters of my research. I am honoured that you reviewed my work.

I want to thank Ana Borba, former employee from the HDR office at Macquarie University. Thank you for being there for me during my time on campus. Thank you for all the

help with administration and for great talks and advice you gave. I want to thank all other staff and colleagues at Macquarie University. Thank you for making my time on campus memorable.

From the University of Zagreb, I want to thank Barbara Malečić for helping me to run the WRF model. Thank you for being there for every question regarding running simulations. It was great to learn from you. Special thanks to Marko Hum who provided an excellent administration support at any time. From the University of Rijeka, I want to thank Boris Mifka and Gordan Janeš for providing me a computing infrastructure and technical support. From the DHMZ I want to say special thanks to wonderful Velimir Milić, kind and supportive colleague who encouraged me to push myself and learn more about programming and visualisation techniques. Thanks to my colleagues from the Agrometeorological Department for support and motivation throughout the years – Petra Sviličić, Jelena Ferina and to retired colleagues, Dražen Kaučić and fire weather researcher Marko Vučetić. Thank you for sharing your knowledge on fire weather with me. I want to thank Kristian Horvath and Endi Keresturi for providing me the ALADIN model data.

Special thanks go to Ivan Kovačević, Commander of the Split-Dalmatia County. Thank you for your collaboration, providing me the data on firefighting intervention and taking me to visit the fire ground. Thank you for answering all my questions on fire behaviour and firefighting intervention during the Split wildfire. Thanks to Mr Zoran Radunić from the Split Firefighting Brigade for great talks regarding fire behaviour and sending me all data I needed. Thanks to all firefighters from the SFB and the Firefighting Brigade Supetar from Island of Brač. I also want to thank firefighters from the Dubrovnik-Neretva County, especially to Commander Ivo Franušić.

Thanks to Zvonimir Barišin, Damira Kalajzić and Ante Mandić for forwarding their photos of the Split wildfire and to Mario Pastuović for helping editing the photos and visualizing the fire progression isochrones. I thank Dr Jonathon Marsden-Smedley for providing the map of the Forcett-Dunalley wildfire and Mrs Janice James for photos.

In the end, I want to thank a special group of people for unconditional support and for reminding me to take breaks, think of my health and have fun along the way. I want to thank my friend, colleague and former roommate Ena Melvan who introduced me to Macquarie's Cotutelle PhD program and encouraged me to apply for the scholarship. I am so grateful that we have fantastic memories together from both sides of the world. I hope we will continue having new ones. From Australia, I want to thank my dear colleague and friend Kellie Cook for fantastic support and acceptance on the campus. Thank you for all the help, advices, confidence talks, even after I left. Thanks to Lisa, Sammy and all wonderful people I met for good times

in Sydney. Huge thanks to my closest Croatian friends who supported me throughout the years – Tea, Marija, Sanja, Tihana, Darija and many more. Thanks to my late friend Željko. I wish we had more time together. I miss you dearly. In the end, I want to thank two very special ladies in my life who took care of me the same way my mum would – Rosetta Trovatiello from Sydney and Marija Frković from Zagreb. You uplifted me so many times and helped me. The words cannot express how grateful I am to have met you and will carry you forever in my hearts.

The last, but not least, I want to express huge gratitude to my family. To my grandparents Vera and Ivan and to my late grandmother Ana. I know you are proud of me. I miss you so much. To the best auntie Marija and mother-in-law Danija. Your support is very important to me. To my rolemodel, forever inspiration and my pillar of strength – my mother Mandica, and to my father Boris and brother Zlatan. In the end, huge gratitude goes to my husband Dario. For your love and trust in me and unconditional support while I am chasing and living my dreams. Thank you. Viva forever.

*Dedicated to firefighters.*

## CONTENTS

Chapter 1 Introduction.....	1
1.1. Background and Justification	1
1.2. Research Objectives	5
1.3. Thesis Outline	6
Chapter 2 Literature Review: Comparison of Wildfire Meteorology and Climate at the Adriatic Coast and Southeast Australia.....	7
2.1. Fire Weather and Fire Regime	7
2.2. Fire Weather in the Mediterranean Basin – Adriatic Coast and Croatia	9
2.2.1. European Wildfire Studies	11
2.2.2. Croatian Wildfire Studies – Wind-Driven	12
2.2.3. Croatian Wildfire Studies – Heat-Driven	17
2.3. Fire Weather in Southeast Australia	18
2.3.1. Synoptic Drivers	18
2.3.2. Surface Drying	23
2.4. Wildfire and Fire Regimes Under Climate Change	26
2.4.1. Fire Weather Indices	26
2.4.2. Future Fire Regimes	28
Chapter 3 Methods.....	31
3.1. Wildfire Reconstruction	31
3.2. Meteorological Observations	31
3.3. Fire Danger Rating	32
3.3.1. The Canadian Forest Fire Weather Rating System (CFFWRS)	32
3.3.2. Forest Fire Danger Index (FFDI) and Forest Fire Danger Rating (FFDR)	33
3.4. Synoptic Analysis	35
3.5. Operational Numerical Model and Reanalysis	35
3.5.1. ALADIN Operational Model	35
3.5.1.1. Low Level Jet	37
3.5.2. BARRA Reanalysis	37
3.6. Numerical Modelling	38
3.6.1. WRF Model	38
3.6.2. WRF SFIRE Model	41

Chapter 4 The Split Wildfire in Croatia.....	45
4.1. Overview of the Split Wildfire	45
4.2. Wildfire Reconstruction	47
4.2.1. Burn Period Split 1: 22:38 (16 July) – 09 UTC (17 July)	48
4.2.2. Burn Period Split 2: 10 – 14 UTC (17 July)	49
4.2.3. Burn Period Split 3: 15 – 21 UTC (17 July)	50
4.2.4. Burn Period Split 4: 22 (17 July) – 04 UTC (18 July)	51
 Chapter 5 The Split Wildfire – Meteorological Analysis.....	 53
5.1. Antecedent Conditions and Fire Danger Rating	53
5.2. Fire Danger Rating	54
5.3. Surface Synoptic Conditions	55
5.4. Surface Conditions – Observations	57
5.5. ALADIN Model	59
5.5.1. Surface Conditions	59
5.5.2. Upper-level Conditions	62
5.5.2.1. Horizontal Fields	62
5.5.2.2. Cross Sections	63
5.5.3. Low Level Jet	65
5.6. Discussion and Conclusions	69
5.6.1. Bura and Upper-level Trough	69
5.6.2. Hydraulic Jump and Dry Air Subsidence	70
5.6.3. Low Level Jet	70
5.6.4. Concluding Remarks on Fire Behavior	71
 Chapter 6 The Forcett-Dunalley Wildfire in Tasmania.....	 73
6.1. Wildfires in Tasmania	73
6.2. Forcett-Dunalley Wildfire	74
6.2.1. Burn Period Dunalley 1: 14 (3 January) – 12 AEDT (4 January)	76
6.2.2. Burn Period Dunalley 2: 13 – 23 AEDT (4 January)	77
6.2.3. Burn Period Dunalley 3: 5 January – 6 January 2013	80
 Chapter 7 Forcett-Dunalley Wildfire – Meteorological Analysis.....	 82
7.1. Climatological Analysis	82
7.2. Fire Danger Rating	83

7.3. <i>Surface Synoptic Conditions</i>	86
7.4. <i>Observations</i>	88
7.4.1. <i>Surface Conditions</i>	88
7.4.2. <i>Upper-level Conditions</i>	91
7.5. <i>BARRA Reanalysis</i>	95
7.5.1. <i>Surface Conditions</i>	95
7.5.2.1. <i>Horizontal Fields</i>	99
7.5.2.2. <i>Cross Sections</i>	101
7.6. <i>Discussion and Conclusions</i>	106
7.6.1. <i>Intense Heat and Severe Ground Conditions</i>	106
7.6.2. <i>Pyroconvection Conditions and Line of Convergence</i>	107
7.6.3. <i>Cold Front Passage</i>	108
Chapter 8 <i>Meteorological Drivers of Extreme Fire Weather in Croatia and Australia – Comparison Study</i> .....	110
8.1. <i>Model Validation</i>	110
8.2. <i>Comparison of Initial Weather Conditions</i>	111
8.3. <i>Comparison of Weather Conditions Coinciding with the Most Extreme Fire Behaviour</i>	115
8.4. <i>Discussion and Conclusions</i>	120
Chapter 9 <i>Preliminary WRF SFIRE Simulations over Croatia</i> .....	121
9.1. <i>Input Data for Coupled WRF SFIRE Simulations</i>	122
9.1.1. <i>Fuel Data</i>	122
9.1.2. <i>Topography Data</i>	124
9.2. <i>Verification of the Split Wildfire Coupled Simulations</i>	125
9.2.1. <i>Initial WRF SFIRE Simulation</i>	125
9.2.2. <i>Reconstruction of the Split Final Burnt Area</i>	127
9.3. <i>Fire-atmosphere Interactions over Adriatic Coast</i>	130
9.4. <i>Validation of the WRF SFIRE Simulations over Croatia</i>	135
Chapter 10 <i>Conclusions</i> .....	137
10.1. <i>Summary and Conclusions</i>	137
10.2. <i>Recommendations for the Improvement of Fire Management in Croatia</i>	142
Prošireni sažetak.....	145

References.....	163
Appendices.....	190
<i>Appendix A</i>	190
<i>Appendix B</i>	193
<i>Appendix C</i>	196
<i>Appendix D</i>	201
Curriculum Vitae.....	203



## CHAPTER 1

### INTRODUCTION

#### *1.1. Background and Justification*

Wildfire is a global ecosystem process and, as an integral part of the natural cycle, it plays a key role in distributing patterns of flora and fauna and helps to shape the landscape mosaic (Flannigan et al., 2000; Keeley, 2012; Keeley and Syphard, 2016). If wildfire starts and spreads quickly in an uncontrollable way, it can cause tremendous destruction and become one of the most severe natural disasters (Meng et al., 2015). On a global scale, we witness reports about the “worst”, “largest”, “longest”, “most expensive” and “record breaking” wildfires and fire seasons (IAWF, 2019).

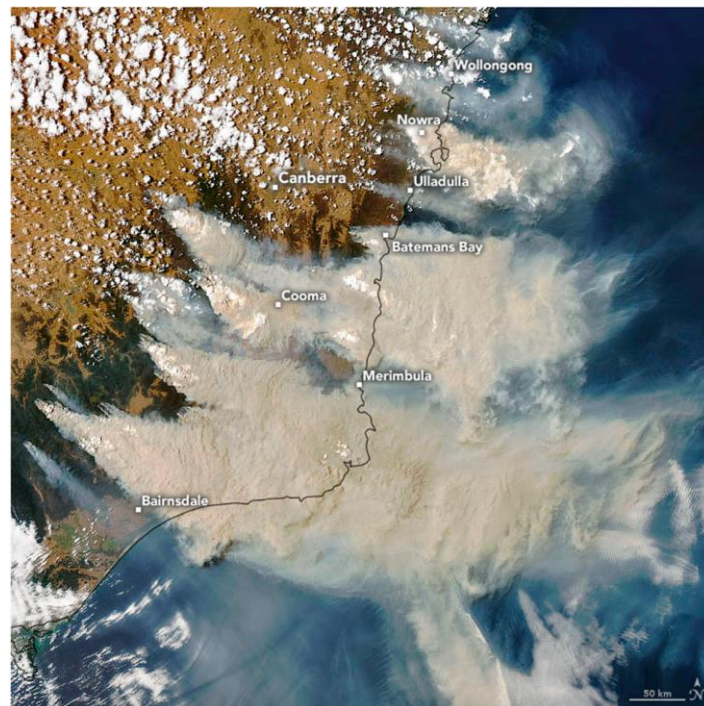


Figure 1.1. Extreme fire events on the 4 January 2020 over southeast Australia as shown by the Moderate Resolution Imaging Spectroradiometer (MODIS) on NASA’s Aqua satellite. In the image, smoke (tan in colour) and clouds (bright white) can be seen, while the white patches above the smoke may be pyrocumulonimbus clouds (source: Earth Observatory of NASA, available at <https://earthobservatory.nasa.gov/images/146110/fires-and-smoke-engulf-southeastern-australia> accessed on 30 April 2022, 16:49 Australian EST).

Year after year wildfires burn with surprising intensity and devastating consequences all across the planet, affecting lives of millions of people and costing billions in direct and indirect damages (Stephenson et al., 2012). Since the turn of the 21<sup>st</sup> century, numerous catastrophic wildfires have captured public attention (Potter, 2012a). For instance, the extent of the 2019/20 fire season in Australia is difficult to comprehend (Borchers Arriagada et al., 2020).

With more than 13 million hectares burnt, tragically dozens of people killed, and up to 1 billion animals dead, this fire season would long be remembered as the “Black Summer” (P Fox-Hughes, 2020, personal communication). These lethal bushfires, which is an Australian term for wildfires, generated an intense smoke that in some places turned day into night. Plumes had not only an immediate local, but a longer-term global impact. Crossing international and continental boundaries smoke from those bushfires affected the air quality in places far away as New Zealand and South America (Figure 1.1).

A series of shock-type wildfire events has not spared the rest of the world either. Apart from the record-setting size of a burnt area, some wildfires in the 21<sup>st</sup> century surprised with major infrastructure damage and human casualties. The deadliest this century in Australia, Black Saturday in 2009, killed 173 people (VBRC, 2009). Moreover, extremely high death tolls occurred on both sides of the Atlantic in 2018 – in Greece, the deadly wildfire near Athens killed 102 people in less than 3 hours (Lagouvardos et al., 2019), while in the United States (California) several wildfires caused 95 deaths, most of which took place in a single fire incident in northern California, the Camp Fire. Apart from human loss, the Camp fire destroyed nearly 19 000 homes and other structures, marking the most expensive wildfire season in California state history (Brown et al., 2020).

In recent years fire activity was observed in other global regions where wildfires are least expected, for example, within the frozen Arctic Circle and Himalayas (You et al., 2018). Latitude and elevation of those fires is of a great concern. Amazonia’s burning crisis in 2019 attracted worldwide media and political attention. Although wildfires within the landscapes of Amazonia rainforest were a consequence of intentional deforestation and extensive agriculture, it was unusual to record an increase in number of wildfires in the absence of a strong drought (Barlow et al., 2019).

Prior to the 21<sup>st</sup> century, there were periodically even larger and more deadly wildfires recorded. According to earlier historical records, Australian bushfires during 1974/75 were nearly apocalyptic. Although fires were concentrated in the central part of Australia, where few people live, numerous blazes burnt 117 million hectares, approximately 15% of Australia’s territory (Cheney, 1976). The largest wildfire disaster in the 19<sup>th</sup> century was the Black Thursday in 1851, which burnt quarter of the State of Victoria (Ellis et al., 2004). The levels of mortality caused by wildfires were exceptionally high in the 19<sup>th</sup> and in the first half of 20<sup>th</sup> century all around the world. For instance, in 1871 an estimated 1,500 people were killed in the firestorm known as the Peshtigo Fire in the United States (Holbrook, 1944). Similar wildfire tragedies marked the history before the era of successful wildfire suppression.

The contrast between such historical events and those occurring today is that catastrophic wildfires occur more often and affect more people despite the modern firefighting equipment and technology (Struzik, 2017). Wildfires today burn in so-called wildland-urban interface (WUI), where millions of people live, work and recreate. Although there was increased number of human caused ignitions, wildfires within WUI, once started, make firefighting operations very demanding. There are three regions of the world where this is especially pronounced: western North America, southeastern part of the Australian continent where majority of the Australian population resides, and the coastal and touristic areas of Mediterranean European countries, where small touristic towns merge with natural and forest areas (Bento-Gançaves and Vieira, 2019). However, the increase of human population and the rapid expansion of WUI are not the only factors affecting our ability to control wildfires. It seems that wildfires today burn differently from the way they used to.

In the 21<sup>st</sup> century we are already experiencing an alarming new category of wildfires – the so-called ‘megafires’ (Williams, 2013). The term ‘megafire’ became widespread in 2002 when the western United States reported their worst wildfires on record and described that ‘incidents were extraordinary and altogether distinct from other large wildfires’ (San-Miguel-Ayanz et al., 2013). Since then, the term has been used to describe massive, intense wildfires in many fire prone regions in the world (Dimitrakopoulos et al., 2011, Coen et al., 2018, de la Barrera et al., 2018), usually larger than 10,000 ha (Stephens et al., 2014). Although extremely infrequent and rare (accounted for only 1% of the total number of fires), megafires may be responsible for more than 90% of burnt area in one fire season (Bartlett et al., 2007, Strauss et al., 1989). Criteria for defining a megafire may vary, and there is no single overarching definition (Buckland, 2019). From fire management and social perspective, it describes a wildfire notable in scale, intensity, expense, necessary resources, and human, economic or environmental impacts (Coen et al., 2018). From the meteorological perspective megafires are high impact wildfires characterized by enhanced dynamical coupling with the atmosphere. In those conditions megafires can generate sufficient energy to modify prevailing meteorological conditions and create their own weather – firestorms (Vines, 1981). Firestorms, as a product of fire-induced interaction with the atmosphere, in severe cases may generate violent pyroconvection, or deep convective column, manifested as special type of clouds – pyrocumulus (pyroCu) or pyrocumulonimbus clouds (pyroCb; Sharples et al., 2016). Convective updrafts and downdrafts within a pyroCu or pyroCb affect fire behaviour by strong and erratic changes in wind speed and direction (Potter, 2012a; Potter, 2012b). Large-scale firestorms may produce pyrogenic lightning and cause additional ignitions kilometres away

from the fire front (Dowdy et al., 2017). In extreme cases pyroconvection can lead to evolution of a disastrous large fire-generated vortex (>100 m diameter) with dynamical similarities to tornadoes. Although very rare, these rotating columns of ash, smoke and flame connected to overlying pyroCb have been documented in Australia (Figure 2.2a; Laureau et al., 2019). At least one intense fire tornado demolished outskirts of Canberra (Australian Capital Territory, ACT) in a series of wildfires in January 2003. The Canberra Firestorm produced fire vortex along 20 km path with the intensity equivalent to an F2 (180–240 km/h) Fujita scale tornado (Cunningham and Reeder, 2009). Since 2003 there were number of cases when wildfires generated catastrophic pyroCbs within hours of their ignition (Fromm et al., 2006; Cruz et al., 2012; McRae et al., 2013; Field et al., 2016; Ndalila et al., 2019).

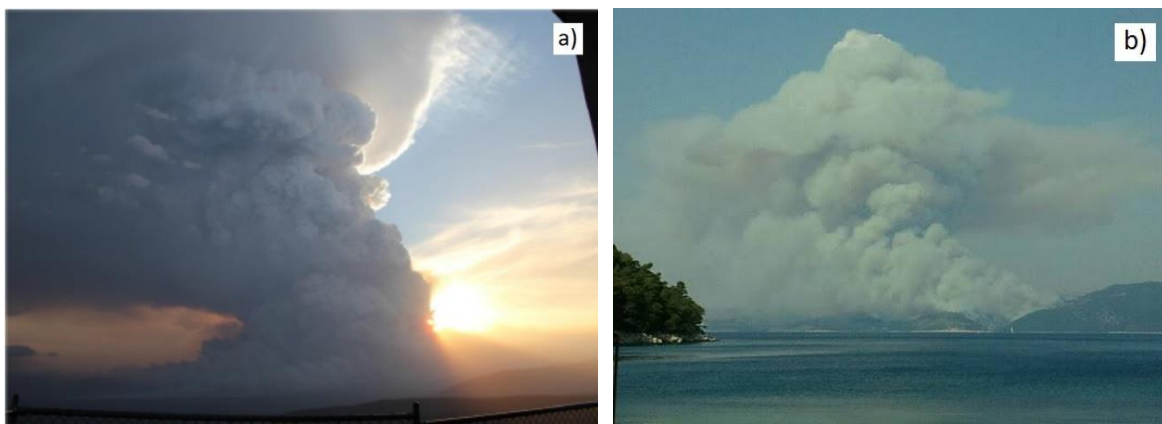


Figure 1.2. a) Photo of pyrocumulonimbus cloud in the Grampians Fire, Victoria, Australia, 21 February 2014 (Photo taken by Randall Bacon; Sharples et al., 2016) and b) pyrocumulus or possible case of pyrocumulonimbus on the island of Brač, Croatia, 14 July 2011 (Photo taken by Siniša Miličić; Mifka, 2012).

Wildfires of this scale have not been reported in Croatia yet, however, pyroconvection has certainly occurred (Figure 1.2b), but it is not clear whether pyroCb have developed. Nonetheless, there have been reports of unusually destructive, uncontrollable and wind-driven wildfires that burned over night without a sign of slowing down, with unstoppable fire progression, widespread flaming, racing downhill and reaching suburban areas that are usually considered protected from such blazes – all of which was reported back in 2017, the worst fire season ever in Croatia. In the recent year's Croatian firefighters and firefighting aircraft often describe wildfires as too intense to fight or even approach, leaving them with the only possibility to remove fuel in front of the fire, which is not safe due to erratic changes in wind. Therefore, Croatia, same as Australia, has recorded unprecedented wildfires and wildfire behaviour, which is meteorologically linked to enhanced fire-atmosphere dynamics, higher level of energy and non-linear effects (Sharples et al., 2016). Regardless of their exact

definition, these events call for special attention and underline the need for researchers to better understand mechanisms causing and driving them.

Rapid wildfire progression that causes huge damage and high mortality mostly occurs in a matter of hours during a wildfires' active period (Wang et al., 2014). Whether a wildfire will exhibit extreme behavior and become a major threat largely depends on weather, or more precisely a certain combination of meteorological conditions (Bradstock et al., 2009). Therefore, in order to accurately forecast and alert rescue and fire officials to wildfires as early as possible, it is timely and important to know a full set of meteorological factors causing wildfires. Comprehensive studies of historical wildfire events may enhance our knowledge on this destructive and powerful phenomenon and significantly contribute to both the science of meteorology and effective decision-making in fire management.

## *1.2. Research Objectives*

The main goal of this Cotutelle PhD is to investigate fire weather of individual extreme wildfire cases, one from each region of interest – the occurred hotspots: Croatia (as part of the Mediterranean) and southeast Australia. Both regions share similar climate and fire weather conditions that contribute to extreme wildfire events in both countries. Croatian case study will include the Split wildfire from 2017 and Australian case study will include the Forcett-Dunalley wildfire in Tasmania from 2013. Although they occurred in different hemispheres, chosen case studies share similar latitude, topography and coastal setting.

The second aim of this research is to draw similarities between dynamic atmospheric processes and mechanisms that occurred in these events. The study's final aim is to determine if wildfires along the Adriatic coast are strong enough to modify the atmosphere in a similar way to those that occur in Australia. For this purpose, a coupled fire-atmosphere model has been implemented in Croatia for the first time.

### *1.3. Thesis Outline*

The dissertation follows a case-study design, combining meteorological observations, climatological analyses, wildfire observations, high resolution numerical meteorological models and a coupled fire-atmosphere model. The overall structure of the dissertation takes the form of ten chapters beginning with this introduction. Chapter 2 is a literature review of previous fire weather research with the focus on Croatia and Australia. Data and methods are described in Chapter 3. The next four chapters will be reconstruction and comprehensive meteorological analyses of two wildfires, one from each country. Chapters 4 and 5 are the reconstruction and meteorological analysis of Croatian case study, while Chapters 6 and 7 of Australian case study. Main research questions will be presented at the end of chapters including reconstruction of each wildfire, while discussion on findings will be presented at the end of chapters including meteorological analysis. Discussion will be also included at the end of the following two chapters. In Chapter 8, the findings from meteorological analysis using high resolution model will be compared in order to identify the most common and uncommon fire weather conditions in selected case studies, while chapter 9 presents preliminary coupled fire-atmosphere simulations for Croatia. Conclusions and further discussion are presented in the last chapter 10. Chapter 2 is published as a recent paper [Tomašević et al. \(2022\)](#), while chapters 4 and 5 are together published in [Čavlina Tomašević et al. \(2022\)](#).

## CHAPTER 2

### LITERATURE REVIEW: COMPARISON OF WILDFIRE METEOROLOGY AND CLIMATE AT THE ADRIATIC COAST AND SOUTHEAST AUSTRALIA

#### 2.1. Fire Weather and Fire Regime

Wildfires are truly global and permanent phenomenon (Camona-Moreno et al., 2005). Generally occurring between 70°S to 70°N, their frequency increases progressively towards the tropics, and drop sharply at the equator (Mouillot and Field, 2005). Although certain regions appear to have a clear 'high' fire season, satellites reveal there is always active fire somewhere on the planet (Flannigan et al., 2009). Around 80–86% of wildfires occur in grasslands and savannahs, primarily in Australia and Africa. The remaining fires occur in forested areas scattered around the globe, but those involve more biomass and sustain the most intense type of wildfires that spread through forest canopy – known as crown fires (Van Wagner, 1976). Crown fires burned in catastrophic wildfires mentioned earlier. Fires in Mediterranean, Australia and California all started in forested areas and quickly reached highly populated urban places causing vast destruction and loss of life. Fire incidents chosen for this meteorological research will include crown type of wildfires.

Here we define *fire weather* as critical atmospheric conditions that enable extreme fire activity, resulting in large and destructive wildfires (Werth et al., 2011; Werth, 2017). Although conclusions on fire weather may differ between locations and at different times at one location, common conditions important for large wildfires include high surface air temperature and low relative humidity, low atmospheric stability, strong surface and upper-level wind, and drought (Luke and McArthur, 1978; Potter, 1996; Lucas, 2010).

Drought is the most obvious factor coinciding with the period prior to a major wildfire, but it is not the sole cause of it and not very useful one for operational fire danger forecasting. Air temperature has an indirect effect on all other meteorological elements, and its small variations can significantly modify direction and magnitude of air-fuel water exchange (Van Wagner, 1979). Air humidity influences fire behavior through fuel moisture. In some cases risk of a severe wildfire is high regardless of relative humidity when air temperature exceeds 40°C, which has been confirmed for major wildfires in New South Wales, Australia (Robin and Wilson, 1958). Wind brings additional supply of oxygen to wildfires' area, enhancing combustion process and consequently increasing wildfires' intensity and radiative energy. Wind also contributes to air-fuel moisture exchange around the combustion region, influences

the rate of spread of a wildfire by changing the angle and distance between flames and fuels (Gisborne, 1928), and carries embers causing additional spotting (Byram, 1940; Byram, 1943, Telitsyn 1965).

Each meteorological property has its own important influence on wildfires; however, these elements are just local and surface manifestations of atmospheric conditions. Both air temperature and humidity depend primarily on air mass characteristics that are normally consistent over large areas and for a significant period of time. On the other hand, wind and precipitation are more dependent on the ever-changing dynamic processes throughout the troposphere, which makes them far more difficult to predict (Brotak, 1976). Therefore, whole set of factors influencing wildfires is determined by horizontal state and vertical structure of the atmosphere, or in meteorological terms – strength and movement of surface lows and highs and associated warm and cold fronts, all known as synoptic scale features (Flannigan et al., 2009). Identification of those synoptic features related to the most extreme wildfire behavior or fire danger, and localizing major wildfires in relation to existing fronts, lows and highs, can contribute to prediction of severe fire weather conditions a day or more in advance (Beals, 1914, Brotak and Reifsnnyder, 2003). *Critical fire weather synoptic patterns can be divided in three categories – the ones causing strong surface wind associated with low relative humidity, the ones causing low atmospheric stability (Werth et al., 2011) and the ones that are combination of both.*

Spatial and temporal pattern of wildfires at certain location and over a given time period defines *fire regime*. The fire regime is characterized by fire *frequency, size, intensity (amount of energy released), severity (measure of fuel consumption), seasonality and type (ground, surface or crown) of wildfires* within a certain spatiotemporal window (Flannigan et al., 2000). These six components of fire regime are determined by key drivers that represent the resources and necessary conditions for fire activity. Those are weather and climate, fuel structure and availability, and ignitions – natural or human related (Flannigan et al., 2009). However, climate and weather are found to be the most important natural drivers influencing fire regimes in many fire prone regions (Flannigan and Harrington, 1988; Johnson and Wowchuk, 1993; Swetnam, 1993; Flannigan et al., 2005; Turco et al., 2017).

Climate controls resources and weather conditions favourable for wildfires. It has a direct effect on fire weather conditions and an indirect, long-term effect on the distribution, moisture and load of available flammable vegetation to burn (Krawchuk et al., 2009). Interplay of mean annual temperature and amount and timing of precipitation determines fuel structure and flammability. While precipitation in wet or winter season proceeding the dry fire season



promotes plant growth and provides sufficient fuel volume to carry fire, warmth during dry or summer season increases evapotranspiration and decreases fuel moisture (Flannigan et al., 2009). Once the favourable conditions are in place, fire start depends on ignitions. The biggest natural source for ignitions is lightning; and lightning activity is again influenced by climate (e.g., Price and Rind, 1994; Flannigan et al., 2009; Romps et al., 2014; Jones et al., 2022). Climate does not only influence fire regime but fire activity can influence climate. Strong thermal convection during large wildfires can cause long-range transport of fire emissions thousands of kilometres away, even to high-latitude glaciers. Black carbon deposits reduce albedo of glaciers and sea ice. As a result, instead of being reflective, ice absorbs more sunlight, which can cause spatially extensive melting events (Keegan et al., 2014). Changes in albedo together with changes in atmospheric concentration of greenhouse gases (Andela et al., 2017), vegetation destruction and accompanying drop in evapotranspiration during and after large wildfires affect energy budget, and therefore climate (Flannigan et al., 2000).

But what do we know about the fire weather that drives wildfires to burn bigger, hotter and faster than ever? The following section contains the review of our best current understanding of fire weather conditions in areas of an interest in this research – Croatia and southeast Australia.

## *2.2. Fire Weather in the Mediterranean Basin – Adriatic Coast and Croatia*

Fire weather conditions in the Mediterranean Basin during summer are mostly characterized by two large semi-permanent synoptic weather systems – the Azores high at the west and the low pressure monsoon system over the far eastern edge (Table 2.1.; Millán et al., 1998) and Ethesian winds over the Eastern Mediterranean (Klaić et al, 2009) as a consequence of the persistent low pressure formed over the Middle East (due to Karachi Depression). The Mediterranean region has a complex orography, which includes extensive coastline, backed by relatively high mountain ranges surrounding the warm Mediterranean Sea (Lionello et al., 2006). Mountain ranges around the Mediterranean act as constraining barriers to the atmospheric flows and can generate mountain-induced aerodynamical vortices or large-scale blocking. Also, the large-scale channeling is common in the entire region (Scorer, 1952). Over the major peninsulas summertime atmospheric circulation can include the formation of extensive and deep convective cells and thermal lows (Hoinka and De Castro, 2003). Other often occurring thermally driven meso-meteorological circulations with diurnal cycle include, for example, sea and land breeze circulations. Their formation during the day, together with their collapse during the night, often involve coupling and/or decoupling with the upper wind

resulting in rapid change in surface wind speed and direction (Telišman Prtenjak et al., 2006, 2010). Therefore, diurnal evolution of such meso-circulations and its interactions with the upper atmospheric flows is necessary for understanding the dynamics of wildfires in the Mediterranean area (Millán et al., 1998).

Summertime synoptic weather patterns related to large wildfires in this region can be loosely distinguished as the ones causing the hottest and driest conditions, and the ones causing windy conditions (Table 2.1.). Extremely warm days in Europe have been associated to atmospheric ‘blocking’ or stationary and persistent anticyclonic situations (Jézéquel et al., 2018). For instance, the location and strength of a North Atlantic ridge, associated with the Azores anticyclone, usually corresponds to the ‘hot and dry’ episodes and heat waves. Depending on the sub-regions in the Mediterranean the anticyclone causes the advection of hot and dry air from the continental Europe and North Africa (Sousa et al., 2018), contributing to high temperature and low relative humidity. Such anticyclonic weather types contributed to the European summer heat wave in 2003. Long-lasting ‘blocking’ nature of the high pressure stretching from the Azores to the Norwegian Sea completely blocked the intrusion of moist and cool air from the Atlantic and the North Sea to central Europe (Fink et al., 2004). The most severe fire weather conditions coincided with the peak of the heat wave in August 2003, which resulted in the most severe wildfires in Portugal in modern times. A devastating sequence of large wildfires burned 450 000 ha in the first two weeks of August in 2003 (Fink et al., 2004). The atmospheric circulation during those wildfires was dominated by the strong North Atlantic ridge, which in one part was situated over the Iberian Peninsula. Near the surface, this ridge enhanced anomalous advection of hot and dry air mass from the northern Africa. This air mass was additionally heated and dried while crossing the central Iberian plateau before reaching wildfires in Portugal (Pereira et al., 2005). This synoptic configuration led to the highest 850-hPa temperatures on record since 1958, together with the all-time Portuguese surface temperature record (47.3°C for maximum and 30.6°C for minimum air temperature on 1 August 2003; Trigo et al., 2006). Similar episodes of ‘blocking’ synoptic conditions, which promote periods of long clear sky and consequently to long-term solar radiative heating and warm surface conditions were found to correlate with severe wildfires in many other Mediterranean countries – Spain (Rasilla et al., 2010; Trigo et al., 2013; Cardil et al., 2014a; Trigo et al., 2016), Italy (Cardil et al., 2014b), Greece (Kassomenos, 2010; Papadopoulos 2013) and Israel (Levin 1999).

The term ‘blocking ridge’ has long been associated with severe wildfires in other mid-latitudes of the Northern Hemisphere (Table 2.1.). For example, various North American

studies (Newark, 1975; Flannigan and Harrington, 1988; Johnson and Wowchuk, 1993; Skinner et al., 1999) confirmed that upper ridges, which can last a week or longer, tend to block or divert moisture-carrying systems to the north or south of the ridge, leaving conditions at the surface warm and dry (Flannigan et al., 2009). Air within a ridge sinks and dries, and after a week or more, irrespective of the antecedent conditions, fuels are dry enough to burn. Although fire danger increases over period of time when ‘blocking ridge’ sits over a certain region and peak in fire danger often correlates with the peak in ridge height (Newark, 1975), it seems that during the ridge breakdown wildfire behavior intensifies in terms of sudden increase in fire intensity and spread. The breakdown of a ridge usually occurs due the passage of a surface cold front and upper-level trough, which brings dry, hot and windy conditions, followed by change in wind direction and transition to cooler, moister air and lighter winds (Nimchuk, 1983). In the Mediterranean Basin these kinds of conditions occur when the Azores or the central European anticyclone weakens and allows the Atlantic depressions moving to the lower latitudes. Summertime Mediterranean cyclones are rare, but when they occur, depressions and accompanying cold fronts sweep the area from the Iberian Peninsula in the west Mediterranean to the Balkan Peninsula in the east (Millán et al., 1998). A summer cold front passage can also leave some regions dry, or without a significant amount of rainfall that can influence vegetation moisture. As the frontal systems cross the region, the wind direction changes from southerlies to northerlies, with the last stage accompanied by a significant increase in wind speed. These synoptic conditions override the regional diurnal coastal circulations, and although it seems the dry cold front passage could be the most intense summer event to influence wildfires persistence and intensity, studies on relationship of this phenomena to wildfires are almost non-existent in the European literature (with the only exception found being Millán et al., 1998).

### *2.2.1. European Wildfire Studies*

Fire weather research in Europe mostly consisted of two kinds of studies – ones focused on analysis of indices representing fire risk, and others using the concept of synoptic climatology for studying the relationships between general atmospheric circulation and extreme wildfires. Work of many European authors, mostly of forestry or agriculture background, were inspired by those topics. Studies of meteorological background are usually climatological studies that link burnt area, fire size and fire frequency with previously defined synoptic weather types. However, different national terms for local winds and often different nomenclature of the same synoptic weather patterns, even for circulations of similar dynamics and driving mechanisms, make the review of European fire weather knowledge base demanding

and confusing. Moreover, averaging of the synoptic circulation, even for specific case studies, and viewing the atmosphere as a steady-state phenomenon does not give a complete answer on the most dangerous possible mesoscale and micro-scale meteorological processes. There is a significant lack in the European literature of an in-depth meteorological studies that use high-resolution numerical mesoscale models in finding the answers on the atmospheric dynamics impacting fire grounds within a complex coastal orography along the Mediterranean Basin. Only three studies were found to use the Weather Research and Forecasting (WRF) model – two of which used a coupled version with a fire-spread model (WRF-SFIRE) to investigate the most catastrophic case of wildfire in Mediterranean that resulted in death of 102 civilians in Eastern Attica, Greece, on 23 July 2018 (Laguardos et al., 2019; Kartsios et al., 2021). Numerical simulations revealed a good span of the various mesoscale atmospheric phenomena influencing wildfires – from induced orographic waves, hydraulic jumps, strong winds on lee slopes and strong downward transport of kinetic energy.

#### 2.2.2. *Croatian Wildfire Studies – Wind-Driven*

Croatia lies within one of the world's most fire prone areas, the Mediterranean Basin. The most fire-prone area in Croatia is the Adriatic Sea coastline, together with its surrounding hinterland and islands, of which there are more than a thousand in the Croatian archipelago. High fire risk is pronounced during summer months, from June to August, when long dry spells and intense heat favor fire ignition and spread through highly flammable Mediterranean vegetation including pine forests and shrubs. Each year, Croatia is affected by a large number of wildfires that are in majority human-caused (> 90%), and only minority is lightning-caused (Mamut, 2011; DUSZ, 2018). The average number of fires per year in the period 2006–2016 was 4 033, with an average burnt forest area of 26 690 ha (DUSZ, 2018). However, wildfire severity has been increasing, which was illustrated by the very hazardous 2017 fire season when the burnt-area escalated with the total of ~87 000 ha in more than 4 100 wildfires along the Adriatic coast, marking the worst fire season in Croatian history.

The need for investigating the relationship between wildfires and weather conditions among Croatian research community was recognized soon after the establishment of the fire danger rating system in 1981 at the DHMZ (Croatian Meteorological and Hydrological Service). Since then, the fire weather research in Croatia evolved in two mayor parallel directions. One kind of studies focused on analysis of the Canadian Fire Weather Index (FWI) representing fire risk, while the other focused on analysis of synoptic and mesoscale conditions during severe wildfire events. Apart from favourable antecedent weather conditions, these

studies revealed certain meteorological phenomena that in some cases triggered an abrupt increase in fire danger, re-activity of already considered controlled wildfires, and in one case – tragic death of firefighters.

The earliest papers that analysed synoptic and mesoscale features revealed that a significant influence on fire weather conditions along the Adriatic coast in Croatia has the placement of the Azores anticyclone over Europe. The persistent or blocking anticyclonic conditions divert cyclonic disturbances away from the Adriatic coastline, situated in the north part of the central Mediterranean. These conditions cause a long period of warm, dry and calm weather, with mostly weak diurnal local coastline circulations such as sea breeze. These conditions are obvious to be favourable for wildfires, but what seems to be crucial for the occurrence of large wildfires in the area is the Azores high displacement to the north. This allows cold fronts to sweep the area of the Adriatic, overriding the local coastline circulations, changing wind direction and increasing wind speed in the region. These summertime cold fronts are usually dry, or bring small amount of precipitation, insufficient for already dry vegetation or to extinguish already started wildfires. In cases of severe wildfire events on the mid-Adriatic islands in 1985 (Vučetić, 1987) and in 1990 (Vučetić, 1992), in spite of low rainfall amount following the cold front passage and decreased fire severity rating, wildfires intensified again after considered to be put under control. The latter case was also the first record of lightning-caused wildfire in Croatia in the scientific literature.

A similar pattern of wind-driven wildfires in Croatia repeated in the following years. For example, in another case of lightning-caused wildfire in July 1997, which followed by the cold front passage (Vučetić, 1998), authors emphasized the important role that wind speed and direction have in severe wildfires cases along the Adriatic coast. Steep mountain ranges descending towards the Adriatic Sea make complex topography in this area that easily modifies the air flow. Also, this study served as the first and the only attempt to date to calculate the speed of the fire front in case of wildfire in Croatia. The best approximation of the maximum fire spreading speed of this wildfire was  $5 \text{ km h}^{-1}$ .

The use of a high-resolution mesoscale ALADIN model made a step forward in fire-weather research in Croatia. It enabled the transition from the two-dimensional to three-dimensional synoptic and mesoscale analysis. Simulation of vertical profiles of wind speed and direction in three case-studies with different synoptic background showed a surprisingly similar atmospheric profile within 3 km above ground – a significant wind speed maximum between 250 and 900 m altitude (Vučetić and Vučetić, 1999). In all three cases with this wind speed maximum aloft (although with different wind directions: SE (*jugo*), NE (*bura*) and NW

(*maestral*)), wildfires on the ground level burned out of control. The earlier research from the United States defined this type of vertical wind speed profile as low-level jet (LLJ) and found it to be among the most dangerous ones (Table 2.1.) – with wildfire behaviour being dominated by the wind, with probable occurrence of large whirlwinds and being very dangerous for towns and villages ahead of the fire front (Byram, 1954).

The same kind of wind speed profile was confirmed, and for the first time defined as a LLJ in Croatian literature in the comprehensive meteorological study of the most tragic wildfire event in Croatian history - the Kornati fire on 30 August 2007, when 12 firefighters died and one was badly injured (Vučetić et al., 2007). The fatal combination of meteorological factors contributing to the tragedy on that day included the annual maximum of the fire danger rating (Vučetić and Vučetić, 2011), a cold front passage related to the cyclonic activity over Adriatic Sea with accompanying 850-hPa trough affecting most of the Western Mediterranean, and on the local scale a shallow meso-cyclone over the wildfire area which created partly cloudy and windy weather with moderate to strong SE wind. The vertical structure of the atmosphere during the most critical wildfire hours consistently included the LLJ. The appearance of the LLJ was associated with a very strong wind shear in the atmospheric boundary layer, together with very high values of turbulent kinetic energy. The study also included the verification of the performance of the ALADIN model to accurately simulate vertical profiles. Comparing to nearby radiosonde measurements it was concluded that ALADIN model tends to underestimate the vertical wind speed. This finding shows the possibility of even more severe conditions in real life scenario. To summarize, this study pointed out two meteorological indicators that can be used as possible additional warning on extreme wildfire behaviour on the Adriatic coast – LLJ with maximum speed exceeding  $12 \text{ m s}^{-1}$  and approaching cold front.

Later studies confirmed a cold front passage and LLJ to be the crucial features of large wildfires at the Adriatic coast, and also reconfirmed the importance of analysis of the vertical structure of the atmosphere. For instance, this typical synoptic pattern and vertical profile was found to occur in cases of all wildfires larger than 500 ha in the period 2001–2010 (Tomašević, 2012). What is interesting is that three out of eight largest wildfires in 10-year period burned simultaneously from 11 to 16 August 2001. Synoptic pattern that influenced the weather conditions on the ground was consistent with the ridge of the Azores anticyclone over the central Europe and shallow cyclone situated over the Gulf of Genoa. The strengthening of the Azores high and transition of the low pressure over the Adriatic Sea generated a strong pressure gradient in the region. The accompanying cold front crossed the area in matter of hours on the night between 11 and 12 August 2001 (Figure 2.1a), changing the wind direction and increasing

the wind speed. This synoptic configuration brings the cool and gusty NE *bura* wind along the Adriatic coast, which is a common feature during winter months. Although it is rare from June to August, studies found that when it occurs it has a drastic influence on wildfire behaviour. Wildfires that started in the night on 11 August 2001 quickly got out of control, one by one, from the north to the south of the Adriatic, coinciding with the increasing prefrontal winds. According to analysis of vertical profiles simulated close to locations of burning wildfires revealed that strong NE *bura* wind dominated in the atmospheric boundary layer, with maximum wind speed of  $25 \text{ m s}^{-1}$  at 640 m altitude (Figure 2.1b). Such strong wind was close to the largest conflagration near the city of Split, the second most populous city in Croatia situated on the coast of the Adriatic Sea. Other wildfires were scattered around the coastline and islands and burned more than 3 000 ha in 5 days (Tomašević, 2012).

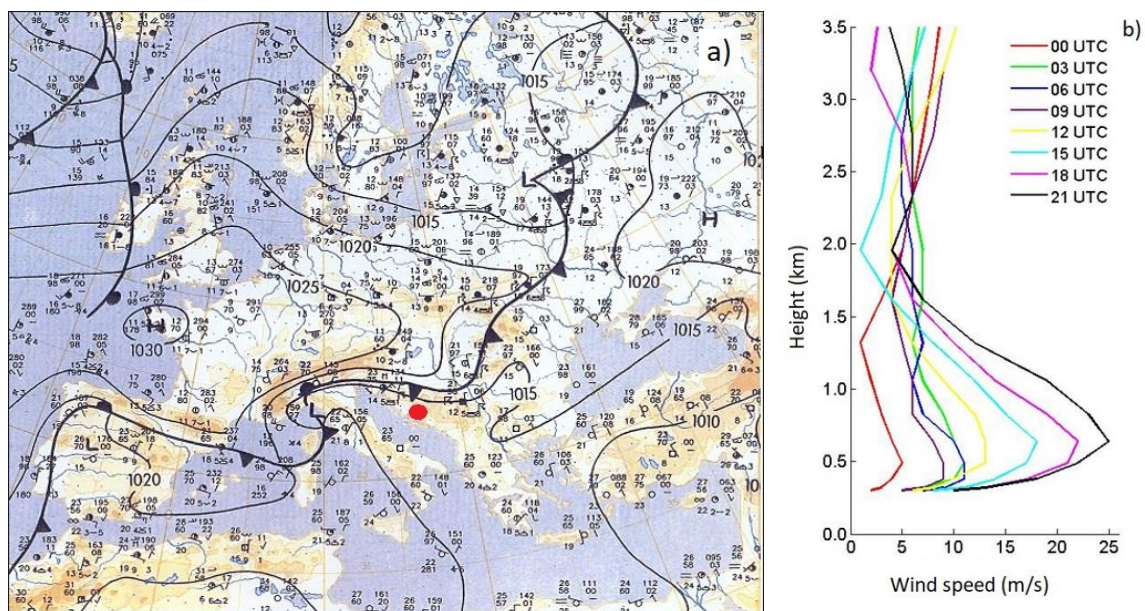


Figure 2.1 a) Mean Sea level pressure analysis over Europe (*Deutscher Wetterdienst*, DWD) at 00 UTC on 11 August 2001 and b) wind speed vertical profile ( $\text{m s}^{-1}$ ) at Split-Marjan meteorological station on the same day, simulated from the numerical mesoscale ALADIN model (Tomašević, 2012).

What is in common between wildfires in 2001 and the rest of the large wildfires that occurred until 2010 is that in all cases wildfires were driven by strong NE *bura* wind. Strong and gusty *bura* wind often prevented firefighting aircraft from participation in the operations, sometimes even making ground troops unable to approach a wildfire. Specifically difficult situation was in 2003 with nine wildfires raging at the same time on the Island of Hvar, some merging into one big conflagration, while on the nearby Island of Brač an already started wildfire rapidly doubled its size in less than 4 h (from 300 ha to 600 ha; Tomašević, 2012). The

total burnt area during these events was larger than 4 200 ha. Another example of extreme wildfire occurred in September 2003 after the usual fire season peak in Croatia, which is in July and August. Cold front, *bura* wind and LLJ aloft again coincided with multiple wildfires on the Adriatic coast, with the largest one threatening residents and tourists on the Island of Lastovo. The total burnt area was 1 800 ha, majority of which (1 200 ha) burned in the first day of the wildfire due to strong *bura* (Tomašević, 2012). To put this spatial scale in the context for defining large wildfires in Croatia – 1 800 ha is more than half of the Lastovo Island. From the fire management perspective, this operation was extremely difficult. Without help from the firefighting aircraft, and with other troops being scattered around the Adriatic coastline, closes being 5 h of a limited boat transfer away from the Island.

In the years that followed similar meteorological conditions continued to trigger large wildfires. The same synoptic configuration (anticyclone over the central Europe and cyclone over southern Italy) caused the strong pressure gradient in the region, creating favourable fire weather conditions during the wildfire in the northern Adriatic on 23 July 2012. Synoptic and mesoscale analysis of this wind-driven wildfire revealed that *bura* wind had a dominant influence on wildfire behaviour (Kozarić and Mokorić, 2012). Measurements from the nearby automatic station showed the maximum average wind speed of  $13 \text{ m s}^{-1}$ , with gusts up to  $30 \text{ m s}^{-1}$ . Relative humidity dropped to 20%, which together with the strong wind, additionally dried fuels. Besides the strong wind on the ground, typical characteristic of *bura* vertical profile is an inversion layer above it, capping the layer of strongest winds. This also influenced the capabilities of fire management on the ground since the thick smoke was trapped below the inversion. Variability in speed is also typical for *bura* wind. The occasionally drop in wind speed caused the rapid change in wind direction due to complex local topography. In those short time periods the topographic influence would be dominant on the fire front, although wildfire could not be contained until the NE *bura* wind completely weakened.

A somewhat different synoptic pattern influenced the weather conditions during the largest wildfire in Croatia to date which burnt 5 600 ha. The wildfire started on the Island of Brač on 14 July 2011, being dominated by the strong southerly wind, which, the next day, turned to NW *maestral* wind, typical for diurnal coastal circulation in the area (Mifka and Vučetić, 2012). The change in wind direction in this case again was followed by the passage of the cold front, although upper-level cyclone was situated over central Europe, unlike the anticyclone in the previous cases. LLJ occurred in this synoptic situation as well, although weaker, with the maximum wind speed of  $9 \text{ m s}^{-1}$  in the layer between 350 and 700 m height.



In the first day wildfire burned 2 000 ha, which refers to an extreme wildfire behaviour. Although synoptic forcing was not as strong as in the *bura* cases, cold front passage, LLJ together with the enhanced local coastal circulation had a significant influence on wildfire behaviour. The probable additional explanation for the extreme behaviour is the altitude of the wildfire, which was around 200 m, making it close to the layer of the LLJ and therefore, increased influence from the jet flow.

### 2.2.3. Croatian Wildfire Studies – Heat-Driven

Besides the most common type of wildfires along the Adriatic coast, which can be classified as ‘wind-driven’, there were few extreme cases of the so-called ‘heat-driven’ wildfires (Table 2.1.). For example, extremely warm and dry weather conditions caused the severe crown wildfire on the Pelješac Peninsula in the Southern Adriatic on 20 July 2015 that burned 2 400 ha (Omazić, 2017). According to measurements from the nearest meteorological station July 2015 was the warmest month in the 1981–2015 period, with 30 days hitting the maximum daily air temperature above 30°C. The closest climatological station recorded its highest values since 1981: daily maximum air temperature reached 38.8°C on the second day of the wildfire, followed by the highest minimum air temperature of 30°C during the following night. Although the ALADIN model simulated a shallow cyclone over the southern Adriatic, there was no significant synoptic forcing that would override the local diurnal circulation. In fact, the local circulation was consistent during the whole active period of the wildfire – with the maximum average speed of the NW *maestral* wind of 9.1 m s<sup>-1</sup>, with the maximum gust of 15.4 m s<sup>-1</sup> on 23 July 2015. During the night wind weakened and turned to N-NE wind, locally known as *burin*. Numerical simulations of vertical profile did not identify the LLJ, however, the temperature profile did indicate an inversion in the ground layer during the first night of the wildfire. That kind of vertical profile enabled the vertical movement of hot air, which was additionally enhanced with the steep orography of the peninsula. These conditions dominated the wildfire behaviour, which was hardly controlled by the firefighters. The fire management operation was also aggravated due to multiple other wildfires that burnt at the same time along the coast and islands.

Wildfires in Croatia do not only occur along the Adriatic coast. In the second decade of the 21<sup>st</sup> century there were some quite severe wildfires in the continental inland. For example, on the mountain Strahinjčica situated 65 km north of the capital city of Zagreb. Although smaller in burnt size (350 ha), this wildfire stood out because it did not appear in the warmest part of the year, or during usual fire season from June to August, but in the first days of spring

from 22 to 27 March 2012 (Kuraži, 2015). For instance, the FWI index is not even operationally calculated for this period in a year. Also, this wildfire was burning oak, beech and conifers forests in contrast to wildfires of dry Mediterranean vegetation along the Adriatic coastline. Extremely dry weather conditions contributed to this wildfire – 11 months prior to the wildfire were drier than average comparing to 1961–1990 period, with March being the driest and the second warmest in the 1994–2012 period (Cindrić et al., 2016). In the first few days of the wildfire wind was weak, however the atmosphere was unstable in the first 1 km. Similar to the Pelješac wildfire, these conditions contributed to the vertical updraft of warm air along the 60° angle of the mountain Strahinjčica, which can be confirmed visually through the vertical column of smoke. In spite of very difficult firefighting operation due to the very steep terrain and the fact that firefighters in continental part never experienced this type of wildfires with massive stump burning and multiple ground fires, which are usually found in the Mediterranean environment, the fire was put under control after 5 days. This is found to be crucial because fire weather conditions got worse right after with the approaching cold front, wind changed to strong and gusty NE wind (up to 12.8 m s<sup>-1</sup>) and the LLJ appeared with maximum speed of 20 m s<sup>-1</sup>. This case in particular serves to illustrate the importance of better future collaboration between firefighting management and meteorologists. It is also worth mentioning that few days before this wildfire on the mountain Strahinjčica there was another wildfire in the eastern inland in the largest swamp area in Europe, Kopački Rit. Multiple wildfires in the continental part of Croatia in the recent years is in the agreement with the results of the SSR rating analysis (discussed below), which found significant increase of the fire danger rating in these regions, once considered safe from these disastrous events (Barešić, 2011). More details can be found in Tomašević et al. (2022).

### *2.3. Fire Weather in Southeast Australia*

#### *2.3.1. Synoptic Drivers*

Early research on synoptic patterns accompanying large wildfires in Australia led to conclusion that two major patterns tend to be present (Foley, 1947). First includes any pattern that carries dry air from the center of the continent to the more fuel enriched periphery, while second pattern corresponds with frontal passages following an anticyclone and is the most common in southeast Australia (Table 2.1.). Indeed, coastline of Victoria, New South Wales and Tasmania often experience a particular feature of fire weather – dry summertime cold fronts, also known as ‘cool changes’ (e.g., Reeder and Smith, 1992). This is the region where

hot continental air mass from the inland merges with cold maritime air over the Southern Ocean. This intersection of air masses intensifies cold fronts as they approach the coastline and interact with coastal temperature gradient (Luke and McArthur, 1978; Mills, 2002). Fronts are usually preceded by pronounced anticyclone, which directs dry air from the heated continental interior with prefrontal N or NE wind. The frontal passage is then followed by S and SW wind and advection of cooler maritime air from the Southern Ocean to regions of southeast Australia (Reeder and Smith, 1992; Reeder and Smith, 1998). A strong cold front is defined as one for which the rate of decrease of maximum daily temperature is from 12 to 17°C ( $12^{\circ}\text{C} < \Delta T < 17^{\circ}\text{C}$ ) on day following the frontal passage, while extreme cold front is defined as one with the difference greater than 17°C ( $\Delta T \geq 17^{\circ}\text{C}$ ). It has been found that this synoptic type has a strong correlation with high fire risk in this area occurring during the most catastrophic wildfires in Australia's history. Meteorological conditions that observed during 24 large wildfires in southeast Australia in the period from 1962 to 2003 showed association to cold fronts; 11 wildfires have been associated with a strong cold front, and 8 with an extreme cold front (Table 2.1.; Mills, 2005; Long, 2006; Reeder, 2015).

Perhaps the most extreme example of this synoptic pattern associated with the cold front as a defining feature occurred during the most catastrophic wildfires in southeast Australia (Victoria) on 7 February 2009, also known as the Black Saturday. Synoptic scale analysis revealed that a strong anticyclone dominated the weather in the week before Black Saturday, leading to very hot and deep air mass over this area (BoM, 2009; VBRC, 2009). On the day of the Black Saturday there was an approaching cold front from the southwest related to the low pressure system farther south and the high pressure system to the east (Figure 2.2.). Northwesterly winds brought exceptionally hot and dry air from the inland, which resulted with the highest daily maximum in 154 years in Melbourne ( $46.4^{\circ}\text{C}$ ), and the historical record in fire danger rating for southeast Australia (BoM, 2009). In addition, a wind direction change (from  $320^{\circ}$  to  $250^{\circ}$  in 14-min period) caused by a cold front passage over the wildfire areas led to extremely dangerous fire behavior in terms of intensity (up to  $88\ 000\ \text{kWm}^{-1}$ ), rate of spread (peaking at  $153\ \text{m min}^{-1}$ , with one fire developing 55 km long headfire in 1 h) and spotting up to 33 km ahead of the fire front (Cruz et al., 2012; Dowdy et al., 2017). The most significant fire on Black Saturday, called the Kilmore East fire, accounted for 70% of all fatalities, burned 100 000 ha and destroyed more than 2 000 buildings in the first 12 h alone. Due to enormous amount of energy released, wildfire generated pyrocumulonimbus cloud, whose top reached at least 13 km, injected vast amount of smoke in the lower stratosphere. A day after the cold front passed this area, daily maximum air temperature dropped to  $20.9^{\circ}\text{C}$  (Engel et al., 2013). Over

the period of 3 weeks, wildfires burned approximately 400 000 ha and resulted in 173 human fatalities.

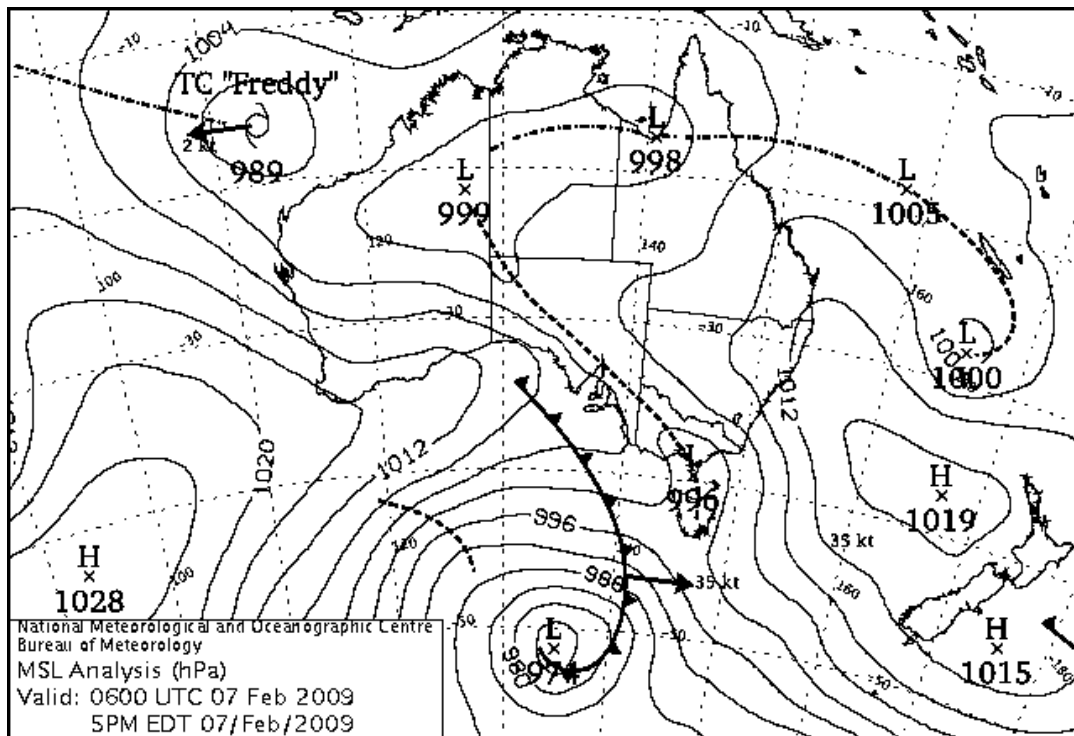


Figure 2.2. The Black Saturday synoptic features represented by mean sea level pressure (MSLP) analysis at 1700 local time (LT) on 7 February 2009 (BoM, 2009).

The extreme fire weather potential observed during Black Saturday wildfires is not unique in southeast Australia (Cruz et al., 2012). Earlier example of a wildfire event associated with the extreme cold front is the Ash Wednesday (South Australia and Victoria) in 1983. Synoptic pattern that included hot and dry northwesterly flow of continental origin caused an extended period with the maximum air temperature exceeding 30°C over much of southeast Australia. Elevated fire danger peaked at the warmest day, which was accompanied by a strong synoptic-scale cold front. Change in wind speed and direction, associated with the cold front passage in this case, contributed to the catastrophe. For instance, literally everyone killed during Ash Wednesday were killed within 1 h after the cold front passed over the wildfires' area (Mills, 2005). Similarly, 'inferno-like' fire weather conditions, when wildfires cause the most damage in a matter of hours, have been documented in a number of other events. The Hobart wildfires (Tasmania) in 1967 (Bond, 1967), Canberra (Australian Capital Territory, ACT) in 2003 (Fromm et al., 2006), Dunalley fire near Hobart (Tasmania) in 2013 (BoM, 2013a) and the Black Summer wildfires (New South Wales) in the late 2019 and early 2020 are cases on point (Collins et al., 2021).

Detailed re-examination of the synoptic and mesoscale features of Ash Wednesday indicated that the strong post-frontal winds were related to unusually deep cool air behind the front (Mills, 2005). The depth or intensity of the cool air behind the front can be determined by *the 850-hPa temperature gradient*, and the value of this gradient in the case of Ash Wednesday was the third strongest in February in 40-year period. Although extreme fire danger and loss of life can also occur with shallow cool changes (e.g., the Dandenong Ranges fire in 1997; Mills, 2002), the extreme values of 850-hPa temperature gradient were found to be the crucial meteorological parameter associated with the most extreme wildfire behavior in a number of other cases (including the 1967 Tasmanian fires). Additional research on synoptic patterns associated with the strongest recorded 850-hPa temperature gradients over southeast Australia revealed similarity in all the cases – a thermal ridge and a baroclinic zone related to a surface trough passage. It is also noted that the temperature gradient in the majority of cases was stronger in east-west rather than the more typical north-south direction, which is to say that isotherms were more meridionally-oriented (Figure 3; Hasson et al., 2009).

Consequently, the magnitude of the maximum thermal gradient in temperature field at 850-hPa has a potential to be used for medium range prediction of extreme days when subsynoptic-scale weather features can possibly lead to ‘blow-up’ fire (as per definition from The Glossary of Wildland Fire Terminology a ‘blowup’ is the ‘sudden increase in fireline intensity or rate of spread of a fire, often accompanied by violent convection that may have other characteristics of a fire storm’; Potter, 2012a). Finally, an assessment of the occurrence frequency of high 850-hPa temperature gradient values over southeastern Australia may also be used in climate change projections to determine possible future changes in severe fire weather (e.g., Hasson et al., 2009; Grose et al., 2014). For example, the study that used projections from a dynamically downscaled climate model, and focused on the southeastern Australian region Tasmania, concluded that under a high emission scenario the incidence of this specific synoptic type is projected to increase until the end of the 21<sup>st</sup> century. The primer driver of this trend is an increase in the temperature of air masses, with little change in the strength of the systems or the intensity of the cold front and prefrontal winds (Grose et al., 2014).

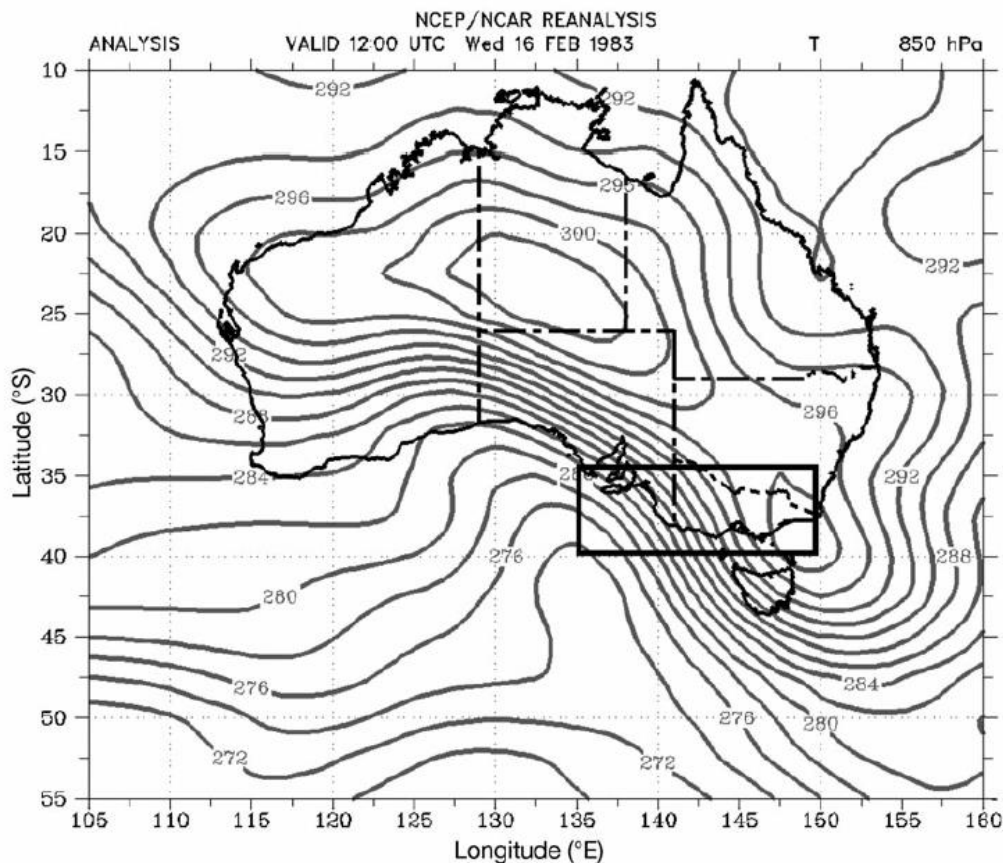


Figure 2.3. The NCEP/NCAR reanalysis of 850-hPa temperature field [K] at 1200 UTC, 16 February 1983 (Ash Wednesday; [Hasson et al., 2009](#)).

Another critical fire weather pattern includes *interaction of synoptic flow with the topography*. For instance, some cases of sudden escalations in local fire danger levels along the mountainous relief in southeastern Australia are related to cross mountain flows and foehn wind occurrence ([Sharples et al., 2010](#)). Foehn is a type of a downslope wind that on the lee side of a mountain range causes abrupt warming and drying through adiabatic compression, accompanied by strong winds and gusts together with turbulent mixing – all features leading to rapid fire spread ([Brinkmann, 1971](#); [Whiteman, 2000](#)). The examination of multiple cases confirming foehn existence in the lee side of the Australian Alps in the southeast connected foehn occurrence with the regional fire danger rating anomalies, at the 95<sup>th</sup> percentile and above ([Sharples et al., 2010](#)). These anomalies could not be explained by the advection of warm and dry air from the inland of the continent alone. The main cause of the abrupt changes in fire danger rating was the decrease of relative humidity, accounting for up to 75% of the changes in the McArthur Forest Fire Danger Index (FFDI; with changes in air temperature and wind speed making up the rest). The analyzed foehn events in southeast Australia also pointed towards certain synoptic precursors for foehn occurrence – low pressure cells or synoptic fronts

passing over the Great Australian Bight and southeast mainland area, generating strong winds perpendicular to the topography of the region. In addition to similarities in synoptic patterns leading to foehn occurrence, mesoscale numerical weather prediction (NWP) model products revealed that foehn was related to partial blocking of humid lower-level air by a mountain barrier and subsidence of drier air on its lee side. Mesoscale analysis also consistently identified the presence of topographically induced atmospheric wave structures connected with foehn occurrence. The combination of the two, foehn and mountain wave structures, results in increased turbulence near the surface. These two features, together with the certain synoptic patterns, seem to be very important in defining critical fire weather conditions in southeast Australia. Along with the Australian mainland, these features were also found to influence fire weather in the eastern part of Tasmania. For instance, foehn-like winds contributed to extreme fire weather conditions during bushfires near Hobart on 6 November 1982 (Marsh, 1987) and again on 12 October 2006 (Fox-Hughes, 2012).

### 2.3.2. *Surface Drying*

For many years fire managers in southeast Australia have been aware of a potential threat of ‘dry air aloft’ causing rapid changes in relative humidity on the surface, which influences fine fuel moisture and therefore fire risk (Table 2.1.). Rapid fluctuations of relative humidity are difficult to observe and forecast, but the use of mesoscale NWP models allowed investigation on these cases. The earliest research on two wildfire events when extreme fire behavior was related to rapid reduction in near-surface relative humidity included devastating wildfires in Canberra (ACT) on 18 January 2003 and on the Eyre Peninsula (South Australia; SA) on 11 January 2005 (Mills, 2008a). The research proposed that the abrupt surface drying in these cases happened due to two reasons. The first included subsidence of extremely dry air from the stratosphere and upper troposphere to the mid-troposphere that created a layer of dry air over the wildfire’s area, while the second process included a development of very deep boundary layer that mixes this dry air from the mid-troposphere to the surface. In the case of the Eyre Peninsula fire, the latter processes occurred in less than an hour, which corresponds to the time scale for fine fuels to respond to changes in atmospheric humidity. The mid-tropospheric dry air was in both cases visible as a dark band in the 6.7  $\mu\text{m}$  ‘water vapor’ channel from a geostationary satellite (WVI) and in both cases dry bands appeared near the time of extreme wildfire activity, which makes this a useful tool in forecasting and nowcasting, and is already in use in Australia and US.

[Mills \(2008b\)](#) presented a synoptic climatology derived from a number of similar cases with the abrupt surface drying in the period from 1999 to 2005. The study found that downward advection of dry stratospheric air from the upper troposphere has been associated with synoptic and mesoscale trough or ridge, while accelerated air was connected with the jet stream circulation. Jet stream entrance and exit circulation induced narrow bands of dry stratospheric air to descend to the mid-troposphere. This circulation was also found in the cases of the Canberra and Eyre Peninsula wildfires. Nevertheless, as it was noted in the aforementioned study, this feature is not the only ingredient needed for the abrupt drying at ground level. There are certain lower tropospheric processes that are needed to link this mid-tropospheric dry air with the surface. One possible low-level process is dry convective mixing in daytime mixed layers, which usually occurs during the afternoon when mixed layers are deepest. The second common feature in most cases are the pre-frontal updrafts that enhance vertical mixing and exchange of air, and therefore, entrainment of mid-tropospheric dry air to the surface. A third possibility for bringing the dry mid-tropospheric air to the surface is the descent from the cool air side of the frontal system, right after the frontal passage. Finally, the cross-mountain flows with topographically induced downward flows can transport the dry air from aloft. All these processes are common along the eastern coast of Australia's mainland and Tasmania and can be used for operational purposes in forecasting dramatic reductions in surface humidity and warning fire officials of possible sudden and extreme wildfire behavior. First, it is necessary to identify areas of upper tropospheric descent of dry air and secondly, to assess whether there is possibility for any of mentioned low-level features to occur to pull this dry air from the mid-troposphere to the surface.

Among all, localized low-level convective processes can turn to be especially dangerous. Apart from enhancing descent of dry mid-tropospheric air to the surface, convective conditions can cause the so-called 'plume-dominated' wildfires – fires in which vertical convection is more relevant than horizontal winds (Table 2.1.). Meteorological conditions which lead to these events have been frequently discussed in Australian literature in the recent decades (e.g., [Dowdy et al., 2017](#); [Cunningham and Reeder, 2009](#); [Fromm et al., 2006](#)). Localized convective processes can be generated in conditions of low wind and low atmospheric stability. Atmospheric stability, as a rate of change of air temperature with altitude, influences fire behavior through its influence on the buoyancy or rate of rise of the convection column (Table 2.1.). Unstable atmosphere usually implies increased kinetic energy and allows development of a deep convective column with strong updrafts leading to strong low-level inflow to the wildfires area and therefore, unexpected wildfire activity ([Byram, 1954](#); [Luke and](#)



McArthur, 1978). Quantitative measure of the potential for vertical atmospheric stability and humidity to influence wildfires is indicated as the Haines Index (HI; Haines, 1988). The Australian region that has most benefited from using the HI index is Tasmania where it is used as complementary information to FFDI in issuing fire weather warnings (Bally, 1995; BoM, 2008a). Other parts of Australia have certain limitations in using HI because high values of the original formulation of the HI occur very frequently in Australian climate and, therefore, make it hard to discriminate days with exceptionally high fire danger due to atmospheric instability. For this reason, Australian researchers developed the extended version of the HI known as Continuous Haines Index (CH; Mills and McCaw, 2010) which is widely used in the rest of the continent to forecast conditions with possible unexpected wildfire behavior associated with dangerous pyroconvection.

Table 2.1. Summary and comparison of the multiscale drivers of wildfire over the Adriatic Coast and Southeast Australia. The last column describes their impacts (Tomašević et al., 2022).

	Adriatic Coast	SE Australia	Impacts
<b>Synoptic Pattern</b>	Azores anticyclone; Karachi (monsoon) depression; Blocking; Blocking ridge	Tasman Sea Anticyclone driving hot and dry air from the centre of the continent; Strong east-west temperature gradient	Set up of background for hot and dry conditions
<b>Strong Winds-Synoptic</b>	Cold front	Cold front, especially summer	Overriding the local coastline circulation; Leading to abrupt change in wind speed and direction
<b>Strong Winds-meso- / micro-scale circulation</b>	Orographic wave; hydraulic jump; Low-level jet (LLJ); Examples are <i>jugo</i> (SE), <i>bura</i> (NE) and <i>maestral</i> (NW) winds	Cross-mountain flow; Foehn wind with topographically induced atmospheric wave; Upper-level jet circulation induces dry air to descend	Downslope transport of energy to the lee side; Abrupt warming and drying through adiabatic compression/introduction of upper tropospheric air
<b>Atmospheric Stability</b>	Unstable atmosphere favourable for updraft of warm air	Unstable atmospheric favourable for updraft; Plume-dominated wildfire	Favourable for low-level fire inflow, smoke removal and pyroconvection
<b>Boundary layer</b>	LLJ leads to strong vertical wind shear and turbulent kinetic energy	Development of deep boundary layer that allows mixing with mid-tropospheric dry air; overnight LLJ development	Favourable for abrupt surface drying and increase in windspeed; overnight progression of elevated fires

Various studies from the short review above demonstrated that in predicting wildfire behavior, in addition to surface meteorological conditions and synoptic circulation patterns, it is of utmost importance to consider lower tropospheric processes. Many Australian studies that investigated low-level processes applied high-resolution NWP model products. Computational capabilities revealed other interesting local atmospheric dynamics influencing wildfires. For example, how atmospheric instability enhanced fire activity in a convergent sea breeze regime or how local boundary layer phenomenon impacted spatiotemporal variation of fire weather

parameters (Fox-Hughes, 2012). Relevant meteorological studies that investigated fire weather during individual wildfire events will be referenced in context in the results chapters.

## *2.4. Wildfire and Fire Regimes Under Climate Change*

### *2.4.1. Fire Weather Indices*

From our previous discussion, fire regime obviously depends on climate and weather, it is also very sensitive to climate change and climate variability (Turco et al., 2019). Climate change, according to scientific consensus, is occurring due to anthropogenic influences (IPCC, 2013), may have significant and potentially unexpected impact on global fire regime (Flannigan et al., 2009). In recent decades, climate scientists frequently confirm correlation between rising global temperatures, long lasting droughts and atmospheric conditions favourable for wildfires (e.g., Jolly et al., 2013; Ellis et al., 2022; Jain et al., 2022). Although there is variability in the spatial extent, majority of studies hold an agreement on the changes in each of six components of fire regime, and provide evidences of increase in frequency, severity, scale and intensity of wildfires, as well as shifts in seasonality and type of wildfires (Collins et al., 2021).

Indeed, similar link between climate change and change in fire regime has been detected in both countries of interest in this research: Croatia, which is within one of the world's most fire prone areas – Mediterranean Basin; and Australia, long known as the 'fire continent' (Flannigan et al., 2009). Although distinct and incomparable in size of territory or scale of wildfires, both countries do have certain similarities. Specifically, southern part of Croatia and south-eastern part of Australia share similar climate with hot and dry summers and mild and wet winters. Both experience droughts and heatwaves accompanied with episodes of strong wind, all contributing to extreme fire weather and wildfire events defined in terms for each country. Although some studies report a decrease in global burned area (Doerr and Santín, 2016), studies from Europe (Amatulli et al, 2013), including Croatia, and Australia (Canadell et al, 2021) report increase in burned area in the last decades.

In representing the climate change influence on weather conditions favourable for wildfires, researchers from both countries frequently use indices. In Australia, climate change studies often focus on analysis of surface fire weather conditions represented by the McArthur Forest Fire Danger Index (FFDI; McArthur, 1967; Luke and McArthur, 1978), and in Croatia on the Canadian Forest Fire Weather Index System (CFFWIS) or Fire Weather Index (FWI; Van Wagner, 1987). Indices are calculated operationally at Meteorological Service of each country (FWI at the Croatian Meteorological and Hydrological Service – DHMZ; and FFDI at

the Australian Bureau of Meteorology – BoM) from daily surface air temperature, relative humidity, wind speed and precipitation (Dowdy and Mills, 2009), and combine fuel dryness and surface soil moisture indices with fire spread rate and/or fire intensity indices. Therefore, the final product describes the joint influence of various meteorological and fuel conditions important to estimate the risk associated with wildfires, and also serve as a broad scale warning in both countries (in Australia for both public and fire management, but in Croatia only for the fire management).

Various climatological studies analysed the FFDI values for Australia (Dowdy et al., 2009; Fox-Hughes, 2011; Clarke et al., 2013; Harris et al., 2017). In its initial formulation, the FFDI was set to have a maximum value of 100 (Luke and McArthur, 1978). This value was described as ‘the near worst possible fire conditions that are likely to be experienced in Australia’. In terms of meteorological values, it includes joint conditions of 40°C air temperature, relative humidity of 15%, wind speed of 15 m s<sup>-1</sup>, and long (6-8 weeks) drought period. In the real world, the upper bound of FFDI was exceeded multiple times (Lucas, 2010). For instance, during the 2009 Black Saturday fires the FFDI value was >150, which forced Australian authorities to redefine the FFDI scale and set a ‘catastrophic’ fire danger for FFDI>100 (Enright and Fontaine, 2013). Another analysis of historical records of FFDI index at 26 meteorological stations in southeast Australia showed that since 1973, 12 stations have recorded ‘catastrophic’ FFDI (Lucas 2007). The most recent study that examined the 67-year period of climate analysis data (from 1950 to 2016) found evident changes of fire weather conditions throughout Australia (Dowdy and Pepler, 2018). Specifically, there is a strong trend toward more severe conditions in southern Australia, where fire danger peaks during spring and summer season (Luke and McArthur, 1978), as well as an increase in frequency and extent of extremes together with earlier onset of the fire season – all pointed out by a higher value of FFDI index in recent decades, including multiple cases of values higher than anything previously recorded.

Climatological research on FWI in Croatia draw similar conclusions as the ones from Australia. The first analysis of FWI along the Adriatic coast in Croatia revealed that historical extreme maximum values are exceeded on almost daily basis during the peak fire season from June to August, specifically in the region of the mid-Adriatic coastline known as Dalmatia (Vučetić, 2001). Later studies in majority examined temporal and spatial distribution of the Monthly Severity Rating (MSR) and the Seasonal Severity Rating (SSR; e.g., Vučetić, 2002; Barešić, 2011; Tomašević and Vučetić, 2014; Bakšić et al., 2015), both derived directly from FWI. The SSR represents the wildfire risk from June to September, and it’s considered to be

extreme if the value exceeds 7. Examination of SSR based on station data (from 1960 to 2018) showed that not only is fire risk increasing in the recent decades within the fire prone coastal area of Croatia, but the high fire risk is spreading from the mid-Adriatic to the northern Adriatic and also to the inland towards regions where wildfires are less expected, such as in the agriculture land in the north east of the country. The same research also included analysis of the fire danger history of even longer, secular measurements, for one coastal station (from 1867 to 2018), which showed that wildfire risk is by 2.4 greater for the period 1981–2010 in regards to the period 1891–1917 (Vučetić and Vučetić, 2019). Furthermore, according to the increasing trend of MSR and SSR (Vučetić et al., 2006; Barešić, 2011), fire seasons in Croatia tend to be longer with an earlier onset and later ending, with almost every season in the 21<sup>st</sup> century exhibiting extreme weather conditions favourable for the most severe type of wildfires. An absolute SSR maximum so far (28.5) was in 2017 (Vučetić and Vučetić, 2019), which was the worst fire season ever recorded in Croatia.

On the whole, the knowledge from a wide range of climatological analyses on fire risk in Croatia and Australia represented by indices derived from station, model or reanalysis data allows a certain degree of confidence in concluding that increase of FFDI and FWI values in the recent decades and century, including their temporal and spatial variability in both countries, are consistent with observed climate change (Flannigan et al., 2009; Dowdy and Pepler, 2018).

#### *2.4.2. Future Fire Regimes*

The future fire regime in regards to climate change is very hard to estimate due to different climate change scenarios and unpredictable human activity related to future fire management, land use or accidental fires (Boegelsack et al., 2018) along with other important factors such as fuel availability and loading (Bowman et al., 2009; Moritz et al., 2012). Nevertheless, projections based on general circulation models (GCMs) in majority agree that due to climate change fire regime components will maintain the aforementioned trend until the end of the 21<sup>st</sup> century (IPCC, 2013; Flannigan et al., 2013).

While there are no studies regarding future fire risk specifically for Croatia, there are few predicting evolution of fire regime in Mediterranean area. According to GCMs projections the Mediterranean basin can be described as a “hot spot”, or the most vulnerable and responsive region to global climate change (Giorgi, 2006). Observations of changes today are considered to be minimal in comparison to the expected future climate change. The most critical issue for this region will be the reduction of precipitation in all seasons, especially in the Balkan Peninsula within which lies the large part of Croatian territory. It is estimated that annual

temperature will become 20 % higher than the global average, with exceptionally high warming in summer with temperature increase from 50% to alarming 100% (i.e., double of the summer mean) in regions north of the Mediterranean basin (Rodríguez et al., 2020). Various studies that used variety of approaches and different global or regional models considering different future climate scenarios consistently indicate that projected changes will consequentially generate certain degree of increase in fire risk within the entire Mediterranean area in the forthcoming decades (e.g. Bedia et al., 2014; Turco et al., 2014; Turco et al., 2018; Fargeon et al., 2020; Dupuy et al., 2020). Although there are no fire risk projections specifically for Croatia, some European studies have found an increase of fire risk along the mid-Adriatic coast and in the aforementioned agricultural land in the north east of Croatia (Camia et al., 2008). Together with an increase in fire risk, another study also found an increase in the length of a fire season and increase in the number of extreme events per season in a part of Croatian territory by the end of the 21<sup>st</sup> century (Moriondo 2006).

Numerous studies have examined possible future changes to FFDI in Australia (e.g. Williams et al., 2001; Cary, 2002; Hennessy et al., 2005; Pitman et al., 2007; Lucas et al., 2007; Bradstock et al., 2009; Clarke et al., 2011, Dowdy et al., 2019). Without exception, studies highlight the potential for significant increase in FFDI in southeast Australia, region with an unusually high frequency of catastrophic wildland-urban fires in the recent decades (Teague et al., 2010). The most recent study based on high resolution projections of the climate change impacts on fire weather conditions generated specifically for this region showed substantially greater FFDI by the year 2080 (Clarke and Evans, 2019). This is especially pronounced in spring season, which suggests intensification and lengthening of fire seasons. Along with increases in severe fire weather conditions, projections also show a decrease in number of prescribed burning days (or reduction burning before the fire season to reduce fire risk; Di Virgilio et al., 2020) or shortage of available prescribed burning windows (up to 10 days in spring). These results reinforced previous findings. For example, research on future impact of climate change on fire weather based on FFDI calculated for 26 stations in south-eastern Australia show the general increase from 10% to 30% in the average cumulative FFDI for the year 2050 with respect to 1990, based on high emissions scenario (Lucas et al., 2007). This increase of accumulated FFDI represents a longer fire season, but can possibly hide the much larger changes in the number of days with high fire risk. The projections of the number of days exceeding the FFDI value of 50 (defined as ‘extreme’) by 2050 show increase of 10-50% for the low scenarios and 100-300% for the high scenarios. As mentioned before, historical analysis of FFDI at 26 meteorological stations revealed that 12 out of 26 stations recorded ‘catastrophic’

FFDI. Projections by 2050, using high emission scenarios, indicate ‘catastrophic’ (FFDI>100) days at 22 out of 26 sites, 19 with return periods of 8 years or less, and 7 sites with 3 years or less. Another research that examined the future frequency of occurrence of specific synoptic patterns causing the most extreme fire weather events over southeast Australia indicates the increase in frequency of such events from about 1 event per 2 years in the late 20<sup>th</sup> century to about 1 event per year in the middle of the 21<sup>st</sup> century and 1 to 2 events per year in the late 21<sup>st</sup> century (Hasson et al., 2009). Likewise, projections of the composite mean sea level pressure pattern (MSLP) associated with elevated FFDI index specifically for the south-eastern state Tasmania show increase in its frequency by the end of 21<sup>st</sup> century (Fox-Hughes et al., 2014). Many other studies in the recent decades consistently confirm that there is a fair probability of a shift to an altered, even more hazardous, near-surface fire weather conditions (Di Virgilio et al., 2019; Dowdy et al., 2019), and fire regime in southeast Australia in the future, and if started, there will be more potential for wildfires to blow up to extreme proportions, burning in uncontrollable way due to extreme fire weather conditions.

## CHAPTER 3

### METHODS

#### *3.1. Wildfire Reconstruction*

In order to associate atmospheric conditions with extreme fire behavior a detailed wildfire reconstructions are provided before the meteorological analyses.

For the Split case study digital time referenced photographs from official firefighting cameras situated at the Zahod tower (Figure 4.2) on the southeast peak of hill Perun (594 m a.s.l.) provided information on time of ignition, propagation and characteristics of the fire front, but only on its eastern side. The wildfire progression was mostly reconstructed from 3 208 radio logs and 1 124 emergency calls obtained from the Split Firefighting Brigade (SFB). This information, together with witness statements and interviews with firefighters and pilots, provided an insight into fire characteristics (flame height, crowning, smoke and plume), spotting, weather conditions on ground and upper-air turbulence. Together with interviews, a large number of photographs was collected. All the information gathered was geo-referenced and used to approximately define fire isochrones. The reconstruction of the fire propagation and fire isochrones were plotted onto the total burnt area isochrone provided by the SFB.

The Forcett-Dunalley wildfire reconstruction is adopted mostly from reports provided by the Bureau of Meteorology (BoM), with the other important findings referenced accordingly. Both wildfires are divided into separate burn periods spanning from the ignitions until the significant ease in fire activity.

#### *3.2. Meteorological Observations*

Surface weather conditions were analyzed using meteorological data from the Split-Marjan station (122 m a.s.l.), the closest station to the wildfire (approximately 16 km west of the ignition location and 4 km from the closest line of the final fire perimeter, Figure 4.2). The Split-Marjan station is situated on the city of Split peninsula and has been operated by the Croatian Meteorological and Hydrological Service (DHMZ) since 1926, with automatic measurements since 2003. The meteorological variables used for this research include 10-minute data of air temperature, relative humidity, mean sea level pressure, precipitation amount, mean and maximum wind speed and direction, and solar radiation, all from July 2017.

Surface weather conditions during the Forcett-Dunalley wildfire were analyzed using meteorological data from automatic weather stations (AWS) closest to the fire site. The selection of meteorological stations included Dunalley (12 m.a.s.l.), Hobart (51 m.a.s.l.), Hobart

airport (4 m.a.s.l.) and Campania (45 m.a.s.l.; Fig. 5.1.b). The meteorological data from 3 to 5 January 2013 included 30-minute (of the hour and half an hour) air pressure, air temperature, relative humidity, precipitation amount, mean and maximum wind speed and direction. Mean and maximum wind speeds are 10-minute values available every half hour. Meteorological stations are operated by the BoM.

Radar data from the Mt Koonya is used in order to determine the maximum injection height of the pyroCb. Mt Koonya weather radar is operated by the BoM (Soderholm et al., 2019). It is located on the Tasman Peninsula, 46 km east-southeast of Hobart and 24 km south of Dunalley, making it ideal for pyroCb tracking in this case. Radar is situated at 515 m height with the elevation scan near Dunalley from 750 m to 25 km height. Radar radial resolution is 250 m and range 150 km with 6-minute reflectivity and velocity scans (Ndalila et al., 2019).

For the Split case study, times are indicated in universal coordinated time (UTC), which is Central European Summer Time (CEST) – 2 h. In the Dunalley case study times are indicated in Australian Eastern Daylight Time (AEDT), which is UTC + 11 h. All measurements were recalculated accordingly.

Antecedent weather conditions of the Split wildfire were analyzed using climatological assessments available from DHMZ. Assessments include the comparison of monthly, seasonal and annual air temperature and precipitation with the climatological period 1961–1990 (from: [https://meteo.hr/klima.php?section=klima\\_pracenje&param=ocjena](https://meteo.hr/klima.php?section=klima_pracenje&param=ocjena)). Air temperature and rainfall patterns preceding the Forcett-Dunalley wildfire were assessed using the climate maps over different timescales across Australia and single states, including Tasmania available from the BoM (<http://www.bom.gov.au/climate/>).

### 3.3. Fire Danger Rating

#### 3.3.1. The Canadian Forest Fire Weather Index System (FWI)

The Canadian Forest Fire Danger Rating System (CFFDRS) (Van Wagner and Pickett, 1985; Stocks et al., 1989) has been implemented in Croatia since 1982 (Dimitrov, 1982) and is used to alert firefighting agencies. CFFDRS has two primary subsystems – the Canadian Forest Fire Behaviour Prediction System and the Canadian Forest Fire Weather Index System (CFFWIS). DHMZ calculates CFFWIS daily from May to September. The final product of the CFFWIS (Canadian Forest Fire Weather Index) system is Fire Weather Index (FWI).

The CFFWIS consists of six sub-indices: Fine Fuel Moisture Code (FFMC), Duff Moisture Code (DMC), Drought Code (DC), Initial Spread Index (ISI), Buildup Index (BUI)



and Fire Weather Index (FWI). FFMC, DMC and DC are fuel moisture indices, while ISI, BUI and FWI fire behaviour indices. All values can be calculated from meteorological data at 12 UTC (14 CEST or local summer time) including air temperature, relative humidity, wind speed and 24-h accumulated precipitation. ISI is function of FFMC and wind, BUI is function of DMC, DC and amount of precipitation in previous 24 hours. In the end, FWI is function of ISI and exponential function including BUI. Along with the FWI (Table 3.1), this study will focus on the ISI (Initial Spread Index; Table 3.2). Details on equations calculating all set of indices can be found in Van Wagner and Pickett (1985).

Table 3.1. Initial Spread Index (ISI) values with according fire spread, speed of the fire front and description of fire behaviour.

ISI	Fire Spread	Speed of the fire front [m min <sup>-1</sup> ]	Description
0–7	Slow	1.5	–
8–12	Moderate	3.0	Torch
13–17	Fast	6.1	Possible crown fire
≥18	Very fast	18.3	Crown fire, multiple fronts

Table 3.2. Fire Weather Index (FWI) and Buildup Index (BUI) values with according fire risk classification.

Fire risk	FWI	BUI
Very low	≤ 4	≤ 48
Low	5–8	49–85
Moderate	9–16	86–118
High	17–32	119–158
Very high	≥ 33	≥ 159

In order to evaluate fire risk in Croatia as a whole, Monthly Severity Rating (MSR) and Season Severity Rating (SSR) will be analyzed. MSR is calculated from Daily Severity Rating (DSR), which is function of FWI, and SSR is calculated from MSR. SSR represents the potential risk of forest fire from June to September (Vučetić, 2001, 2002).

### 3.3.2. Forest Fire Danger Index (FFDI) and Forest Fire Danger Rating (FFDR)

In Australia the Forest Fire Danger Index (FFDI) and the Grassland Fire Danger Index (GFDI) are routinely used to quantify fire weather risk. These indices have been defined by McArthur (Luke and McArthur, 1978) in the late 1960s to assist in estimation of fire behavior related to the weather. FFDI is calculated using the McArthur Mark 5 Forest Meter (McArthur,

1967) with the inputs of air temperature, relative humidity, average 10-minute wind speed and the drought factor, a measure of the state of the fuel.

Specifically, FFDI is calculated according to the following equation:

$$FFDI = 1.2753^{(0.9871\log DF + 0.0338T + 0.0234V - 0.0345RH)};$$

where DF is drought factor, T is air temperature in degrees Celsius, V is wind speed in  $\text{kmh}^{-1}$  and RH is relative humidity in percentage.

**Table 3.3.** Forest Fire Danger Index (FFDI) values and corresponding Forest Fire Danger Rating (FFDR) and description of difficulty of suppression (Lucas et al., 2007; Vercoe, 2003).

Forest Fire Danger Index (FFDI)	Forest Fire Danger Rating (FFDR)	Difficulty of suppression
0–11	Low-Moderate	Fires easily suppressed with hand tools or fire usually suppressed with hand tools and easily suppressed with bulldozers.
12–24	High	Fire generally controlled with bulldozers working along the flanks to pinch the head out under favourable conditions. Back burning may fail due to spotting.
25–49	Very high	Initial attack generally fails but may succeed in some circumstances. Back burning will fail due to spotting. Burning-out should be avoided.
50–74	Severe	Fire suppression virtually impossible on any part of the fire line due to the potential for extreme and sudden changes in fire behaviour. Any suppression actions such as burning out will only increase fire behaviour and the area burnt.
75–99	Extreme	
100 or higher	Catastrophic	

The drought factor (DF) is a function of daily rainfall and the period of time elapsed since the last rain (Finkele et al., 2006). It is calculated according to the Griffiths (1999) formulation and using the Keetch-Byram Drought Index to estimate the deficit of the soil moisture (Keetch and Byram, 1968). The FFDI calculation assumes fixed value of 12.5 tons per hectare of fuel load and it does not take into account the slope of the landscape. In Tasmania, as in other Australian states, forest fire danger is numerically represented by FFDI and descriptive as FFDR, which assists to fire agencies on determining the possible fire behavior and the difficulty to control a fire (Table 3.3). The FFDI vales have been calculated from selected AWS closest to the wildfire site. FFDI and FFDR are calculated on 1-minute and 1-hour basis from 05 AEST to 23 AEST on 4 January 2013, or the period of the most extreme wildfire activity. Two periods of data were excluded from the analysis. The first is from Hobart station from 16:35 AEST to 17:58 AEST when the wet bulb reservoir dried out, which affected the humidity observations. The second period is from 16:19 AEST to 18:06 AEST at Dunalley station when the Forcett-

Dunalley wildfire burnt in the close vicinity of instruments, leading to highly variable air temperature.

### *3.4. Synoptic Analysis*

The data used to examine the synoptic environment prior to and during the Split wildfire included synoptic surface and upper-level analysis obtained from the German Meteorological Service (Deutsche Wetterdienst, DWD, [www1.wetter3.de/Archiv/](http://www1.wetter3.de/Archiv/)). The products used included 850-hPa and 300-hPa wind and relative vorticity charts, 500-hPa geopotential (gpdam), surface pressure and relative topography (RT, between 500 hPa and 1000 hPa levels).

Synoptic analysis related to the Forcett-Dunalley wildfire was based on analysis from the National Meteorological and Oceanographic Centre (NMOC) available at the BoM web page (<http://www.bom.gov.au/australia/charts/archive/>). The data included mean sea level pressure analysis for the period from 3 to 8 January 2013, available at 6-hours intervals at synoptic hours for each day.

### *3.5. Operational Numerical Model and Reanalysis*

#### *3.5.1. ALADIN Operational Model*

Numerical simulations for the Split case study were performed using the operational limited area mesoscale numerical weather prediction model ALADIN/HR (ALADIN International Team, 1997). Details on model setup and configuration can be found in Tudor et al. (2013, 2015). For the purpose of this research, ALADIN/HR model was initialized at 00 UTC for each day of the Split wildfire, from 16 to 25 July 2017, with the hourly output data. Simulation ran with two nested domains (in operational use in DHMZ) in 4 km horizontal resolution (ALADIN-HR44) up to 72 hours forecast. The outer domain covers a 1900 km x 1700 km area, while inner domain is zoomed on the area covering 550 km x 550 km over Croatia (Figure 3.1). ALADIN model also provides dynamical adaptation of wind fields (ALADIN-HRDA) with 2 km horizontal resolution which has in a number of cases improved near surface wind representation in complex terrain such as the Adriatic Sea coastline (e.g., Hrastinski et al., 2015). Dynamically downscaled surface wind fields with a grid spacing of 2 km for the purpose of this study covered an additional sub-domain of 250 km x 250 km around Split.

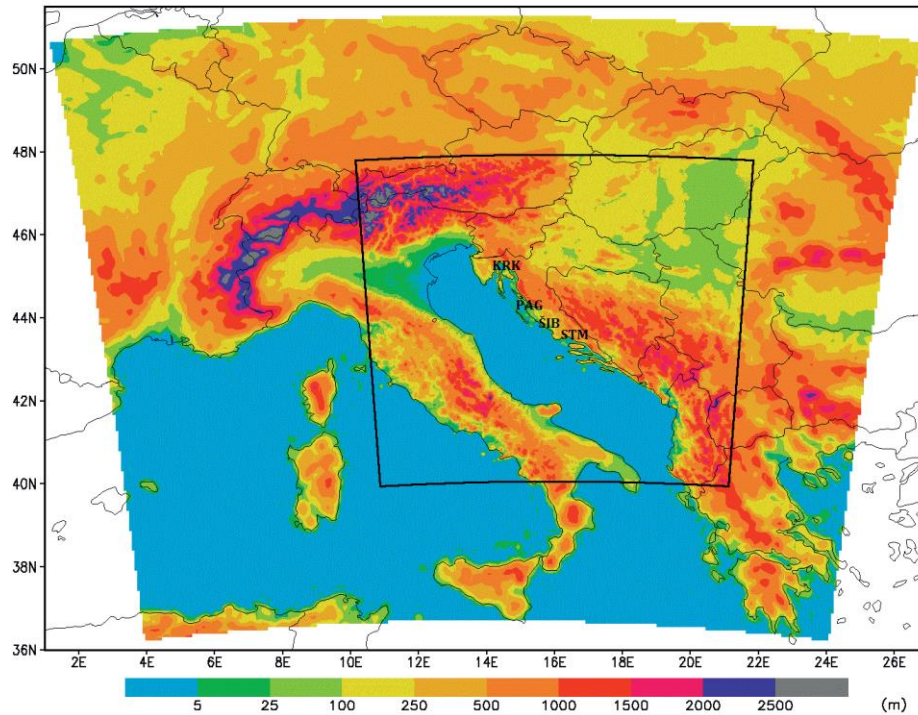


Figure 3.1. ALADIN/HR model domain at 4 km horizontal grid spacing (outer domain) and at 2 km horizontal grid spacing (inner domain) with corresponding orography (adopted from [Hrastinski et al., 2015](#)).

Numerous validation and verification methods, both in operational and in research context, applied over the years confirmed that ALADIN model also provides very good representation of the vertical state of the atmosphere (e.g., [Horvath et al., 2009](#); [Ivančan-Picek et al., 2016](#); [Stanešić et al., 2019](#)). Vertical grid in products of 4 km grid spacing is stretched with 73 hybrid sigma-pressure levels with the lowest vertical level at approximately 10 m above ground level, while dynamic adaptation products have 15 vertical levels (with 8 levels in the first 1000 m). Vertical profiles in this case are simulated for Split location (43.525°N, 16.506°E), and included air pressure, air temperature, dew point temperature, wind speed and wind direction.

Finer-scale atmospheric features were additionally examined by vertical cross sections of horizontal wind speed and direction combined with air temperature, relative humidity, potential temperature and  $z$ -wind covering 300 km horizontally and 5 km in height. The location of vertical cross sections from ALADIN model can be seen in [Figure 4.1a](#).

### 3.5.1.1. Low Level Jet

For the purpose of this research, a new ALADIN model product, a spatial distribution of LLJ is introduced. Vertical profiles were simulated for each grid point at 4 km resolution and plotted over inner domain over Croatia for each hourly time step. LLJ at grid point was defined according to one of four criteria (Bonner, 1968):

- a wind speed maximum between 10 and  $< 12 \text{ ms}^{-1}$  with a wind speed decrease aloft by  $4 \text{ ms}^{-1}$  up to the 3 km height, noted as LLJ criterion 0;
- a wind speed maximum between 12 and  $< 16 \text{ ms}^{-1}$  with a wind speed decrease aloft by  $6 \text{ ms}^{-1}$  up to the 3 km height, noted as LLJ criterion 1;
- a wind speed maximum between 16 and  $< 20 \text{ ms}^{-1}$ , with a wind speed decrease aloft by  $8 \text{ ms}^{-1}$  up to the 3 km height, noted as LLJ criterion 2;
- a wind speed maximum  $\geq 20 \text{ ms}^{-1}$  with a wind speed decrease aloft by  $10 \text{ ms}^{-1}$  up to the 3 km height, noted as LLJ criterion 3.

The LLJ criterion 0 was additionally implemented since some of the previous studies indicated that ALADIN may underestimate near-surface wind speed (e.g., Vučetić et al., 2007). To our knowledge, a spatial distribution of LLJ speed and height has never been applied in fire weather research to date.

### 3.5.2. BARRA Reanalysis

The BoM's high-resolution Regional Reanalysis for Australia (BARRA) is used for the Forcett-Dunalley case study. BARRA is atmospheric regional reanalysis covering Australia, New Zealand, Southeast Asia and south to the Antarctic ice edge (Su et al., 2019). The BARRA reanalysis includes 29-year period from 1990 to 2018 and involves two suites. The first suite is whole-domain (identified as BARRA-R) at approximately 12 km resolution and the second suite is centered around Tasmania (BARRA-TA) and downscaled at 1.5 km resolution (Figure 3.2).

The reanalysis is produced in two steps. In the first step for initialization and boundary conditions BARRA-R uses the European Center for Medium-Range Weather Forecasts (ECMWF) coarse-scale ( $\sim 80 \text{ km}$ ) global atmospheric reanalysis (ERA-Interim; Dee et al., 2011). BARRA-R further combines conventional observations and short model forecasts to provide the best representation of the atmosphere at approximate 12 km horizontal resolution with 70 vertical levels extending up to 80 km into the atmosphere (50 levels up to 18 km and 20 model levels above 20 km). The second step includes a convective-scale downscaling model

over Tasmania. This downscaling model has 1.5 km horizontal resolution and 70 vertical levels up to 40 km in the atmosphere. The sub-domain for Tasmania stretches from 142.5°E to 150.5055°E and from 46.0°S to 39.1555°S. Both reanalysis and downscaled suite for Tasmania run four times a day, with data covering a 24-hour period. BARRA-TA produces hourly outputs of meteorological variables (BoM, 2018). BARRA-R and its subdomains, including BARRA-TA, give a realistic reproduction of weather conditions at and near surface and provide an opportunity to analyze past weather, including extreme events and have various implications for users from fields such as it is fire management. More details on the BARRA reanalysis and evaluation can be found in Su et al., 2019. BARRA reanalysis data is available online at: [https://dapds00.nci.org.au/thredds/catalog/cj37/BARRA/BARRA\\_TA/v1/forecast/catalog.html](https://dapds00.nci.org.au/thredds/catalog/cj37/BARRA/BARRA_TA/v1/forecast/catalog.html).

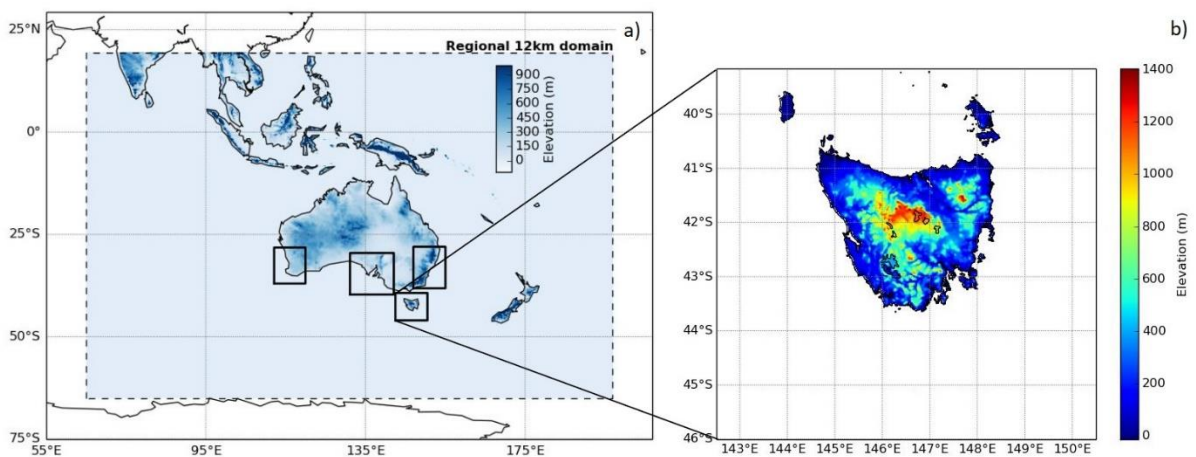


Figure 3.2. BARRA-R domain (left) and BARRA-TA subdomain with orography at 1.5 km resolution (right; BoM, 2018).

### 3.6. Numerical Modelling

#### 3.6.1. WRF Model

The Weather Research Forecasting (WRF) model, supported by the National Center for Atmospheric Research (NCAR), is a three-dimensional, non-hydrostatic atmospheric model developed for numerical weather prediction (NWP) and research (Skamarock et al., 2008). WRF calculates set of equations for fluid motion, mass conservation and atmospheric thermodynamics, together with predictive equations for water states in order to produce a three-dimensional forecast of air temperature and velocity, water vapor, cloud water, rain and ice (Coen et al., 2013). WRF users are able to simulate weather over large domain and high spatiotemporal resolution of airflow characteristics in inner domain using model's nesting capabilities. WRF is therefore able to simulate various atmospheric phenomenon related to

catastrophic wildfires, including fronts, windstorms or convective updrafts. For instance, high resolution WRF runs provided an insight into finer-scale features of downslope windstorms that caused dangerous wind-driven wildfires, such as hydraulic jump and strong surface winds along and near lee slopes (e.g., Telišman Prtenjak et al., 2010, 2015; Nauslar et al., 2018; Brewer and Clements, 2020). Consistent with previous research and in order to investigate synoptic, mesoscale and microscale drivers related to two catastrophic wildfires, one from Croatia and one from Australia, high resolution WRF simulations were used from the model version 4.1.5.

Two sets of WRF simulations were run, one for each case study. Both simulations were initialized using the ERA-Interim reanalysis, provided by the European Centre for Medium-Range Forecasts (ECMWF) on a regular grid spacing of  $0.75^\circ \times 0.75^\circ$  and temporal resolution of 6 h (Dee et al., 2011). Simulation for the Croatian case study ran for 60 hours from 12 UTC 16 July 2017–00 UTC 19 July 2017 and for Australian case study for 72 hours from 00 UTC 3 January 2013–00 UTC 6 January 2013. Both simulations were made with output at 1-hour interval. A two-way coupling approach (Tudor et al., 2015) was used to define four nested domains (Figure 3.3. and 3.4.) of grid spacing ratio 1:2:3:3 and with spatial resolution 9 (d01), 4.5 (d02), 1.5 (d03) and 0.5 km (d04) for both case studies (Table 3.4).

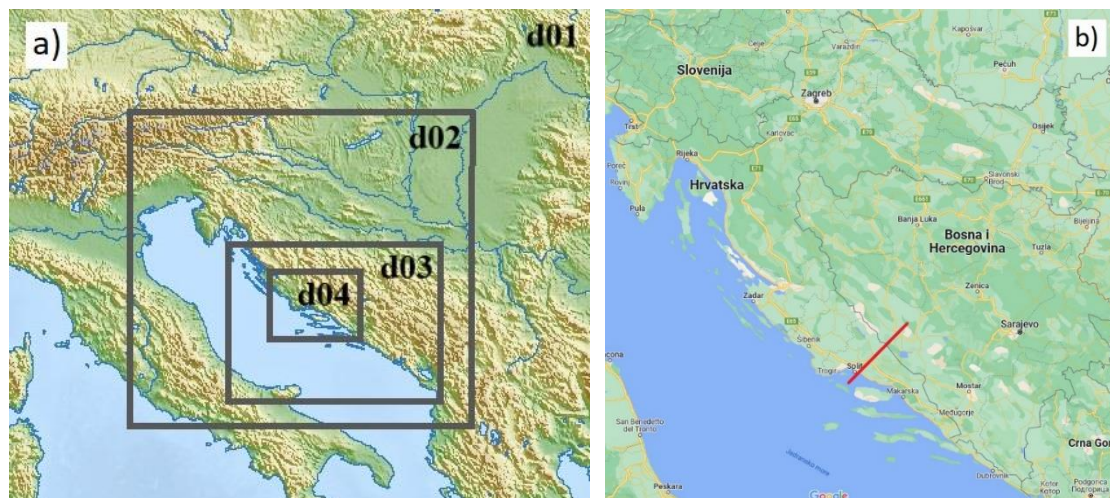


Figure 3.3. a) Domains used in WRF simulation for Croatian case study and b) location of cross section in the innermost domain. (Basic topography from freeworldmaps.net).

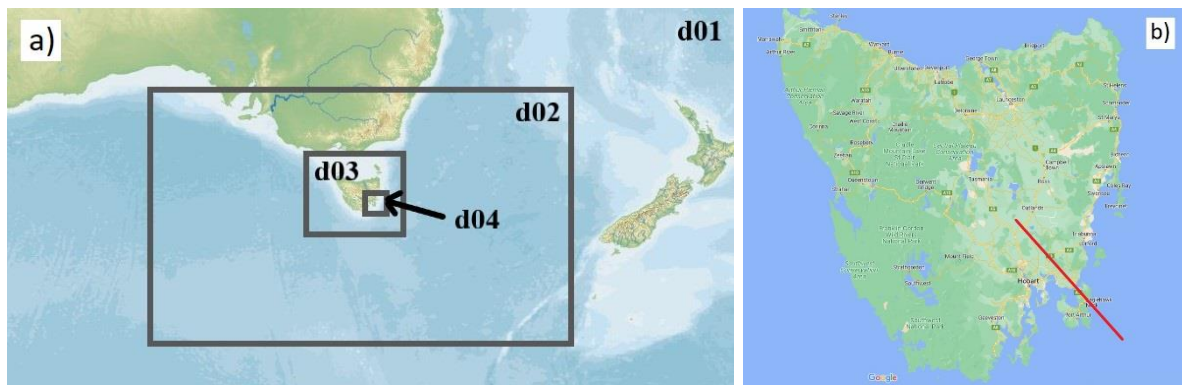


Figure 3.4. a) Domain used in WRF simulation for Australian case study and b) location of cross section in the innermost domain. (Basic topography from freeworldmaps.net).

In the vertical, there were 66 hybrid levels, from approximately 10 m up to 18 km above terrain height, with increasing resolution near the surface to realistically represent atmospheric processes in planetary boundary layer (PBL). Physics options for both simulations included Mellor-Yamada-Nakanishi-Niino boundary layer (MYNN2.5; [Nakanishi and Niino, 2006](#)) scheme, in combination with the Quasi-Normal Scale Elimination PBL surface physics scheme. The rapid radiative transfer model scheme (RRTM) ([Mlawer et al., 1997](#)) is used for longwave radiation and the Dudhia scheme ([Dudhia, 1989](#)) for shortwave radiation. The chosen microphysical scheme was Morrison double-moment scheme (MORR) ([Morrison et al., 2009](#)) and in the outermost domain, convection was described using the Kain-Fritsch scheme ([Kain and Kain, 2004](#)). While for the Australian case, topographic data at 30 s (USGS), and a landuse (MODIS) data at 15 s were employed, for Split simulation, topographic and land-cover data were used from the 100 m resolution of the SRTM (Shuttle Radar Topographic Mission) digital topographic database and the 100 m resolution CORINE (Coordination of Information on the Environment Land Cover) database, respectively. Simulations were run using the infrastructure on the supercomputer called “Bura” from the University of Rijeka in Croatia.



Table 3.4. Number of grid points in simulations for two case studies. There are 66 hybrid levels for both simulations.

WRF simulation domain and resolution	Number of grid points (west-east x south-north x hybrid levels) and size of domain	
	Croatian case study	Australian case study
<b>d01 (9 km)</b>	110 x 110 x 66 990 km x 990 km	434 x 392 x 66 3906 km x 3528 km
<b>d02 (4.5 km)</b>	151 x 153 x 66 679.5 km x 688.5 km	457 x 423 x 66 2056 km x 1903.5 km
<b>d03 (1.5 km)</b>	244 x 223 x 66 366 km x 334.5 km	352 x 331 x 66 528 km x 496.5 km
<b>d04 (0.5 km)</b>	196 x 202 x 66 98 km x 101 km	346 x 310 x 66 173 km x 155 km

### 3.6.2. WRF SFIRE Model

WRF capabilities expand beyond weather by two-way coupling. The coupling option used here is between atmosphere dynamics and fire. The fire physics module within the WRF (available later than the WRF 3.2. version) that provides a detailed study of fire's effects on atmospheric dynamics and feedback to fire behavior is called WRF SFIRE (Spread FIRE). It allows the simulated fire to “create its own weather” and users are able to investigate fire effects on the surrounding atmosphere together with the fire growth and decay (Coen et al., 2013). The WRF SFIRE simulations were used from the model version 4.2.2., the latest available at time.

WRF model is coupled with a fire spread model using the level-set method which calculates the fire front across terrain. The algorithm for fire spread and fuel combustion are based on Rothermel model (Rothermel, 1972) which uses the fuel characteristics based of Anderson (Anderson, 1982). A detailed description of the physical model, numerical algorithms and software of the coupled atmosphere-wildland fire (WRF SFIRE) model can be found in Mandel et al. (2011). In summary, a computation within the atmospheric and fire component of the model is as follows: in each time step throughout the simulation the winds from the atmospheric model grid are interpolated into a fire model grid, which is situated in the innermost domain. Local near surface winds from the atmospheric model together with the fuel properties and topography of the fire model then determine the rate and direction of a fire’s spread. As a fire consumes fuel defined in each fire cell within the fire domain it releases heat and water vapor fluxes. Before the completion of the model’s time step the sensible and latent energy released by a fire is returned into the lowest levels of the atmospheric model (Figure 2.4.). Thus,

in the next time step of the WRF model simulation, the atmosphere fields are influenced and modified by the energy released by the fire (Peace et al., 2015).

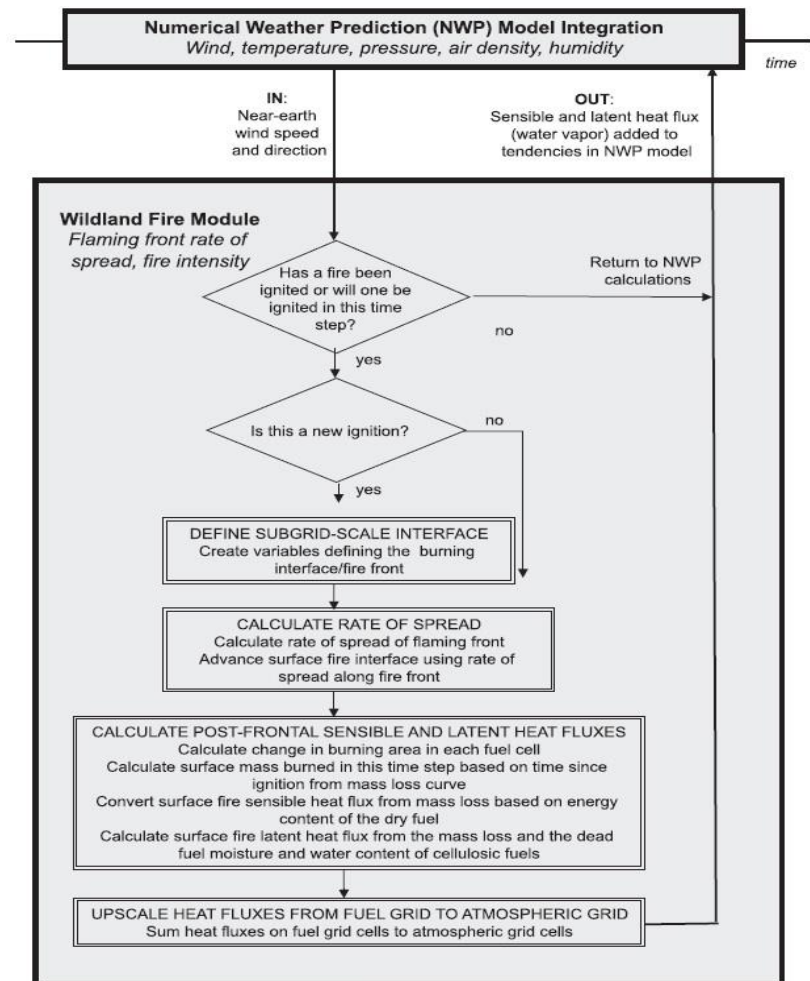


Figure 3.5. Schematic of process components of the WRF-SFIRE coupled model (from Coen et al., 2013).

The WRF SFIRE model has proved to be a very important tool in fire management worldwide (e.g., Peace et al., 2015, 2016; Coen et al., 2013) and has been used to validate the model against real fire events (e.g., Kochanski et al., 2013) and to investigate the dynamics of fire and atmosphere interactions (e.g., Peace, 2014). By using the WRF SFIRE model simulations this research aims to: 1) demonstrate the possibility to successfully run the model for Croatian fire event, 2) validate the model data against the beforehand reconstructed wildfire and 3) investigate the possible fire-atmosphere interactions for an event from Croatia by testing the approach from previous studies which ran simulations in two modes – feedback ‘on’ and feedback ‘off’. These options in the model differ inclusion and exclusion of the energy fluxes that are being exchanged between the fire and the atmosphere. This method provides the assessment on if and how the simulated fire might change the local surrounding atmosphere (Peace, 2014).

The simulations for this study were made from the most recent available WRF SFIRE model version, which at time was the version 4.2.2. In order to initialize the WRF SFIRE simulations atmospheric state, terrain and spatial distribution of fuels were defined together with location and time of fire ignition (or multiple ignitions). The numerical simulation of the Croatian wildfire case study ran for 48 hours, from 12 UTC on 16 July 2017, which is 10 h prior the wildfire ignition (to allow for the model’s spin-up time) until 12 UTC on 18 July 2017. Initial and boundary conditions for the WRF SFIRE simulations were the same as for WRF simulations using the ERA-Interim reanalysis at 6-hourly intervals. The simulations ran in four nested domains of a same position as in WRF simulations (Figure 3.3) and with the same resolution, i.e., number of grid points and vertical levels (Table 3.4). The fire model was initiated in the inner most atmospheric domain (d04) which was additionally refined at the ratio of 1:15, resulting in a surface fire grid cell size of 33.3 m (Table 3.5). Model output for the inner most domain was available at interval of 10 minutes.

Table 3.5. Fire grid properties in the innermost domain of WRF SFIRE simulation.

<b>FIRE GRID</b>		
D04 refinement ratio	Cell size	Number of grid points
1:15	33.3 m x 33.3 m	2940 x 3030

In order to successfully represent the topography and fuel distribution in the innermost domain, WRF SFIRE requires high resolution topographical and fuel cover data. Only available topography data for Croatia that was converted in the form suitable for WRF was at 100 m resolution, which is the innermost (fire) domain interpolated to 33.3 m resolution. Since there is no open-source high resolution fuel data available for Croatia, for this purpose is used the CORINE Land Cover (CLC) dataset also available at 100 m resolution. Following the methods from Kartsios et al. (2021), the CLC raster data was reclassified into 13 categories of the Northern Forest Fire Laboratory (NFFL) classification (Table 3.6.; Anderson, 1982). The 13 categories define various vegetation categories while category 14 is assigned to ‘no fuel’. Together with water areas category 14 also consists wildland-urban interface. This dataset was additionally resampled (nearest neighbor) to 33.3 m spatial distribution (Kartsios et al., 2021).

Table 3.6. NFFL fuel categories and fuel types according to [Anderson, 1982](#).

FUEL CATEGORIES	FUEL NAME
1	Short grass (1 ft, ≈ 30 cm)
2	Timber (grass and understory)
3	Tall grass (2.5 ft, ≈ 75 cm)
4	Chaparral (6 ft, ≈ 180 cm)
5	Brush (2 ft, ≈ 60 cm)
6	Dormant brush, hardwood slash
7	Southern rough
8	Closed timber litter
9	Hardwood litter
10	Timber (litter + understory)
11	Light logging slash
12	Medium logging slash
13	Heavy logging slash
14	No fuel

In order to simulate fire spread WRF SFIRE needs additional fuel characteristics of 13 NFFL fuel categories, such as fuel load (namelist name: fgi) and depth (fueldepthm; for predicting the fire ignition, rate of spread and intensity), wind adjustment factor (windrf), ‘surface-to-volume-ratio’ (savr), moisture of extinction (fuelmce; the one at which a fire will no longer spread) and mineral content (st). These fuel characteristics are represented by certain average values that have been previously defined in laboratory experiments and field research in the USA ([Rothermel, 1972](#); [Albini, 1976](#); [Baughman and Albini, 1980](#); [Anderson, 1982](#)). The set of these values is provided externally to the fire model without any adjustment for Croatian case study.

## CHAPTER 4

### THE SPLIT WILDFIRE IN CROATIA

#### 4.1. Overview of the Split Wildfire

The most fire-prone area in Croatia is the Adriatic Sea coastline (Figure 4.1a), together with its surrounding outback and islands, which Croatia has more than a thousand in its archipelago. High fire risk is pronounced during summer months, from June to August, when long lasting dry spells and intense heat favour fire ignition and spread through highly flammable Mediterranean vegetation – pine forests and shrubs. The average annual burnt area in Croatia is ~18 400 ha in ~2500 wildfires (DUZS, 2018). The burnt-area figure escalated in 2017 with the total of ~87 000 ha in more than 4100 wildfires along the Adriatic coast, which marked the worst fire season in Croatian history. The most catastrophic wildfire of the season and in Croatia to date, was the Split wildfire that occurred in July 2017.

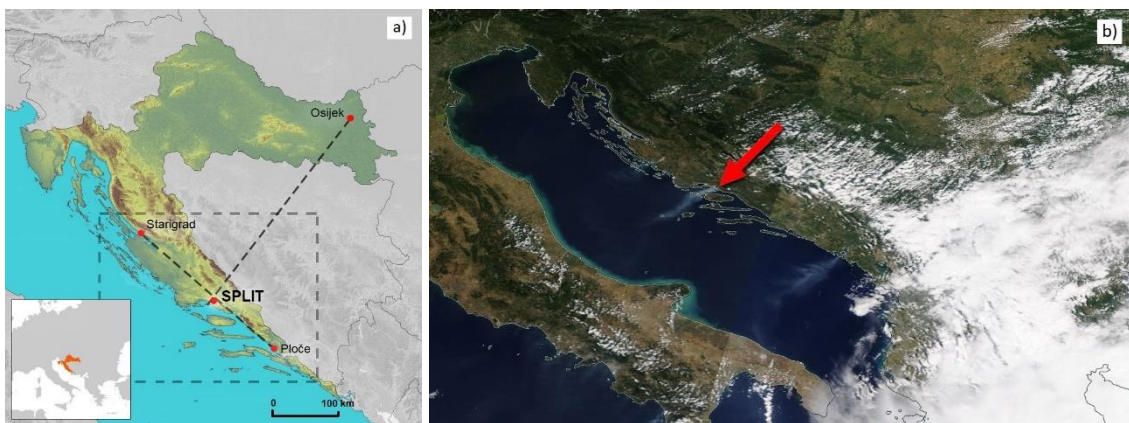


Figure 4.1. a) Location of the Split wildfire in Croatia with positions of vertical cross sections (dashed lines) and location of the inner nested domain used in the ALADIN model simulation (dashed rectangle) and b) Terra satellite MODIS image on 17 July 2017 shows active fire areas along the Adriatic Sea coast (<https://worldview.earthdata.nasa.gov>).

Split is historical and touristic city, listed as a UNESCO World Heritage Site List (Kapusta, 2017). Its wider urban area counts up to 300 000 citizens, with more than 720 000 tourists visiting in 2017 (Ministry of Tourism, 2017), mostly in July and August, when majority of wildfires occur. The Split wildfire occurred on the last night of the Ultra festival, which attracted more than 150 000 visitors into the city that weekend alone. The city is situated on a peninsula surrounded by gulfs to the west and mountain and hills in the east (Figure 4.2). The wildfire started 15 km southeast from the city, in the valley between hills parallel to the Adriatic coast and orientated north-west to south-east (Figure 4.2, 4.3a and A1). Further inland lies the highest mountain Mosor (1339 a.s.l.) in which south foothill, towards the Adriatic Sea, lie three

lower hills – Makirina (Figure 4.2; C; 723 a.s.l.), Sridivica (B; 420 a.s.l.) and Perun (A; 533 a.s.l.). The peaks are from 2 to 8 km away from the sea, which make this highly urbanized coast very narrow. This type of topography, consistent of the steep mountain range backing the coastline, can significantly influence air flows and create complex atmospheric dynamics in the area. The hinterland landscape is dominated by Mediterranean Aleppo pine forests (*Pinus halepensis* Mill.), scrubs and maquis intermixed with small agricultural fields within scattered villages (Figure 4.3a). The area is well-known to be prone to fires, but mostly with minor wildfire incidents each year. The last significant conflagration near Split, similar to the one from 2017 in terms of area burnt and firefighting demand, was in 2001 (Tomašević, 2012). However, it took that wildfire 4 days to reach the same impact as the one from the 2017 had in less than 30 hours (Francetić, 2017). The wildfire was stopped only 4 km from the city centre.

The Split wildfire lasted nine days, from 16 to 25 July 2017, and burned 5122 ha (Jovanović and Župan, 2017), most of which within 30 hours of ignition. The total cost of the Split wildfire is estimated at US\$ 20.6 million. It burned three houses and damaged 46 others, burned 18 cars, 11 olive groves and two greenhouses. It threatened agriculture fields, olive groves, churches, substations, power lines, gas stations, police station, court building, hotels and cities main landfill (DUZS, 2018). The plume from the wildfire crossed the Adriatic Sea and reached the coast of Italy, and it was clearly visible from space (Figure 4.1b). Ash was observed up to 25 km south of the conflagration. Within the city smoke turned day into night and drastically lowered an air quality. The cause of the wildfire is declared to be from an open flame or ember of an unknown origin. Given the size and rapid rate of spread of the fire, which made multiple runs into densely populated area, it is miracle that no lives were lost as a direct result of the wildfire. Due to intense fire activity, unexpected fire escalations, and enormous demands on property protection, mostly without aircraft support and with limited water supplies, the number of ground firefighting forces had to increase rapidly. During the early stages of the wildfire, many citizens joined the intervention until additional firefighting resources and personnel came from other parts of Croatia, including from the closest island, which is unprecedented in firefighting history. In total 168 vehicles, 796 firefighters, and more than 200 soldiers were deployed. To date firefighters refer to the Split wildfire as the “Mother of all fires”.

#### 4.2. Wildfire Reconstruction

The Split wildfire was characterized by four very active fire runs in the first 30 hours from ignition (Figure 4.2). Those four periods of broad fire spread accompanied by erratic fire behaviour and air turbulence will be noted as SPLIT 1 through 4. SPLIT 1 will refer to the first 11 hours of the wildfire, or a period from the late-night ignition to the morning hours the following day when fire activity slightly eased. Within this period firefighting aircraft could not join the intervention due to air turbulence. The SPLIT 2 period will refer to early afternoon fire reactivation and further spread of the fire zone with mosaic fire front. SPLIT 3 will refer to the late afternoon escalation in fire activity around all zones with the most significant downhill fire run into the city. The fourth and final period SPLIT 4 will refer to the night time downhill fire run into the eastern suburbs of the city. It should be noted that during defined periods wildfire was simultaneously progressing and remaining active while also reactivating at locations impacted beforehand.

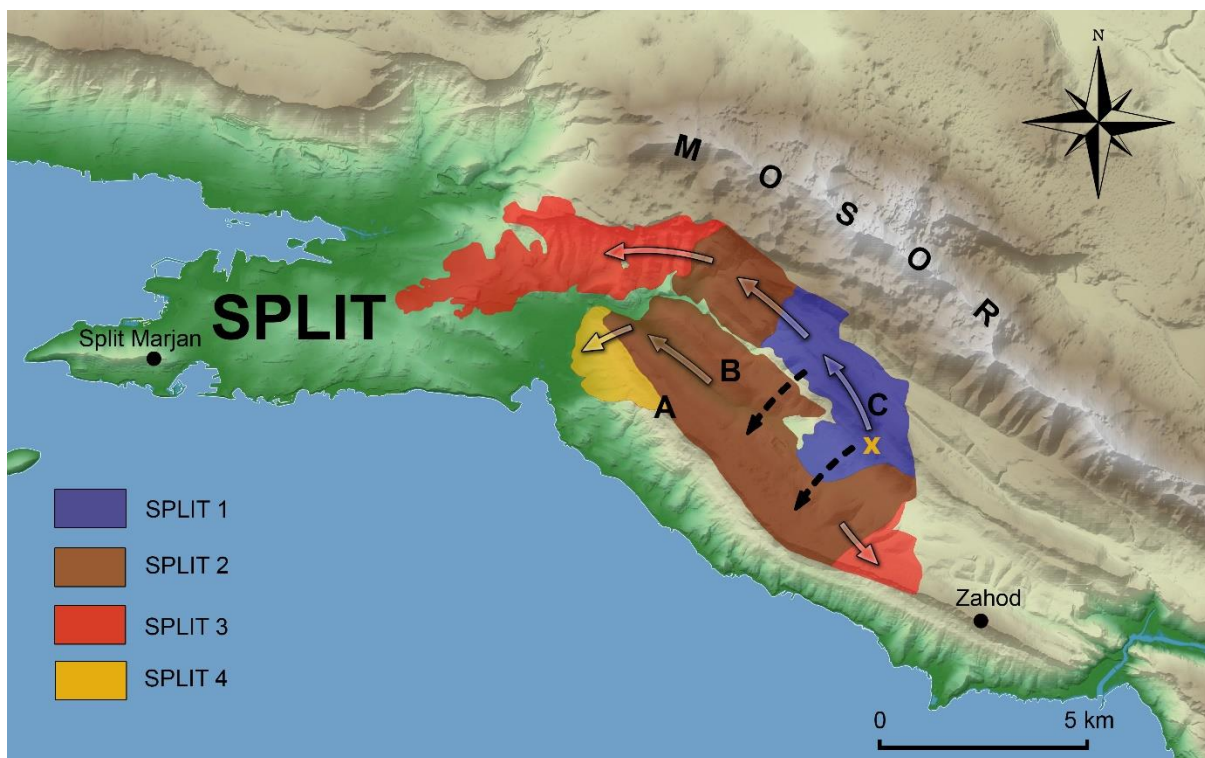


Figure 4.2. Map of the Split wildfire with the final perimeter and four prominent progressions in growth, noted as SPLIT 1 to SPLIT 4, over the first 30 hours from ignition (from 22:38 UTC on 16 July 2017 to 04:00 UTC on 18 July 2017). Ignition location is noted as X. Black dots indicate locations of Split Marjan meteorological station and tower (Zahod) with cameras used for fire detection and surveillance. Letters indicate hills Perun (A; 533 a.s.l.), Sridivica (B; 420 a.s.l.) and Makirina (C; 723 a.s.l.), all part of Mosor (1339 a.s.l.) mountain range. (Basic topography from [geoportal.dgu.hr](http://geoportal.dgu.hr)).

#### 4.2.1. Burn Period Split 1: 22:38 (16 July) – 09 UTC (17 July)

The wildfire was reported in the evening on 16 July 2017 at 22:38 UTC (00:38 CEST on 17 July), 15 km east from the city, on the south foothill of Makirina (C; Figure 4.2). Landscape and ignition location can be seen in Figure 4.3a. Within minutes surveillance camera detected a very fast fire growth (Figure 4.3b). This was confirmed by the first firefighters on the site who reported a burnt area of 6000 m<sup>2</sup> in 5 minutes. Wildfire developed under a very strong and gusty north-easterly *bura* wind, which pushed the fire in southwest direction, into the valley. However, between strong *bura* gusts fire progressed northwards, burning uphill Makirina (C; Figure 4.2), threatening villages in higher altitudes and the astronomical observatory. From the ignition, the wildfire was characterized by erratic behaviour and high rate of spread. Depending on available fuels, it easily transitioned to crown fire.

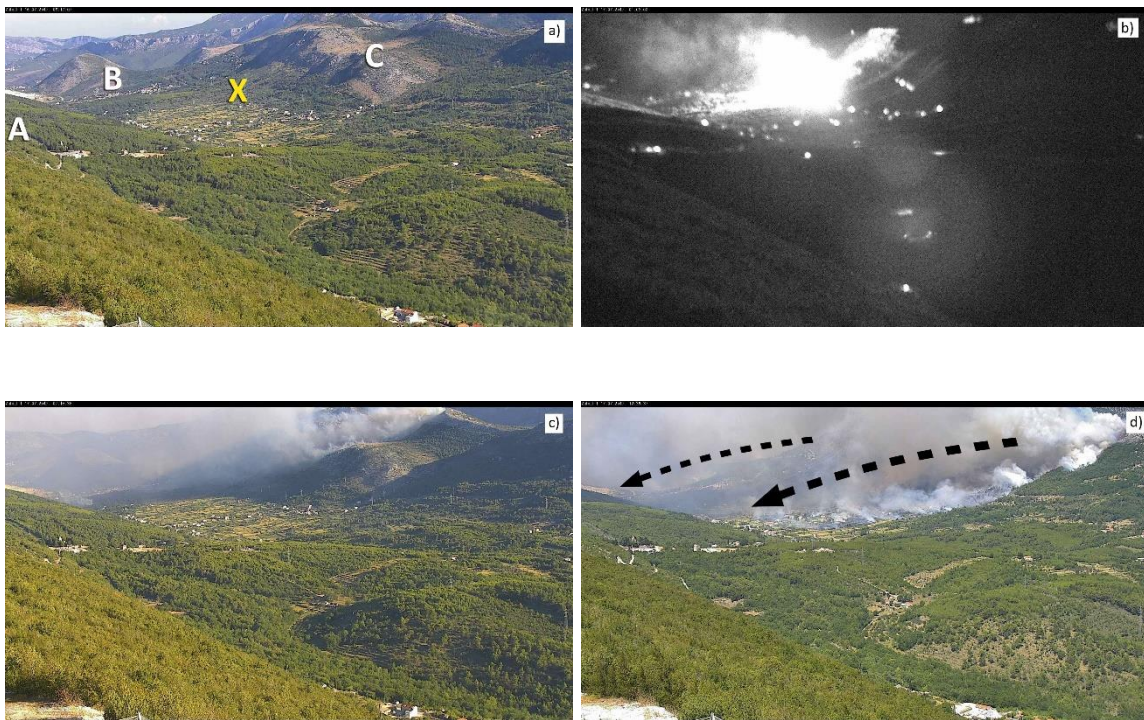


Figure 4.3. Photographs from Zahod location show: a) area affected by the Split wildfire with noted hills Perun (A), Sridivica (B) and Makirina (C) and ignition location (X), b) fire spread 28 minutes after the ignition (23:06 UTC on 16 July 2017), c) fire front in higher altitudes of Makirina hill (C) in the early morning hours on 17 July during the SPLIT 1 period (at 05:15 UTC, which is also the time of the first attempt by firefighting aircraft to approach the fire site) and d) mosaic fire front and wildfire spread down into the valley in SW direction between SPLIT 1 and SPLIT 2 period (at 10:39 UTC on 17 July).

When the fire affected suburban settlements in the valley and at higher altitudes, demand for firefighting troops increased drastically. Only 3 hours after ignition firefighting aircraft were requested as soon as daylight allowed. From 05 UTC to 13 UTC on 17 July 2017 firefighting aircraft made multiple attempts to join the intervention, but were unable to approach the site



due to severe turbulence. According to fire officials, at one period during the early morning fire activity slightly eased and wildfire could potentially have been controlled with air assistance at higher altitudes (Figure 4.3c and 4.5a) while ground troops focused their suppression efforts on keeping the fire away from villages at lower altitude.

#### 4.2.2. Burn Period Split 2: 10 – 14 UTC (17 July)

The significant shift in fire activity occurred around 10 UTC on 17 July. While still flanking along the hill Makirina, mostly towards the north-west towards the city of Split, a southern flank of the fire front reactivated and spread further into the valley (as seen in Figure 4.3d and noted as dashed arrows in Figure 4.2). Multiple spot fires created a mosaic fire front, and forced firefighting crews to scatter troops to protect people's homes. Photograph from the camera at Zahod location (Figure 4.2), revealed fire smoke rising in different directions within the valley and surrounding hills (Figure 4.4). At Makirina hill (C) smoke was rising in SW direction, within the valley in NW direction and at foothill of Perun (A) vertically. Wildfire easily crossed the main road in the middle of the valley and lower hill Sridivica (B) and burned upslope the north side of hill Perun (A; Figure 4.2 and A5a). At some locations wildfire crossed the hill A and threatened to run downslope towards the sea (which happened in the late evening of the same day during the SPLIT 4 period). At this time it was prevented by the firefighting aircraft which could join the intervention only at south side of hill Perun between 13 UTC and 14 UTC. After 14 UTC weaker turbulence enabled firefighting aircraft to approach villages in the valley, but it had only minor impact on the fire (Figure 3.6a). By 15 UTC, the north-western flank of the wildfire which was progressing towards the city, had travelled 6 km, 13 hours after ignition.



Figure 4.4. Fire smoke rising in different directions in early afternoon hours during the SPLIT 2 period (at 12:30 UTC on 17 July).

#### 4.2.3. Burn Period Split 3: 15 – 21 UTC (17 July)

During this burning period fire activity escalated around all fire zones (Figure 4.2). The north-western flank of the wildfire, which was by 15 UTC located 10.5 km from the city centre, turned southwest and started its downslope run towards the city from the nearby hills and mountain Mosor. The fire burned into dense pine forest in the north eastern higher altitudes of the wider city area. This area also consists a possible minefield, a leftover from the war in 1990s, which meant fire burned into plenty of long unburned dry fuels. As the main fire front entered heavy fuel, smoke and ash developed into the extensive convection plume (Figure 4.5b).

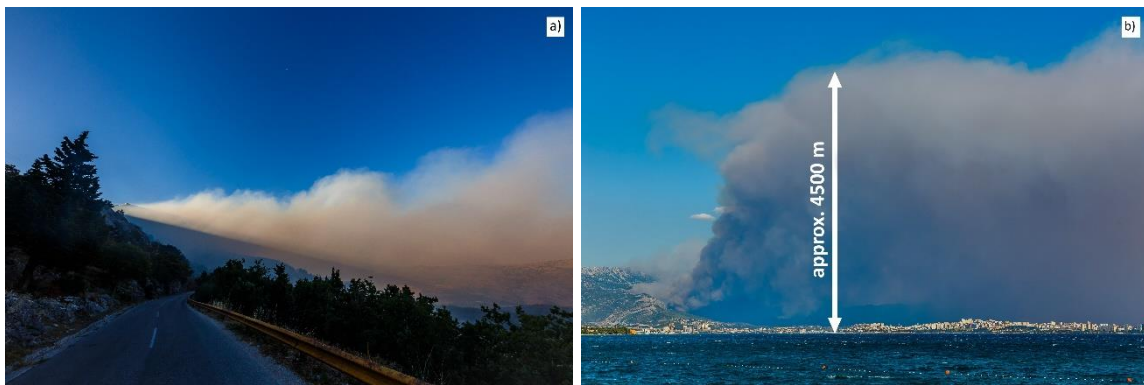


Figure 4.5. Fire smoke a) in the early morning on 17 July (04:52 UTC) during the SPLIT 1 period and b) in afternoon hours (15:09 UTC) during the SPLIT 3 period (photographed by Zvonimir Barišin).

Also, a number of spot fires were reported ahead of the main front, some ignited up to 500 m by flying pinecones. It is striking that between 15 UTC and 16:20 UTC, wildfire crossed additional 2.8 km, which makes the average forward rate of fire spread for this period to be  $35 \text{ m min}^{-1}$ . According to a firefighter witness, six fire whirls were spotted in the northern city suburbs, along the foothill of mountain Mosor. Due to wildfire's high intensity, erratic behavior and fast spread, constraining the propagation of the main fire front was not possible. Active fire suppression could only be organized in defensible space around people's homes. Local firefighters and self-organized citizens defended residential neighborhoods before additional help arrived. Situation within the city in this period can be described as chaotic. Fire threatened, among other, gas stations, substations and cities main landfill. Observed spread rates within the inner suburbs between 16:30 UTC and 20 UTC were estimated to be from 500 m to 1 km per hour. The propagation of this flank of the wildfire was constrained due to fuel discontinuity and massive suppression efforts of firefighters, self-organized citizens and military. This flank of the wildfire was stopped only 4 km from the historical city centre, and brought under control by 21:00 UTC. Overall, in less than 6 hours wildfire travelled additional 6.5 km. Although

wildfire did not travel far east, along the valley where it started, drastic reactivation of the fire front on this side occurred simultaneously with the downslope fire run into the Split urban area (Figure 4.2) which contributed to chaos in already strained fire management. Firefighters on this side reported 3 km long fire front, extensive spotting and at one point flames up to 30 m high (Figure 4.6b).



Figure 4.6. The eastern part of the fire front: a) fire smoke in SW direction and Canadair firefighting aircraft in operation (at 16:33 UTC on 17 July) and b) flames higher than 30 m with fire smoke in SW direction (at 18:57 UTC on 17 July), both during the SPLIT 3 period.

#### 4.2.4. Burn Period Split 4: 22 (17 July) – 04 UTC (18 July)

By this time another flank of the wildfire drastically reactivated on the hill Perun (A, Figure 4.2 and 4.7a). Wildfire crossed the hill multiple times on 17 July, but only around 21:30 UTC its activity escalated and could not be stopped before it ran downslope towards the sea. Wildfire burned into a native downy oak (*Quercus pubescens*) forest on the top of the hill and spread rapidly downhill reaching narrow and densely populated coastal area at the bottom of the hill within minutes (Figure 4.7b, A2a and A2b).

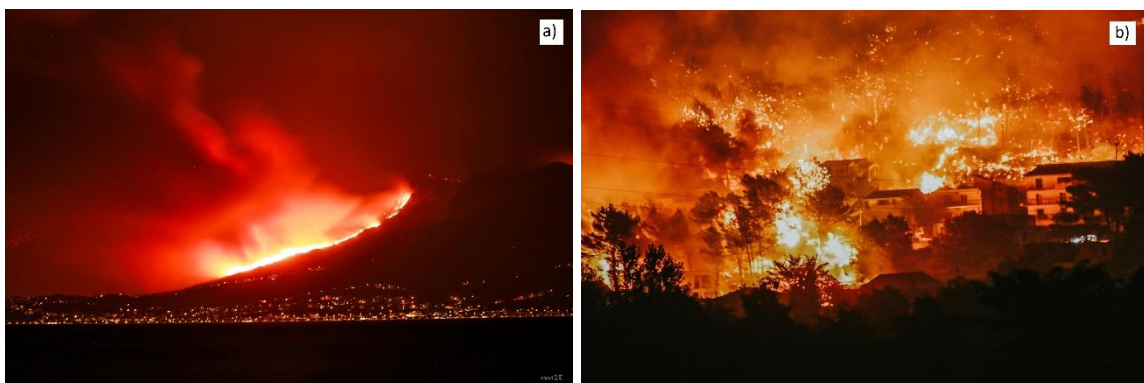


Figure 4.7. Wildfire's downslope run on the south side of hill Perun (A) during the SPLIT 4 period: a) a view of the wildfire from the nearby Island of Brač, approximately 13 km south (photographed by Ante Mandić) and b) fire burning into the highly populated coastal area (photographed by Damira Kalajzić).

Crown fire propagated down slopes inclined at approximately 20°, and in less than 30 minutes burned 1 km of forest before it reached houses. This flank of the fire front was 700-800 m long, with the average forward rate of fire spread of 2 km h<sup>-1</sup> or 33 m min<sup>-1</sup> (Figure 4.8a and 4.8b). According to witnesses, pinecones from the burning forest on the hill started several isolated spot fires up to 800 m ahead of the fire front. Flames from the crown fire reached heights in a range from 10 to 30 m above the canopy. Considerable suppression efforts were focused on defending people’s homes, hotels, a school and church. This flank of the wildfire was controlled around 4:00 UTC in the morning on 18 July 2017. The majority of 5122 ha burned by this time. Only small additional areas burned until the wildfire was declared contained nine days after ignition, on 25 July. More aerial photos of final fire scar taken few days after the wildfire with indicated fire spread direction can be seen in Appendix A.

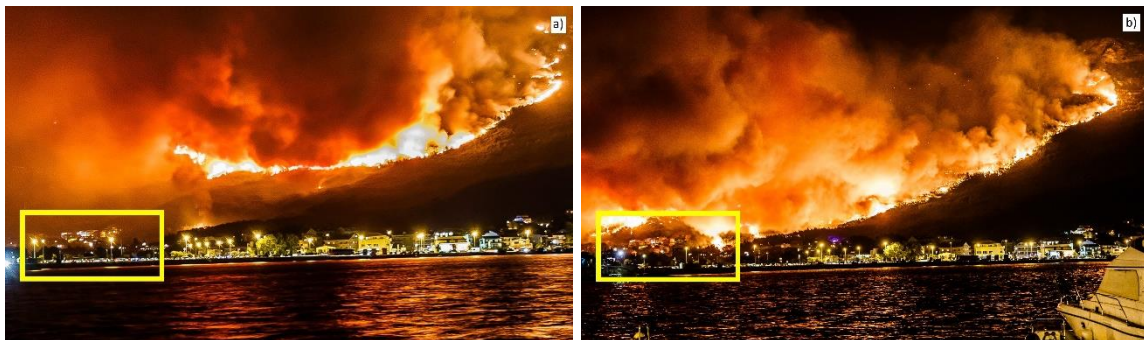


Figure 4.8. Wildfire’s downslope run into the coastal area on the south side of hill Perun (A) during the SPLIT 4 period a) at 22:05 UTC and b) 13 minutes later, at 22:18 UTC on 17 July 2017 (photographed by Zvonimir Barišić).

The meteorological analysis in the Chapter 5 aims to answer the questions about the role that fire weather conditions played in the most significant fire runs:

1. Which meteorological conditions occurred prior and right after the ignition of the Split wildfire in late night hours on 16 July 2017?
2. What conditions prevented firefighting aircraft from joining intervention from the early morning to late afternoon on 17 July (the SPLIT 1 period)?
3. What conditions contributed to sudden fire reactivation around the noon on 17 July (transition between periods SPLIT 1 and SPLIT 2)?
4. What meteorological conditions accompanied total fire escalation around all zones and downslope run into the cities area in the late afternoon on 17 July (the SPLIT 3 period)?
5. Which fire weather conditions occurred together with another downslope run during the night time between 17 and 18 July 2017 (the SPLIT 4 period)?

## CHAPTER 5

### THE SPLIT WILDFIRE – METEOROLOGICAL ANALYSIS

#### 5.1. Antecedent Conditions and Fire Danger Rating

The summer season in Croatia in 2017 was extremely warm and dry with air temperature at the Split-Marjan meteorological station  $3.1^{\circ}\text{C}$  above average, and with only 6% of the 30-year (1961–1990) mean rainfall (Figure 5.1).

Extreme weather conditions during the summer were extension of a long dry period that started in the preceding spring season. Spring was very warm and dry, with the last significant rainfall in Split two months prior to the wildfire (on 26 May, 10.5 mm). Weather conditions in June were extremely warm and dry, with an air temperature  $3.3^{\circ}\text{C}$  above average, and 8% of the 30-year average rainfall at the Split-Marjan meteorological station. Similar weather conditions continued until the Split fire in mid-July and remained extreme until the end of the summer 2017.

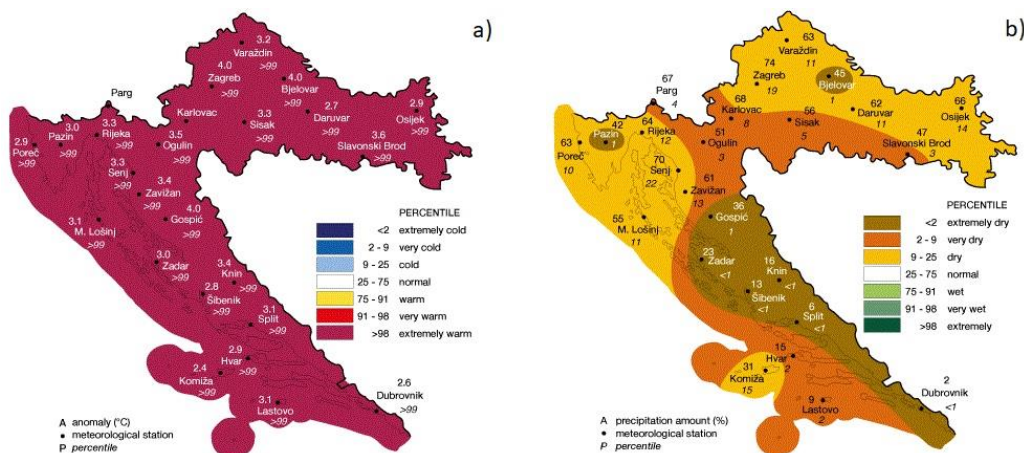


Figure 5.1. a) Average summer (June-August) 2017 air temperature ( $^{\circ}\text{C}$ ) and b) total precipitation (mm) at meteorological stations in Croatia compared to climatological period 1969-1990. The number above each station indicates the anomaly of air temperature (a, in  $^{\circ}\text{C}$ ), and the percentage of average precipitation accumulated in that period (b, in %). The number under each station indicates the percentile according to which stations are classified in certain category (from extreme cold to extreme hot; extreme dry to extreme wet). From [https://meteo.hr/klima.php?section=klima\\_pracenje&param=ocjena](https://meteo.hr/klima.php?section=klima_pracenje&param=ocjena).

## 5.2 Fire Danger Rating

The lack of precipitation accompanied by higher-than-average air temperature in the months prior to the wildfire led to continued drying of fuels in the region and consequently had an impact on fire danger rating. According to the SSR (Figure B1a and B1b), the most endangered area in summer 2017 was the mid-Adriatic known as Dalmatia, especially its outback where majority of the fires occurred (Ferina and Vučetić, 2018). If greater than 7, SSR and MSR indicate very high meteorological fire danger. MSR in July at Split-Marjan meteorological station was 20.7, and at nearby Split airport 37.7. SSR at Split-Marjan and airport reached 13.4 and 25.1, respectively, which are some of the highest values ever recorded (Table B1). Fire danger rating in the Split area was much above average during 2017 when compared with monthly and seasonal severity values for the period 1981–2010 (Figure 5.2).

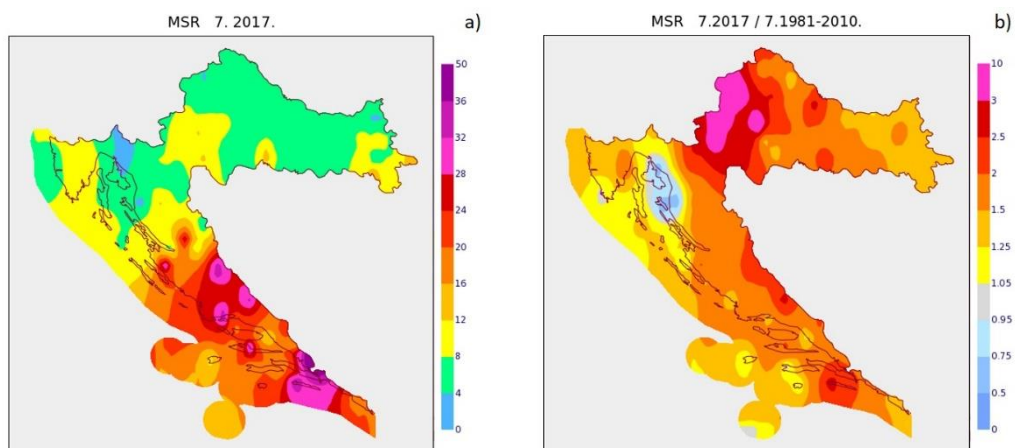


Figure 5.2. a) Monthly Severity Rating (MSR) index for July 2017 and b) MSR of July 2017 in comparison with July 30-year period (1981–2010).

Fire danger was very high for more than 20 consecutive days prior to the Split wildfire. On the day of the fire, FWI reached its annual maximum and ISI reached the seasonal maximum (Figure 5.3). This confirms that the most severe fire weather conditions in 2017 occurred exactly on 16 July, the first day of the Split wildfire.

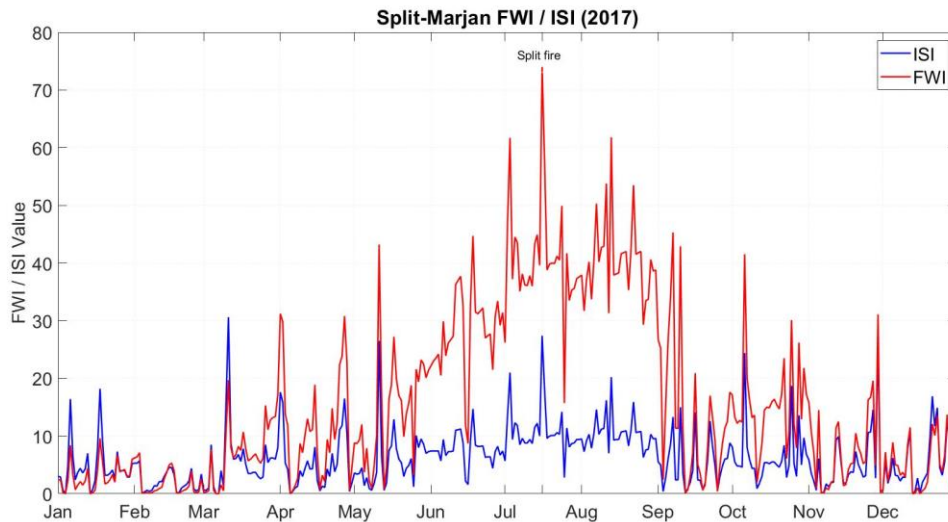


Figure 5.3. Daily course of Initial Spread Index (ISI) and Fire Weather Index (FWI) at 12 UTC from 1 January 2017 to 31 December 2017 at Split-Marjan meteorological station.

Additionally, according to the definition of ISI, if it is greater than 18, then the estimated speed of a fire front is  $18.3 \text{ m min}^{-1}$ . Seasonal peak value of ISI (27.4) also pointed out that, along with rapid spread, wildfire may create multiple fire fronts and develop into a crown wildfire, the most dangerous type of fire. According to wildfire reconstruction, this type of fire behavior occurred exactly in the first 30 hours of the Split wildfire.

### 5.3. Surface Synoptic Conditions

The synoptic analysis revealed that prior to and during the first 30 hours of the Split wildfire there was a strong pressure gradient over the Adriatic coast (Figure 5.4a). On 16 July and most of the day on 17 July Croatian territory was placed between front of the Azores anticyclone and rear of the cyclone over SE Balkan Peninsula. Consequently, the strong pressure gradient over 600 km long coastline was created, with pressure varying from approximately 1023 hPa to 1010 hPa, which was followed by an advection of strong NE airflow. This gradient remained strong in the morning on 17 July when aircraft reported severe turbulence. The pressure gradient along the Adriatic eventually weakened on 18 July and was replaced by almost non-gradient conditions which lasted for several days until a low pressure system on 24 July brought light rain over the fireground. These conditions helped firefighters to completely extinguish the wildfire on 25 July 2017.

The upper-level charts revealed that synoptic conditions coinciding with the Split wildfire featured a large amplitude upper-level trough extending from the Baltic Sea in the north to the Adriatic Sea in the south (Figure 5.4b). The trough amplified in the hours prior to the wildfire. Around the time of ignition, the trough attained maximum strength and traveled slightly east,

placing the wildfire's area exactly on its west side. Analysis of 500 hPa chart (not shown) revealed stronger wind speed here ( $25.7 \text{ m s}^{-1}$ ), accompanied by a 300 hPa jet stream (Figure 5.4c; up to  $46.3 \text{ m s}^{-1}$ ). This western flank of the jet stream and trough is associated with air subsidence, which can be further confirmed by the advection of the vorticity maximum away from the wildfire's location. The region right behind the vorticity maximum is linked to the strong sinking motion.

A large amplitude and shortwave trough are known to be dynamically unstable and also associated with fast upper-level cut-off processes (Jurčec, 1989). The cut-off process in this case started at 00 UTC (Figure 5.4b) and further deepened by 06 UTC on 17 July becoming a cut-off cyclone, which can be seen over SE Balkans and Greece. Upper-level trough acted as a boundary between two airflows. On its west side, immediately above the wildfire's location, it brought a cool change with strong NNE airflow, while on the east side it brought ESE airflow with cloudiness and development of storm centers, which can be seen over SE Balkan Peninsula on satellite in Figure 4.1b.



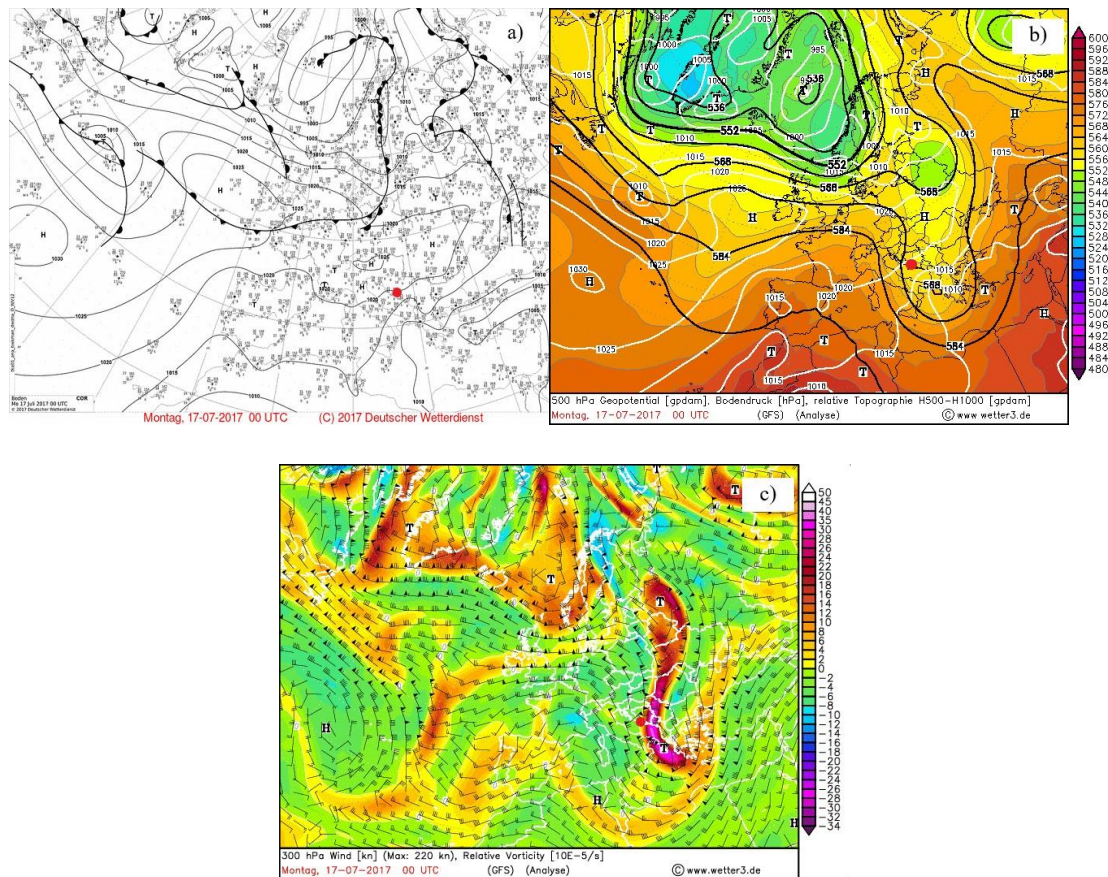


Figure 5.4. Analysis charts for Europe at 00:00 UTC (approximately two hours after the ignition) on 17 July 2017 of a) mean sea level pressure (hPa; black contours) and fronts, b) 500 hPa geopotential (gpdam; black contours), surface pressure (hPa; white contours) and relative topography RT 500/1000 (gpdam; coloured) and c) 300 hPa wind (kt, where 1 kt = 0.51 ms<sup>-1</sup>; wind barbs) and relative vorticity (10<sup>-5</sup>s<sup>-1</sup>; coloured). Split wildfire location on charts is indicated as red dot. (The charts are available from: [http://www1.wetter3.de/archiv/.](http://www1.wetter3.de/archiv/))

#### 5.4. Surface Conditions – Observations

Automatic measurements from Split-Marjan station recorded the cool outbreak as a drop in maximum daily air temperature by 5°C, from 33.3°C to 27.0°C between 15 and 16 July (Figure 5.5a). This was followed by a drop in relative humidity, which remained between 18% and 38% for two consecutive days, on 16 and 17 July.

Wind measurements at Split-Marjan station confirm the NE airflow during the first 30 hours of the wildfire (Figure 5.5b, c). A sudden increase in wind speed is evident in the afternoon on 15 July, with the strongest gust of the month: 19.9 m s<sup>-1</sup>. Wind gusts remained strong throughout 16 July, although decreasing to 4.5 m s<sup>-1</sup> by the time of the wildfire’s ignition (Figure 5.5b). Wind speed and gusts increased again (to 12.7 m s<sup>-1</sup>) in the morning on 17 July, at the time of the reported air turbulence by firefighting aircraft. Wind speed slightly eased at times during the mid-day on 17 July, and intensified again right at the time of a downslope run

towards the city of Split (the SPLIT 3 period). Wind direction remained persistent as NE *bura* wind, which can be also seen by direction of the fire smoke which was perpendicular to the coast and traveled across the Adriatic Sea towards Italy (Figure 4.1b). The smoke also caused a drop in the total solar radiation at Split-Marjan station (not shown). Wind dropped in speed and changed direction to SW in the morning on 18 July, which helped firefighters to control the fire spread. Light rain on 24 July (1.2 mm) and 25 July (1.6 mm), also the most significant rainfall in two months, additionally helped to finally extinguish the wildfire.

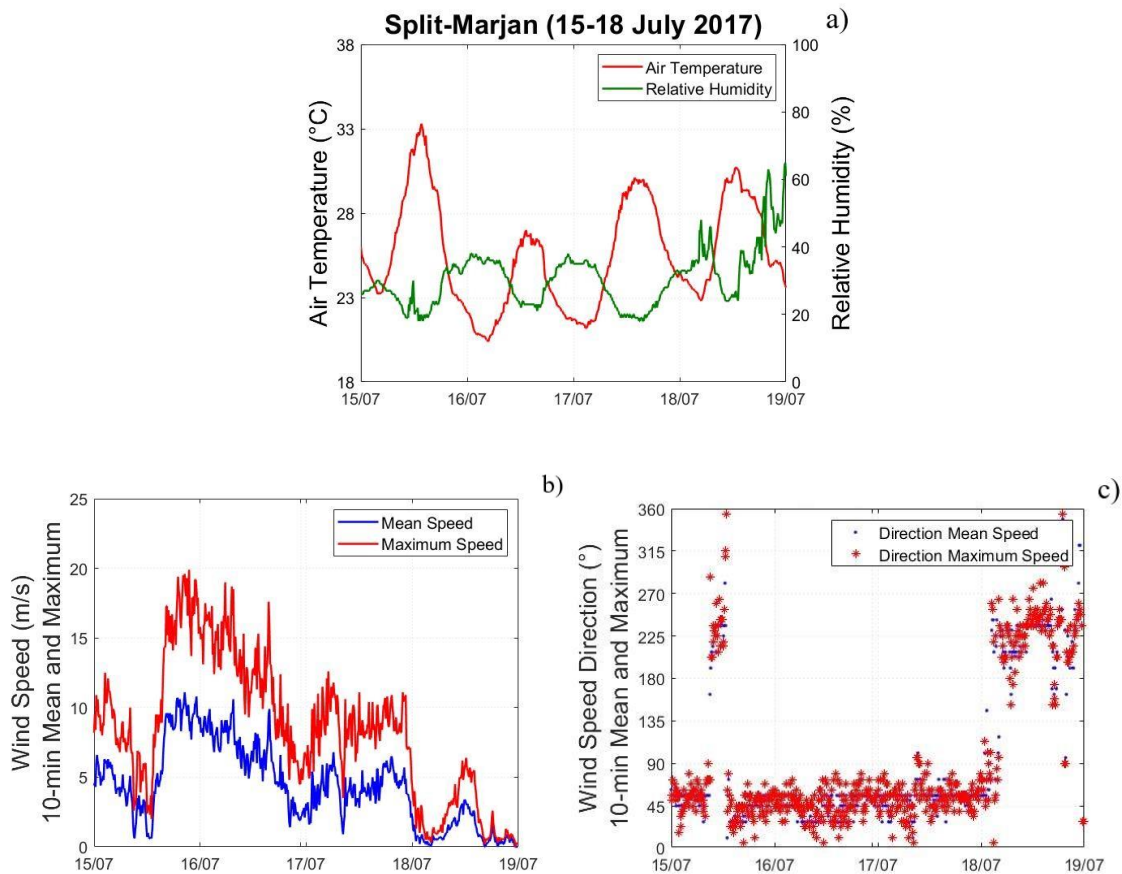


Figure 5.5. Split-Marjan automatic weather station 10-minute observations of a) air temperature (°C) and relative humidity (%), b) mean and maximum wind speed ( $\text{m s}^{-1}$ ) and c) mean and maximum wind speed direction (°) from 15 to 18 July 2017.

## 5.5. ALADIN Model

### 5.5.1. Surface Conditions

Model data corroborate the surface pressure analysis and depict the strong pressure gradient over the wildfire's area prior to ignition and until midday on 17 July (transition from SPLIT 1 to SPLIT 2 period). The wildfire location (43.5°N, 16.6°E) of ignition was placed in the narrow band of tight pressure gradient between 1020 hPa to 1012 hPa over 100 km of N-S line (between 43°N and 44°N; [Figure 5.6a](#)). This tight pressure slightly eased during the day on 17 July (SPLIT 2 to SPLIT 4), and was replaced by a non-gradient field in the midday on 18 July.

Simulated air temperature and relative humidity follow the in-situ observation data and give insight into broader conditions in the mountainous outback where wildfire started. Maximum values here on 16 and 17 July were between 25°C and 29°C ([Figure 5.6c and e](#)), with minimum values on the night of the ignition between 13°C and 19°C, depending on the elevation. The overnight relative humidity, during the first hours of wildfire, reached the maximum of 60% at the elevated terrain ([Figure 5.6b](#)). Early morning on 17 July brought a drop in relative humidity as expected ([Figure 5.6d](#)), however, relative humidity in the area remained below 40% the following the night (between SPLIT 3 and SPLIT 4 period; [Figure 5.6f](#)).

The dynamical adaptation of ALADIN model at 2 km horizontal resolution gave more detailed spatial structure of near-surface winds in the area. Model data reveals that during the SPLIT 1 period, *bura* wind in the coastal outback where the wildfire was burning at the time (foothill of C; [Figure 4.2](#)) had a speed between 5.5 m s<sup>-1</sup> and 8.0 m s<sup>-1</sup> with gusts between 13.9 m s<sup>-1</sup> and 24.5 m s<sup>-1</sup>. *Bura* retained this strength by 5 UTC on 17 July, when the aircraft tried to approach the fire site ([Figure 5.7a](#)). At the same time the wind dropped in speed away from the coast. The area of a low wind offshore and perpendicular to mountain range during *bura* flow is known as wake ([Grubišić, 2004](#)). This low wind zone corresponds to the successful aircraft operation at another wildfire site on the island 35 km south, which burned simultaneously with the Split wildfire. It is worth mentioning that the Croatian firefighting aviation is one of the rare operations which descend to 20 m or even 10 m height ([Željko Žugaj, personal communication](#)).

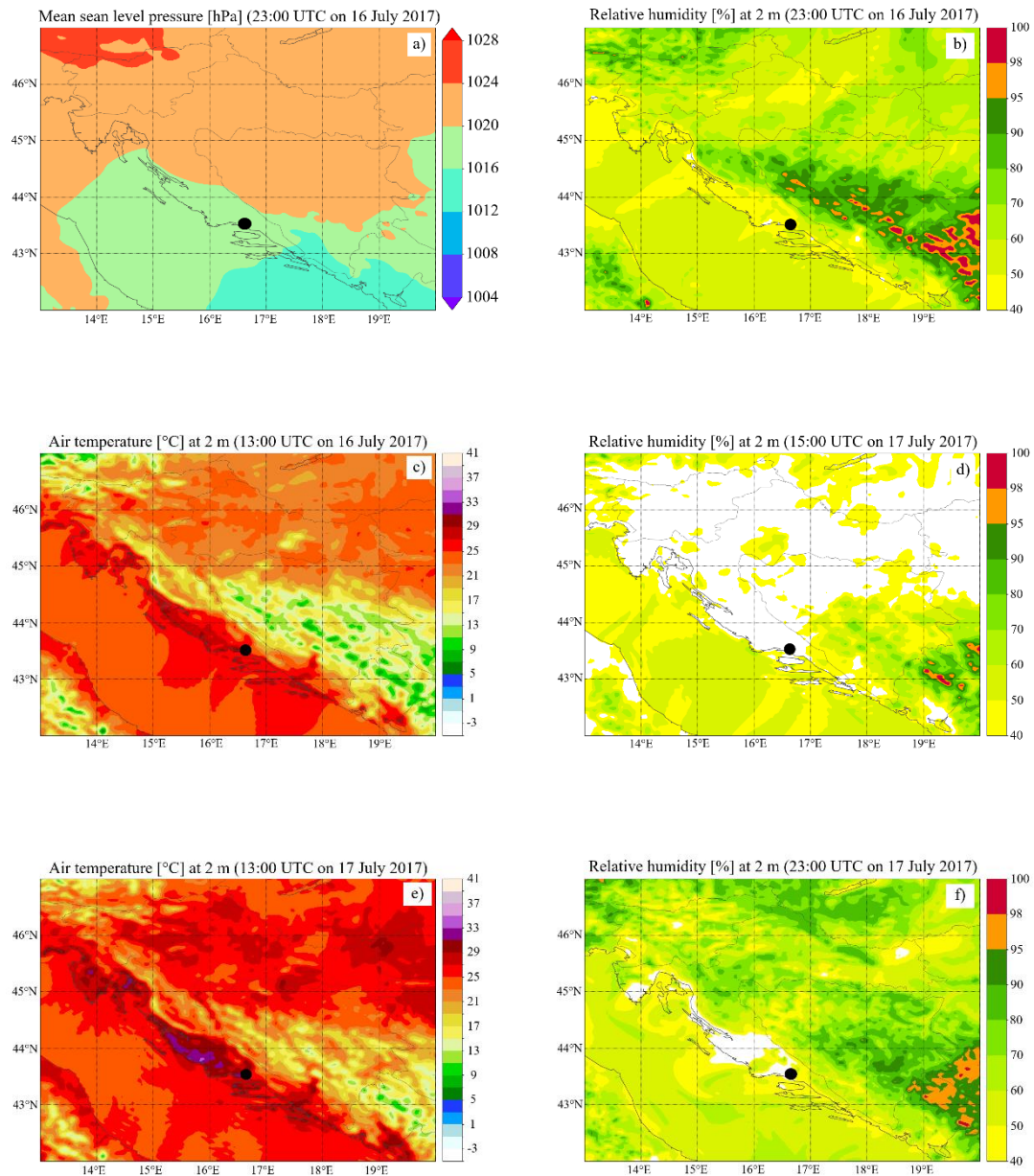


Figure 5.6. a) Mean sea level pressure (hPa; coloured), b) relative humidity (%; coloured) at 2 m, both valid for 23 UTC on 16 July, c) air temperature (°C; coloured) at 2 m valid for 13 UTC on 16 July, d) relative humidity (%; coloured) at 2 m valid for 15 UTC, e) air temperature (°C; coloured) at 2 m valid for 13 UTC and f) relative humidity (%; coloured) at 2 m valid for 23 UTC, all valid for 17 July 2017 from ALADIN-HR44 model. Split wildfire location on charts is indicated as black dot.

During the SPLIT 2 period, *bura* retained strength in the area closest to mountain Mosor, however, narrow bands of weak wind started to appear over the continental area in the NE section of the domain (Figure 5.7b). One such band of weak wind was located over the Split peninsula, Perun hill (A, Figure 4.2) and the outback valley where wildfire reactivated and started its reverse spread. Weaker wind speed along the hill A also contributed to successful

aircraft operation on its southern side. During the SPLIT 2 period, wind was westerly along the southern foothill of A and northeasterly along the hill C (Figure 4.2).

At the time of the SPLIT 3 downslope fire run, *bura* wind over the landward part of the city's peninsula, at the location of the NW flank of the wildfire (Figure 4.2), remained strong with speed between  $5.5 \text{ ms}^{-1}$  and  $10.8 \text{ ms}^{-1}$  and gusts to between  $10.8 \text{ ms}^{-1}$  and  $24.5 \text{ ms}^{-1}$  according to the model (Figure 5.7c). The speed of *bura* and its gusts persisted during the most critical hours of fire burning within the city, after which it eased down to between  $3.4 \text{ ms}^{-1}$  and  $8.0 \text{ ms}^{-1}$  with gusts between  $8.0 \text{ ms}^{-1}$  and  $13.9 \text{ ms}^{-1}$  until the evening on 17 July (end of SPLIT 3 period, Figure 5.7d).

Although weakening in the broader Split area and in contrast to the previous 48 hours, the *bura* wind continued into the late evening and during the SPLIT 4 period, preserving its aforementioned wind speed and gusts until morning on 18 July, after which it further weakened and wind turned westerly.

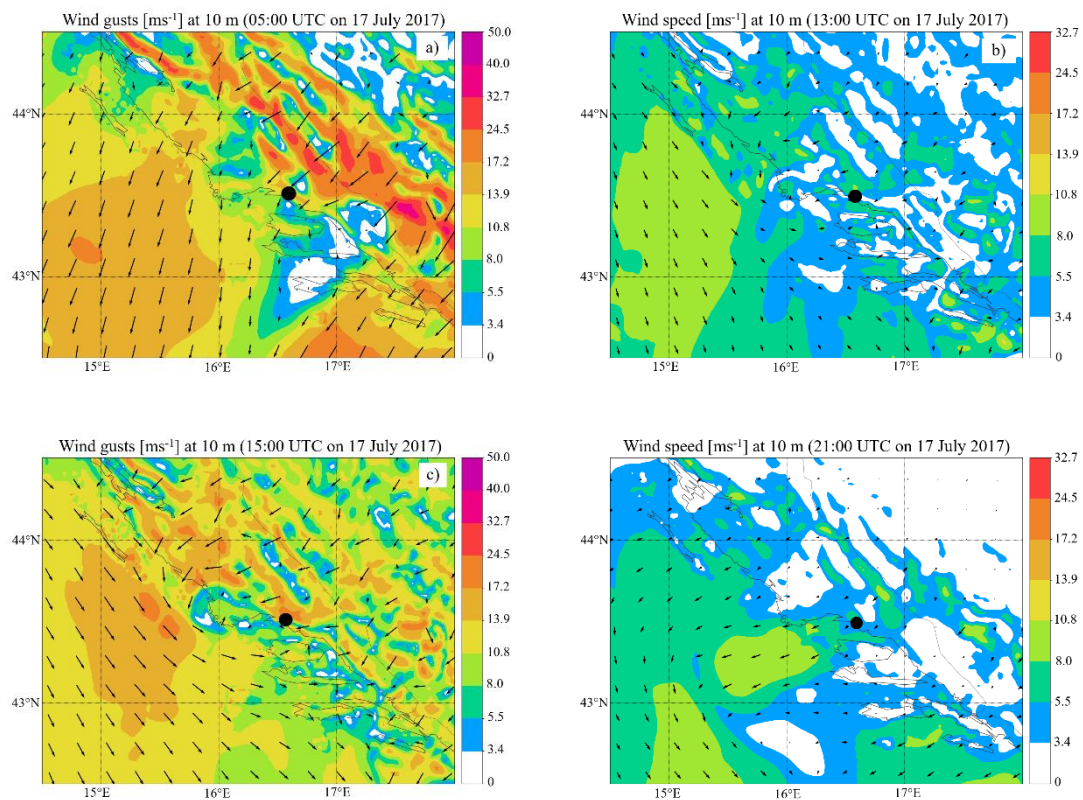


Figure 5.7. a) Wind gusts ( $\text{m s}^{-1}$ ; coloured and array) at 05 UTC, b) wind speed ( $\text{m s}^{-1}$ ; coloured and array) at 13 UTC, c) wind gusts ( $\text{m s}^{-1}$ ; coloured and array) at 15 UTC and d) wind speed ( $\text{m s}^{-1}$ ; coloured and array) at 21 UTC, all valid for 17 July 2017 at 10 m from ALADIN-HRDA model. Split wildfire location on charts is indicated as black dot.

## 5.5.2. Upper-level Conditions

### 5.5.2.1. Horizontal Fields

The model provides an accurate location of the upper-level shortwave trough stretched over the study area at 500 hPa, at the time of the wildfire's ignition (Figure 5.8a-c), however, the cut-off process appeared earlier (by 16 UTC on 16 July) in ALADIN simulations in relation to synoptic analysis and a little dislocated towards the Adriatic Sea. By the time of the ignition, Split wildfire was exactly on the western or rear edge of the upper-level cyclone, which caused the cool air outbreak from the north of the continent (Figure 5.8a), bringing very dry air (Figure 5.8b) and leaving clear skies over the entire Croatian territory, as can be seen in the satellite imagery (Figure 4.1b). After the ignition, upper-level cyclone progressively dissipated until the midday on 18 July 2017. During the whole study period (SPLIT 1 to SPLIT 4) the Croatian territory was placed in a narrow dry area of subsiding flow (Figure 5.8b).

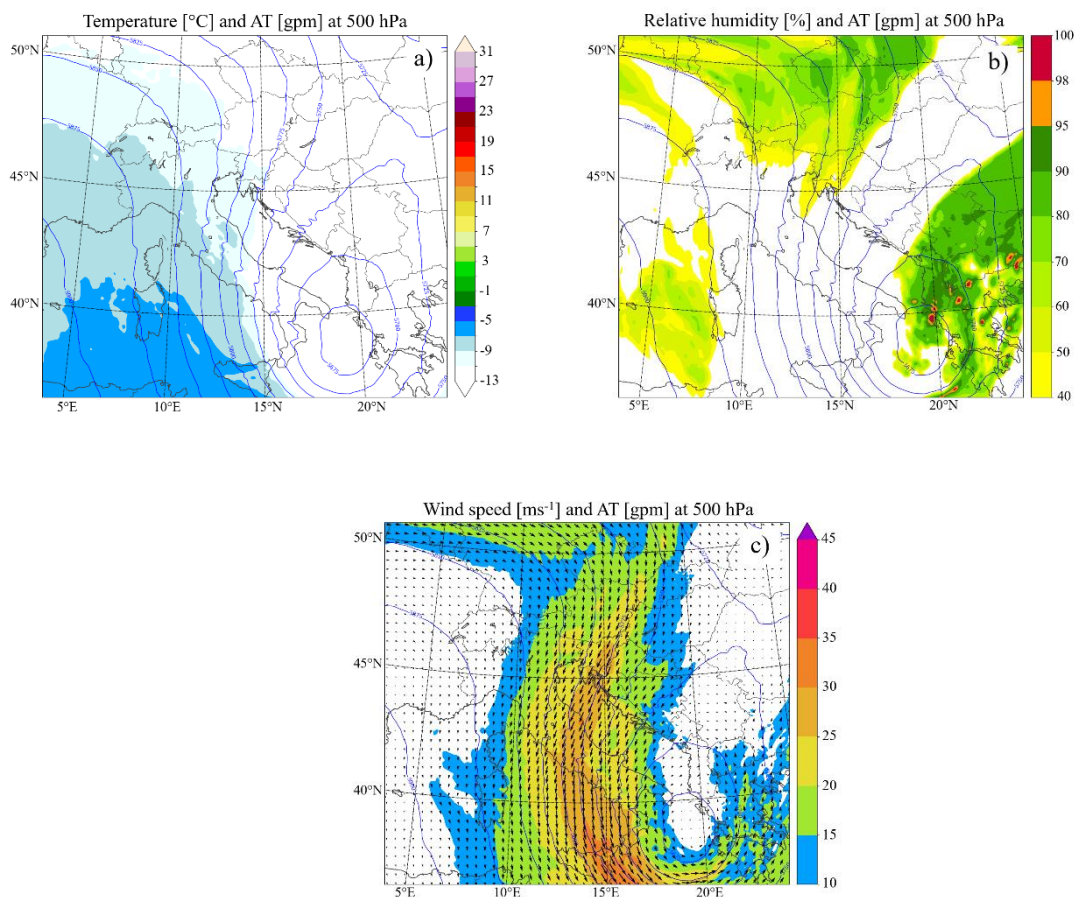


Figure 5.8. a) Temperature (°C; coloured), b) relative humidity (%; coloured) and c) wind speed (ms<sup>-1</sup>; coloured), all including AT (gpm; blue contours) at 500 hPa from ALADIN-HR44 model valid for 16 July 2017 at 23 UTC.

Wind pattern at 500 hPa also confirms the cool air outbreak from the north (Figure 5.8c). A jet-like shape following a jet streak and jet stream aloft embedded the NE circulation in the morning on 16 July. As jet streak was situated on the west side of the trough, it pointed to its amplification, which occurred hours prior to the ignition. The band of accelerated air further intensified and positioned the edge of its core immediately above the ignition location at ignition time.

#### 5.5.2.2. Cross sections

Vertical cross sections reveal a hydraulic jump-like structure over the coastal mountain slopes at the time of the wildfire's ignition (Figure 5.9a and 5.9c). The *bura* flow was strongest between 600 m and 1 700 m above ground level, immediately upstream of the wildfire's location, with the maximum horizontal wind speed close to  $30 \text{ m s}^{-1}$ . Above this strong *bura* flow was a layer of weak NE wind at altitude between 2 300 m and 4 300 m. This deep layer of weak wind on top of the wind maximum in the lee of the coastal range indicates a possible wave breaking below, which is the mechanism of a hydraulic-like flow. The presence of the hydraulic jump was also suggested by the positive vertical wind component at the downstream end of the hydraulic jump, with the maximum value of  $+2 \text{ m s}^{-1}$  at this side (in combination with  $-2.5 \text{ m s}^{-1}$  within the downstream flow; Figure 5.9b). Hydraulic jump flow culminated right at the time of the ignition, after which it dissipated by the end of the SPLIT 1 period.

The acceleration of the *bura* flow within the 1 km height throughout the day on 16 July is also apparent from the potential temperature in the same cross section line (Figure 5.9c). While the potential temperature field did not change significantly on the windward side of the *bura* flow indicating the statically stable lower atmosphere during the observed period, on the left side of the panel, or above the Dinarides and Split area, isentropes deformed during the day of the wildfire suggesting a decrease in stability here. By 23 UTC on 16 July (ignition time) isentropes became densely packed with steep downward, nearly vertical slope right above the mountain crest in the vicinity of the wildfire and jump-like recovery downwind, also indicating a hydraulic jump. Deformation of isentropes occupied a deep layer from 800 m to 3 500 m height. Together with accompanied hydraulic jump this dense packing of isentropes signal existence of the orographic gravity-wave breaking, known to generate strong *bura* flows (Gohm and Mayr, 2005). The sharp potential temperature gradient shows the gravity wave right above the leeward side of the Dinarides (Figure 5.9c). Peak gravity-wave activity occurred at the ignition time, after which it weakened until the following morning (end of SPLIT 1). A descending slope of isentropes above coastal mountains at the ignition time, when the gravity-

wave was the most amplified, clearly indicates the strong flow acceleration and formation of the jet in the lee of the mountains.

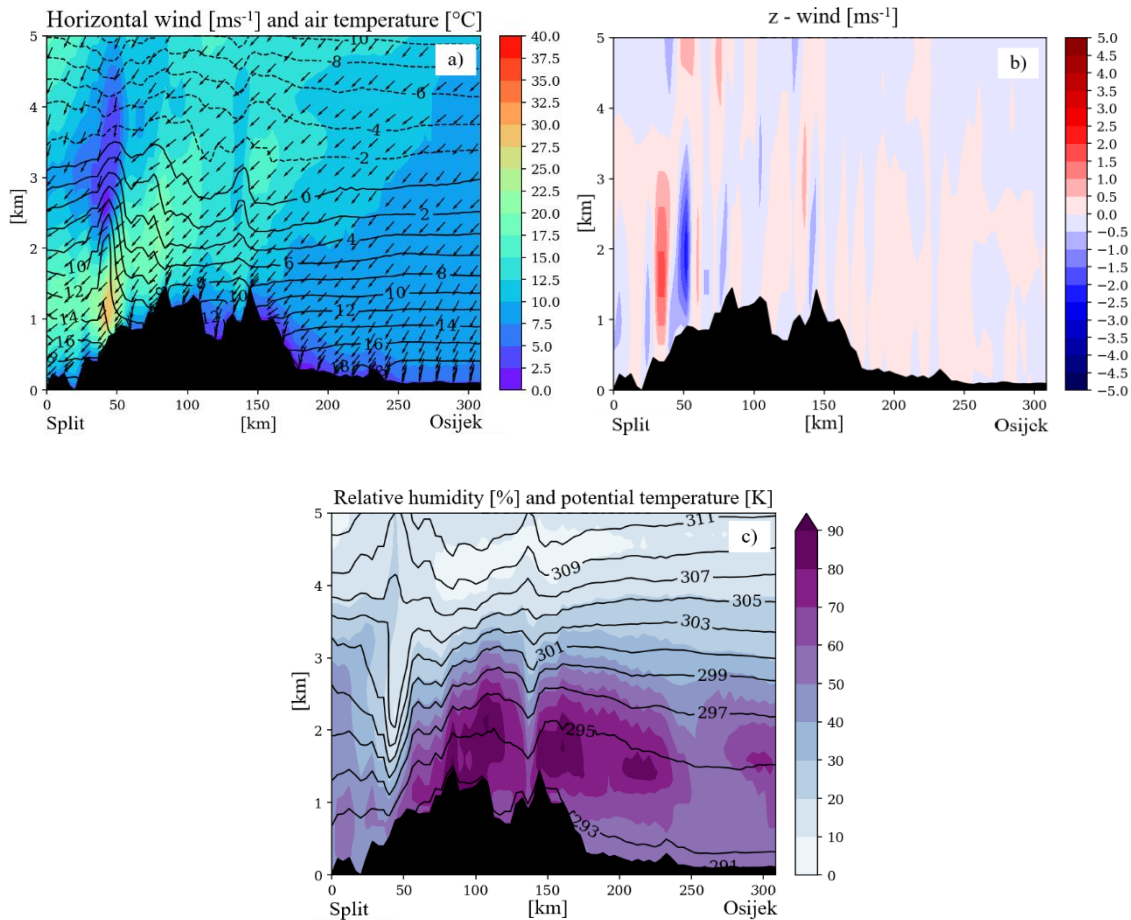


Figure 5.9. Vertical cross sections from ALADIN-HR44 model of (a) horizontal wind speed ( $\text{m s}^{-1}$ ; coloured) and direction (array) and temperature ( $^{\circ}\text{C}$ ; black contours for  $\geq 0^{\circ}\text{C}$ , dashed contours for  $< 0^{\circ}\text{C}$ ), (b) z-wind ( $\text{m s}^{-1}$ ; coloured) and (c) relative humidity (%; coloured) and potential temperature (K; black contours every 2 K) all valid for 23 UTC on 16 July 2017 from ALADIN model. The bottom black area depicts the terrain. Location of cross section between cities Split and Osijek is indicated in Figure 4.1a. Each section is 300 km long and 5 km high, oriented northeast to southwest and perpendicular to Adriatic coast with Split situated approximately 20 km from the left bottom corner. Air flow in each panel is from right to left.

Appearance of sharper potential temperature gradient was accompanied by a significant drop in relative humidity. Cross section of relative humidity reveals that the most prominent dry air descent occurred right at the ignition time (Figure 5.9c). A tongue of low relative humidity ( $< 30\%$ ) extended downward to 1 300 m height coinciding with the most intense sloping of isentropes. Moving forward in time, the model indicated the relative humidity drop for the entire vertical column above the wildfire area, which from early afternoon on 17 July had relative humidity under 30%. This low relative humidity persisted during the overnight hours between 17 and 18 July (SPLIT 3 and SPLIT 4 periods) in the first 1 000 m height and



decreased further under 10% to 3 500 m height above the wildfire. This dry air subsidence is in agreement with the upper-level analysis, which also suggested a possible dry air subsidence due to position of the upper-level cyclone in relation to the wildfire.

### 5.5.3. Low level Jet

*Bura* flow meets the characteristics of LLJ (defined in Section 3.5.1.1). Mechanisms recognized to cause LLJ include synoptic pressure gradients, cold front passage, mountain waves, cyclogenesis in mid-latitudes and upper-level jet streak dynamics (Uccellini, 1980; Jurčec, 1992).

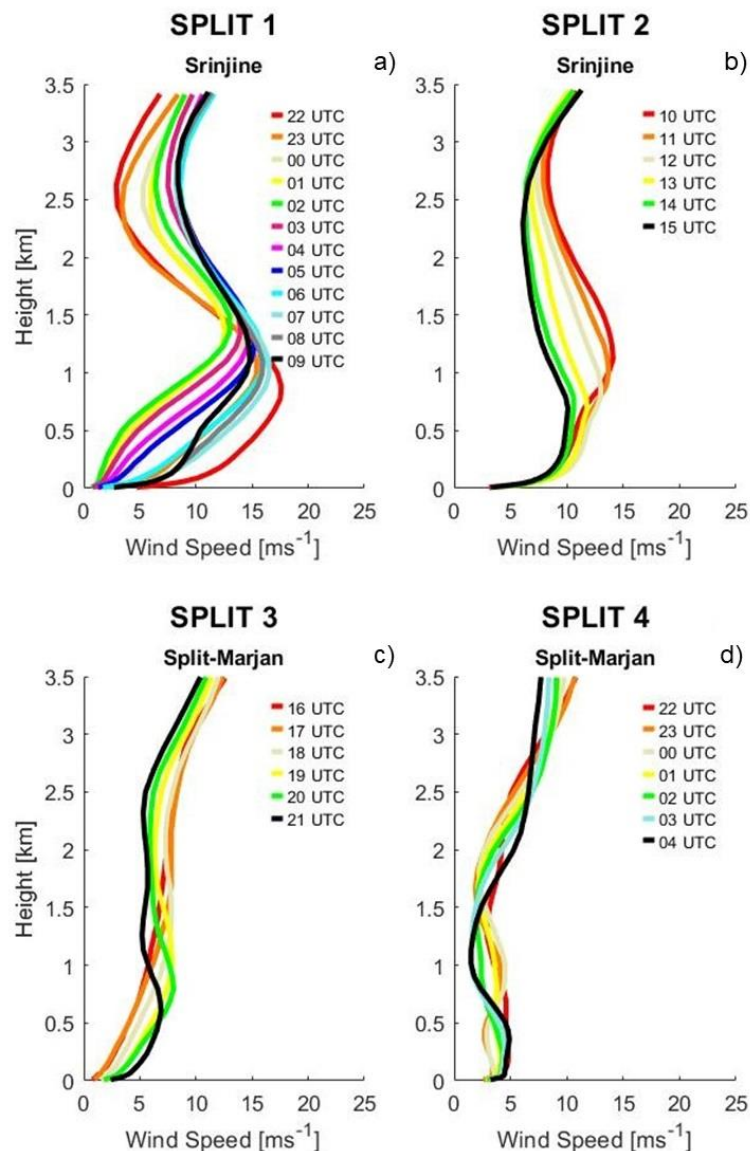


Figure 5.10. Vertical profiles of wind speed ( $\text{m s}^{-1}$ ) at Srinjine and Split-Marjan locations for periods a) SPLIT 1 (from 22 UTC on 16 July 2017 to 09 UTC on 17 July 2017), b) SPLIT 2 (from 10 UTC to 14 UTC on 17 July 2017), c) SPLIT 3 (from 15 UTC to 21 UTC on 17 July 2017) and d) SPLIT 4 (from 22 UTC on 17 July 2017 to 04 UTC on 18 July 2017) from ALADIN model. See Figure 4.2 for location of Split-Marjan and Srinjine (noted as S).

Pseudotemps or vertical profiles from ALADIN model permit analysis of the temporal evolution of LLJ during the *bura* flow since radiosonde measurements at the closest station (Zadar airport) were not obtained (observations declared invalid) during the study period. A sequence of vertical profiles was simulated for locations closest to wildfire at key times – at village Srinjine in the coastal hinterland (relevant for periods SPLIT 1 and SPLIT 2) and Split-Marjan station (relevant for periods SPLIT 3 and SPLIT 4; [Figure 5.10](#)). The vertical wind profiles reveal the existence of a strong LLJ with a peak wind maximum above the wildfire's location two and half hours before the ignition ( $19.1 \text{ ms}^{-1}$ , LLJ criterion 2). During the first few hours of the wildfire, LLJ eased to criterion 1 and remained this strength until the end of SPLIT 1 period ([Figure 5.10a](#)) and throughout the SPLIT 2 period ([Figure 5.10b](#)). At 12 UTC on 17 July the LLJ speed was  $13.0 \text{ ms}^{-1}$  between 786 m and 891 m height. As hill C has 723 m elevation, this corresponds to the plume direction at the top of this hill (upper right corner in [Figure 5.10b](#)). The LLJ was not found in this area after the SPLIT 2 period.

In general, LLJ appearance and temporal evolution in the rough topography of Mosor mountain and the one from the coastal location of Split followed the same pattern throughout the study period. However, at the location of Srinjine, LLJ was slightly weaker with higher positioned maximum. This discrepancy in height of a LLJ core between coastal and outback location is in agreement with previous studies on *bura* flow that found the center of the maximum flow higher in the outback and lower along the coast ([Lepri et al., 2015](#)). At all times at both locations, whether during the mature stage of the LLJ or in its complete absence during the periods SPLIT 3 and SPLIT 4 ([Figure 5.10c and d](#)), wind was persistently NE up to 3000 m height.

The vertical profile up to 10 km revealed that upper jet stream had a peak strength right prior to ignition ( $57.3 \text{ ms}^{-1}$ ) and during the SPLIT 1 period. At all times during the study period, wind direction throughout the troposphere was N to NE (with some exceptions in the first 1000 m height during the SPLIT 3 and SPLIT 4 periods), illustrating that this was a deep *bura* event ([Gohm and Mayr, 2005](#)). Vertical profiles of air temperature ([Figure 5.11c](#)) reveal the absence of the inversion in both lower and upper troposphere. The lower troposphere lacked the inversion at all times significant to strong *bura* flow, even during the hydraulic jump appearance. Vertical profiles of both air and dew point temperature ([Figure 5.11c, d](#)) reveal their considerably different values for the entire study period, which indicates very dry conditions. Dry conditions might be explained by the complete absence of the tropopause, which potentially led to larger vertical motion and dry air subsidence from the stratosphere. Dry upper-tropospheric air advection to the mid and lower troposphere was generated by the jet

stream dynamics situated above the study region. Vertical cross sections revealed that the dry air started to persistently dominate the fire ground after the SPLIT 1 period until the end of the study period. The presence of a ribbon of dry air (Figure 5.8b) with large potential vorticity (Figure 5.4c) suggests the translation and descent of a tropopause fold into the study area.

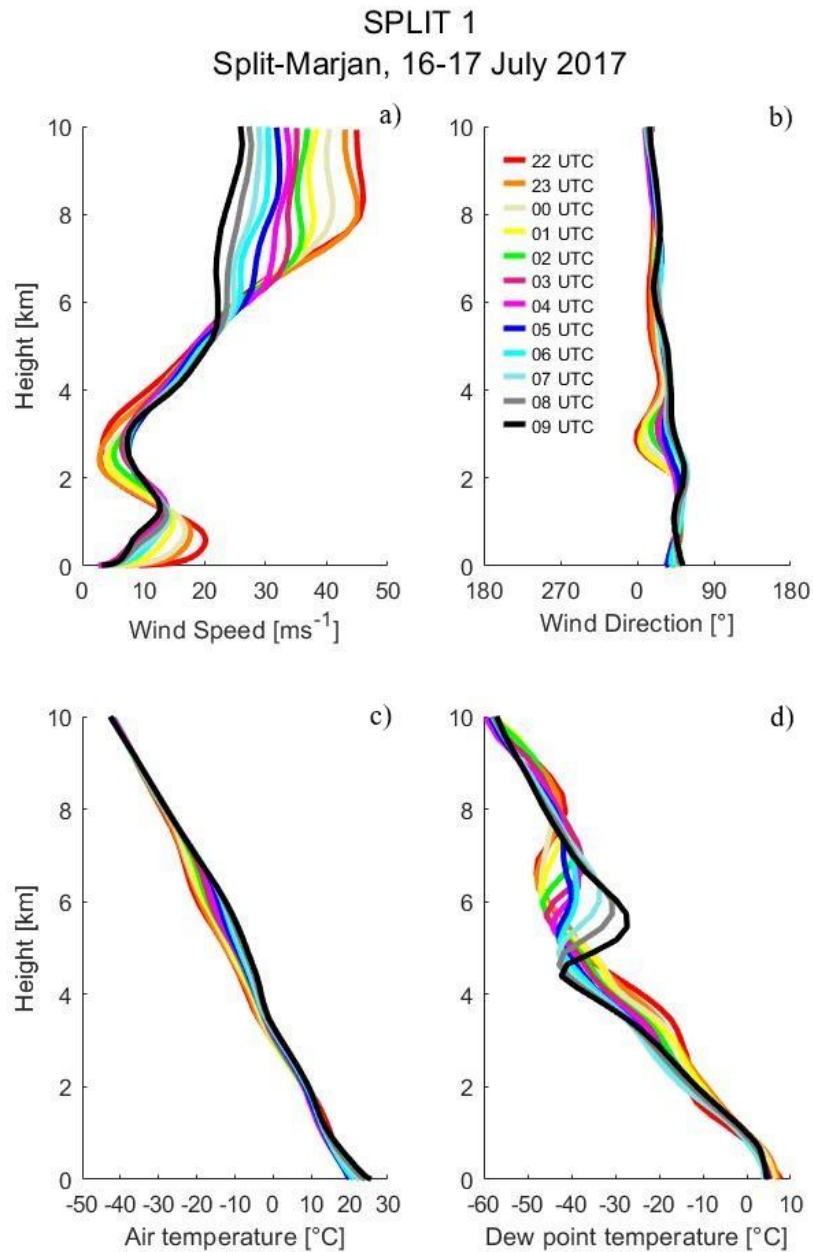


Figure 5.11. Vertical profiles of a) wind speed ( $\text{m s}^{-1}$ ), b) wind direction ( $^{\circ}$ ), c) air temperature ( $^{\circ}\text{C}$ ) and d) dew point temperature ( $^{\circ}\text{C}$ ) at Split-Marjan locations for period SPLIT 1 (from 22 UTC on 16 July 2017 to 09 UTC on 17 July 2017) from ALADIN model. See Figure 4.2 for location of Split-Marjan.

Previous studies suggested that LLJ is a weather phenomenon of considerable spatial extent (e.g., Vučetić, 1988; Gohm and Mayr, 2005), however, this conclusion was drawn from simulated vertical profiles at various locations. This is the first study to present the spatial distribution of LLJ in Croatia or, according to authors knowledge, elsewhere.

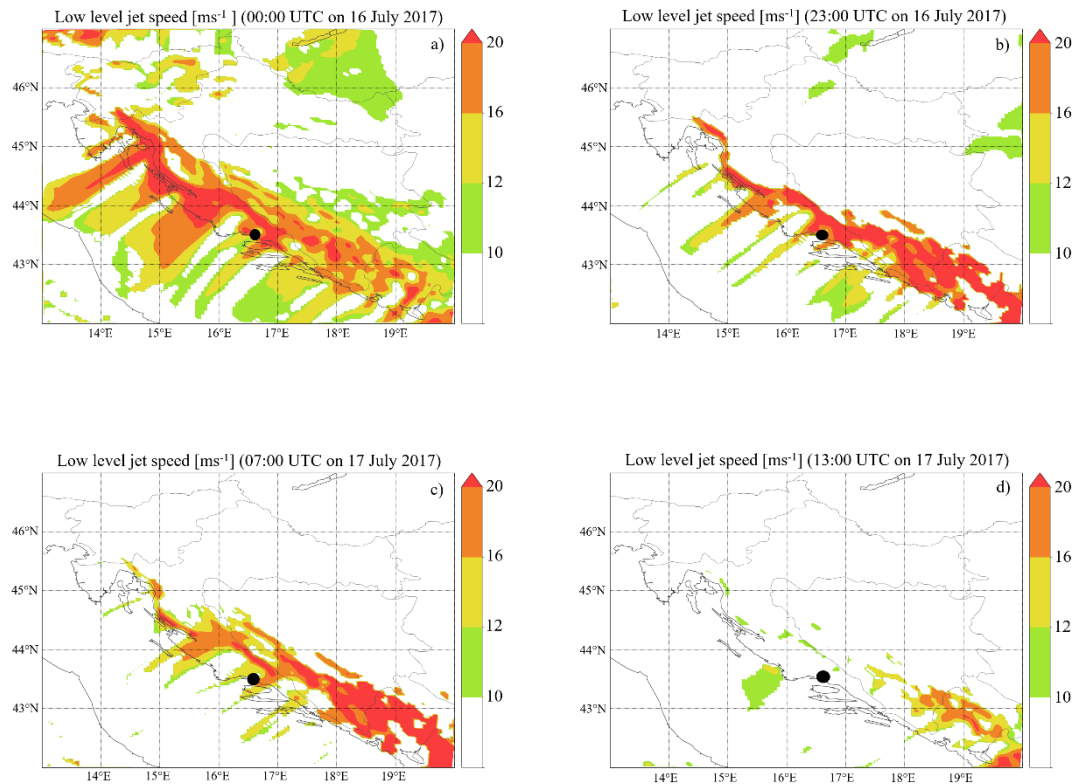


Figure 5.12. Spatial distribution of low level jet defined by criterion 0 to 3 ( $\text{ms}^{-1}$ ) at a) 00 UTC on 16 July 2017, b) 23 UTC on 16 July 2017 (SPLIT 1 period – ignition time), c) 07 UTC on 17 July 2017 (SPLIT 1 period – aircraft approach) and d) 13 UTC on 17 July 2017 (SPLIT 2 period) from ALADIN-HR44 model. Split wildfire location on charts is indicated as black dot.

The spatial extent of LLJ reveals that the strongest jet defined as criterion 3 occurred over the highest coastal mountains, extending from NW to SE, with parts of the flow stretching more than 100 km over the Adriatic Sea accompanied by wakes in between. This spatial distribution of the strongest flow and wakes between the jet wind region over Adriatic confirms the expected flow pattern formed by topographic incisions along the coast. The greatest extent of LLJ defined by criterion 3 appeared 23 h prior to the wildfire (Figure 5.12a) after which it slightly reduced its strength and coverage during the midday on 16 July before it intensified again over the entire coast in the late afternoon hours, culminating two and half hours before the ignition. The location of the wildfire during the SPLIT 1 period was situated in the wake-like region of the much stronger flow in the outback, where the LLJ defined as criterion 3

coincided with the location of the hydraulic jump that appeared in vertical cross sections. The LLJ at the wildfire's location during the morning on 17 July (end of SPLIT 1 period) was classified as criterion 1 and 2 and stretched over the valley between hills A and C, right at the time of the reported turbulence by firefighting aircraft. During the SPLIT 2 period the LLJ flow within the valley was classified by criterion 0 after which it completely disappears from the area. Although LLJ appeared at the southeastern and northwestern edge of the wildfire during the SPLIT 3 period, it gradually disappeared over the entire Adriatic region by the end of the study period or SPLIT 4.

## 5.6. Discussion and Conclusions

The Split wildfire in July 2017 was one of the most severe wildfires in Croatian history given the size, unexpected fire behavior and rapid spread, which included two downslope runs into the densely populated area of the second largest city in the peak of the tourist season. In the months leading up to the Split wildfire a prolonged period of extremely warm and dry conditions caused continuous drying of fuels in the area and an increase of the fire danger which culminated exactly on the day of the ignition. The annual maximum of FWI on 16 July 2017 at Split-Marjan station highlights the state of fuels as very dry and flammable with the possibility for rapid fire spread, multiple fire fronts and crown fire, all of which occurred during the Split wildfire. These fire weather conditions mirror the state across the rest of the Mediterranean region affected by abnormal drought and heat waves during the particularly severe and record breaking fire season of 2017 (e.g. [Turco et al., 2019](#); [Sanchez-Benítez et al., 2018](#)).

### 5.6.1. Bura and Upper-level Trough

The sequence of severe antecedent meteorological conditions, combined with the specific synoptic situation that occurred prior to the ignition, contributed to the acute fire weather in the Split area. The favorable fire weather synoptic pattern in this case included: 1) a strong surface pressure gradient caused by the presence of an Azores anticyclone stretching towards central Europe and low pressure area over the southeastern Balkans and 2) long amplitude and shortwave upper-level trough extending from the Baltic Sea to Ionian Sea with the accompanying upper-level cut-off cyclone over SE Balkans. The synchronization of the low surface pressure area with the upper tropospheric trough produced a deep northeasterly *bura* flow over the Adriatic Sea. Deep *bura* flow, in contrast to shallow *bura*, extends throughout the troposphere and is typical for colder months ([Grisogono and Belušić, 2009](#)). As aforementioned, *bura* is a gusty downslope windstorm that blows from NE quadrant

perpendicular to Adriatic coast and the adjacent Dinarides. In this case, *bura* coincided with the wildfire ignition and strongly contributed to it becoming a large conflagration. Although *bura* in this case was weaker (with mean wind speed up to  $10.5 \text{ ms}^{-1}$  and gusts up to  $19.9 \text{ ms}^{-1}$  at Split-Marjan station) and does not fulfil the criteria for severe *bura* (mean hourly speed  $> 17 \text{ m s}^{-1}$ ), it occurred during summer when such episodes are rare. *Bura* dominated the fire ground during each of the most significant wildfire progression periods.

### 5.6.2. Hydraulic Jump and Dry Air Subsidence

In general, *bura* flow over the Adriatic can be described by dynamic processes presented in hydraulic theory (Long, 1953) where orographic wave breaking plays a key role for strong surface downslope windstorm occurrence (e.g., Smith, 1985; Vučetić, 1993). The theory includes acceleration of the flow upslope as well as an abrupt acceleration of the flow downslope in the lee with a hydraulic jump gradually restoring subcritical conditions (Cesini et al., 2004). Hydraulic jump is a frequent feature of strong *bura* flow over the Adriatic (e.g., Grisogono and Belušić, 2009; Telišman Prtenjak and Belušić, 2009). Hydraulic flow is found to coincide with the Split wildfire ignition. It is marked by a wave-breaking aloft, an abrupt tilt of streamlines, accelerated wind on the leeward slopes and strong turbulence immediately above (Sharples, 2009; Whiteman, 2000; Smith, 1985; Jurčec and Visković, 1989).

Another significant finding from the Split wildfire, documented in association with severe fire weather conditions found in other catastrophic wildfires (e.g. Mills, 2008a; Mills, 2008b), is the influence of dry air subsidence. Descent of dry air occurred in conjunction with upper-level trough and jet stream dynamics above the study area. The subsidence process started 24 hours prior to the wildfire, with the dry air descending sharply towards the wildfire right at the ignition time. This dry air descent was enhanced by the topographically-induced hydraulic *bura* flow on the downstream side of Dinarides. The dry air was further transported towards the already fast-growing wildfire with the deepening of the daytime mixed layer on 17 July 2017. These processes resulted in significant reduction in relative humidity during the downslope fire runs in this case.

### 5.6.3. Low Level Jet

LLJ is of interest here not only as a phenomenon itself, but because of its effect on a wildfire behavior and aircraft operations. Previous studies suggest that LLJ is associated with turbulent kinetic energy that can be mixed down to the fireground and cause rapid fire growth (Charney et al., 2003). Early US research (Byram, 1954) described vertical profiles similar to

those found in this case as the most dangerous for fire weather, especially in the mountainous area. The reason for that lies in the intersection of the LLJ core and the elevated forested terrain, which in the case of a fire ignition can lead to blow-up fire behavior. Also, the fire behavior characteristics described for this type of wind profile include possible appearance of fire whirlwinds. LLJ was found prior the ignition and during the most significant fire runs of the Split wildfire, as well as to coincide with most extreme fire behavior in this case.

#### 5.6.4. Concluding Remarks on Fire Behavior

Based on the nexus of meteorological and fuel conditions in combination with complex topography, the most significant fire progressions during the Split wildfire from July 2017 can be explained as follows:

1) Both synoptic and upper-level conditions that coincided with the wildfire ignition are recognized to be among the most dangerous in fire weather literature. Strong surface pressure gradient with a source of dry air from the upper atmosphere that was transported to the surface by the hydraulic *bura* flow led to rapid fire growth immediately following ignition. In the first few hours of the nighttime SPLIT 1 period, strong NE *bura* pushed the fire downhill on south facing slopes of hill C (Figure 4.2), into the valley, where the fire was eventually stopped by firefighters. Wildfire also burned upslope on hill C for two reasons. The first is due to buoyancy effects on flames and smoke between *bura* gusts and the second is potentially due to eddies and rotors in the lee, under the accelerated LLJ stream embedded in the *bura* flow (e.g., Gohm et al., 2008; Telišman Prtenjak and Belušić, 2009).

2) The complexity of the flow at the wildfire's location was especially pronounced during the SPLIT 2 period (Figure 4.3d). The sudden fire reactivation and its run downhill of C (Figure 4.4) surprised firefighter crews who had to redefend settlements in the valley that had been considered safe from the fire burning at higher altitude. Why the fire front could return into the valley and burn upslope on hills B, and afterwards A, may again be explained by the vertical wind profile, which revealed lowering of both LLJ speed and height. By lowering its height, the core of LLJ now coincided with the top of the hill C where the wildfire was burning. As wind dropped in speed it may have resulted in more laminar and attached flow over the terrain which therefore pushed the fire again downslope of hill C with flying embers creating a mosaic fire in the valley. The LLJ weakening is related to daytime *bura* weakening, typical for a *bura* episode in its decaying stage (e.g., Gohm and Mayr, 2005) as was the case during the SPLIT 2 period.

3) The total fire escalation around all zones occurred during relatively benign fire weather conditions. *Bura* weakened by the beginning of the SPLIT 3 period (Figure 5.7c) and the firefighting aircraft could join the intervention. However, the location of the wildfire at the time together with local atmospheric conditions are likely to be crucial for the rapid downslope fire run into the city area. By the beginning of the SPLIT 3 period, the NW flank of the wildfire (Figure 4.2) burned into abundant dry fuels on the city edge on the slopes of Mosor. Covered by dense pine forest and long unburnt fuels this elevated terrain was aligned with the *bura* flow. The NE *bura* was still moderate to strong in this elevated area, contributing to a channeling effect and pushing the fire down the SW oriented slopes, towards Split. Such dynamic fire channeling is considered impossible to control due to high fire spread rate and intensity (Sharples, 2009), as was the case in this event. Furthermore, the rugged terrain with favorable fire weather and plenty of dry fuel available caused fire whirls and spotting. Simultaneously, mosaic fire that was still flanking in the higher elevated valley between hills A and C on the eastern side of the wildfire (Figure 4.2) merged into a single fire front. Intensification of the wildfire on this side was most likely caused by burning into heavier fuels and turbulent effects associated with the LLJ that persisted in the surrounding mountainous area.

4) Another downslope fire run during the nighttime SPLIT 4 period are presumably associated with moderate *bura* in the area (Figure 5.7d) which pushed the wildfire over the top of hill A towards its southern side (Figure 4.2). Its downslope run was therefore amplified by *bura* and additionally favored by nighttime reduction in relative humidity, most likely caused by dry upper tropospheric air drawn down to the surface by the daytime mixed layer during the previous fire progression period SPLIT 3. Furthermore, on its downslope path the fire burned into downy oak forest resulting in significant fire escalation before it reached the urban area in the foothill of A in a matter of minutes (Figure 4.8a and b). Again, such fire behavior is extremely dangerous for firefighters, communities and assets in the path of such a rapidly advancing downslope fire.



## CHAPTER 6

### THE FORCETT-DUNALLEY WILDFIRE IN TASMANIA

#### *6.1. Wildfires in Tasmania*

Tasmania, the island state of Australia, shares a history of frequent wildfire events with the mainland. Situated 240 km south of the continent between 41°S–44°S and 145°E–149°E (Figure 6.1.a), the island's topography includes mountainous region and a high plateau extending from the central west to southeast, where some peaks higher than 1200 m, like Mt Wellington on the edge of the state's capital city of Hobart, approach the coastline. The eastern and southeastern coastline is additionally extended by numerous narrow peninsulas with undulating terrain. Tasmania is surrounded by more than thousand islands. The vegetation of the main island is dominated by dry eucalypt forests in the east, wet eucalypt forests in the north, west and far south and agricultural grasslands in the inland east. The southwest part of the state is declared as the Tasmanian Wilderness World Heritage Area containing endemic vegetation.

Fire plays an important role in Tasmania's ecosystem. Some native flora in Tasmania recovers well from fire or even relies on fire for regeneration (Yospin et al., 2015; French et al., 2016; Kirkpatrick et al., 2018). For thousands of years fire has been used by Indigenous people for land management purposes, maintaining biodiversity and hunting (Marsden-Smedley, 2014). These practices have been inherited by European settlers and used in 19<sup>th</sup> and most of the 20<sup>th</sup> century (Von Platen et al., 2011). The tradition was gradually abandoned, especially after several disastrous fire seasons and catastrophic wildfires. For example, during fire seasons of 1897-98 and 1933-34 approximately 2 000 000 ha (a third of the state) and 1 000 000 ha, respectively, were burnt. The deadliest wildfire that occurred in Tasmania to date entered the city of Hobart, killed 62 people, destroyed 1400 buildings and burnt 250 000 ha, mostly in a single day on 7 February 1967 (Marsden-Smedley, 2014).

The main causes of wildfires in Australia are together lightning strikes and human activities, with number of ignitions caused by lightning strikes increasing in the recent decades (Zylstra, 2018). Recent studies suggest that most wildfires in Tasmania to date are still human-caused (Nampak et al., 2021). In the period between 2011 and 2019 ignition causes were classified as accidental (25%), deliberate (11%), planned burn (22%), undetermined (36%), and lightning induced (7%). However, despite being the least frequent of the ignition sources,

lightning was responsible for 53% of the state's total burned land throughout the period (Nampak et al., 2021).

The peak fire weather in Tasmania occurs in late summer and early autumn (Luke and McArthur 1978), however, recent studies also revealed a springtime peak in fire danger, which appears approximately once every two years (Fox-Hughes, 2008). The most fire-prone area is the southeast of the state (Fox-Hughes, 2008). The average burnt area in the period 2002–2011 was 51 920 ha in 65 wildfires per year. The burnt area escalated in fire season 2012-13 when 128 wildfires burnt 119 267 ha. The most catastrophic wildfire of that season, and in the last five decades, was the Forcett-Dunalley wildfire in January 2013 (Marsden-Smedley, 2014).

## 6.2. Forcett-Dunalley Wildfire

The Forcett-Dunalley wildfire started from an accidental ignition at 14 AEDT (UTC + 11 h) on 3 January 2013 in the rural locality of Forcett, 35 km northeast of Hobart, the state's capital. The Forcett-Dunalley wildfire was one of four fires ignited accidentally or by lightning on the same day (Figure 6.1.a, Table 6.1.). Although it was not the largest considering final burnt area, this wildfire threatened people's lives and almost completely destroyed the township of Dunalley. The fact that this wildfire burned 25 950 ha, mostly in only 6 hours (Marsden-Smedley, 2014; Ndalila et al., 2018) and produced pyrocumulonimbus (pyroCb), the first on record in Tasmania (Ndalila et al., 2019), point towards extreme fire behavior and, together with the rest of the severe wildfires that burned almost 87 000 ha statewide (Table 6.1.), to extreme fire weather conditions during this event. In this context, Forcett-Dunalley wildfire presents an opportunity to study some of the most severe fire weather recorded to date in Tasmania.

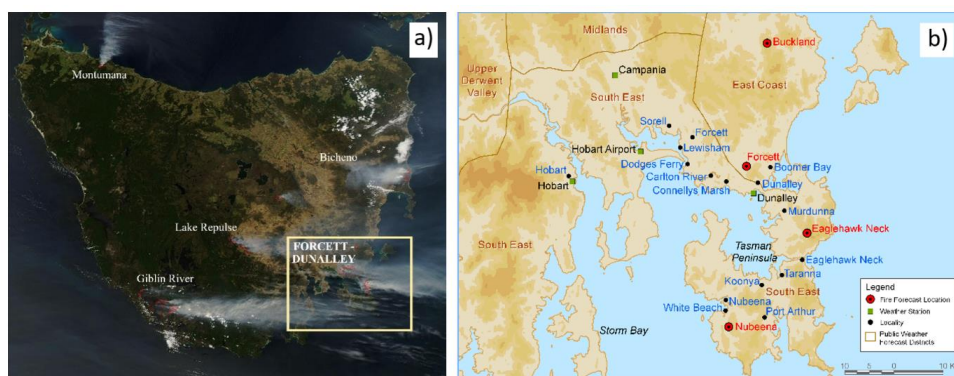


Figure 6.1. a) Satellite image of Tasmania with noted area of interest and smoke plumes visible from the MODIS Aqua satellite on 5 January 2013 (Image: MODIS Rapid Response, NASA) and b) weather station locations and localities in the Forcett-Dunalley area (BoM, 2013a).

The Forcett-Dunalley fire lasted 16 days, from 3 to 18 January 2013, but was declared completely extinguished only on 20 March 2013. The wildfire quickly gained global media attention ([The Guardian, 2013](#)). It destroyed or damaged 431 properties, including primary school and police station in Dunalley and forced people to jump into sea to avoid death. One firefighter involved in the intervention lost his life, but not as a direct result from a fire. The wildfire burnt 25 950 ha of native forests, agriculture land, forest plantations, more than 660 km of commercial fencing and killed 10 000 livestock, mainly sheep. The Forcett-Dunalley wildfire had negative effect on businesses including tourism, livestock farming, agriculture, seafood industries etc. The total financial cost of Tasmanian wildfires from January 2013 is estimated at US\$ 71.9 million, without emergency response and recovery operations costs ([Marsden-Smedley, 2014](#)).

Table 6.1. Summary of five wildfires started from 3 to 5 January 2013 in Tasmania.

FIRE	LAKE REPULSE	FORCETT-DUNALLEY	GIBLIN RIVER	BICHENO	MONTUMANA
IGNITION CAUSE	Escaped campfire	Re-ignition campfire	lightning	lightning	lightning
IGNITION TIME (AEST)	11:30 3.1.2013.	14:00 3.1.2013.	afternoon 3.1.2013.	approx. 20:00 3.1.2013.	approx. 08:00 5.1.2013.
CONTAINMENT	18.2.2013.	18.1.2013.	22.1.2013.	9.1.2013.	20.1.2013.
BURNT AREA	10637 ha	25950 ha	45124 ha	4939 ha	3158 ha
FINAL PERIMETER	121.5 km	310 km	387 km	41.3 km	28.5 km

The wildfire occurred in southeast Tasmania ([Figure 6.1a](#)), along the highly indented coastline with numerous peninsulas, bays and islands. Topography of the region is notable for its undulating terrain, with mean slopes  $> 10^\circ$  ([Ndalila et al., 2018](#)). The wildfire mostly burned in a southeasterly direction from its ignition location in Forcett. The hills around Forcett and Dunalley, as well as on the nearby Forestier and Tasman Peninsulas southeast of these townships, are approximately 200 m to 400 m high. Similar undulating, but higher elevated terrain is situated northwest of the ignition location with hills between 500 m and 750 m a.s.l. The landscape is dominated by dry and wet *Eucalyptus* forests, dry sclerophyll forests, scattered agriculture with a minor component of *Pinus radiata* plantations ([Ndalila et al., 2018](#)).

The Forcett-Dunalley wildfire is defined as a megafire ([Ndalila et al., 2018](#)) according to earlier described criteria ([Cruz et al., 2012](#)) for a wildfire exhibiting extreme behavior, causing vast environmental damage, large burnt area and property destruction. The violent pyroconvective storm, the only known case to date in Tasmania ([Figure 6.2.](#)), occurred in less than an hour, reaching 15 km height and causing at least two lightning strikes ([Ndalila et al.,](#)

2018). The Forcett-Dunalley wildfire was described by firefighting pilots ‘like nothing ever seen before’ and behaving in a way they didn’t think it could ([The Guardian, 2013](#)).

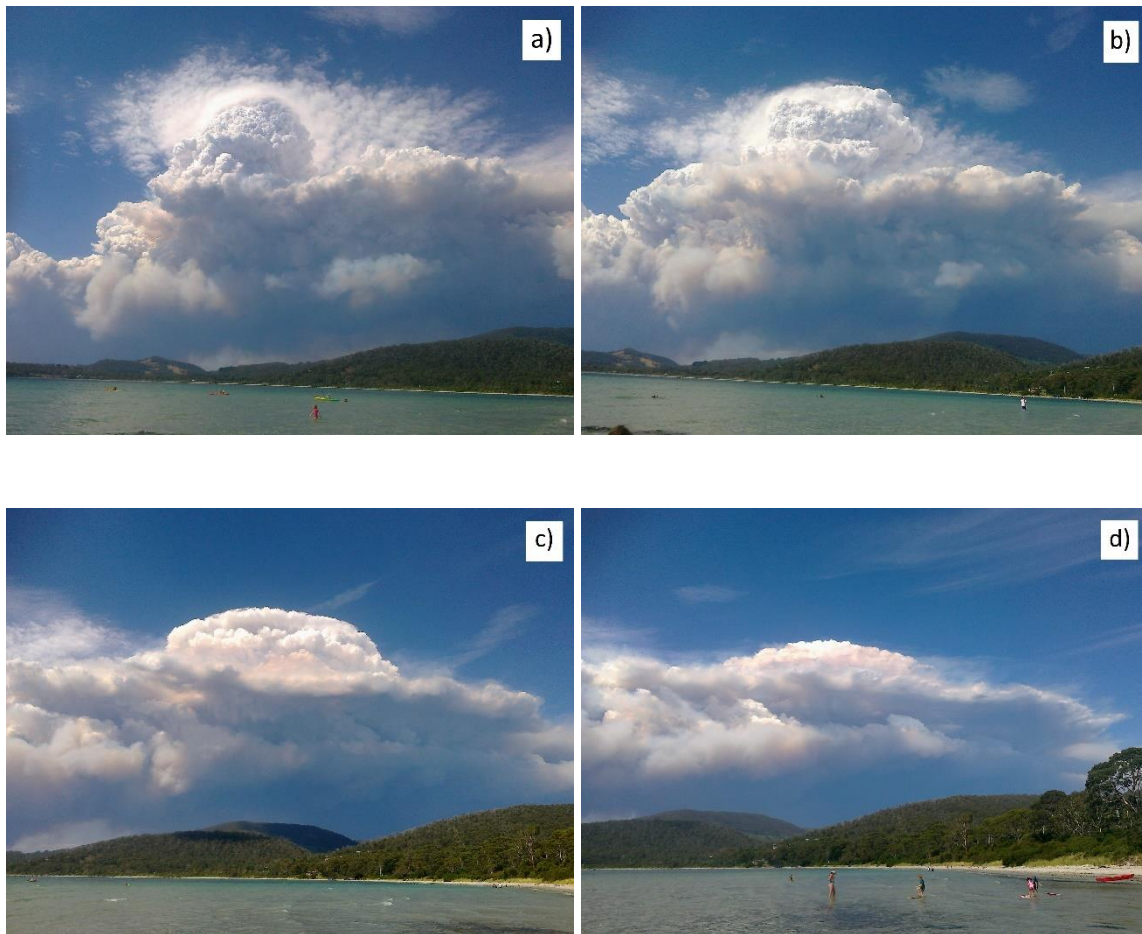


Figure 6.2. Pyrocumulonimbus occurred during the Forcett-Dunalley wildfire at about 15:55 AEDT on 4 January 2013 (photo by Janice James).

For the purpose of this study the first 82 hours of the Forcett-Dunalley wildfire will be noted as DUNALLEY from 1 to 3. The DUNALLEY 1 will refer to first 23 hours of the wildfire, or a period from the re-ignition on 3 January to midday on 4 January, immediately before the escalation in fire activity. The DUNALLEY 2 period will refer to the violent firestorm that occurred in the afternoon hours on 4 January. The third and final period DUNALLEY 3 will refer to change in fire front direction on 5 January and back-burning on 6 January. The time zone used in the wildfire description and further meteorological analysis is Australian Eastern Daylight Time (AEDT), which is UTC + 11 h.

#### *6.2.1. Burn Period Dunalley 1: 14 (3 January) – 12 AEDT (4 January)*

The Forcett-Dunalley wildfire started as a re-ignition from a campfire that had been lit inside an old tree stump on 28 December 2012. In following days most probably a slow

combustion took place within tree roots in very dry soil, until fire reached the surface and wind lifted embers and spread the fire in nearby grass (BoM, 2013a). The official cause of the Forcett-Dunalley wildfire is declared to be an accident.

From the time of the re-ignition at 14 AEDT on 3 January near the locality of Forcett, the fire progressed in southeast direction, down the slope of 5°, with an average speed from 6 to 8 m min<sup>-1</sup>. Within an hour the fire burnt 2.5 ha and had a perimeter of 0.7 km. Flame height was up to 5 m, and spotting reached distance to 2.5 km. In the period between 15 and 17:30 AEDT fire progressed eastwards increasing spread rate up 43 m min<sup>-1</sup>. By 17:30 AEDT, or 3.5 hours after the ignition, the fire travelled 5.9 km, burned 506 ha and had a perimeter of 14 km.

During the night between 3 and 4 January the fire activity eased. Although it continued to burn southeast, its overnight spread rate decreased to 2 m min<sup>-1</sup> and the uncontained southeastern fire front decreased to 12 km in length. The next significant change in fire behavior occurred in the early morning on 4 January. While still slowly progressing south, by 06:45 AEDT the burnt area increased to 973 ha and fire perimeter to 19.6 km. After this time fire persistently increased its spread rate and intensity and by 12:30 AEDT had a size of 1586 ha with perimeter of 21.7 km (Figure 6.4.a).

#### 6.2.2. Burn Period Dunalley 2: 13 – 23 AEDT (4 January)

The fire activity escalated after 13 AEDT on 4 January 2013. In following hour and half the fire tripled in size, doubled a perimeter and increased its speed rate to 58.3 m min<sup>-1</sup>. By 14:30 AEDT, 24 hours after the ignition, the wildfire had size of 5819 ha and perimeter of 42.8 km (Figure 6.4.b). Fire was further progressing southeast, mainly as a high intensity crown fire. Fire intensity, which is determined by fire spread rate, fuel height and fuel load, was estimated at 30 000 kW m<sup>-1</sup>. According to known categorizations the fire intensity between 7000 and 70 000 kW m<sup>-1</sup> with flame height >15 m classifies a fire as complete crown fire, essentially unstoppable, with firestorm conditions (if reaching an upper limit of fire intensity; Cheney, 1991). Nevertheless, more detailed analysis (Ndalila et al., 2018) found that the fire intensity in the case of the Forcett-Dunalley wildfire during the six-hour period, between 16 AEDT and 22 AEDT, was even higher and reached 68 571 kW m<sup>-1</sup>. This was estimated for the periods when severe fire weather conditions (according to FFDI value) coincided with fire spreading in the wind direction and in the upslope trajectory burning through dry *Eucalyptus* forests. To put this into perspective, during the most catastrophic fires in Australian history, the 2009 Black Saturday fires, fire intensity reached 88 000 kW m<sup>-1</sup> (Cruz et al., 2012).

The additional proof of extreme fire behavior in the case of Forcett-Dunalley wildfire is the appearance of violent pyroconvection. Pyroconvection can be manifested as pyrocumulonimbus (pyroCb) cloud, which in Australia had been confirmed in 65 fire cases to 2019 (Ndalila et al., 2019), noting that during the 2019-20 southeastern Australian "super outbreak" an additional 38 pulses of pyroCb activity occurred (Peterson et al. 2021). PyroCb in the case of Forcett-Dunalley wildfire is the first and only known in Tasmania (Figure 6.2.). The evolution of PyroCb occurred between 13 AEDT and 17 AEDT on 4 January 2013 and was captured by the nearby weather radar operated by the Bureau of Meteorology (BoM; Soderholm et al., 2019). This Doppler radar is located at the Mt Koonya on the Tasman peninsula (Figure 6.1.b), only 24 km south of Dunalley, which made it ideal for pyroCb tracking in this case. The plume height increased from 1 km at 13 AEDT to 8 km at 15 AEDT, after which the convection column rapidly increased and in only 30 minutes reached 15 km height. The peak of violent pyroconvection with the injection of smoke into the stratosphere at the maximum height of 15 km lasted for 18 minutes, between 15:30 AEDT (Figure 6.3.a) and 15:48 AEDT. The thunderstorm developed within this time and moved southeasterly over the Tasman Sea, culminating with two lightning strikes around 16:10 AEDT (BoM, 2013a). The precipitation captured by the radar occurred in higher altitudes, but evaporated before reaching the ground. The cool air as a result from this evaporation descended towards the surface and caused erratic winds and gusts that impacted the fire ground.

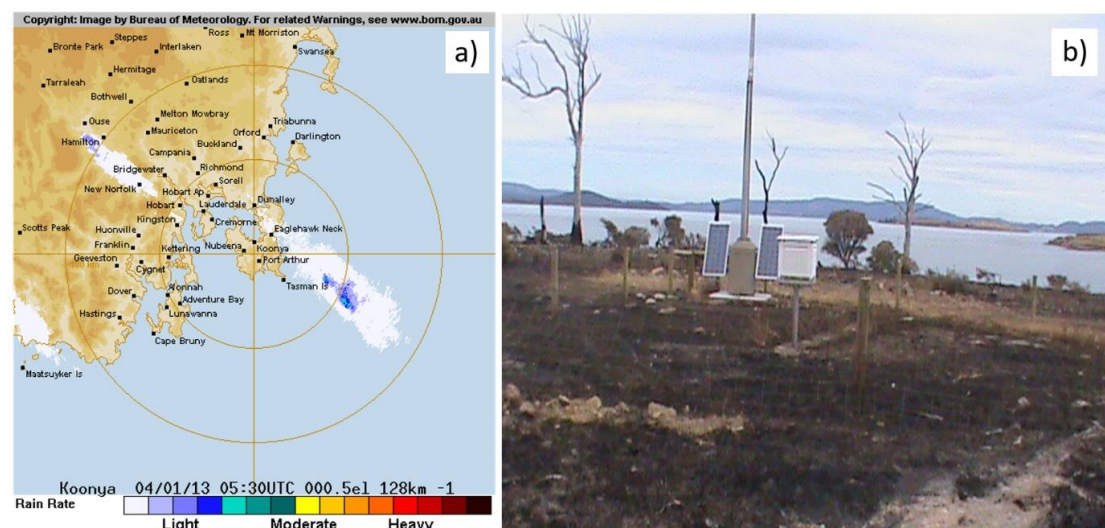


Figure 6.3. a) Smoke visible from radar image at 15:30 AEDT from Mt Koonya radar and b) weather station enclosure in Dunalley burnt in the wildfire between 16:19 AEDT and 18:06 AEDT on 4 January 2013 (BoM, 2013). Mt Koonya Doppler radar and weather station are operated by BoM.

The peak pyroconvection coincided with the fire arrival in Dunalley at 15:25 AEDT. Beforehand fire travelled more than 15 km in just two hours ([The Guardian, 2013](#)). The arrival of the wildfire in Dunalley was accompanied by ember storm, which caused multiple spot fires throughout the town and forced evacuation. Multiple aircraft water bombing the fire could not contain it. After good flying conditions in the early morning, firefighting pilots reported worsening of the conditions in the afternoon due to smoke, heat and the wind strengthening. Upon arrival in Dunalley, the fire spread rate was 45 to 50 m min<sup>-1</sup>. The plume from the wildfire extended in southeast direction over the Tasman Sea and its height decreased to 7 km by 16:42 AEDT, after which the pyroCb most likely dissipated. After 17 AEDT the plume stabilized its height at 3 km and, as seen from satellite ([Figure 6.1.a](#)) and radar images ([Figure 6.3.a](#)), had a persistent southeast direction until the end of the day. After arriving in Dunalley fire at one point easily crossed more than 3 km of open water ([The Guardian, 2013](#)) and narrow land neck that connects Forestier Peninsula with the rest of Tasmania before it continued flanking over the peninsula in a southeasterly direction. Along with a third of the Dunalley township wildfire also damaged the weather station operated by the BoM ([Figure 6.3.b](#)), strongly affecting the temperature records ([BoM, 2013a](#)).

Around 17:30 AEDT, while progressing across the Forestier peninsula, a probable minor wind change slightly turned fire direction from southeast to south-southeast and pushed the fire towards already hazard reduced dry forest east of the Murdunna township ([Figure 6.1.b](#)), which explains why there was fewer houses lost in comparison to Dunalley. Between 17:30 AEDT and 20 AEDT the fire had an average spread rate of 32.4 m min<sup>-1</sup> and during this time period the burnt area increased from 9623 ha to 13 277 ha, and perimeter from 93.6 km to 146.8 km.

By 23 AEDT the wildfire reached Eaglehawk Neck, the southernmost locality in the Forestier peninsula and spotted across the bay onto the Tasman Peninsula ([Figure 6.1.b](#)). This spotting occurred over a distance of approximately 2.5 km. By the end of this progression period, the wildfire had size of 15 322 ha and a perimeter of 166.9 km. Overall, in 11 hours the wildfire progressed approximately 27 km ([Figure 6.4.c](#)).

### 6.2.3. Burn Period Dunalley 3: 5 January – 6 January 2013

Between 01 AEDT and 02 AEDT on 5 January wind change stopped the wildfire progression towards southeast and turned the fire front in east-northeast direction. By 20:30 AEDT the same day fire was 19 692 ha in size with perimeter of 246.6 km.

Large scale back-burning occurred on 6 January northeast of ignition location in Forcett. The burnt area by 21 AEDT on 6 January was 20 981 ha with a perimeter of 269.1 km. The majority of total fire area burned by this time. Only small additional areas burned until the wildfire was contained 16 days after the ignition, on 18 January 2013 (Figure 6.4.d).

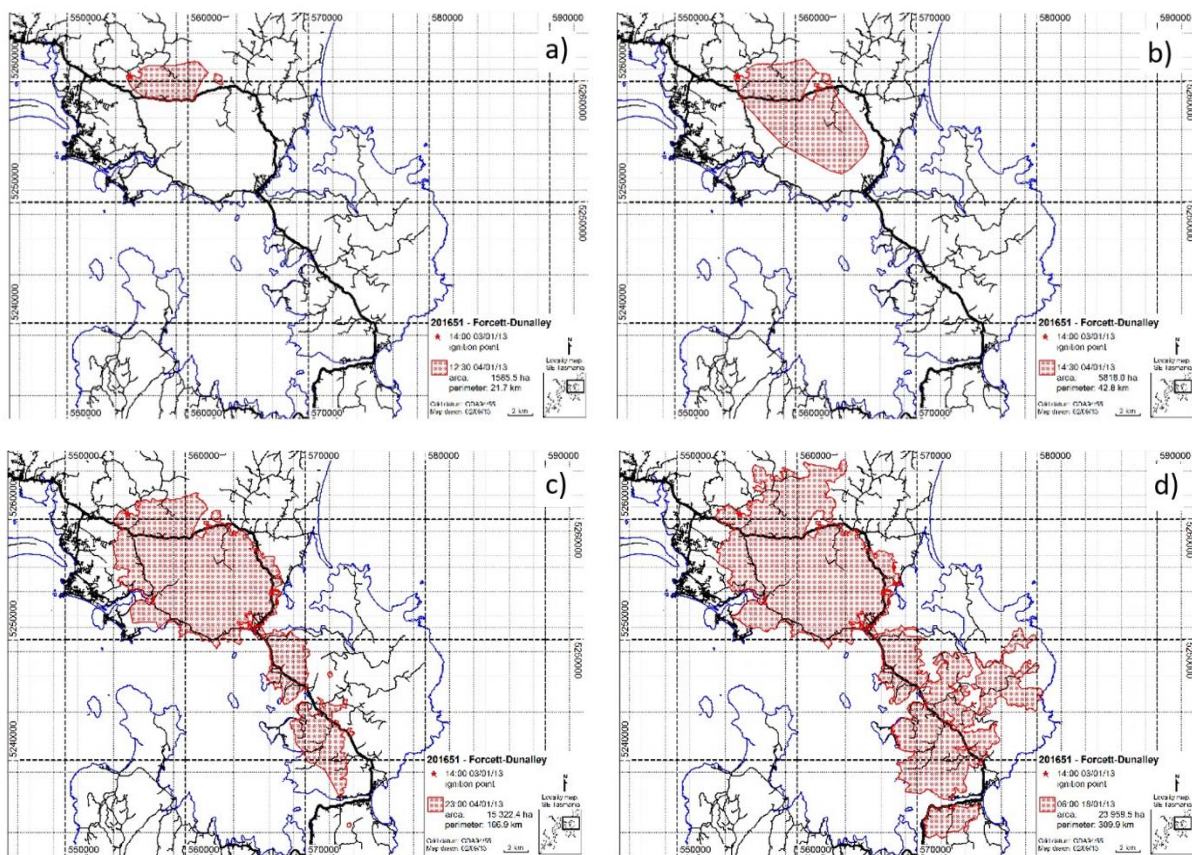


Figure 6.4. Map of the Forcett-Dunalley wildfire with the final perimeter and three prominent progressions in growth. Burnt area a) by the end of DUNALLEY 1 period, b) at the beginning of pyroconvection in the DUNALLEY 2 period, c) by the end of DUNALLEY 2 period and d) after wildfire's containment on 18 January 2013. Ignition location is noted as red star. Images credit: Dr Jonathon Marsden-Smedley, as part of work completed for the Bushfire and Natural Hazards Co-operative Research Centre.



The meteorological analysis in the Chapter 7 aims to address the following questions:

1. Which antecedent weather conditions contributed to the Forcett-Dunalley wildfire?
2. Which fire weather conditions coincided with the ignition of the wildfire?
3. Which weather conditions followed the ease in fire activity in nighttime between 3 and 4 January, as well as the conditions contributing to change in fire behavior in the morning on 4 January (the DUNALLEY 1 period)?
4. Which upper-level atmospheric conditions enabled the violent firestorm development and allowed pyroconvection to evolve to extent it was observed in this case during the afternoon on 4 January (the DUNALLEY 2 period)?
5. Which weather conditions caused the change in the fire front direction and back-burning on 5 and 6 January (the DUNALLEY 3 period)?

## CHAPTER 7

### FORCETT-DUNALLEY WILDFIRE – METEOROLOGICAL ANALYSIS

#### 7.1. Climatological Analysis

Long term antecedent conditions in the decade prior to Forcett-Dunalley wildfire (from hereafter Dunalley wildfire) in Tasmania are characterized as drier and warmer than average (BoM, 2013a). From 2003 to 2012, total rainfall in the Dunalley area was very much below average comparing to 10-year periods from 1900 to 2011. Although altogether rainfall deficiency was more frequent, in some years it was not that extreme. For example, the total rainfall in the eastern part of Tasmania in 2009 and 2011 was above or very much above average (BoM, 2013a). These infrequent, yet relatively wet, conditions most likely contributed to vegetation growth in the Dunalley area before the wildfire in January 2013.

Short term antecedent conditions included total rainfall below average (Figure 7.1a, From: <http://www.bom.gov.au/climate/>) and air temperature above average (Figure 7.1b, C1b) for most of the Australian continent in months prior to the Dunalley wildfire. From October to December 2012 rainfall deficiency is evident for most of eastern Australia, including Tasmania (Figure C1a), where the total 3-month rainfall in the Dunalley area was below average which contributed to drying out fuels immediately prior to the wildfire.

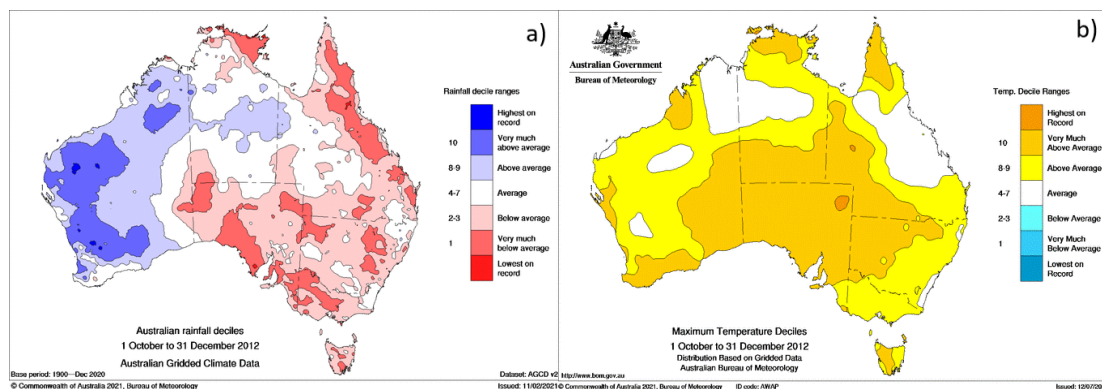


Figure 7.1. a) Rainfall deciles and b) maximum temperature deciles for Australia for the period from 1 October to 31 December 2012 (BoM).

Last months of 2012 were very much above average considering maximum daytime temperature (Figure 7.1b). The culmination of the prolonged warmer than average period was an extreme heatwave that occurred between 25 December 2012 and 19 January 2013. This heatwave was characterized by its unusual spatial extent and duration of high air temperature. A new record for the hottest day for Australia as a whole was set on 7 January 2013, with an averaged maximum temperature of 40.3°C (previous record of 40.17°C was set on 21 December

1972). Furthermore, the area-averaged temperature for Australia exceeded 39°C for seven consecutive days, from 2 to 8 January 2013. To put this into perspective, until 2013 there had been only 21 days in 102 years when the averaged maximum air temperature exceeded 39°C. Overall, January 2013 was the hottest month on record in Australia with both mean and maximum air temperature setting record of 36.92°C and 39.68°C, respectively, which is 2.28°C and 1.77°C above the average from the climatological period 1961–1990 (BoM, 2013b).

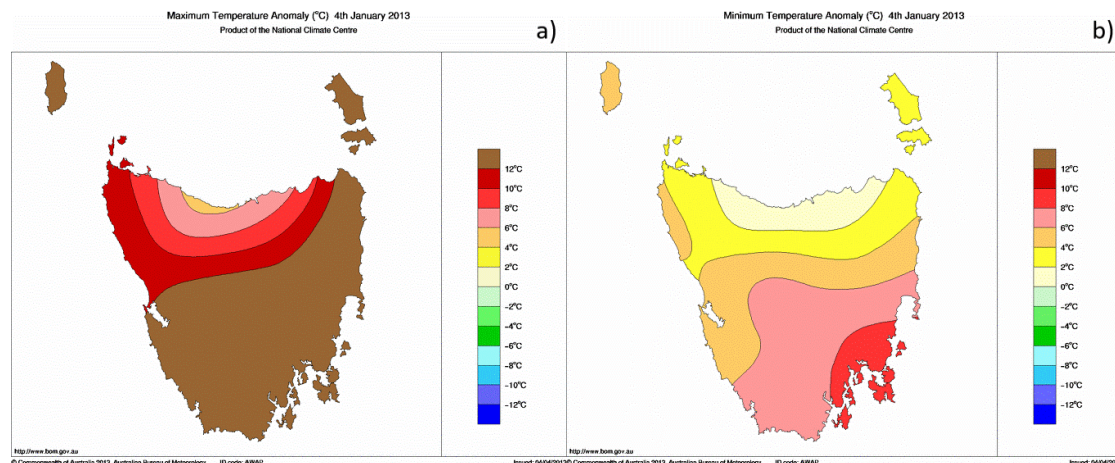


Figure 7.2. a) Maximum air temperature anomaly and b) minimum air temperature anomaly for Tasmania on 4 January 2013 (National Climate Centre, BoM).

The culmination of the heatwave in Tasmania occurred on 3 and 4 January 2013, the first two days of the Dunalley wildfire. The maximum air temperature anomaly on both days was 12°C above average (Figure 7.2a and C2a), with the minimum air temperature anomaly 8°C above average on the morning of 4 January 2013 (Figure 7.2b and C2b).

## 7.2. Fire Danger Rating

The long-term lack of precipitation accompanied by the extreme heatwave in transition between December 2012 and January 2013 led to the increase in the Forest Fire Danger Index (FFDI) and Forest Fire Danger Rating (FDR) in Tasmania at the beginning of January 2013. FFDI index gives information on fire danger characteristics on 1-hour and 1-minute basis throughout a day. In contrast, FWI, which is operationally used in Croatia, provides the information on fire danger rating only for the warmest part of a day (at 12 UTC).

According to 1-hour FFDI values, Hobart and Campania stations recorded a catastrophic fire danger rating in the afternoon on 4 January 2013 (Table 7.1). The catastrophic range occurred at 15 AEDT, coinciding with the violent pyroCumulonimbus (pyroCb) development within the DUNALLEY 2 period (from 13 AEDT to 23 AEDT on 4 January

2013). At Hobart station FFDR was set at very high danger rating since the early morning on 4 January, and held this or even higher danger rating class for the rest of the day.

Table 7.1. Forest Fire Danger Rating (FFDR) and Forest Fire Danger Index (FFDI) at Hobart, Hobart airport, Dunalley and Campania for in the period from 05 AEDT to 23 AEDT on 4 January 2013. Data outages were at Hobart and Dunalley stations between 17 and 18 AEDT. Unavailable data at Dunalley station refer to time when wildfire burnt in close proximity to the automatic weather station.

	HOBART		HOBART airport		DUNALLEY		CAMPANIA	
<i>Time (AEST)</i>	<i>FFDR</i>	<i>FFDI</i>	<i>FFDR</i>	<i>FFDI</i>	<i>FFDR</i>	<i>FFDI</i>	<i>FFDR</i>	<i>FFDI</i>
05:00	Very High	25	Low-Moderate	9	Low-Moderate	5	High	14
06:00	Very High	26	Low-Moderate	7	Low-Moderate	6	High	14
07:00	Very High	29	Low-Moderate	10	Low-Moderate	7	Low-Moderate	11
08:00	Very High	32	High	12	Low-Moderate	9	High	12
09:00	Very High	31	High	14	Low-Moderate	10	High	17
10:00	Very High	30	High	15	Low-Moderate	9	High	21
11:00	Very High	29	Very High	25	Low-Moderate	9	Very High	36
12:00	Severe	74	Very High	39	High	20	Severe	57
13:00	Severe	72	Extreme	93	Very High	25	Extreme	77
14:00	Extreme	77	Severe	66	Severe	56	Extreme	75
15:00	Catastrophic	112	Severe	69	Severe	72	Catastrophic	112
16:00	Extreme	81	Extreme	77	Severe	70	Extreme	85
17:00	n/a	n/a	Extreme	76	n/a	n/a	Extreme	88
18:00	Severe	54	Severe	56	n/a	n/a	Severe	53
19:00	Very High	45	Severe	56	Severe	63	Very High	46
20:00	Very High	33	Very High	39	Very High	38	Very High	38
21:00	Very High	30	High	22	Very High	35	Very High	25
22:00	High	22	Very High	28	High	21	High	19
23:00	Very High	25	Very High	26	Very High	26	High	21

In Tasmania, a very high fire danger rating class is used as an indicator of potentially dangerous fire weather and has an operational importance for issuing fire weather warnings. Also, FFDI > 50 or severe rating (Table 3.3) is considered a rarity in Tasmania (Fox-Hughes, 2008). During the second day of the Dunalley wildfire FFDI exceeded this value from 12 AEDT (end of DUNALLEY 1 period) until evening hours (DUNALLEY 2 period). According to previously defined fire behavior in relation to FFDI value, if exceeded 50, fire suppression is considered impossible due to the potential for sudden changes in fire behavior (Table 3.3.; Vercoe, 2003). Also, any suppression efforts would only increase the fire activity and the burnt

area. The maximum FFDI in this event reached 112, which is close to the all-time FFDI record for Tasmania that occurred on 7 February 1967, known as Black Tuesday, the most catastrophic day of the deadly wildfire near Hobart. The absolute record of FFDI in Tasmania during the Black Tuesday peaked at 128 (Fox-Hughes, 2008).

More detailed insight into the FFDR gives 1-minute FFDI data for selected meteorological stations (Figure 7.3.). Available data confirms a diurnal variability in fire danger rating with its broad increase in the midday on 4 January 2013, the second day of the wildfire. The rapid ‘spike’ in FFDI values occurred after 11 AEDT, and peaked within the DUNALLEY 2 period at all stations – at Hobart airport at 13:10 AEDT, in Hobart at 14:30 AEDT, Campania at 15 AEST and latest in Dunalley at 15:38 AEDT, when it reached the catastrophic fire danger rating which again corresponds with the time of the peak PyroCb activity. The 1-minute FFDI values also reveal that catastrophic value, 100 and higher, has been reached multiple times outside the synoptic observation hours at most of the stations.

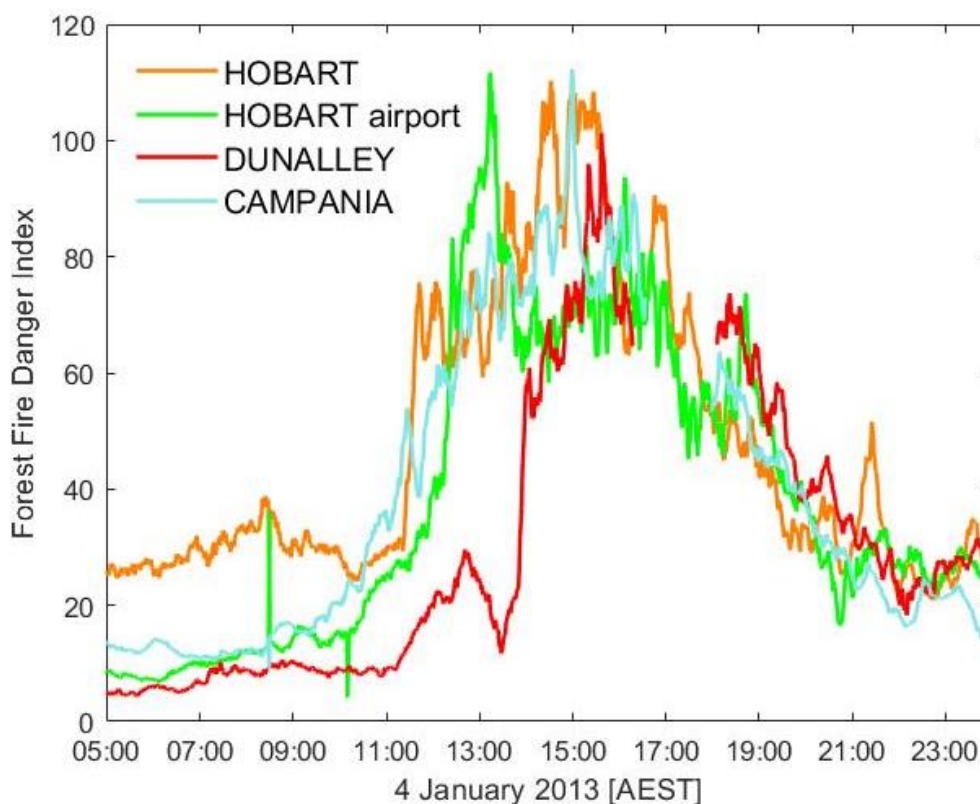


Figure 7.3. Forest fire danger index (FFDI) at Hobart, Hobart airport, Dunalley and Campania based on 1-minute air temperature, dew point temperature and wind speed averaged over 10-minutes for the period from 05 AEDT to 23 AEDT on 4 January 2013. Values between 16:19 AEDT to 18:06 AEDT on 4 January 2013 at Dunalley station are officially omitted due to corrupted measurements when the wildfire affected instruments.

### 7.3. Surface Synoptic Conditions

Important fire weather synoptic conditions in the case of the Dunalley wildfire included anticyclone situated over the Tasman Sea, northeast of the state, and an approaching cold front, west of the state. In days prior to ignition, from 1 to 3 January 2013, the high pressure anticyclone moved across the Great Australian Bight and over southeast Australia towards the Tasman Sea (Figure 7.5.a), i.e. from the northwest to the northeast of Tasmania. This caused a strong north to northwesterly flow of hot and dry air to blow off the central Australian mainland towards southeast of the continent, including Tasmania. On the evening on 3 January (DUNALLEY 1 period) a cloud band stretching from Western Australia to Tasmania (Figure 7.4a and 7.5a) reached the southwest and eventually southeast coasts of Tasmania, bringing thunderstorms, yet with less than 1 mm of precipitation in 24 hours (until 09 AEDT on 4 January; BoM, 2013a). Lightning had been detected in the area of Forcett and Dunalley, however, no fires were ignited here (Figure 7.4b). This cloud band was caused by the line of convergence which moved from the Western Australia towards the southeast.

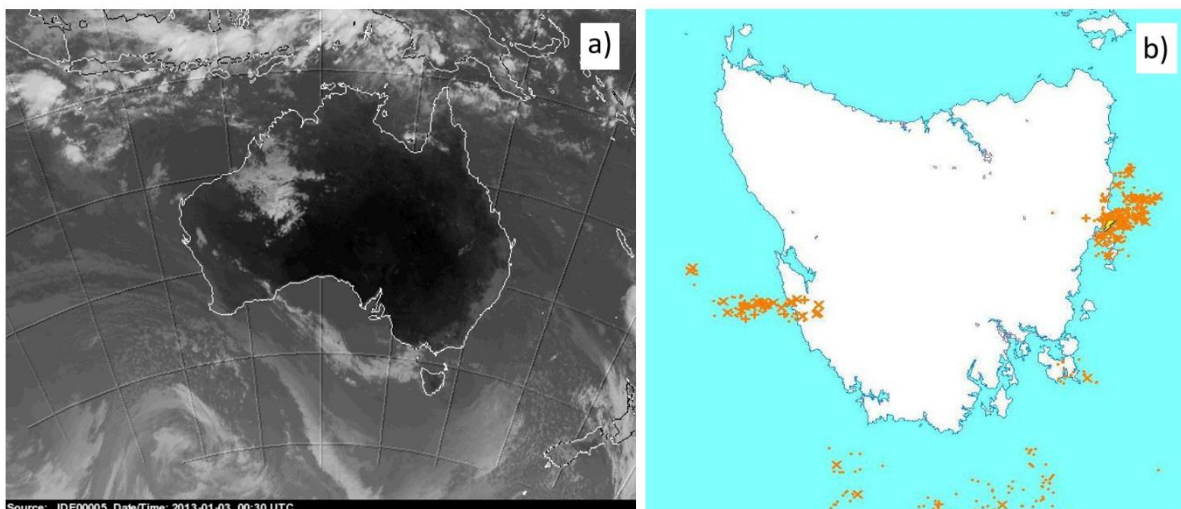


Figure 7.4. a) Infrared satellite photo at 11 AEDT on 3 January 2013 (Image: MTSAT-2, Multifunction Transport Satellite, JCAB and JMA) and b) lightning over Tasmania detected in the period from 20:35 AEDT on 3 January to 02:35 AEDT on 4 January 2013 (Image: GPATS Pty Ltd).

The anticyclone over the Tasman Sea remained persistent in its position and strength, with central air pressure ranging from 1017 hPa to 1020 hPa. Meanwhile, the cold front was progressing steadily eastward from Western Australia since 2 January. On 4 January, or by the time of the pyroCb development (DUNALLEY 2 period) a pressure gradient of 8 hPa extended over Tasmania, between 1000 hPa and 1008 hPa, which became stronger with the approaching cold front from the west (Figure 7.5b). Nevertheless, the line of convergence, which determines a region of rising air, arrived over Tasmania before the cold front and might have had a

dominant influence on weather conditions during the DUNALLEY 2 period. According to synoptic analysis at the time of pyroconvection the convergence line stretched from the southern Australian mainland towards the northwest of Tasmania (Figure 7.5b).

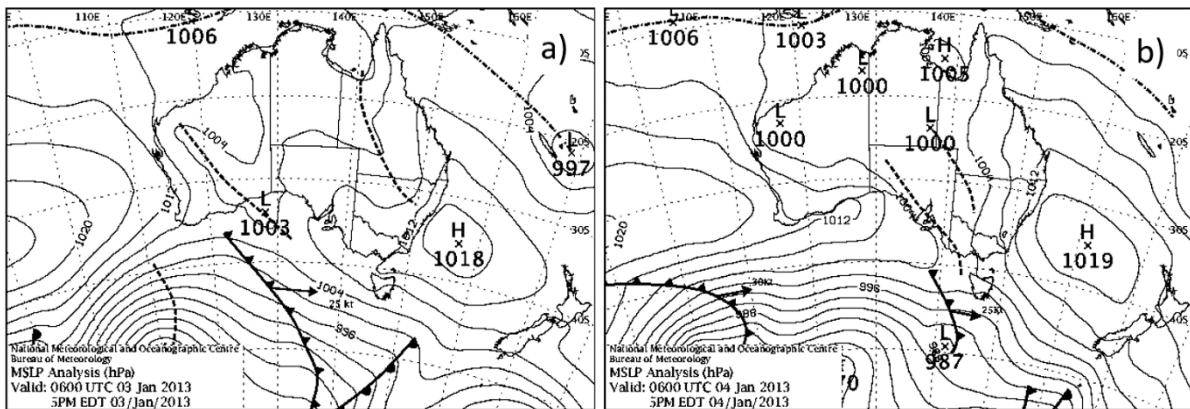


Figure 7.5. Mean sea level pressure (hPa) analysis for a) 17 AEDT on 3 January and b) 17 AEDT on 4 January 2013. Images: The National Meteorological and Oceanographic Centre (BoM).

Cold front reached Tasmania by the end of the DUNALLEY 2 period and crossed it in the night between 4 January and 5 January (Figure 7.6a) or in the first hours of DUNALLEY 3 period. Cold front passage was accompanied by the wind direction change, from northwesterly to southwesterly and southeasterly, and isolated showers across western Tasmania which did not bring any significant rainfall on the night and morning on 5 January (Figure 7.6a; BoM, 2013a). Cold front passage was followed by a ridge of high pressure (Figure 7.6b), which remained over Tasmania until 7 January 2013.

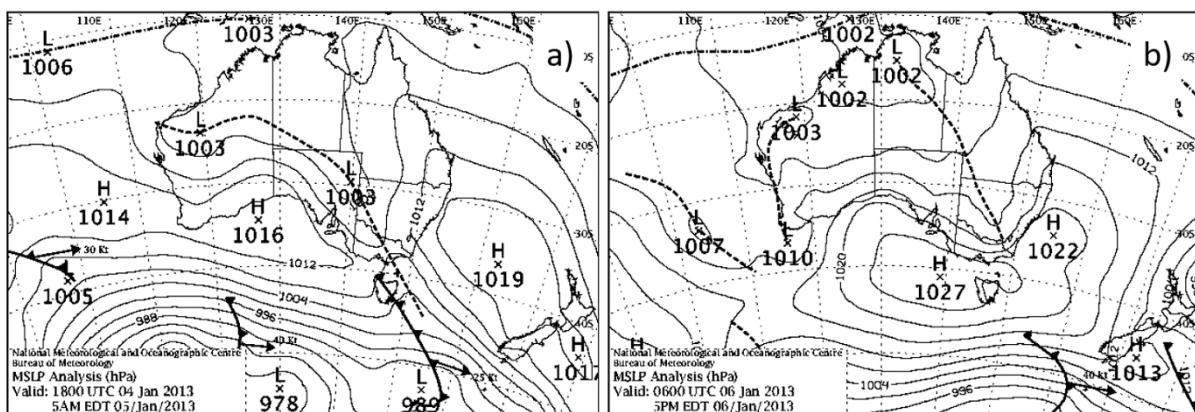


Figure 7.6. Mean sea level pressure (hPa) analysis for a) 05 AEDT on 5 January and b) 17 AEDT on 6 January 2013. Images: The National Meteorological and Oceanographic Centre (BoM).

## 7.4. Observations

### 7.4.1. Surface Conditions

Mean sea level pressure observations reflect the synoptic analysis. Air pressure continually dropped from 3 January until the peak pyroCb activity on 4 January (the DUNALLEY 2 period). The drop occurred from 1013.8 hPa (Figure 7.7a) to the minimum value of 997.5 hPa at 15:23 AEDT on 4 January (Table 7.2), coinciding with the most significant period of pyroconvection. From 5 January 2013 (the beginning of DUNALLEY 3 period) air pressure recovered and in just 24 hours reached 1022.3 hPa (by 6 January 2013; Figure 7.7a). Automatic weather stations in Hobart and at Hobart airport confirm the same pattern (Figure C3a and C4a). All stations also recorded the oscillation in pressure in the evening on 3 January when thunderstorms crossed the area of Hobart and Dunalley.

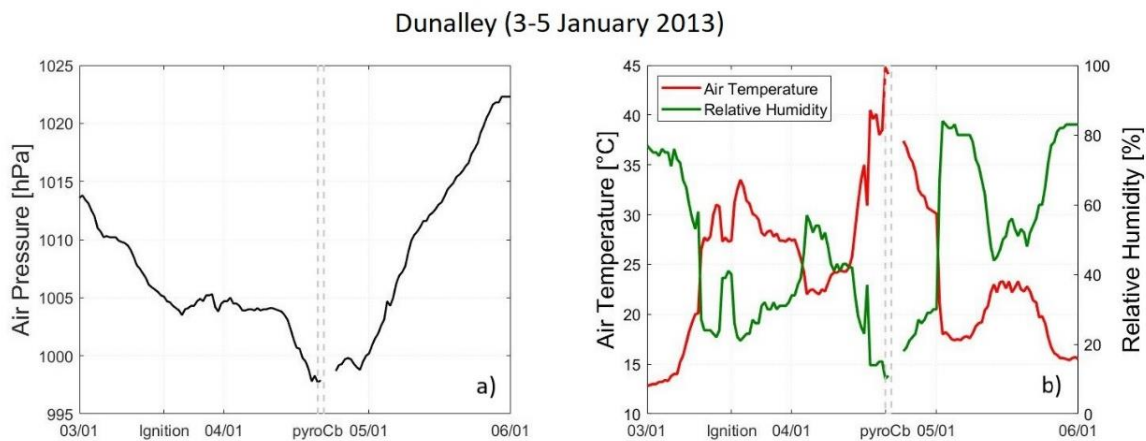


Figure 7.7. Dunalley automatic weather station 30-minute observations of a) air pressure (hPa) and b) air temperature (°C) and relative humidity (%) from 3 to 5 January 2013. Values between 16:19 AEDT to 18:06 AEDT are officially omitted due to corrupted measurements. Data recorded earlier, from about 15:20 AEDT, was most likely still affected at times and should be viewed with caution. Dashed grey lines indicate the peak activity of the pyroCb, between 15:30 AEDT and 16 AEDT on 4 January 2013 (the DUNALLEY 2 period).



Table 7.2. Observations at Dunalley station between 15 AEDT and 16 AEDT on 4 January 2013. The selected times included 30-minute with additional significant observations that were most likely affected at times and should be viewed with caution and not as official meteorological data.

<i>DUNALLEY 4 January 2013</i>						
Time (AEST)	Air temp. (°C)	Relative hum. (%)	Wind speed (ms <sup>-1</sup> )	Direction (°)	Wind gust (ms <sup>-1</sup> )	MSLP (hPa)
15:00	38.5	15	11.3	300	17.5	998.3
15:22	<b>54.9</b>	<b>6</b>	10.3	300	22.6	997.7
15:23	49.9	8	10.8	300	22.6	<b>997.5</b>
15:26	44.5	10	10.8	300	22.6	997.9
15:30	<b>44.8</b>	10	11.8	300	18	997.7
15:37	47.2	9	11.8	340	17.5	997.8
16:00	44.1	11	10.8	340	19.5	997.9

Temperature records were set on 4 January 2013. With 41.8°C Hobart station recorded its highest air temperature in 120 years (BoM, 2013a), which is also an all-time record for southern Tasmania. On the same day Hobart and at Hobart airport recorded their highest minimum air temperature in January. On the night between 3 and 4 January 2013 air temperature did not drop below 20°C (Figure C3c and C4c).

Air temperature at Dunalley station, which is not an official record due to wildfire effect on measurements, reached 44.8°C at 15:30 AEDT (Figure 7.7c), and in between half hour measurements even higher, 54.9°C at 15:22 AEDT (Table 7.2.). However, the survival of Dunalley station is fortunate and obtained records are rare and valuable representation of conditions in the close proximity to the wildfire when it entered the township of Dunalley during the peak of pyroCb activity (the DUNALLEY 2 period).

High surface air temperature was accompanied by low relative humidity. At the ignition time on 3 January relative humidity dropped to 26 % in Dunalley and to 14 % in Hobart and at Hobart airport (DUNALLEY 1 period). Short recovery occurred during the night between 3 and 4 January, coinciding with disturbances that did not bring any rain in the area. At peak pyroconvection in the early afternoon on 4 January (DUNALLEY 2 period) relative humidity dropped to its lowest values in this case with only 10 % in Dunalley, 11 % at Hobart airport and 12 % in Hobart, all at 15:30 AEDT (Figure 7.7c). Therefore, as it might be expected, both surface air temperature and relative humidity confirm the severe hot and dry weather conditions during the first 24 h of ignition.

Another significant feature of this event was a strong and gusty northwesterly wind that peaked at two occasions – right after the ignition and during the firestorm. At Hobart (Figure C3b) and Hobart airport (Figure C4b) stations stronger peak occurred right after the ignition on

3 January (DUNALLEY 1 period) while at Dunalley station stronger wind occurred during the pyroconvection (DUNALLEY 2 period). Wind speed in Dunalley was also strong during the day of the ignition on 3 January, significantly dropped in the night on 4 January, and regained its strength rapidly by the end of DUNALLEY 1 period (Figure 7.8a). Maximum 10-min wind speed and wind gust in Dunalley was recorded on 4 January at 14:30 AEDT, 13.4 m s<sup>-1</sup> and 21.6 m s<sup>-1</sup>, respectively. Wind remained strong with the approaching fire storm with gusts between 17.5 m s<sup>-1</sup> and 19.5 m s<sup>-1</sup> when the wildfire burned near the station.

All stations recorded a sharp change in wind direction right at midnight on 5 January, indicating the cold front passage. Wind direction in Dunalley (Figure 7.8b) and at Hobart airport (Figure C4d) turned from northwesterly to southwesterly, only in Hobart wind changed to southeasterly (Figure C3d).

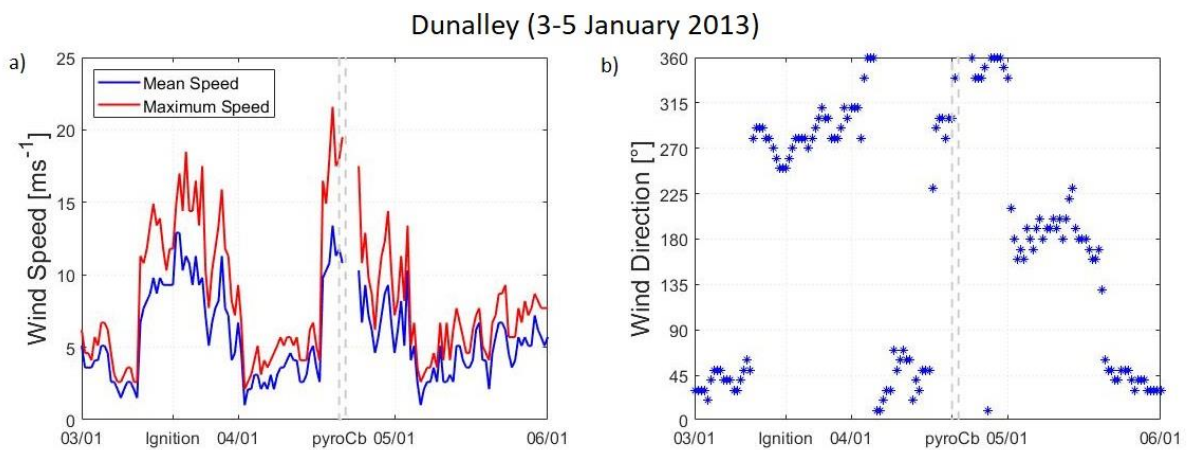


Figure 7.8. Dunalley automatic weather station 30-minute observations of a) mean and maximum wind speed (m s<sup>-1</sup>) and b) mean wind speed direction (°) from 3 to 5 January 2013. Mean and maximum wind speeds are 10-minute values available every half hour. Values between 16:19 AEDT to 18:06 AEDT are officially omitted due to corrupted measurements. Dashed grey lines indicate the peak activity of the pyroCb, between 15:30 AEDT and 16 AEDT on 4 January 2013 (the DUNALLEY 2 period).

#### 7.4.2. Upper-level Conditions

The radiosonde data from Hobart airport (25 km northwest of Dunalley) on 4 January 2013 (Figure 7.9), 5 hours before the peak of pyroconvection represents the favorable vertical profile for PyroCb development, similar to well-known inverted-V profile. A classic inverted-V sounding has been reported in literature to illustrate conditions favorable for pyroconvection and intense fire activity (e.g., Rosenfeld et al., 2007; Cunningham and Reeder, 2009; Fromm et al., 2012, Johnson and Wowchuk, 2014). The temperature profile on the right side and moisture profile on the left side of an inverted-V profile indicate a deep well-mixed boundary layer conditions and moist unstable middle troposphere, which supports the moist convective plume (Tory et al., 2016). The inverted-V profile also points to possible downburst development which can significantly influence fire ground and pose a great threat to firefighters (e.g., Kaplan et al., 2021). The sounding data before the peak of pyroCb activity in the case of Dunalley indicated a very dry boundary layer up to 600 hPa, with one shallow layer of weak temperature inversion around 750 hPa. Cloud base was situated roughly at 550 hPa with the level of condensation up to 400 hPa. The tropopause was detected between 300 hPa and 275 hPa ( $\approx 10.5$  km), with dry stratospheric air above.

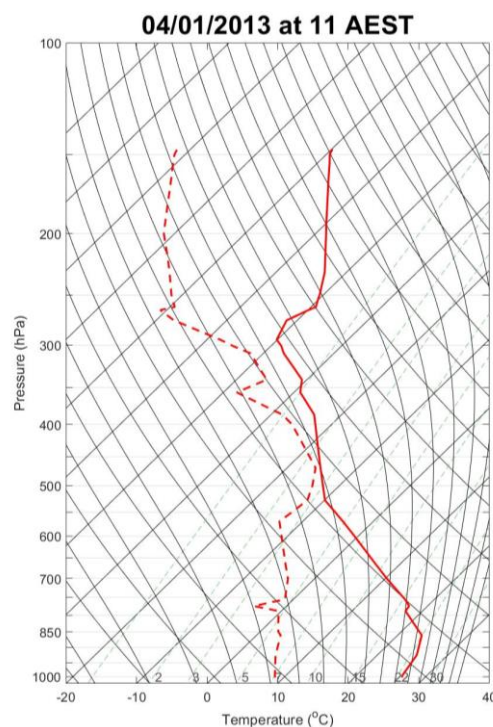


Figure 7.9. Hobart airport thermodynamic sounding at 10 AEDT on 4 January 2013. The red line corresponds to air temperature ( $^{\circ}\text{C}$ ) and red dashed line corresponds to dew-point temperature ( $^{\circ}\text{C}$ ), both as a function of altitude.

Wind speed and direction together with air and dew-point temperature from radiosonde measurements presented as vertical profiles reveal more details on vertical conditions in the atmosphere. Two soundings prior the pyroconvection (at 23 AEDT on 3 January and 11 AEDT on 4 January) present the appearance of low-level jet in lower troposphere (Figure 7.10a). The wind speed of the night-time low level jet was  $28 \text{ m s}^{-1}$  and of the one preceding the pyroconvection was  $24.2 \text{ m s}^{-1}$ . Although the low-level jet definition (Subsection 3.5.1.1) requires certain decrease of wind speed aloft it will be considered that low level jet of criterion 3 occurred in this case. By definition if low level jet is greater than  $20 \text{ m s}^{-1}$  the wind speed should decrease by  $10 \text{ m s}^{-1}$  up to 3 km height. In this case the wind speed decreased by  $9.5 \text{ m s}^{-1}$  and  $8.2 \text{ m s}^{-1}$ , respectively. The wind speed profile also reveals increase of upper-level wind and the jet stream appearance at the tropopause. The jet speed increased to maximum of  $44.2 \text{ m s}^{-1}$  at 22 AEDT on 4 January, right before the cold front passage. The wind in the pre-frontal air mass on the day of the pyroconvection had northwest direction throughout the whole troposphere (Figure 7.10b). Air and dew point temperature vertical profiles reveal a dry mid-level air and two temperature inversions up to 2 km height right before the ignition at 10 AEDT on 3 January (Figure 7.10c and d). The tropopause altitude on the morning sounding on 4 January, before the pyroconvection, was at 10.4 km with air temperature of  $-39.9^{\circ}\text{C}$ , while the evening sounding depicts the elevation of the tropopause to altitude of 12.2 km with air temperature of  $-49.3^{\circ}\text{C}$ .

### Hobart airport radiosonde

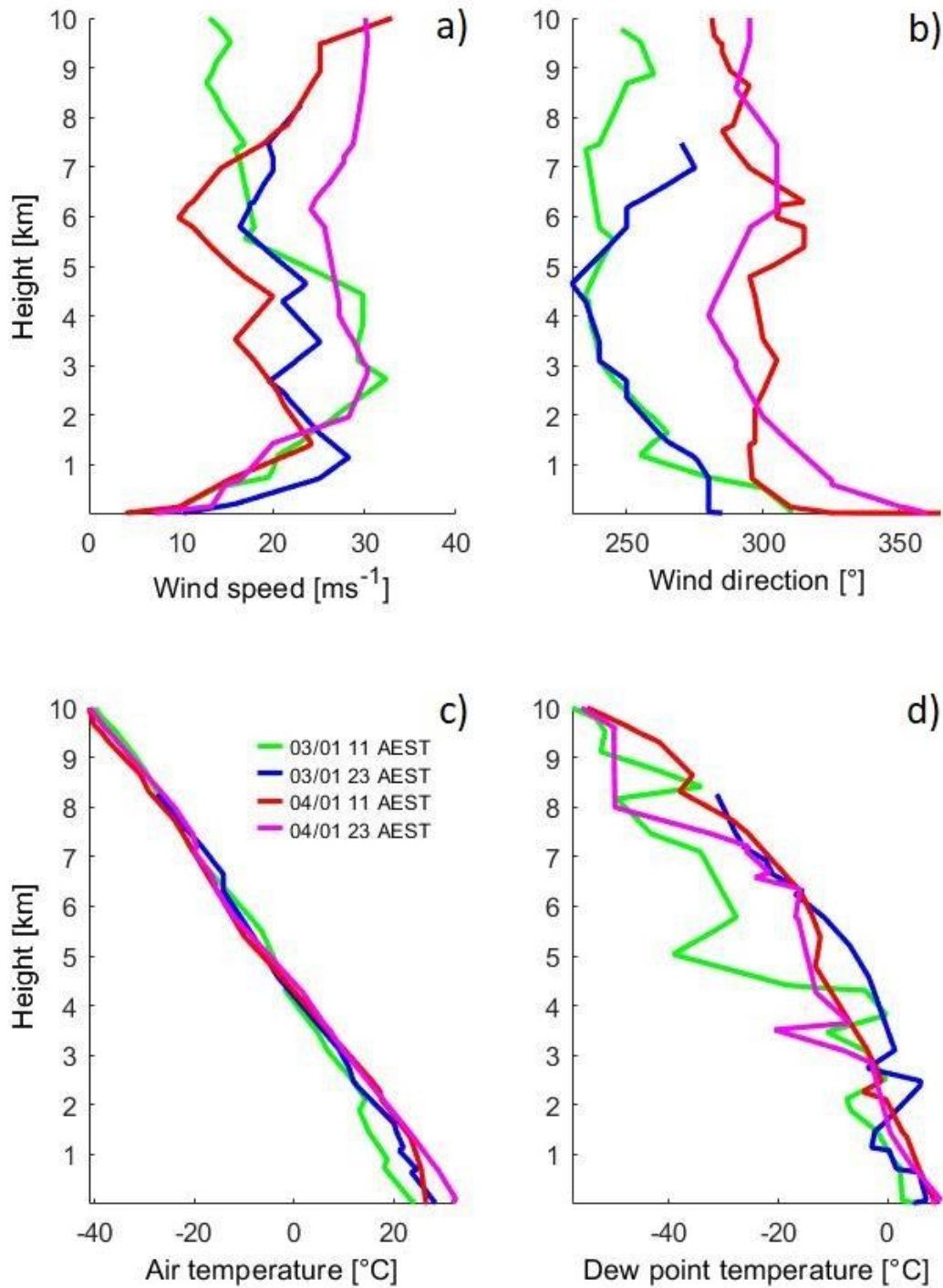


Figure 7.10. Vertical profiles of a) wind speed ( $\text{m s}^{-1}$ ), b) wind direction ( $^{\circ}$ ), c) air temperature ( $^{\circ}\text{C}$ ) and d) dew-point temperature ( $^{\circ}\text{C}$ ) up to 12 km height, from Hobart airport soundings at 11 AEDT (00 UTC) and 23 AEDT (12 UTC) on 3 January and 4 January 2013.

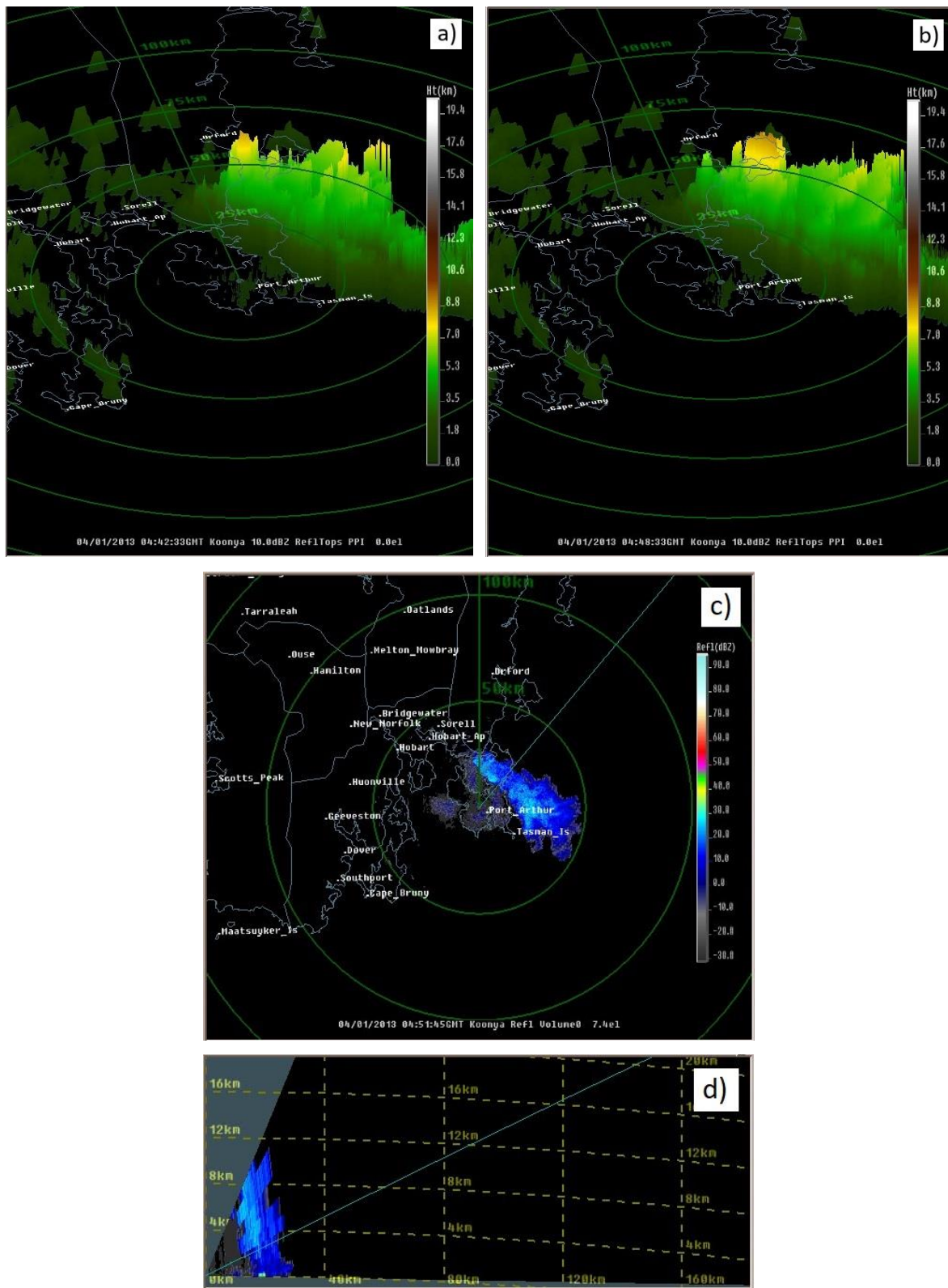


Figure 7.11. Mt Koonya radar output on 4 January 2013 a) 3D representations of reflectivity data at 15:42 AEDT, b) at 15:48 AEDT, c) plan-position indicator (PPI) view of reflectivity data at 7.4-degree elevation (elevation indicated by diagonal line in panel (d)) and d) range-height indicator RHI (orientation of RHI indicated by diagonal line in panel (c)) Both c) and d) valid at 15:51 AEDT.

Radar from Mt Koonya, situated 24 km south of Dunalley, covered pyroconvection from Dunalley in three dimensions (Figure 7.11). Radar detected echoes connected to the wildfire that peaked from 15:30 AEDT to 16 AEDT on 4 January (Ndalila et al., 2019), spreading southeast for more than 60 km. Echo-tops calculations provided by the BoM reveal that pyroconvective column mostly reached 5 to 7 km height between 15 AEDT and 16 AEDT (Figure 7.11a). At the peak of pyroconvection between 15:48 AEDT and 15:51 EADT (Figure 7.11b and c) echo-tops extended up to 8 km with the strongest echoe as high as 11 km (Figure 7.11d) which is 3–4 km lower than the previous research stated (Ndalila et al., 2019).

## 7.5. BARRA Reanalysis

### 7.5.1. Surface Conditions

The reanalysis data corroborate the surface synoptic pressure analysis and AWS data from Dunalley and Hobart airport. BARRA depicts the strong pressure gradient over Tasmania at the time of wildfire's ignition on 3 January (Figure 7.12a). The strong pressure gradient from the south to the north of the state, approximately over 300 km distance varied from 1002 hPa to 1013 hPa, with the lowest mean sea level pressure in close proximity to wildfire's location. The pressure gradient eased towards the evening on 3 January and the following day, bringing the minimum mean sea level pressure to fire ground around the time of pyroconvection (Figure 7.12b). According to the BARRA reanalysis the minimum mean sea level pressure at wildfire's location was between 997 hPa and 1002 hPa from 15 AEDT to 21 AEDT on 4 January, which corresponds to AWS measurements at Dunalley station (Figure 7.7a). As the cold front crossed Tasmania overnight on 4-5 January the mean sea level pressure increased to between 1007 and 1010 hPa in the area of the wildfire, which corresponds to AWS data.

Extreme surface weather conditions are illustrated by highest skin and air temperature and lowest relative humidity right before and during the first 34 hours of ignition (DUNALLEY 1 and 2 periods). According to BARRA meteorological values peaked at 11 AEDT on the first two days at the wildfire's location and over the majority of southeast Tasmania (Figure 7.13). Severe conditions on 3 January, right prior the ignition, were marked with skin temperature between 32 and 34°C, air temperature between 30 and 34°C and relative humidity below 10% (Figure 7.13a, c and e).

On 4 January weather conditions got even more extreme (Figure 7.13b, d and f). State wide skin temperature exceeded 30°C while relative humidity remained below 10%. Dunalley area again stood out with absolute maximum temperature values of the day. In hours prior the

pyroconvection skin temperature exceeded 40°C while air temperature was between 36 and 38°C. The fact that the BARRA reanalysis slightly underestimated measured values (not only of those from Dunalley station that were affected by the fire) highlights the severity of this case. The reanalysis confirmed warm surface conditions in the night between 3 and 4 January when air temperature in the area of Hobart and Dunalley did not drop under 20°C and relative humidity remained below 20 % (Figure C5a and b). The change in broader weather conditions after the cold front passage (DUNALLEY 3 period) which caused cool outbreak and increase in relative humidity was also evident from the reanalysis data (Figure C5c and d).

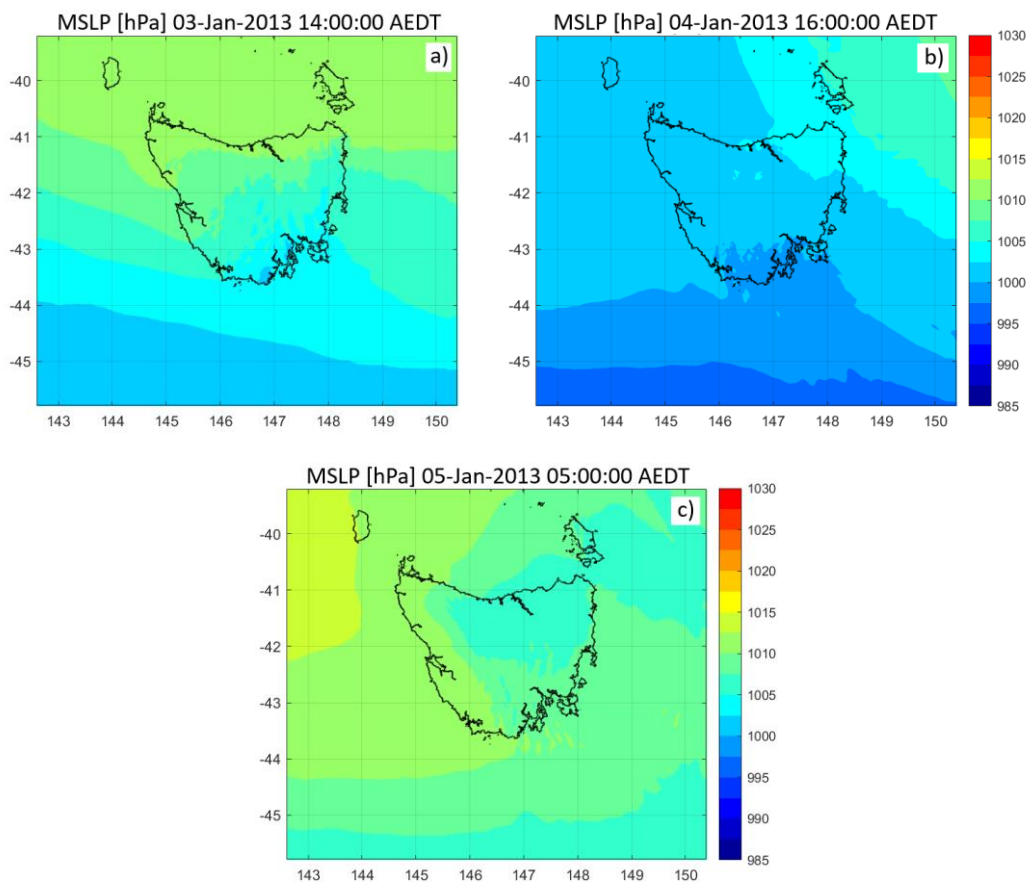


Figure 7.12. Mean sea level pressure (hPa) at a) 14 AEDT on 3 January, b) 16 AEDT on 4 January and c) 05 AEDT on 5 January 2013 from BARRA reanalysis.

After the ignition the wildfire was carried by the northwesterly airflow which was persistent in Dunalley area during DUNALLEY 1 and DUNALLEY 2 periods (from 14 AEDT on 3 January to 23 AEDT on 4 January). According to BARRA, west to northwest wind in the area of the wildfire was strong right before and at the ignition time with mean speed between 8 and 12 m s<sup>-1</sup> and wind gusts up to 16 m s<sup>-1</sup>. At some locations, mostly upwind and further from the coast wind gusts at narrow bands reached strong gale force up to 24 m s<sup>-1</sup> (Figure 7.14a and



b). Decrease in wind speed occurred throughout the night between 3 and 4 January, when its mean speed remained under  $8 \text{ m s}^{-1}$ . A sudden increase in wind speed up to  $16 \text{ m s}^{-1}$  and wind gusts up to  $24 \text{ m s}^{-1}$  is evident again between 9 AEDT and 15 AEDT on 4 January or by the end of DUNALLEY 1 and in the first hours of DUNALLEY 2 period. This strong wind of persistent northwest direction, perpendicular to the coast coincided with increase in fire activity in the morning on 4 January and right before the pyroconvection.

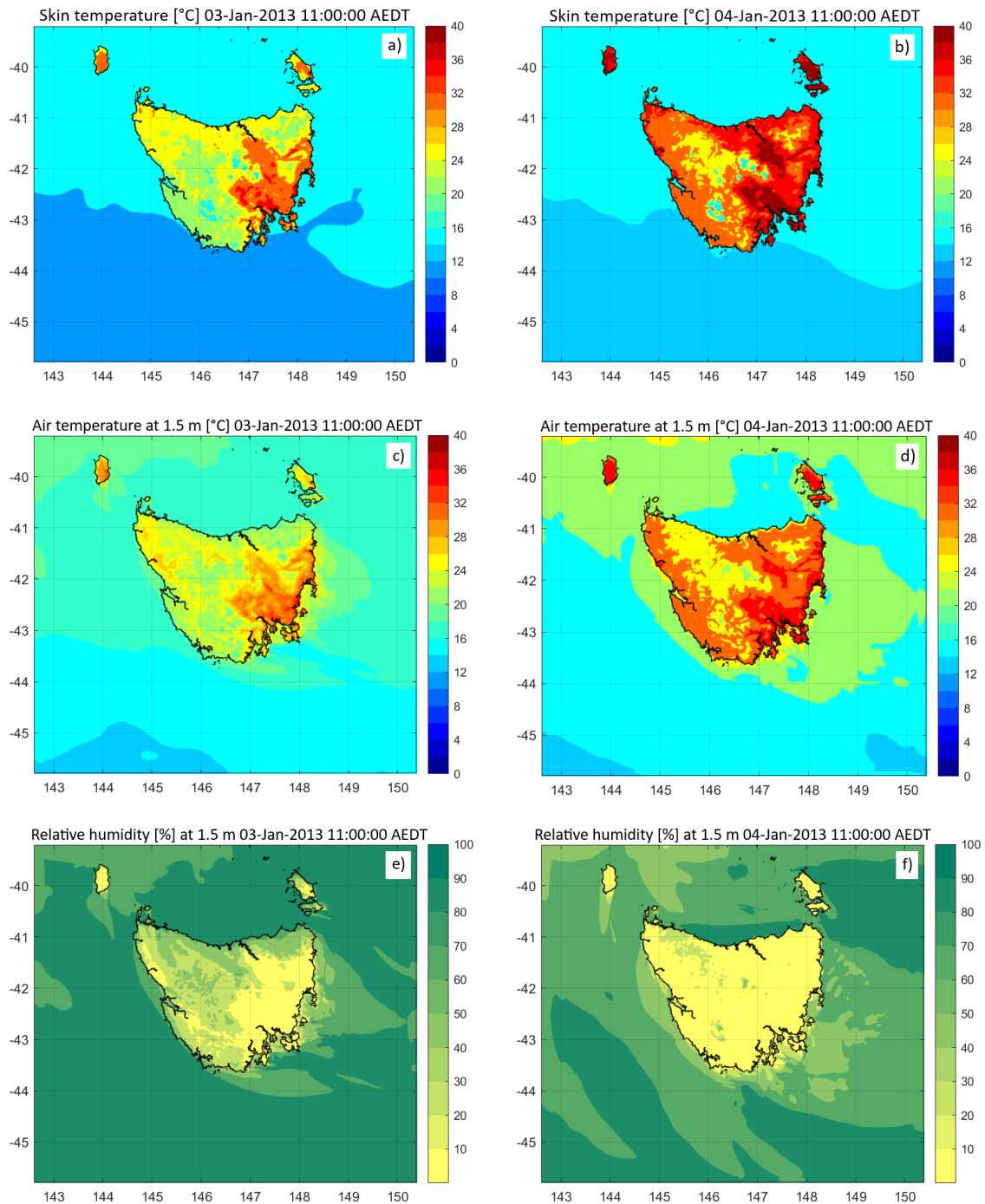


Figure 7.13. Skin temperature ( $^{\circ}\text{C}$ ; top), air temperature ( $^{\circ}\text{C}$ ; middle) and relative humidity (%; bottom) at a), c) and e) 11 AEDT on 3 January and b), d) and f) 11 AEDT on 4 January 2013 from BARRA reanalysis.

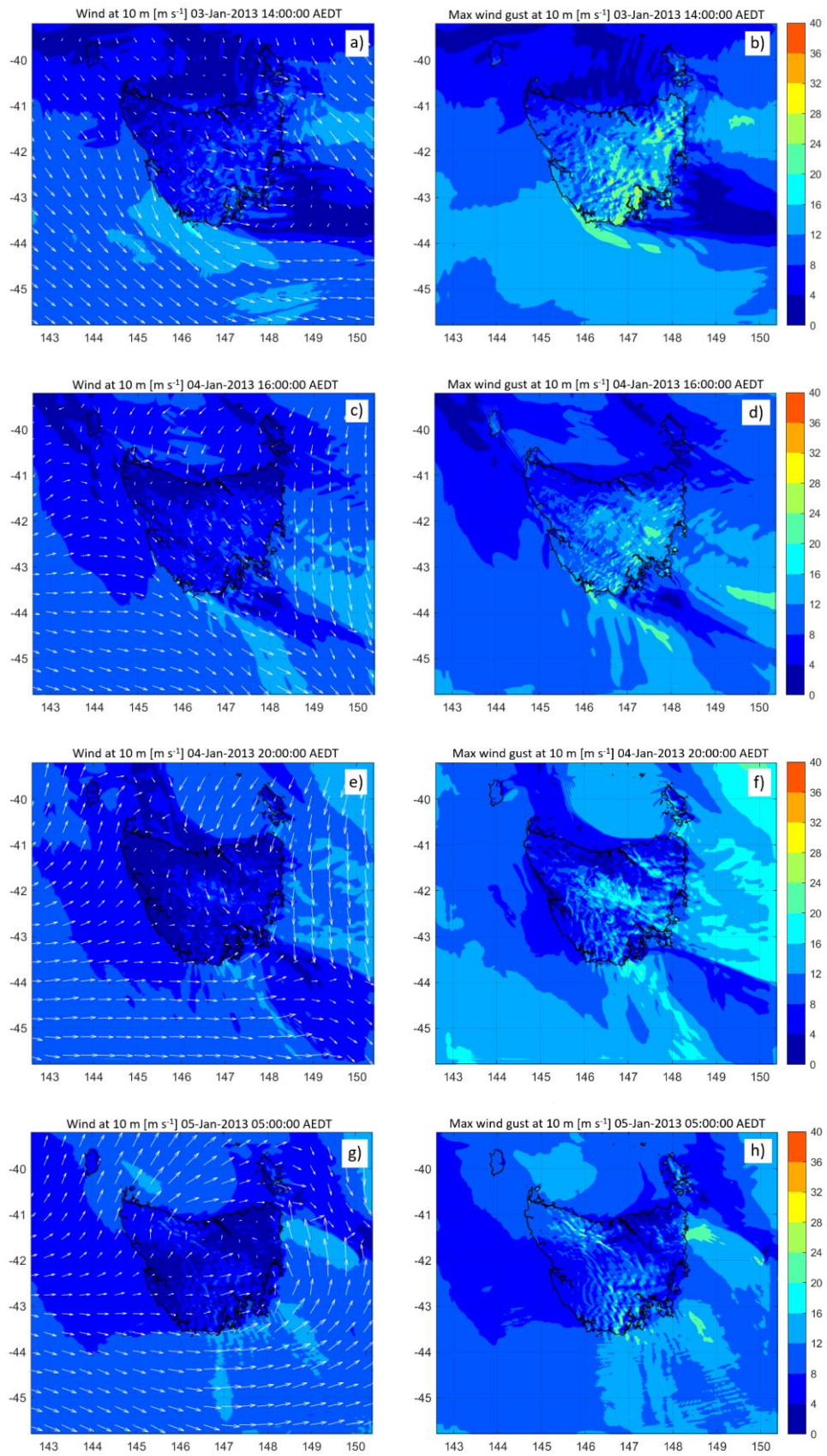


Figure 7.14. Wind speed ( $\text{m s}^{-1}$ ; left) and direction and maximum wind gust ( $\text{m s}^{-1}$ ; right) at 10 m at a) and b) 14 AEDT on 3 January; c) and d) 16 AEDT on 4 January, e) and f) 20 AEDT on 4 January and g) and h) 05 AEDT on 5 January 2013 from BARRA reanalysis.

By the time of the peak pyroconvection wind gusts maintained strong to gale force upwind of the fire location (Figure 7.14d). However, in the downwind area, over the Tasman Peninsula and further offshore, wind slightly eased in strength. This is due to approaching line of convergence which edge reached the Tasman Peninsula by the time of peak pyroconvection (Figure 7.14c). The line of convergence corresponds to lower wind zone offshore the southeast Tasmania. According to BARRA the convergence line crossed the wildfire's area around 20 AEDT on 4 January (Figure 7.14e and f).

The line of convergence was followed by the cold front passage at the end of DUNALLEY 2 period. This is evident in further ease in wind speed in broader area and abrupt change in wind direction to southwest during the first hours of DUNALLEY 3 period. The timing of the cold front passage over Tasmania is represented accurately when compared to synoptic analysis. BARRA in general represented the measurements from local meteorological station well, with the noted discrepancy to AWS data at the peak of pyroconvection due to fire approaching the station and influencing instruments.

#### *7.5.2.1. Horizontal Fields*

The upper-level evolution of air temperature, relative humidity and wind provides more evidence on severity in this case and gives an insight into upper-level conditions that occurred during the pyroconvection. Warm and dry conditions at 850 hPa were persistent throughout the DUNALLEY 1 and 2 periods (Figure 7.15 and C6). At the ignition time at 14 AEDT on 3 January air temperature at 850 hPa over Tasmania was between 16 and 19°C (Figure 7.15a). Moving forward towards the evening air temperature did not drop. On the contrary, upper-level conditions got even more severe, with air temperature eventually reaching the maximum of 25°C in the night between 3 and 4 January (DUNALLEY 1 period; Figure C6a). This very warm air remained and covered the wildfire's area for a period of 24 hours, between 22 AEDT on 3 January (DUNALLEY 1 period) until 22 AEDT on 4 January (end of DUNALLEY 2 period), including the period of pyroconvection (Figure 7.15c). Extreme warmth at 850 hPa was also followed by reduction in relative humidity which remained between 20 and 40 % during the first 34 hours of ignition or during DUNALLEY 1 and 2 periods (Figure 7.15b and d, C6b). The warm and dry air mass covered the area of the state until the cold front passage over Tasmania and advection of cool and moist air from the southwest in the night on 5 January (DUNALLEY 3 period; Figure C6c and d).

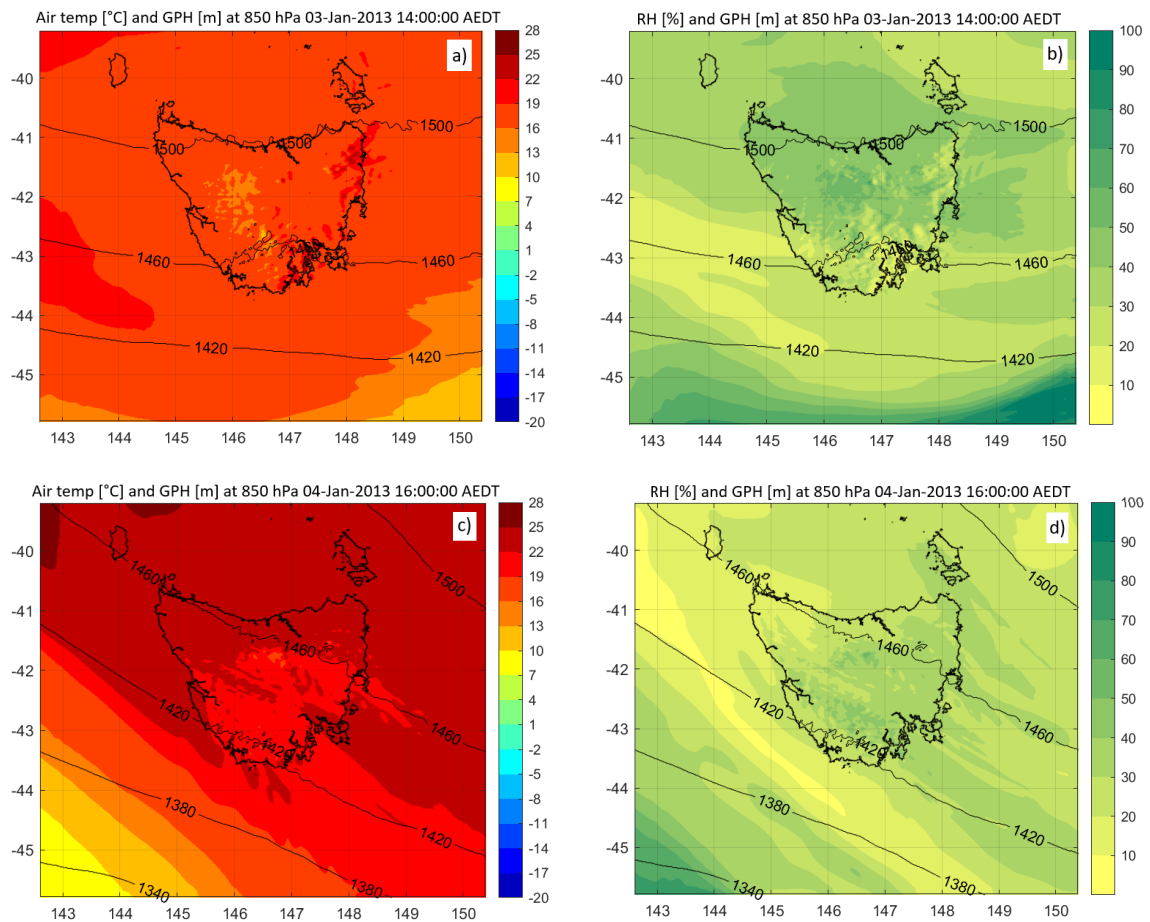


Figure 7.15. Air temperature ( $^{\circ}\text{C}$ ; left) and relative humidity (%; right), both with geopotential height (m; contours) at 850 hPa at a) and b) 14 AEDT on 3 January and c) and d) 16 AEDT on 4 January 2013 from BARRA reanalysis.

Northwest wind dominated upper-level air flow over Tasmania during all burn periods of Dunalley wildfire (DUNALLEY 1 to DUNALLEY 3). Although at the ignition time (at 14 AEDT on 3 January) airflow was mostly southwest to west (Figure C7), significant direction shift to northwest occurred at 06 AEDT on 4 January. Direction shift started at 850 hPa and 500 hPa levels and by the end of DUNALLEY 1 period expanded up to 300 hPa (at 11 AEDT on 4 January). While the northwest wind expanded in coverage by the end of DUNALLEY 1 period, it also increased in speed. This is especially evident during the DUNALLEY 2 period at higher altitudes of 500 hPa and 300 hPa. At 850 hPa northwesterly wind eased in strength from 10 AEDT to 18 AEDT, which includes pyroconvection period. At the peak pyroconvection northwest wind at 850 hPa had speed from 12 to 16  $\text{m s}^{-1}$  right above the wildfire's area (Figure 7.16a). In particular, this was the region of lowest wind which corresponded to pyroCb location. During the peak convection northwesterly wind at 500 hPa had speed between 20 and 24  $\text{m s}^{-1}$  and at 300 hPa between 24 and 28  $\text{m s}^{-1}$  (Figure 7.16b and c). By the end of DUNALLEY 2 wind speed further increased and by the end of DUNALLEY 3 period reached maximum speed

of  $40 \text{ m s}^{-1}$  at mid and upper troposphere. Meanwhile wind speed at 850 hPa eased and shifted to southwest with the approaching cold front. It is also important to note that findings from BARRA reanalysis correspond to radiosonde measurements. For instance, the reanalysis accurately presented upper-level jet speed as well as the shift in wind direction (Figure 7.11a and b).

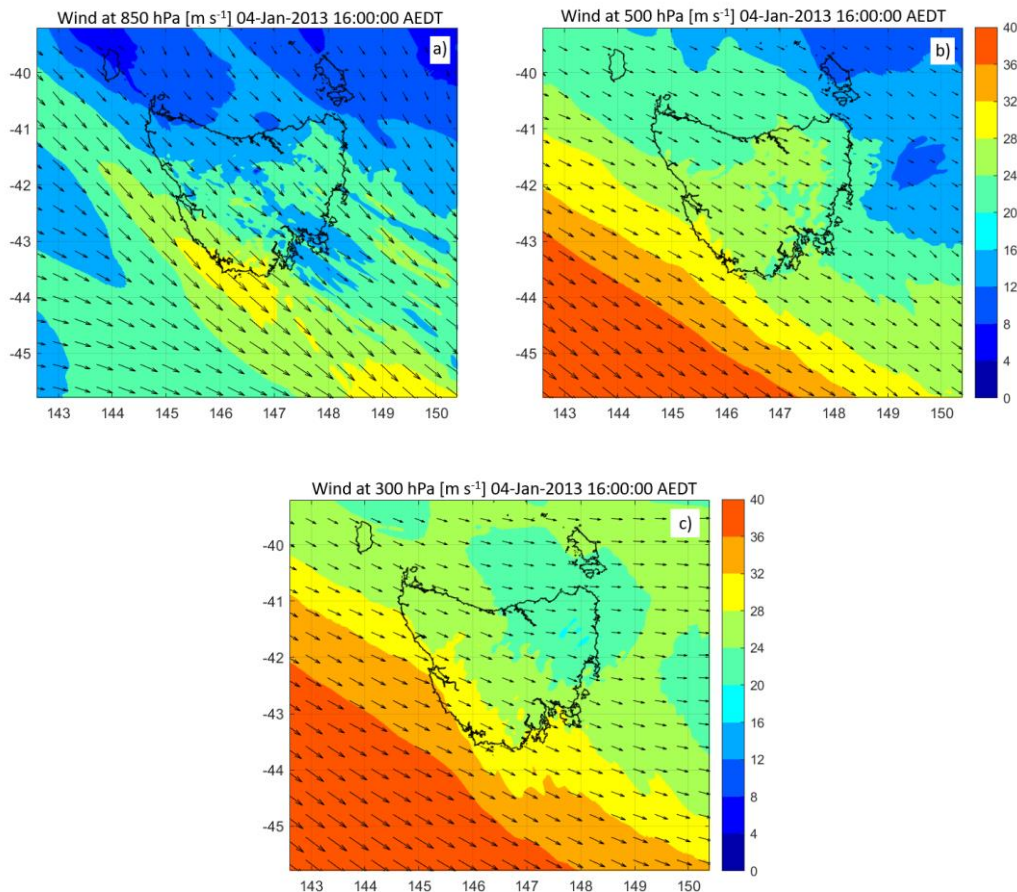


Figure 7.16. Wind speed ( $\text{m s}^{-1}$ ) and direction at a) 850 hPa, b) 500 hPa and c) 300 hPa all at 16 AEDT on 4 January 2013 from BARRA reanalysis.

### 7.5.2.2. Cross Sections

Vertical cross sections up to mid (500 hPa) and top (300 hPa) of the troposphere are derived along the 120 km line that extends from the interior of Tasmania, through Dunalley wildfire location and over the Tasman Sea following the northwesterly airflow (Figure 3.4) and also being perpendicular to the Tasmanian Sea coast.

Vertical cross sections of z wind reveal that the largest and strongest area of upward motion was right at the time of pyroconvection. Between 11 AEDT (end of DUNALLEY 1 period) and 16 AEDT on 4 January (DUNALLEY 2 period) the largest area of upward vertical wind speed covered the location immediately downwind of Dunalley (Figure 7.17a, c and e).

The maximum positive vertical wind component of  $+3 \text{ m s}^{-1}$  extended over Tasmanian Peninsula and Tasman Sea at 12 AEDT (Figure C9a) and again at 16 AEDT (Figure 7.17e), coinciding with the exact time of peak pyroconvection which is a significant finding.

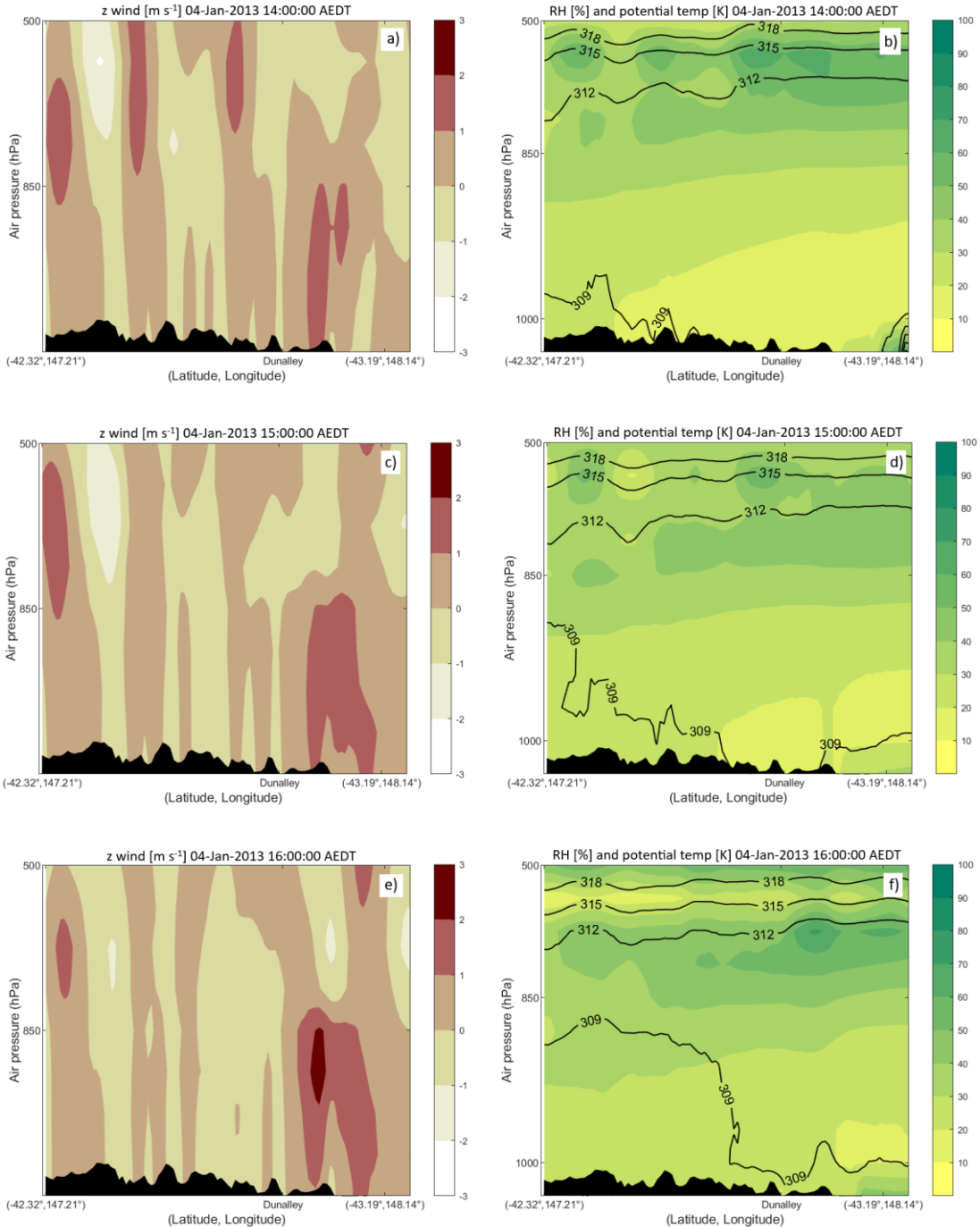


Figure 7.17. Vertical cross sections of  $z$  wind ( $\text{m s}^{-1}$ ; left), relative humidity (%) and potential temperature (K; right) at a) and b) 14 AEDT, c) and d) 15 AEDT and e) and f) 16 AEDT on 4 January 2013 from BARRA reanalysis. The bottom black area depicts the terrain. Location of cross sections is indicated in Figure xx. Each section is 120 km long with height up to 500 hPa, oriented northwest to southeast and perpendicular to Tasmanian Sea coast with Dunalley situated approximately 45 km from the right bottom corner. Air flow in each panel is from left to right.

The strongest upward vertical motion covered the layer up to 850 hPa with additional areas downwind of Dunalley area extending up to 500 hPa. This region of positive vertical wind speed mostly dissipated by 17 AEDT, which corresponds to time of dissipation of pyroCb over the Tasman Sea (Figure C9b).

Strong vertical mixing is additionally confirmed by the lack of any significant potential temperature gradient above wildfire's area. Sparse distribution of isentropes that appears as a large gap between potential temperature of 309 K and 312 K on cross sections occupied a deep layer from 1000 hPa up to 600 hPa in the period from 11 AEDT to 16 AEDT on 4 January, i.e., indicating the well-mixed layer. Therefore, strong vertical mixing occurred right at the time of pyroconvection (Figure 7.17b, d and f). Absence of potential temperature gradient was accompanied by low relative humidity, which by the time of pyroconvection dropped under 30 % in the layer from 1000 hPa up to 850 hPa (Figure 7.17b). The only surface layer with higher relative humidity remained over the Tasman Sea. Cross sections of relative humidity also corroborate the previous synoptic analysis and confirm the advection of moisture over Tasmania in the night on 3 January and after the cold front passage. The former layer of moist air was between 500 hPa and 300 hPa (Figure C8b), while the latter extended throughout the entire troposphere.

Vertical cross sections of wind speed reveal the upper-level divergence at the ignition time (DUNALLEY 1) which was followed by the northwesterly airflow throughout the troposphere (DUNALLEY 1 and 2) and gradually strengthening of upper-level jet during the cold front passage (DUNALLEY 2 and 3).

Divergence at the ignition time occurred in the layer of 600 hPa and divided the slower northwesterly air flow below and more accelerated southwest flow above (Figure 7.18a). The maximum wind speed in the layer of southwesterly flow was between 25 and 27.5 m s<sup>-1</sup>, which corresponds to radiosonde measurements obtained few hours before the ignition at Hobart airport (Figure 7.11a and b). While the lower northwesterly air flow was dry (originated from Australian mainland), the upper-level air flow coming from the southwest was moist, which can be seen in relative humidity increase above 500 hPa after the ignition and during the night between 3 and 4 January (Figure 7.18b and C8b). Moving forward in time during the DUNALLEY 1 period southwesterly air flow eased (Figure C8a) and direction of the wind aloft gradually aligned with the wind at lower levels. At 06 AEDT on 4 January the northwesterly air flow extended throughout the entire troposphere (Figure 7.20a) and remained persistent until the cold front passage at the end of DUNALLEY 2 period.

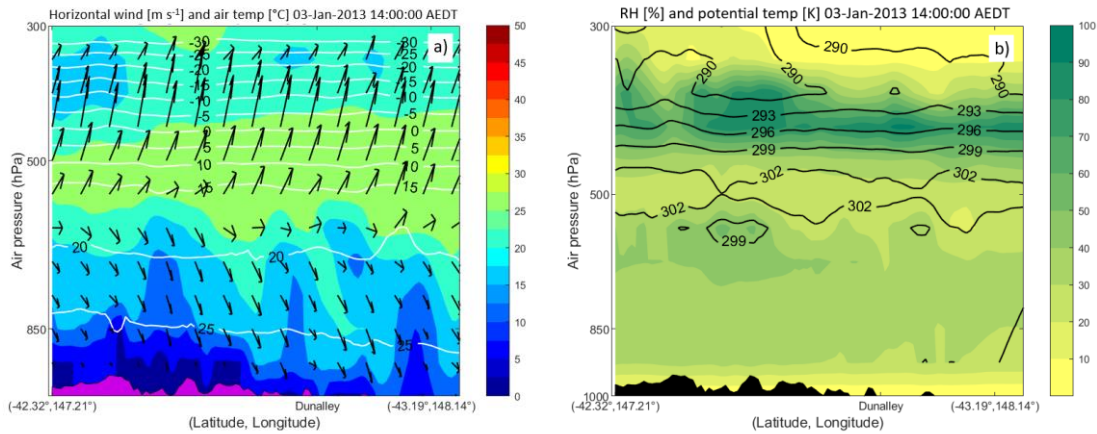


Figure 7.18. Vertical cross sections of a) wind speed ( $\text{m s}^{-1}$ ) and direction and b) relative humidity (%) and potential temperature (K) both at 14 AEDT on 3 January 2013 from BARRA reanalysis. The bottom violet area depicts the terrain. Air flow in each panel is from left to right.

From the time of wind direction alignment (DUNALLEY 1 period) and during the DUNALLEY 2 period upper-level northwesterly wind accelerated. This acceleration was more evident at upper levels, while at lower levels wind speed remained largely constant. During the pyroconvection the horizontal wind speed was between  $2.5$  and  $12.5 \text{ m s}^{-1}$  up to  $900 \text{ hPa}$  and between  $15$  and  $17.5 \text{ m s}^{-1}$  up to  $600 \text{ hPa}$  (Figure 7.19). These layers are most evident above and downwind of wildfire's area or above Tasman Peninsula and Tasman Sea right at the peak pyroconvection (Figure 7.19c). This region corresponds to pyroCb location and to the location of the maximum upward wind speed found in  $z$  wind cross sections. After 17 AEDT or after the pyroconvection wind speed also increased in lower levels, with the maximum closest to surface between  $20$  and  $22.5 \text{ m s}^{-1}$  at 20 AEDT on 4 January.

Another change in upper-level conditions was evident by the end of DUNALLEY 2 and DUNALLEY 3 periods. The cross section of the troposphere was again divided with two airflows – the area of low wind up to  $850 \text{ hPa}$  and the strong jet stream above. While the cold front affected the wind at lower levels, decreasing its speed and turning direction to southwest, the upper-level northwesterly wind peaked. The northwest airflow accelerated and by the end of DUNALLEY 3 period (at 05 AEDT on 5 January) reached the maximum speed of  $45 \text{ m s}^{-1}$  in the deep layer between  $600 \text{ hPa}$  and  $300 \text{ hPa}$  (Figure 7.20b).



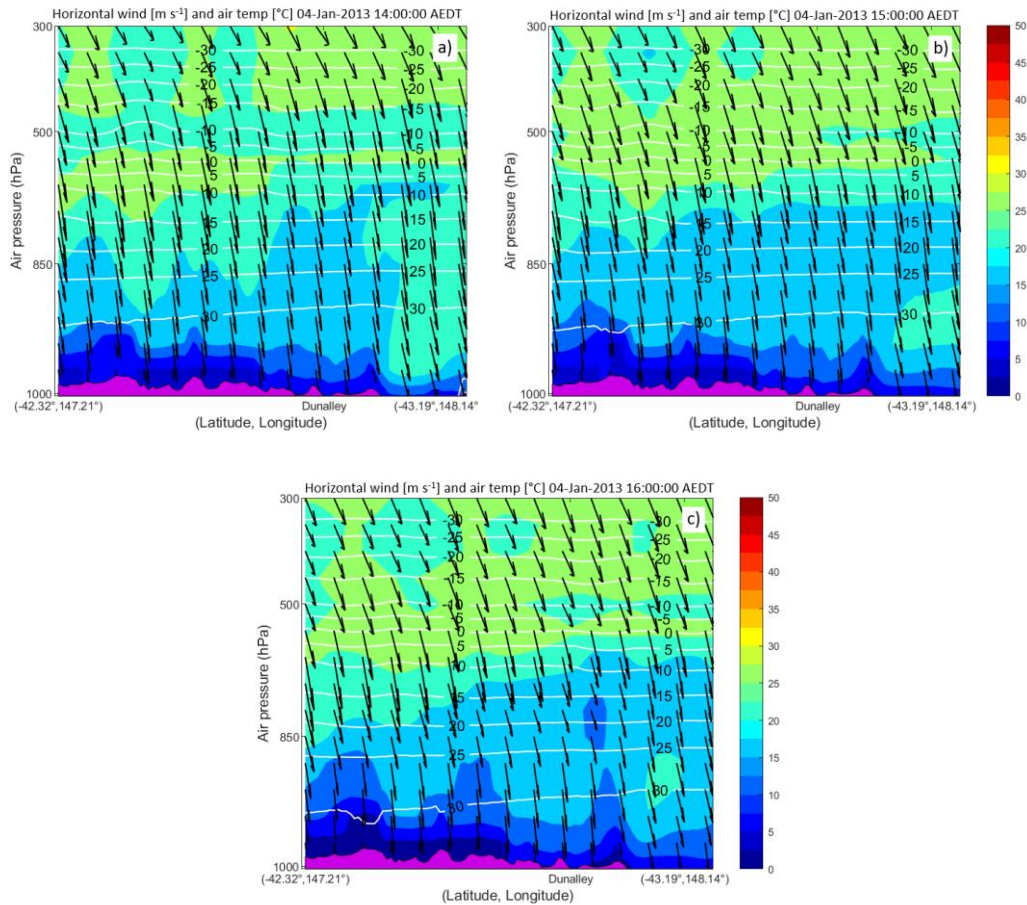


Figure 7.19. Vertical cross sections of horizontal wind speed ( $\text{m s}^{-1}$ ) and direction and air temperature ( $^{\circ}\text{C}$ , white contours) at a) 14 AEDT, b) 15 AEDT and c) 16 AEDT on 4 January 2013 from BARRA reanalysis. The bottom violet area depicts the terrain. Air flow in each panel is from left to right.

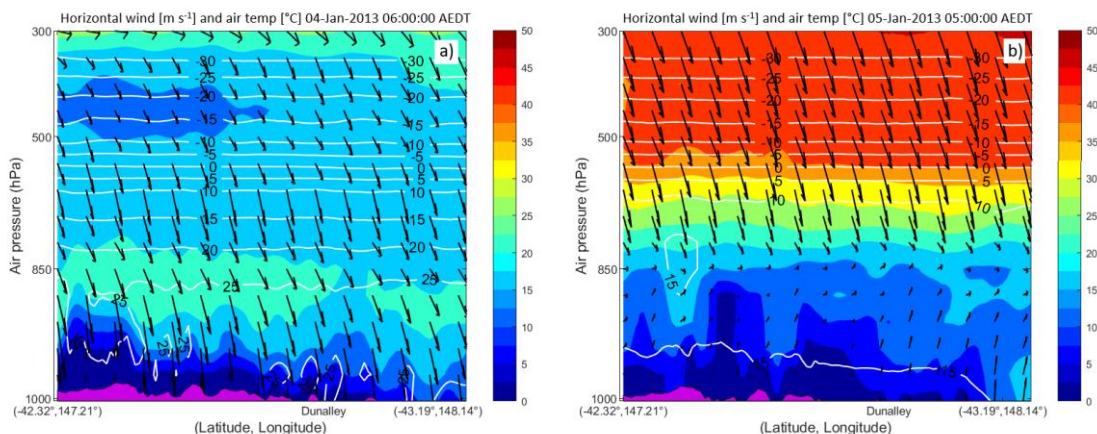


Figure 7.20. Vertical cross sections of wind speed ( $\text{m s}^{-1}$ ) and direction and air temperature ( $^{\circ}\text{C}$ ; white contours) at a) 06 AEDT on 4 January and b) 05 AEDT on 5 January 2013 from BARRA reanalysis. The bottom violet area depicts the terrain. Air flow in each panel is from left to right.

## 7.6. Discussion and Conclusions

The Dunalley wildfire occurred during an episode of severe weather conditions and in an environment favoring extreme fire behavior.

### 7.6.1. Intense Heat and Severe Ground Conditions

Going back in time, in the decade prior the wildfire, combination of frequent long term warm and dry weather with occasional rainfall above average contributed to vegetation growth and subsequent drying of the fuels in the area, which was further enhanced in the months immediately prior to the wildfire. The ignition of the wildfire coincided with the culmination of prolonged heatwave that was unusual in its spatial extent and duration and resulted in the hottest month on record in Australia, including Tasmania. The peak of the heatwave occurred during the first two days of the wildfire, on 3 and 4 January 2013 setting the maximum air temperature anomaly  $12^{\circ}\text{C}$  above average and minimum air temperature  $8^{\circ}\text{C}$  above average. The heatwave led up to all-time air temperature record for southern Tasmania. On 4 January 2013 Hobart station measured  $41.8^{\circ}\text{C}$ , which is its highest air temperature in 120 years. The intense heat in Tasmania was caused by the strong northwesterly airflow which brought hot and dry air from the central interior of Australian mainland. The northwesterly wind was a result of strong pressure gradient in the area caused by synoptic configuration consisting of the anticyclone situated in the Tasman Sea, northeast of Tasmania, and approaching cold front from the west.

The northwest wind determined the fire activity during the DUNALLEY 1 period. Since the ignition the strong surface northwest wind with occasional gale force gusts pushed the fire in southeast direction, towards the township of Dunalley, at the spread rate at one point reaching  $43\text{ m min}^{-1}$ . Only the general ease in wind speed during the night between 3 and 4 January decreased and almost stopped any fire activity and progression. However, air temperature remained high ( $>20^{\circ}\text{C}$  up to 850 hPa) and relative humidity low ( $<30\%$ ) which did not allow for the overnight process of cooling and fuel moisture recovering in the area of the wildfire. The re-activation and escalation of fire activity in the morning on 4 January and until the end of DUNALLEY 1 burn period coincided with the significant upper-level wind conditions that included strong low level jet and the alignment of the northwest wind throughout the troposphere. These surface and upper-level conditions introduced the atmosphere environment that became favorable for the pyroconvection during the DUNALLEY 2 period.

### 7.6.2. *Pyroconvection Conditions and Line of Convergence*

In the afternoon on 4 January 2013, during the DUNALLEY 2 burn period, fire activity escalated and Dunalley wildfire blew up into pyroCb storm, the only known in Tasmania to date. Extreme surface weather conditions leading up to and coinciding with the peak pyroconvection included maximum air temperature approaching and exceeding 40°C, relative humidity dropping to 10 % and northwesterly wind increasing, which altogether subsequently produced the catastrophic fire danger rating (FFDI of 112) – a rarity in Tasmania.

Violent firestorm development from the Dunalley wildfire was associated with highly unstable atmosphere and triggered by the approach of the line of convergence in the hours prior to the cold front passage. PyroCb formed in the lower wind zone situated along the line of convergence, which extended immediately downwind and southeast of the wildfire location. Having a source of energy from the escalated wildfire upwind of the northwesterly air flow and a source of moisture over the Tasman Sea in the southeast, over which the plume extended, the pyroCb gained strength for extensive vertical development. Although the pyroCb formed over a period of a few hours, the cloud's peak explosive development lasted only for a few minutes. While the surface meteorological conditions found at the location of the pyroCb aligned to support the fire storm, upper-level conditions were not sufficiently favorable for the peak stage of the pyroCb to last for more than few minutes.

The vertical development of the wildfire's plume was supported by the combination of the convergence of the surface wind field and positive vertical wind speed up to 850 hPa downwind of Dunalley area. Also, the sounding in the pre-frontal air mass indicated very unstable, warm and dry air up to 600 hPa and combustion processes within the wildfire further enhanced instability and contributed to already severe conditions favorable for the blow-up fire. Heat source from the fire burning through dry eucalyptus vegetation was sufficiently large and intense and the energy release must have been enormous so that vertical injection could reach the tropopause height at around 300 hPa, as the previous research on Forcett-Dunalley pyroCb suggested (Ndalila et al., 2019). This is because of increasing horizontal wind speed at upper-levels which reached gale force and speed of a jet stream (at 500 hPa and 300 hPa up to 24 m s<sup>-1</sup> and 28 m s<sup>-1</sup>, respectively).

Once the convection had been initiated at the surface the vertical development of the smoke column started to be visible on imagery from the nearby Mt Koonya radar. According to radar data the overshooting of the cloud top at one instance was up to 11 km, which is 3 to 4 km lower than the previous research suggested. Also, as per photographs of the fire plume and

other majority of radar images at the peak of pyroCb development, the smoke plume mostly resided at altitudes around 400 hPa or ~7.5 km, which is more realistic considering horizontal wind speed above this height. The additional confirmation for the pyroCb cloud top height are altocumulus clouds that formed next to the pyroCb (Figure 6.2). However, the pyroCb plume did gain enough energy to maintain the vertical axis and to breach the strong horizontal jet stream aloft for a few minutes.

Forcett-Dunalley pyroCb produced two lightning strikes, which in this case did not ignite additional fires due to pyroCb moving over Tasman Sea. Favorable conditions needed for the electrification of pyroCbs include air temperature around or below -20°C (Williams, 1989). The sounding data right from before the pyroconvection confirmed this condition at ~7.5 km height, which corresponds to the top of the Forcett-Dunalley pyroCb.

The lack of precipitation in this case confirms the common feature of strongly polluted pyroCbs that usually suppress the precipitation due to high aerosol concentration (Tory et al., 2016). However, if precipitation did occur and evaporated before reaching the ground it points towards development of dangerous downbursts (e.g., Rothermel 1991). Downbursts can influence ambient winds in terms of strength and direction under which a burning wildfire can become very unpredictable and pose a great threat to firefighters (e.g., Fromm et al., 2006; Trentmann et al., 2006; Fromm et al., 2012). The classic inverted-V sounding found in this case also indicates that downbursts from the pyroCb potentially occurred, which also provides an explanation for escalation in fire activity and size of burnt area by the end of the DUNALLEY 2 period and subsequent frontal passage.

### *7.6.3. Cold Front Passage*

The wind in the pre-frontal air mass on the day of the pyroconvection had northwest direction throughout the troposphere. The change in airflow occurred with cold front passage in the first hours of 5 January 2013, denoted as DUNALLEY 3 period. Passing through Tasmania surface wind sharply changed in direction from northwesterly to southwesterly and locally, near Dunalley, to southeasterly. This change influenced the wildfire by stopping the escalation in its activity and progression towards southeast, over the Tasman Peninsula. While the cold front at first affected the wind at lower levels, the upper-level northwesterly jet stream at first peaked, but eventually also decreased in speed and aligned to southwesterly direction on 6 January. The cold front passage brought the general ease in wind speed and advection of cool and moist air from the southwest and caused the wildfire to extend back-burning northeast

of ignition location, further inland, while the fire front along the Tasman Peninsula stopped its progression.

Many cases to date documented the pyroCb environment associated and influenced by a cold front passage (e.g., [Fromm et al., 2006](#); [Luderer et al., 2009](#); [Fromm et al., 2012](#)). Although the cold front passage in this case occurred ~10 hours after the peak of pyroconvection, the prefrontal dynamics were favorable for its initiation and blow up. To conclude, the presented meteorological analysis indicated that the combination of heat from the wildfire, strong wind and atmospheric instability ahead of the cold front passage triggered the explosive pyroCb development in the case of the Dunalley wildfire.

## CHAPTER 8

### METEOROLOGICAL DRIVERS OF EXTREME FIRE WEATHER IN CROATIA AND AUSTRALIA – COMPARISON STUDY

Previous meteorological analyses of the Split wildfire in Croatia and Forcett-Dunalley wildfire (from hereafter Dunalley wildfire) in Tasmania were performed using the ALADIN model and BARRA reanalysis, respectively. In order to compare fire weather characteristics of both wildfires high resolution simulations were performed using WRF model. The simulations involved a nested model runs with an ERA-Interim reanalysis initial conditions. In total, there were four nested domains with 500 m resolution of the innermost domain.

#### *8.1. Model Validation*

The WRF model results can be validated against AWS data in the case of the Split wildfire and against AWS and radiosonde data in the case of Dunalley wildfire. The simulations of mean sea level pressure, 2-metre air temperature and relative humidity and 10-metre wind were quite satisfactory in both cases. The afternoon maximum temperature at 2-metre temperature was slightly overestimated (up to 2°C) in the case of the Split wildfire (Figure 5.5a) and underestimated in the case of Dunalley (Figure 7.7b). On the day when Dunalley wildfire turned into firestorm (4 January 2013) maximum simulated air temperature is 38°C in the contrast to record breaking 41.8°C measured in Hobart (Figure C3). The morning maximum and the afternoon minimum relative humidity at 2 meters is simulated well, with the moisture advection accompanying cold front passage in the case of Dunalley a bit delayed (Figure 5.5a and 7.7b). Horizontal wind at 10-meters was slightly underestimated in both cases, more evidently in the case of Dunalley. The wind direction changes from northeast to southwest by the end of the Split case study period was not evident (Figure 5.5c) and the timing of the primary wind change after the cold front passage in the case of Dunalley was about 1 hour late (Figure 7.8). Compared to radiosonde measurements in the case of Dunalley (Figure 7.10a and b) upper-level wind speed was well estimated with the WRF model.

The WRF model results of outer domains with lower resolution can be compared with operational the ALADIN model and BARRA reanalysis. The tendency of the wind speed and direction within the Split wildfire area and its wider region over the Adriatic coast is consistent between ALADIN and WRF models. However, although simulated wind speed from the WRF model generally corresponds to measurements from the Split-Marjan station (Figure 5.5b, c), situated on the Split city peninsula, wind speed in wider area is stronger wind than in ALADIN

(Figure 5.7). This includes the wildfire's area in the outback of Split. Also, the discrepancy in the simulated data can be found in the timing of the offshore wind change which occurred during the day of the downslope wildfire run (SPLIT 2 and 3 periods on 17 July 2017). The turn from northeast *bura* wind to northwest was simulated 4 hours earlier than in the operational model ALADIN. Although both models simulated the general ease in wind speed at the end of analysed period, neither did present the wind direction change from northeast *bura* wind to southwest, which was observed at the Split-Marjan station. Peak in upper-level wind speed is in agreement in both models.

The WRF model simulated the convergence line that appeared in the case of Dunalley, presenting it closer to the pyroCb location at the time of its peak than the BARRA reanalysis (Figure 7.14c). In general, upper-level wind speed achieved its maximum approximately 4 hours later in WRF. Thus, upper-level wind speed at the time of the peak pyroCb was weaker than in BARRA (Figure 7.16), presenting more favourable conditions for the pyroCb development in this case. The discrepancy found more favourable for the pyroCb in the BARRA reanalysis data was the vertical wind speed (Figure 7.17e). In the WRF simulation the maximum vertical wind speed covered the smaller area downwind of Dunalley and appeared one hour earlier. However, these results presumably provide more realistic conditions due to more vertical levels in WRF (66 hybrid levels in contrast to 37 levels in BARRA).

## 8.2. Comparison of Initial Weather Conditions

Similar surface conditions at the ignition time for both wildfires include strong gusty wind as a result of tight pressure gradient over their areas (Figure 8.1a, b and 8.2a, b). Coincidentally, both wildfires were fanned by the wind blowing in direction from an inland towards a coast. From the ignition the Split wildfire was pushed towards the Adriatic Sea by the northeast *bura* wind, while Dunalley was carried towards the Tasman Sea by northwest wind. According to the WRF model *bura* wind at the Split wildfire location had speed between  $8 \text{ m s}^{-1}$  and  $12 \text{ m s}^{-1}$ , and in the case of Dunalley northwest wind had speed between  $4 \text{ m s}^{-1}$  and  $8 \text{ m s}^{-1}$ . However, as previous analyses presented, mean wind speed in both cases is slightly underestimated here.

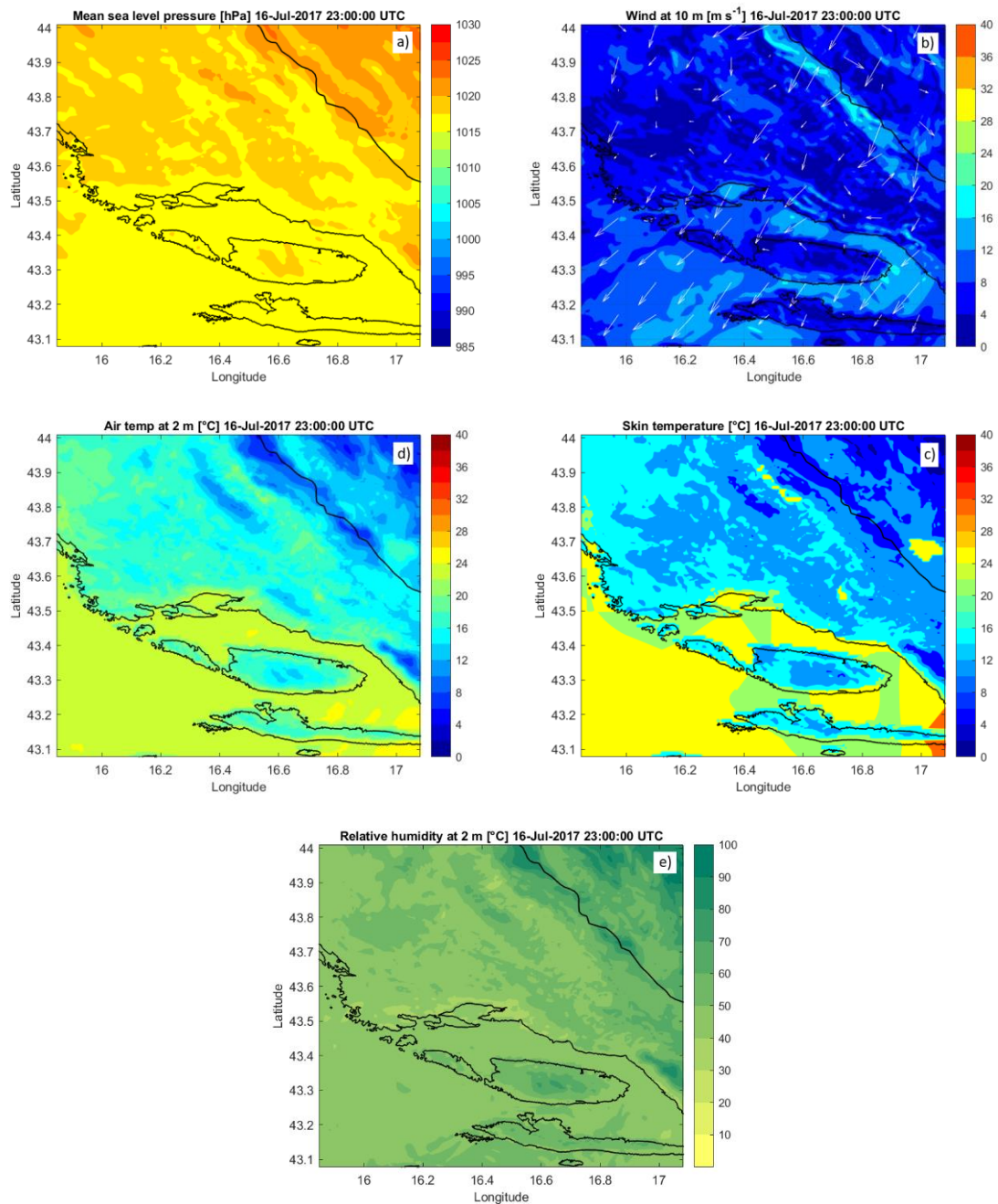


Figure 8.1. WRF model results at 500 m resolution for the Split case study: a) mean sea level pressure (hPa); b) wind at 10 m ( $\text{m s}^{-1}$ ); c) skin temperature ( $^{\circ}\text{C}$ ); d) air temperature ( $^{\circ}\text{C}$ ) at 2 m and e) relative humidity (%), all at 23 UTC on 16 July 2017.

Along with strong wind determining fire activity, other meteorological conditions coinciding with the wildfire's ignition were severe in both cases in their own terms. While ignition of Dunalley wildfire coincided with the culmination of the heat wave in Tasmania, the Split wildfire occurred after the cool change. It is also important to remember that Dunalley wildfire started around the midday, while the Split wildfire started in the evening. While northeast *bura* wind in the case of Split located in Croatia in the northern hemisphere means



advection of the cool air in summertime, the northwest wind in Tasmania in southern hemisphere means advection of hot and dry air from the central Australian mainland. This brings to conclusion why air and skin temperature and relative humidity values differed in these cases. According to WRF model the initial surface weather conditions in the Split case included air and skin temperatures up to 20°C and 16°C, respectively, and relative humidity under 50 % (Figure 8.1c, d and e). In the case of Dunalley simulated surface weather conditions were air and skin temperatures up to 32°C and 36°C, respectively, and relative humidity under 30 % (Figure 8.2c, d and e).

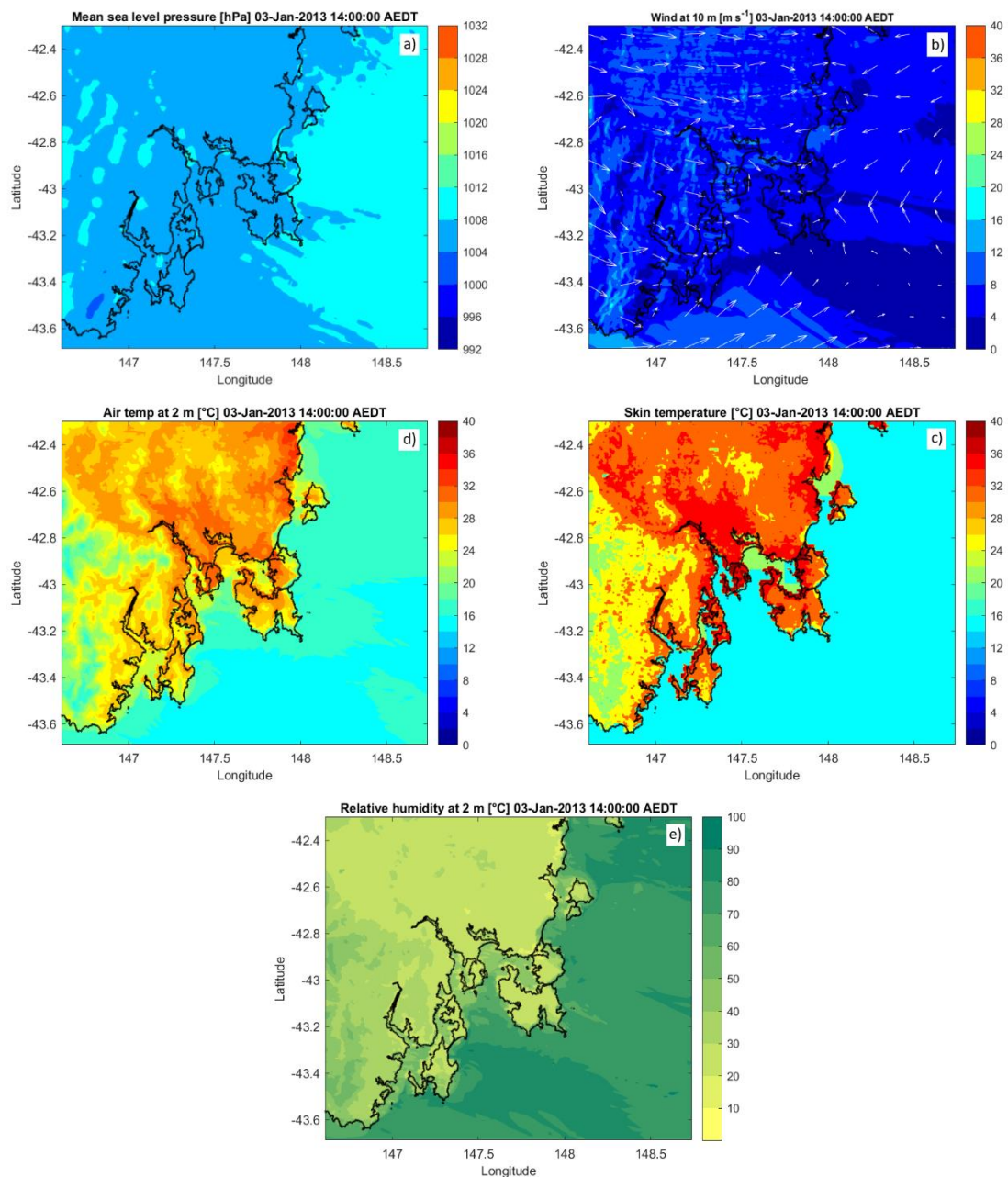


Figure 8.2. WRF model results at 500 m resolution for Dunalley case study: a) mean sea level pressure (hPa); b) wind at 10 m ( $\text{m s}^{-1}$ ); c) skin temperature ( $^{\circ}\text{C}$ ); d) air temperature ( $^{\circ}\text{C}$ ) at 2 m and e) relative humidity (%), all at 14 AEDT on 3 January 2013.

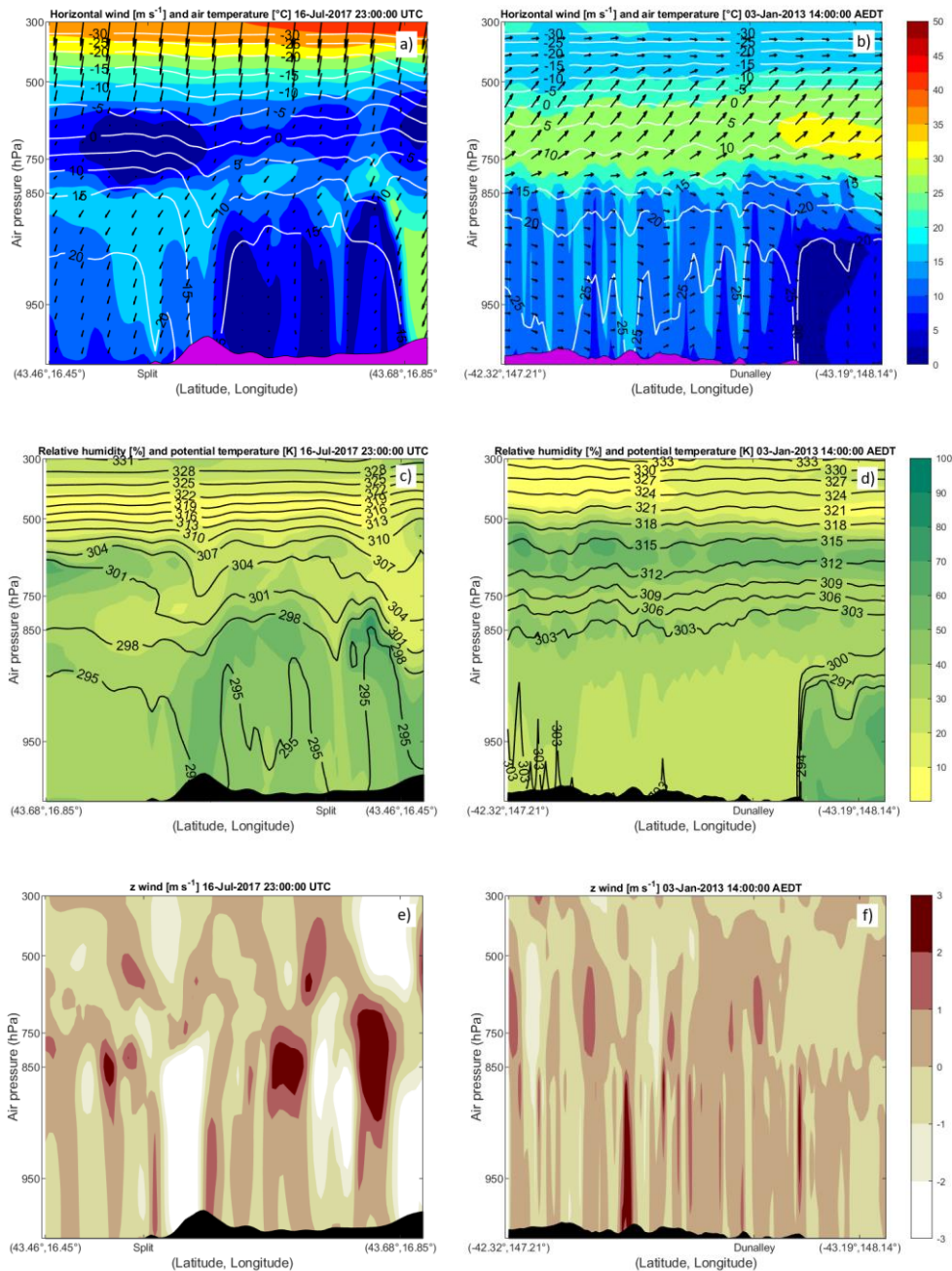


Figure 8.3. Cross section of wind speed ( $m s^{-1}$ ) and direction ( $^{\circ}$ ) and air temperature ( $^{\circ}C$ ; top); relative humidity (%) and potential temperature (K; middle) and z wind ( $m s^{-1}$ ; bottom) at a), c) and e) at 23 UTC on 16 July 2017 for the Split case study and at b), d) and f) at 14 AEDT on 3 January 2013 for the Dunalley case study, all from WRF model.

Different synoptic background caused different dynamics at the ignition time in both cases, which is the most evident from cross sections. On the one hand, in the Split case there is wind flow alignment throughout the troposphere presenting a deep *bura* case with the jet stream at the tropopause (Figure 7.3a), while on the other hand in Dunalley case there is the upper-level divergence at approximately 800 hPa level (Figure 7.3b). In the Split case a deep northeast *bura* flow was caused by synchronisation of the low surface pressure area with the

upper-level trough. In the case of Dunalley, the divergence was caused by the anticyclone situated northeast of Tasmania, over the Tasman Sea, supporting advection of northwest warm and dry air from the Australian mainland in the lower-levels while the southwest air flow remained in the upper-levels.

The cross sections of relative humidity reveal other significant upper-level differences in these two cases. In the Split case there was high relative humidity over the inland and lower relative humidity over the Adriatic Sea (Figure 8.3c) and in Dunalley case it was opposite with the warm and dry air over inland and moist air over the Tasman Sea (Figure 8.3d). Likewise, the differences are found in the cross sections of vertical wind speed which indicate strong downward motion above wildfire's area in the case of Split (Figure 8.3e), and upward motion in the case of Dunalley (Figure 8.3f). It is also interesting to note that in the contrast to ALADIN model, WRF simulation does not clearly indicate the hydraulic jump accompanied by strong *bura* flow in cross sections of horizontal wind speed. However, WRF does present strong subsidence or downward motion in the area of the Split wildfire.

### 8.3. Comparison of Weather Conditions Coinciding with the Most Extreme Fire Behaviour

The most severe hours of analysed wildfires included the escalation around all zones including the downslope run towards the city of Split and extreme fire behaviour in a form of pyroconvection near Dunalley.

The peak in extreme fire behaviour in both cases occurred in the afternoon hours, when surface weather conditions are usually the most severe and favourable for wildfire development. The WRF model results confirmed worst surface weather conditions in the case of Dunalley. This is because the downslope run in the Split case occurred after the cool change, while the pyroconvection in the case of Dunalley coincided with the culmination of the heatwave, when Hobart station recorded its highest air temperature in 120 years. According to the model both cases included very hot and dry conditions with air temperature up to 36°C, skin temperature up to 40°C and relative humidity under 20 % (Figure 8.4 and 8.5). As presented in the previous analysis, the actual air temperature in Dunalley was even higher. It is also noteworthy to mention that night before the most extreme fire behaviour in both cases did not allow for cooling and fuel moisture recovering, which was again more extreme in the case of Dunalley.

Surface wind field in both cases confirm persistent wind direction from the ignition until the most extreme fire behaviour in both cases. In the case of Split it was northeast *bura* wind and in the case of Dunalley northwest. As aforementioned, wind flow in both cases was oriented from the inland, where fires were burning, towards the coastline. At the time of the extreme fire

behaviour in both cases wind field in the innermost domain reveal the appearance of line of convergence. In the case of Dunalley this line of convergence got parallel to the main northwest wind flow and was closer to Dunalley area (Figure 8.5c). In the case of Split the line of convergence appears further offshore where the northeast *bura* flow perpendicularly coincided with the northwest flow (Figure 8.4c), which is common wind appearing over the Adriatic Sea during a daytime in summer known as *maestral*. Although surface wind speed in both cases was between  $4 \text{ m s}^{-1}$  and  $8 \text{ m s}^{-1}$ , comparing to measurements this wind speed in underestimated.

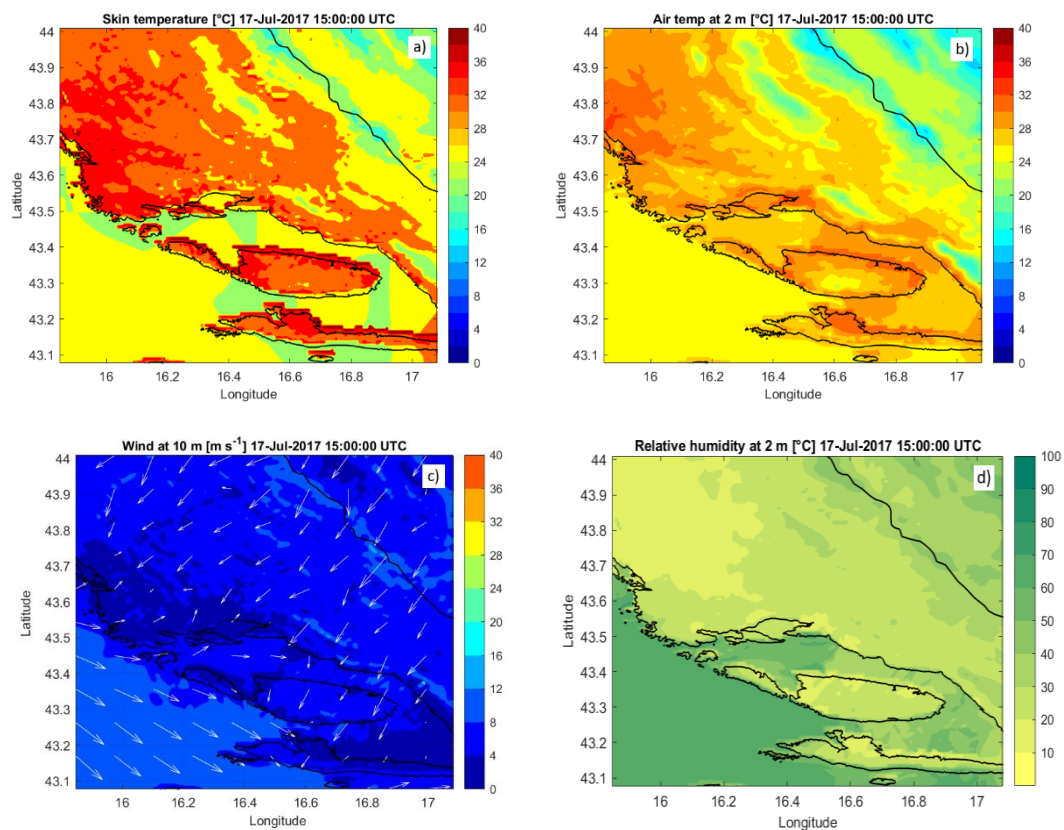


Figure 8.4. WRF model results at 500 m resolution for the Split case study: a) skin temperature ( $^{\circ}\text{C}$ ); b) air temperature at 2 m ( $^{\circ}\text{C}$ ); c) wind at 10 m ( $\text{m s}^{-1}$ ) and d) relative humidity (%), all at 15 UTC on 17 July 2017.

Upper-level conditions coinciding with the most extreme fire behaviour in both cases included alignment of wind flow throughout the troposphere, i.e., persistent wind direction from the surface up to the tropopause (Figure 8.7a, b). In the case of Split wildfire this occurred in hours prior to ignition and during all burn periods, while in the case of Dunalley the alignment occurred after the ignition and prior the pyroconvection. Therefore, in the Split case study plume extended in southwest direction and in Dunalley case in southeast direction or in both cases the plume extended from the mainland towards a sea. According to previous Split wildfire

reconstruction its extensive plume was sheared off sharply at approximately 4500 m altitude (Figure 4.5b), while Dunalley plume blew out into the pyroCb. The reason why the plume in Split case was cut off sharply is the gale force wind at 500 hPa (Figure 8.6b). Although the wind at upper-levels in case of Dunalley was even stronger (Figure 8.6c, d), the high fire intensity in the combination with unstable atmosphere in the pre-frontal air mass was enough for extensive convection up to the tropopause, although it lasted only for a few minutes.

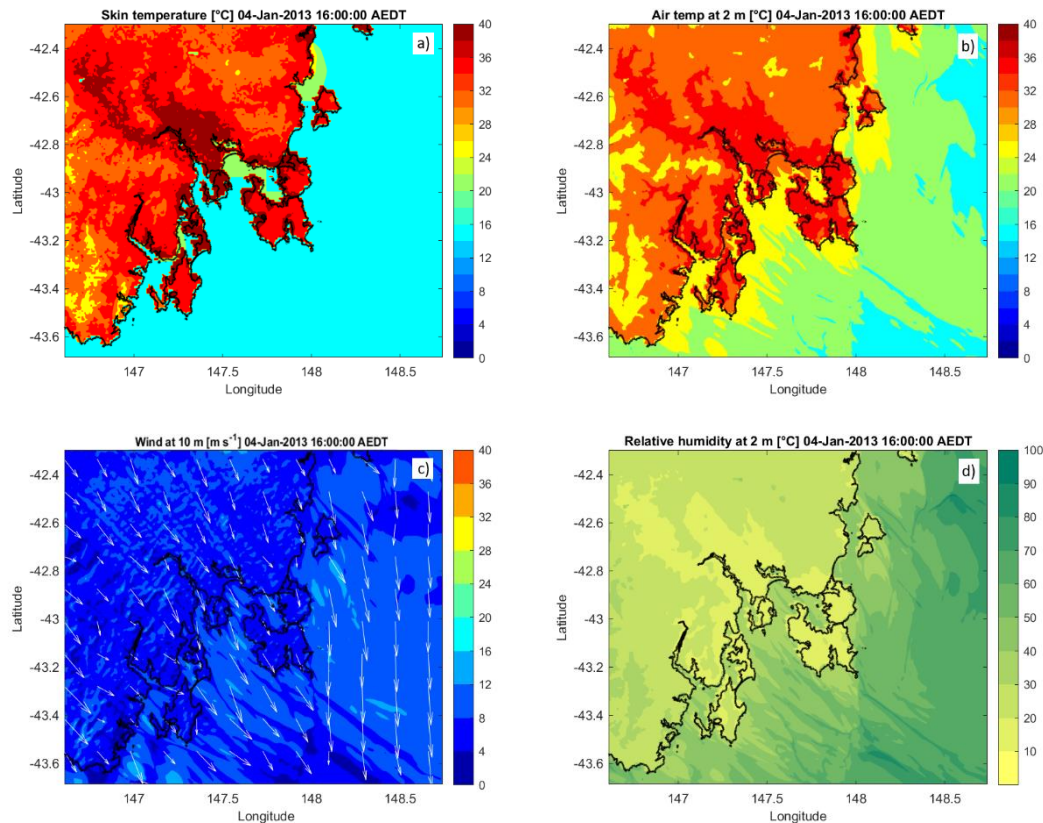


Figure 8.5. WRF model results at 500 m resolution for the Dunalley case study: a) skin temperature ( $^{\circ}\text{C}$ ); b) air temperature at 2 m ( $^{\circ}\text{C}$ ); c) wind at 10 m ( $\text{m s}^{-1}$ ) and d) relative humidity (%), all at 16 UTC on 4 January 2013.

Other upper-level weather conditions coinciding with the most extreme fire behavior included persistent downward motion in the case of Split and upward and well-mixed boundary layer conditions in the case of Dunalley. The difference between upper-level conditions between ignition time and the most severe wildfire hours included lowering of wind speed across the troposphere in the case of Split, and strengthening of wind speed in the case of Dunalley. In both cases upper-level fire weather conditions could not be straight forward classified to cause such extreme fire behavior as it occurred in these catastrophic wildfires. By the time of the downslope fire run in the case of Split *bura* flow eased and was weaker than 24

hours prior (Figure 8.7a). However, as the meteorological analysis showed, wildfire burned into plenty of dry fuels in higher altitudes in mountainous outback of Split where the *bura* flow was still moderate to strong. The topography of the area provided ideal conditions for channeled downslope fire run towards the city. Although not that extreme as at the ignition time, the cross sections at the time of the downslope fire run in the case of Split still indicated sinking motion and dry upper troposphere caused by trough crossing the wildfire's area (Figure 8.7c and e).

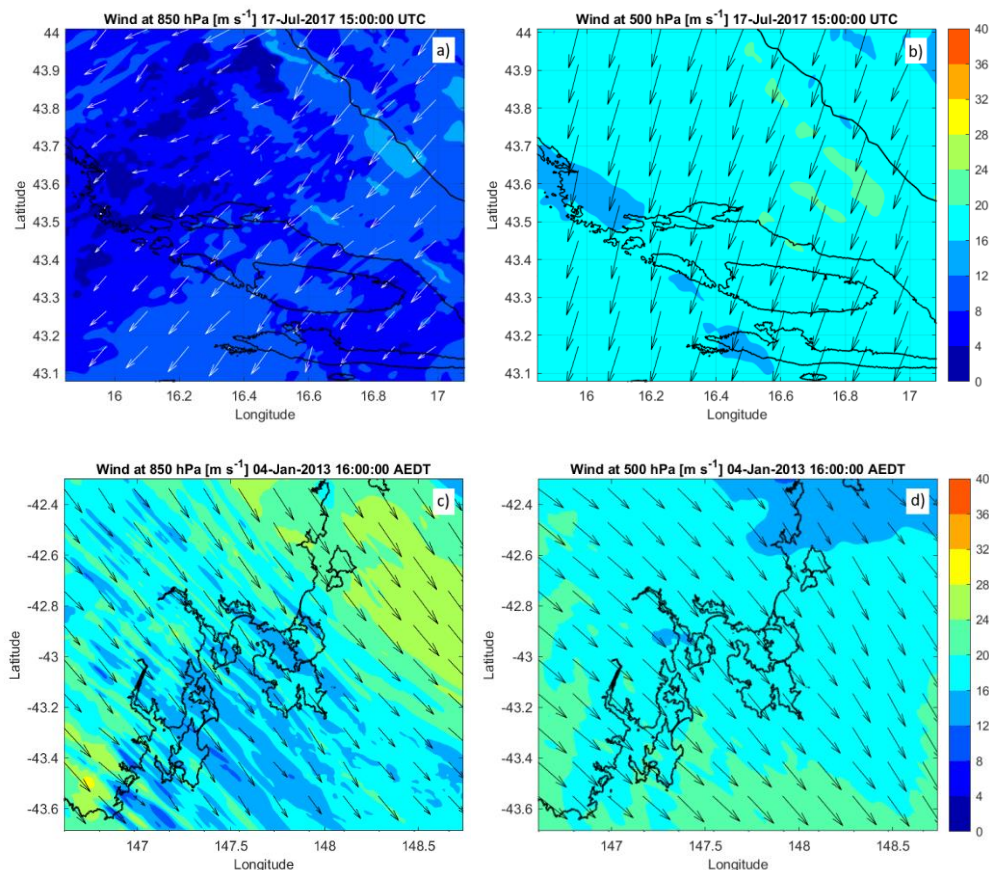


Figure 8.6. WRF model results from the finest domain at 500 m grid spacing of a) and c) wind at 850 hPa ( $\text{m s}^{-1}$ ) and b) and d) wind at 500 hPa ( $\text{m s}^{-1}$ ) for the Split case study at 15 UTC on 17 July 2017 (top) and Dunalley case study at 16 AEDT on 4 January 2013 (bottom).

In the case of Dunalley, stronger northwest wind flow than 24 hours prior contributed to fire spread rate and pushed the fire towards the area of dry eucalyptus forests, which in the end enhanced fire intensity and blew it into extensive plume. The wildfire's plume eventually evolved into pyroCb in spite of strong and gale force upper-level horizontal wind (Figure 8.7b). PyroCb managed to break this strong horizontal northwest air flow in the mid-troposphere and inject over the tropopause for a few minutes. However, the vertical development of the firestorm in the case of Dunalley was supported by the unstable conditions, strong vertical mixing and

upward motion over the wildfire's area together with the source of moist air in the upper troposphere and over the Tasman Sea (Figure 8.7d).

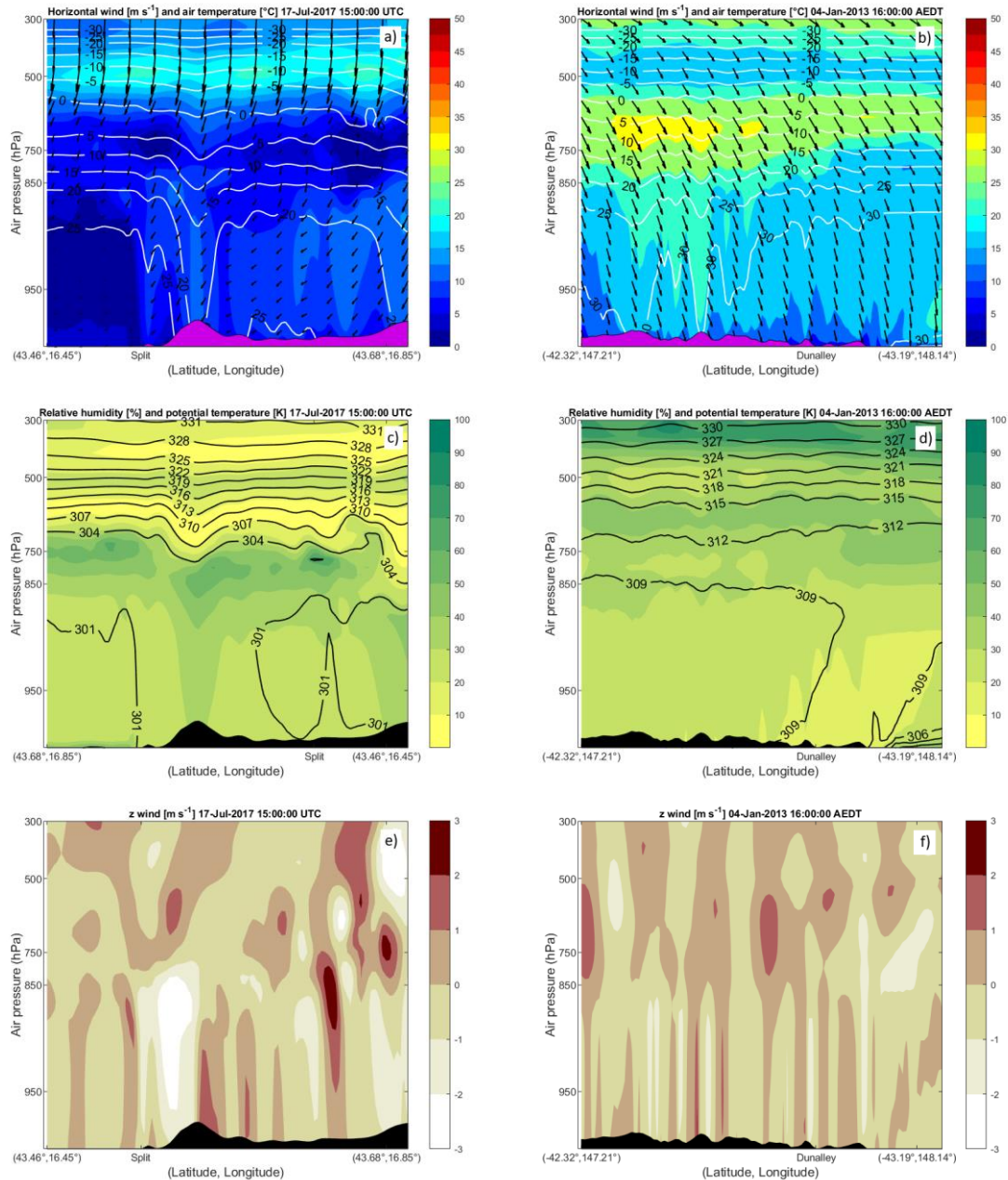


Figure 8.7. Cross section of wind speed ( $\text{m s}^{-1}$ ) and direction ( $^{\circ}$ ) and air temperature ( $^{\circ}\text{C}$ ; top); relative humidity (%) and potential temperature (K; middle) and z wind ( $\text{m s}^{-1}$ ; bottom) at a), c) and e) 15 UTC on 17 July 2017 for the Split case study and at b), d) and f) 16 AEDT on 4 January 2013 for the Dunalley case study, all from WRF model.

#### 8.4. Discussion and Conclusions

Two catastrophic wildfires from opposite sides of the world and different hemispheres do share some similarities in fire weather associated with their occurrence. Antecedent conditions in both wildfire events were undeniably similar with the lack of precipitation and higher-than-average air temperature in months' prior both wildfires. Extreme antecedent weather conditions consequently had an impact on fire danger rating which was extreme in both cases. High fire danger rating pointed out to possible extreme fire behaviour, which includes rapid fire spread, multiple fire fronts and fire burning in crown of trees. According to reconstruction of wildfires, this type of fire behaviour occurred in both cases.

The initial surface ignition conditions differed in air temperature and relative humidity, but were similar in wind conditions. The difference in air temperature and relative humidity was due to Split wildfire ignition occurring in the late evening hours on a day after the cool change, while Dunalley wildfire was re-ignited from an old fire stamp in the early afternoon, a day before the culmination of the heatwave in Tasmania. However, in the subsequent hours after the ignition surface conditions in Split case also aligned with hot and dry conditions found in Dunalley case. From the ignition both wildfires were fanned by strong surface wind.

The upper-level atmospheric conditions in analysed cases were different due to different synoptic background. The catastrophic wildfire in Split coincided with the upper-level trough and accompanied deep and strong *bura* flow which favoured sinking motion of dry air from aloft, while the most extreme fire behaviour in Dunalley case occurred at the peak of the heatwave and right prior to the cold front passage. The extreme fire behaviour in analysed wildfires included downslope fire run in the Split case and pyroconvection in Dunalley case. In conclusion, the Split wildfire can be defined as wind driven wildfire, while the Forcett-Dunalley wildfire was a combination of wind driven and buoyancy driven type of wildfire.



## CHAPTER 9

### PRELIMINARY WRF SFIRE SIMULATIONS OVER CROATIA

A step further in wildfire analysis and understanding the impacts fires can have on the surrounding atmosphere is possible by using coupled fire-atmosphere models. A physically-based coupled fire-atmosphere modelling system applied to various wildfire cases in the recent decade is the WRF SFIRE model. Previous studies that used WRF SFIRE simulations investigated winds in the vicinity of fires, estimated a fire growth and fire intensity and their dependence on varying wind speed and direction, topography and fuel characteristics (e.g., [Coen et al., 2013](#); [Simpson et al., 2013 and 2015](#)). For instance, Australian case studies found that fire progression was highly sensitive to small changes of environmental and fire modified wind speed and direction ([Peace et al., 2015, 2016](#)). Australian cases also confirmed that energy released by a fire can be strong enough to cause significant modifications to the surrounding atmosphere ([Peace et al., 2015](#)) and that accounting for the fire's influence on atmosphere evolution, and not only vice versa, is of utmost importance in representing fire behavior. Furthermore, high resolution coupled WRF SFIRE model simulations related rapid fire spread with the passage of mesoscale convective cells ([Peace et al., 2016](#)) and have been able to represent larger fire whirls, among the other fire phenomena ([Peace et al., 2015](#)). WRF SFIRE can be linked to the NWP in near real-time and be used for fire weather forecasting (e.g., [Kochanski et al., 2013](#)). WRF SFIRE model has been applied for multiple wildfire cases in Australia, but never to a wildfire event from Croatia. Therefore, this study provides an opportunity to present the first WRF SFIRE simulations over Croatia with the Split wildfire in July 2017 selected as the first case study.

The aims are to:

- 1) demonstrate the possibility to successfully run the WRF SFIRE model for Croatian fire event,
- 2) provide a verification of the model data. Specifically, the earlier reconstruction of the wildfire gives a valuable and rare opportunity for detailed verification of the fire progression in coupled simulations, and
- 3) investigate the possible fire-atmosphere interactions during the Split wildfire by testing the approach from previous studies which ran simulations in two modes – feedback ‘on’ and feedback ‘off’. The energy fluxes that are exchanged between the fire and the atmosphere are included or excluded in these model options. This method is used to determine whether and

how a simulated fire might affect the local atmosphere (e.g., [Peace, 2014](#)), which would be the first evidence of these processes occurring in a fire event from Croatia.

## 9.1. Input data for Coupled WRF SFIRE Simulations

### 9.1.1. Fuel Data

The fuel map prepared for initializing high resolution coupled simulations included the information available from Corine Land Cover (CLC). Following the methods from [Kartsios et al., 2021](#), the CLC raster data was reclassified into 13 categories of the Northern Forest Fire Laboratory (NFFL) classification ([Anderson, 1982](#)). The 13 categories define various vegetation categories ([Table 3.6.](#)) and [Figure 9.1.](#)), while category 14 is assigned to ‘no fuel’. No-fuel category consists of water bodies and wildland-urban interface. Finally, as the spatial distribution of the converted dataset is at 100 m, it was additionally resampled to 33.3 m to fit the fire domain by using the nearest-neighbor average option. The final fuel load map used for the Split fire simulation is presented in [Figure 9.1.](#)

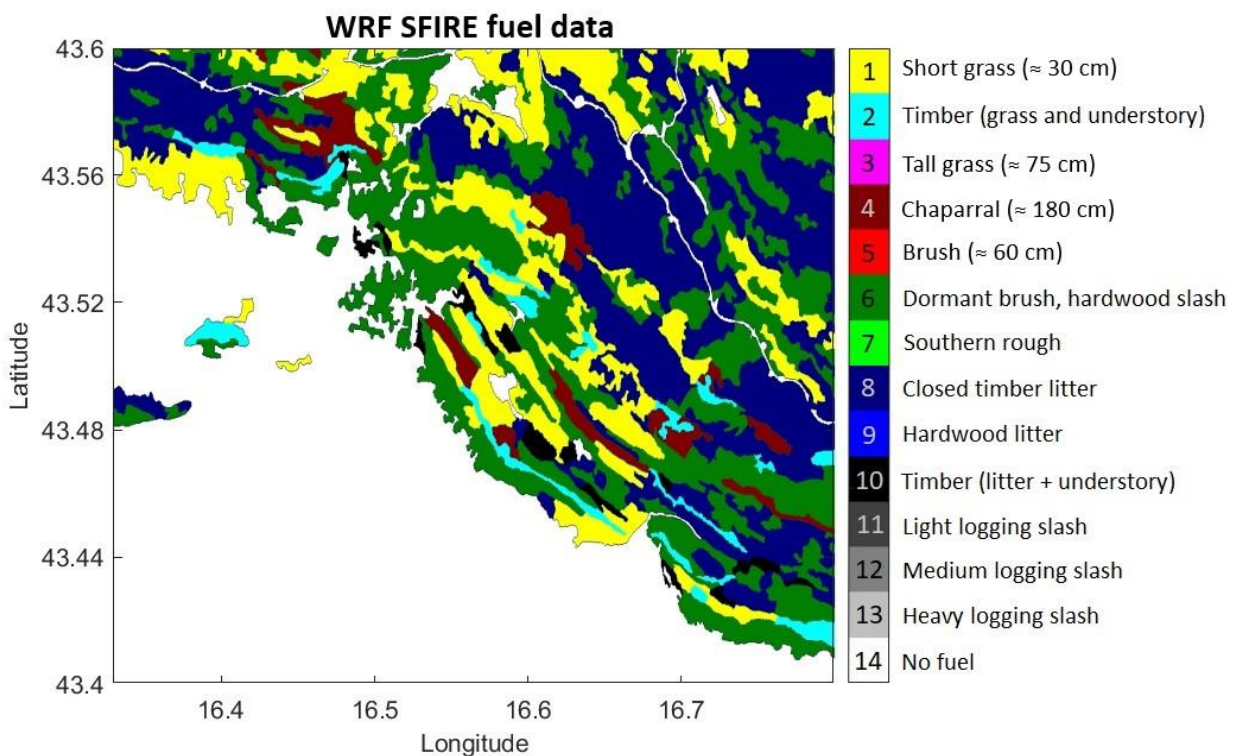


Figure 9.1. Fuel map in the WRF SFIRE simulation from CLC and according to fuel categories from [Anderson \(1982\)](#).

According to the presented classification fuel map the Split wildfire was ignited ( $43.49^\circ$  N,  $16.62^\circ$  E) in the area of short grass (category 1, yellow in [Figure 9.1](#)) and hardwood shrubs (category 6, dark green). The short grass ( $\approx 30$  cm) fuel model describes a fire spread through

fine cured herbaceous fuels, which can also consist of shrub or timber up to one-third of the area. Fires burning within this fuel model are surface fires that can move rapidly. Fire spread through the fuel model of hardwood shrubs requires moderate winds ( $> 3.6 \text{ m s}^{-1}$ ) at the mid-flame height (6.1 m). While flanking over the hill C during the SPLIT 1 period and in the valley between hills A and C during the SPLIT 2 period (Figure 4.2.) fire also spread through chaparral fuel (category 4, dark red), which is typical for Mediterranean area (Figure D2.b). Mediterranean chaparral includes flammable foliage and live and dead woody material in the crowns of pine or mature shrub stands that together with possible deep litter layer contributes to fire intensity and cause fast-spreading wildfires. Another fuel type that Split wildfire burned into at the top of the hills A and C is timber (grass and understory, category 2, cyan). This fuel type carries surface fires, which can be intensified by additional litter and dead stem woods from the open shrub or pines. Open shrub lands and pine stands may cover one-third to two-thirds of the area. Such stands may contribute to higher fire intensity and may produce firebrands (Anderson, 1982).

Table 9.1. Fuel depth (m) and fuel load ( $\text{kg m}^{-2}$ ) for fuel categories dominating the Split wildfire area.

Fuel category	Fuel depth (m)	Fuel load ( $\text{kg m}^{-2}$ )
1	0.305	0.166
2	0.305	0.897
4	1.829	2.468
6	0.762	1.345
8	0.061	1.121
10	0.305	2.694

The significant groups of fuel models affected by the Split fire also include fuel model 8 and 10. Those fuel models are situated in the far southeastern corner of the final fire perimeter and in the area of the northwestern flank (border between SPLIT 2 and SPLIT 3 periods in Figure 4.2. and D4) and both burned simultaneously during the SPLIT 3 period. Fuel model 8 (closed timber litter) include closed canopy stands of conifers or hardwood with the compact litter layer consisting of needles, leaves and twigs. This fuel model supports slow burning ground fires, with possible occasional flare up due to heavy fuel load. These fuels can become fire hazard under severe fire weather conditions that include high air temperature, low relative humidity and strong winds. Timber (litter and understory) which describes the fuel model 10 includes large load of dead material on the forest floor of any type. It causes crown fires, spotting and torching of individual trees (Anderson, 1982). Additional photos of described fuel types in the Split wildfire area can be seen in photos in Appendix F (Figures D1 to D4). Details on fuel model depth and load used in WRF SFIRE simulations can be found in Table 9.1.

### 9.1.2. Topography Data

The topography used in coupled simulations are from the dataset with spatial distribution of 100 m which has additionally been interpolated to resolution of 33.3 m in the WRF preprocessing system to fit the fire domain. Although high topographic resolution has been accomplished by interpolation, the terrain height still reveals complex local topography, which includes the mountain Mosor with peaks higher than 1400 a.s.l. close to the Adriatic Sea (Figure 9.2). WRF SFIRE terrain height of the Split wildfire area also includes hills Perun, Sridivica and Makirina (A, B and C, respectively, in Figure 4.2 and Table 9.2) elongated parallel to the coastline with the highest peaks of Mosor. Small discrepancy in topographic data and the overlaid coastline in Figure 9.2 is due to different data sources. The coastline is retrieved from the open-source Database of Global Administrative Areas (GADM) and overlaid for reference of the fire area and the nearby city of Split peninsula.

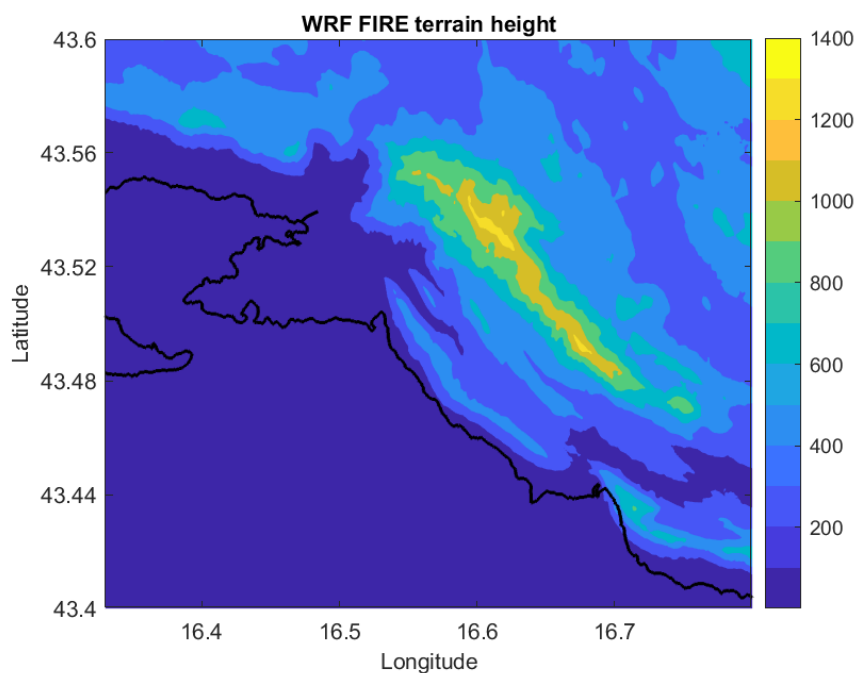


Figure 9.2. Terrain height in the innermost domain from WRF SFIRE and overlaid coastline from GADM data (the Database of Global Administrative Areas).

## 9.2. Verification of the Split Wildfire Coupled Simulations

Detailed reconstruction of the Split wildfire provides a valuable and rare opportunity for verification of not only simulated final fire perimeter, but as well the simulated fire spread. Precise information on ignition time and location together with mapped fire progressions and spotting within the first 30 hours of the wildfire were used for both – to initialize simulations and to evaluate the model's ability to simulate fire's propagation and final fire scar.

### 9.2.1. Initial WRF SFIRE Simulation

Based on information from the reconstruction, the fire was ignited in the innermost domain (d04) at 22:38 UTC on 16 July 2017, 10 hours and 38 minutes after the simulation start to allow for model spin up. The ignition shape was defined as a square of 40 m  $\times$  40 m size at the grid point that corresponds to coordinates (43.492° N, 16.624° E) of the real ignition location. As WRF SFIRE has no mechanism to stop the simulated fire (with the exception of the lack of fuel or if the fuel moisture exceeds the fire extinction threshold) it requires to define the time when the 'final' perimeter is reached. The Split wildfire progressions are previously mapped as four distinct spread periods, named SPLIT 1 to SPLIT 4 (Chapter 3). Therefore, as per beforehand prepared reconstruction, the time of the final perimeter will be defined as the end of the SPLIT 4 burn period or at 04 UTC on 18 July 2017. It is also important to note that WRF SFIRE model does not take into account the effect of firefighting suppression.

The first WRF SFIRE model result over Croatia partially reconstructs the observed fire perimeter (Figure 9.3). In comparison with the actual final fire perimeter (Figure 4.2) simulated fire underestimates the final burned area. After ignition, simulated fire propagated towards southwest, driven by northeasterly *bura* wind (4–8 ms<sup>-1</sup>, Figure 9.5a) which is consistent with the real fire. However, in 11 hours, or by the end of the SPLIT 1 period (purple contour in Figure 9.3), simulated fire advanced by 4 km and burned all the way to the Adriatic coast, omitting only no-fuel areas in this part of domain in village Srinjine and Tugare (northwest and southeast, respectively, contoured shapes inside of the fire perimeter). In the real fire case scenario by the end of the SPLIT 1 period the fire front was stopped by firefighting ground troops in the valley between hills A and C or on the half way between ignition location and Adriatic coast.

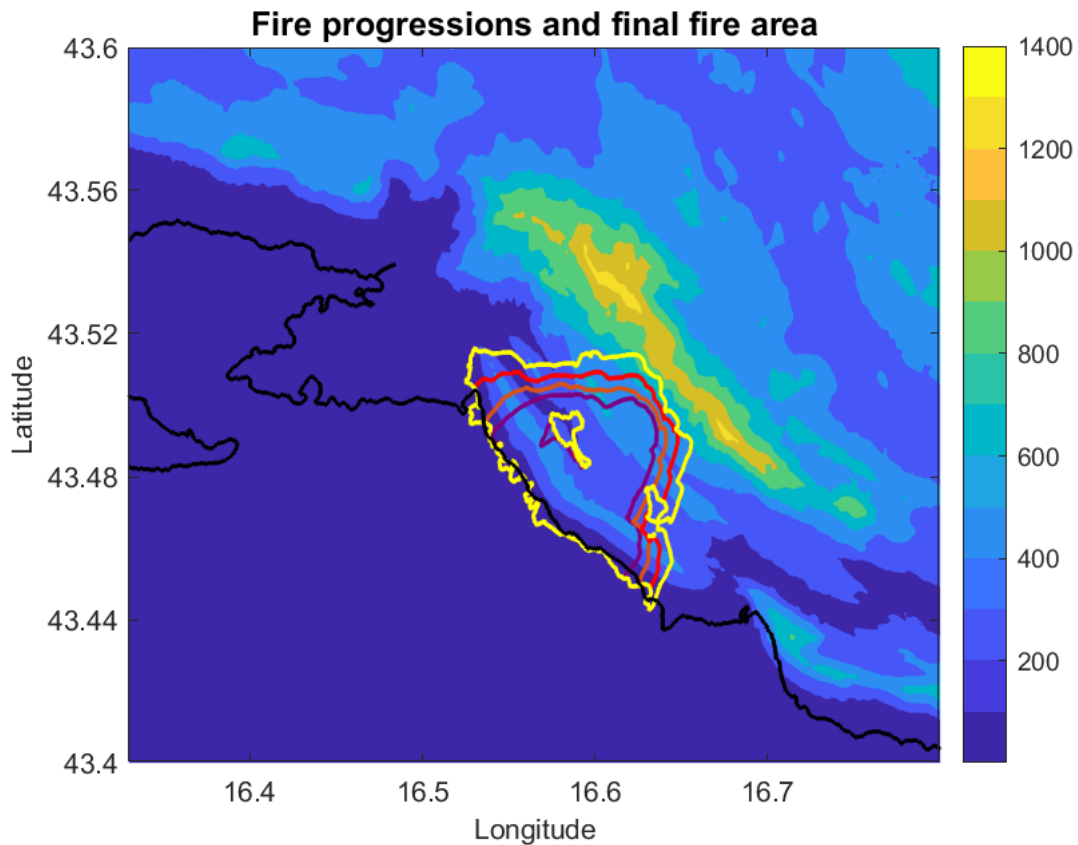


Figure 9.3. Final fire perimeters of four distinct fire progressions: SPLIT 1 (at 10 UTC on 17 July 2017; purple contour), SPLIT 2 (at 15 UTC; brown), SPLIT 3 (at 21 UTC; red) and SPLIT 4 (at 04 UTC on 18 July 2017, yellow) with terrain height (as presented in Figure 8.2). The difference between the fire front and the coastline contours is due to a slightly inconsistent coastline dataset in comparison to the topography and fire boundary datasets.

After reaching the Adriatic coast simulated fire slowed its progression and followed the available fuels along the coast in two separate directions, with the northwestern flank spreading further than the southeastern flank of the fire (brown, red and yellow contours in Figure 9.3.). The northwestern flank along the hill A and in between hills A and B (Table 9.1) reconstructs the real fire well. The real fire front along the hill A was stopped by the firefighting aircraft, while the front in between hills A and B was not a priority at time because it is mostly an uninhabited area. Firefighter efforts were focused around settlements in the valley between hills A and C, around villages Srinjine and Tugare, and around the flank progressing between hills B and C. The major discrepancy between the real and simulated burnt area are probably due to efficient firefighting suppression here. However, the real fire did eventually progress as presented in simulation, during the SPLIT 2 period.

Simulated fire did not capture the propagation of the northwestern flank between hills B and C, which in afternoon hours on 17 July (SPLIT 2 and 3) caused the fast topographically enhanced downward spread towards the city of Split. Also, during all four burn periods fire did

not progress much north after the ignition, which is consistent with the real case scenario, although the simulated fire did burn across the hill C to the north, not just to its peak.

Overall, WRF SFIRE overestimated the initial fire spread during the SPLIT 1 period after which it decelerated in comparison to the real fire. The northwestern flank of the simulated fire between hills B and C did not reach the real fire location at the foothill of mountain Mosor and therefore, did not reproduce the fast downhill spread towards the city of Split. In the end, due to this difference the simulated fire underestimated the size of a burnt area during the SPLIT 2, 3 and 4 periods. However, it is important to emphasize that the model gives the result of the influence of meteorological conditions and fuel material without taking into account the actions of firefighters, which can give an idea in which direction the spread of the fire is most prevented.

### *9.2.2. Reconstruction of the Split Final Burnt Area*

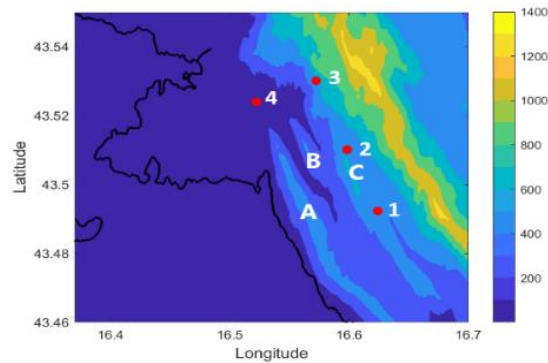
Three additional simulations were initialized in order to more accurately reproduce the final burnt area with the emphasis on the northwestern flank of the real wildfire, which caused the fast downhill fire spread towards the city of Split. Following the previously prepared detailed reconstruction (Chapter 3) it was possible to ignite more fire grids in the model that would coincide with locations where the real fire front was at time. This approach would also resolve the simulation of possible spotting (Kochanski et al., 2013) that occurred in this case. Therefore, the second simulation had one additional ignition (next to the initial one) at the Saint Luka church (noted as no. 2 in Table 9.2). The third simulation consisted of three ignitions – the first two as from the previous simulations and the third one is in suburban settlement of Amižići (no. 3). The final, fourth simulation, had four ignitions – three from the previous simulations and the fourth at Kučinsko field (no. 4) which is situated in the back of the city of Split peninsula. This ignition reconstructs the spotting that occurred during the downslope fire run into the city.

The most accurate final burnt area was simulated using four distinct ignitions (Figure 9.4). There was no significant difference between the simulation with only initial ignition (Figure 9.3) and two ignitions (not shown) as well as between simulations with three (not shown) and four ignitions. Third and fourth ignition together (Amižići village and Kučinsko field, Table 9.2) were the best option to reconstruct the northwestern flank of the real wildfire. Simulated fire fairly reproduced the rapid fire spread between SPLIT 2 and SPLIT 3 periods (difference between brown and red contours, Figure 9.4), although the area between hills B and C, which was the origin of the northwestern flank in the real fire, partially remained omitted. The fire spread rapidly from the ignition point 3 towards the southwest in two directions divided

by a no-fuel area – towards the city of Split, merging with the ignition point 4, and further south towards the active fire flank that was propagating along the hills A and B.

Table 9.2. Location and time of four distinct ignitions in WRF SFIRE simulations. All ignitions in the model were lit for 60 s within a square of 40 m x 40 m size. Letters A, B and C denote hills Perun (533 a.s.l.), Sridivica (420 a.s.l.) and Makirina (723 a.s.l.), respectively.

WRF SFIRE IGNITIONS			
Ignition	Name	Coordinates	Time
1	Initial ignition	43.492° N, 16.624° E	22:38 UTC, 16 July
2	Saint Luka church	43.510° N, 16.598° E	07 UTC, 17 July
3	Amižići village	43.530° N, 16.572° E	14 UTC, 17 July
4	Kučinsko field	43.524° N, 16.522° E	16:30 UTC, 17 July



The fast fire spread in this area (difference between brown and red contour, [Figure 9.4](#)) can be explained by *bura* wind ([Figure 9.5c](#)), topography and higher fuel loads of prevailing fuel categories of chaparral and timber ([Figure 9.1](#)). As noted, Mediterranean chaparral comprises of flammable live and dead material in crowns of pine trees with possible deep litter layer, which contributes to fire intensity and spread, while timber fuel includes large loads of dead material and causes crown fires and spotting. This type of fire behavior was observed during the SPLIT 3 and SPLIT 4 periods.

The flank of the simulated fire towards the city of Split peninsula penetrated deep into the urban area until it was constrained by the no-fuel category ([Figure 9.1](#)). The simulation here agrees with the real case scenario ([Figure 4.2](#)), however with a delay of few hours ([Figure 9.4](#)). The flank of the wildfire within the city of Split burned until the end of the SPLIT 3 period in the real fire in contrast to the end of the SPLIT 4 period in simulation.

The other flank of a downhill spread from the ignition point 3 merged with the flank of the fire that steadily progressed northwestward along the hills A and B. The notable difference between the simulated and the real fire is in the area is along the northwestern tip of the hill A. Timber fuels here (and downy oak forest, [Figure D3.b](#)) burned during the SPLIT 4 period in the night between 17 and 18 July 2017, in contrast to simulated fire which burned this area earlier in simulation (by 21 UTC on 17 July during the SPLIT 3 period, [Figure 9.3](#)). This discrepancy could be due to neglecting the firefighting suppression in the simulation. Thus, from earlier description of the fire progression, the firefighting aircraft extinguished the wildfire at the top of the hill A (approximately in the middle of A) in early afternoon on 17 July, stopping



its spread downhill towards the Sea and also towards northwest. Had this not occurred, as simulation is suggesting, the fire would advance along the hill A until it finally reached the northwestern tip of the hill where the downy oak forest is situated. This location eventually did burn in real case (during the SPLIT 4 period) in a downslope spread coming from its north side on the far western edge. The rest of the simulated final burnt area and fire spread corresponds to the simulation with only one initial ignition.

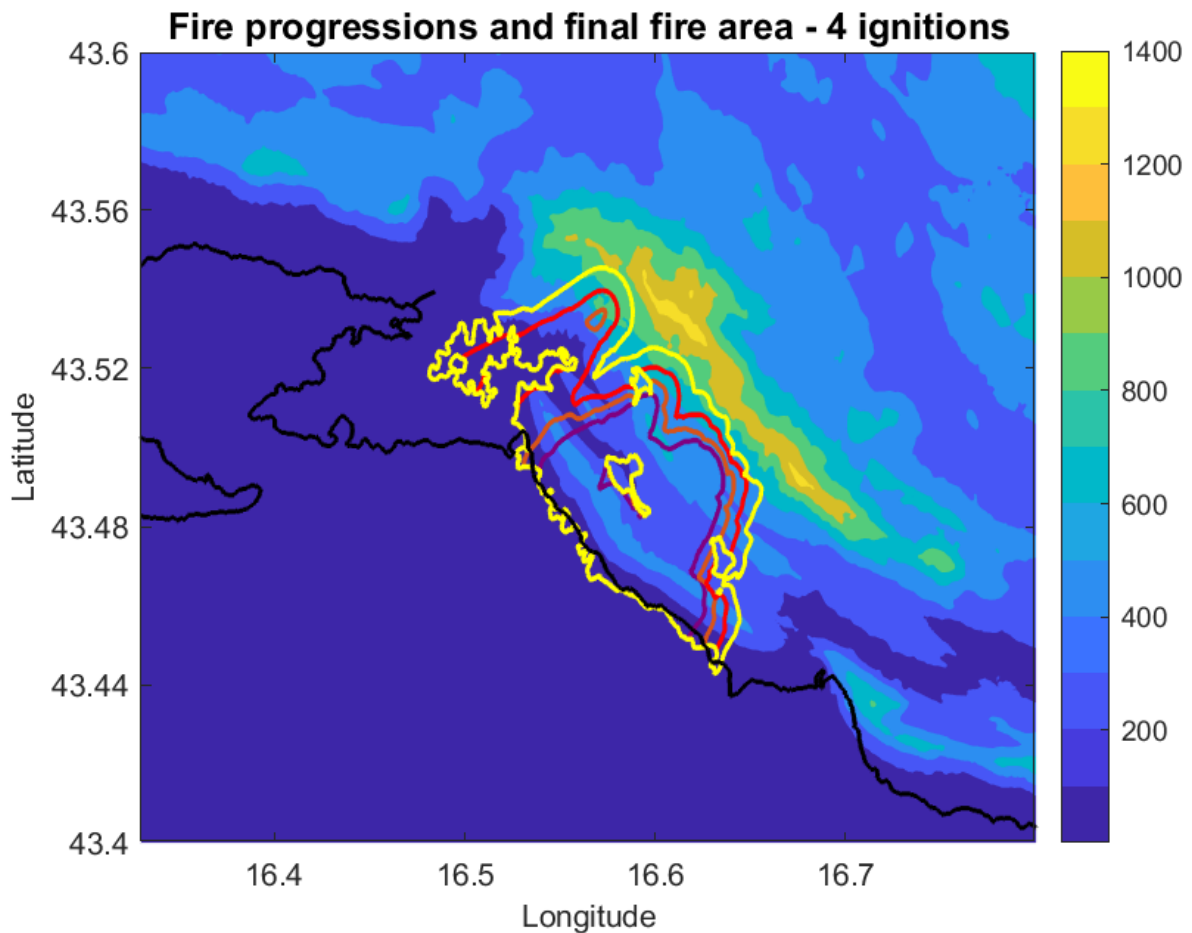


Figure 9.4. Final fire perimeters of four distinct fire progressions: SPLIT 1 (at 10 UTC on 17 July 2017; purple contour), SPLIT 2 (at 15 UTC; brown), SPLIT 3 (at 21 UTC; red) and SPLIT 4 (at 04 UTC on 18 July 2017, yellow) with terrain height. The difference between the fire front and the coastline contours is due to a slightly inconsistent coastline dataset in comparison to the topography and fire boundary datasets.

### 9.3. Fire-atmosphere Interactions over Adriatic Coast

To investigate possible fire-atmosphere interactions in the case of the Split wildfire simulations were run in feedback ‘on’ and feedback ‘off’ mode. The difference is in the inclusion and exclusion of energy fluxes between the fire and the atmosphere. Coupled simulations provide good representation of fire-atmosphere interactions in this case regardless the discrepancy between simulated and the real fire, which most probably occurred due to coarse fuel spatial distribution and topography input data and suppression efforts that the WRF Sfire model does not take into account.

The difference in fire area in feedback ‘on’ and ‘off’ simulations (left and right panels in Figure 9.5) present the sensitivity to inclusion of fire-atmosphere feedback. Although very similar, fire areas at the end of each burn period are overall greater in feedback ‘off’ simulation. The difference in wind fields and fire areas also provide evidence of fire-atmosphere interactions in this case. The most significant difference between feedback ‘on’ and ‘off’ simulations can be seen in wind field at the end of the SPLIT 1 period (Figure 9.5a, b). In the feedback ‘on’ simulation fire induced greater wind speed in the area between hills A and C where *bura* was accelerated from 4–8 m s<sup>-1</sup> to 8–12 m s<sup>-1</sup>. The most significant fire effect on environmental winds (shift in wind direction caused by the fire) can be seen at the NW tip of the hill A (Figure 9.5a). Detailed view of this section of fire perimeter reveals the shift in wind vectors around the fire front (Figure 9.7). This is the area that mostly burned during the SPLIT 4 period, while in the feedback ‘off’ simulation it reached this location earlier, by the end of the SPLIT 2 period. Coupled simulations confirm that *bura* dominated fire ground during all four burn periods, which is consistent with measurements and both ALADIN and WRF model. Moderate to strong *bura* pushed the fire rapidly towards the Adriatic coast in the southwest by the end of the SPLIT 1 period, while fire growth was constrained towards north. Weak *bura* periods allowed the fire spread through unburned fuels in the northwest and northeast, which is the most evident during SPLIT 2 and SPLIT 4 periods and especially in the feedback ‘off’ simulation (Figure 9.5c, d,g,h). At the end of the SPLIT 2 both ‘on’ and ‘off’ simulations (Figure 9.5c, d) depict weak westerly wind over the Adriatic Sea and the convergence zone south of the fire perimeter and the hill A. This weak wind zone downstream of *bura* allowed successful aircraft operations in real fire along the hill A together with smoke convection at this location (Figure 4.2).

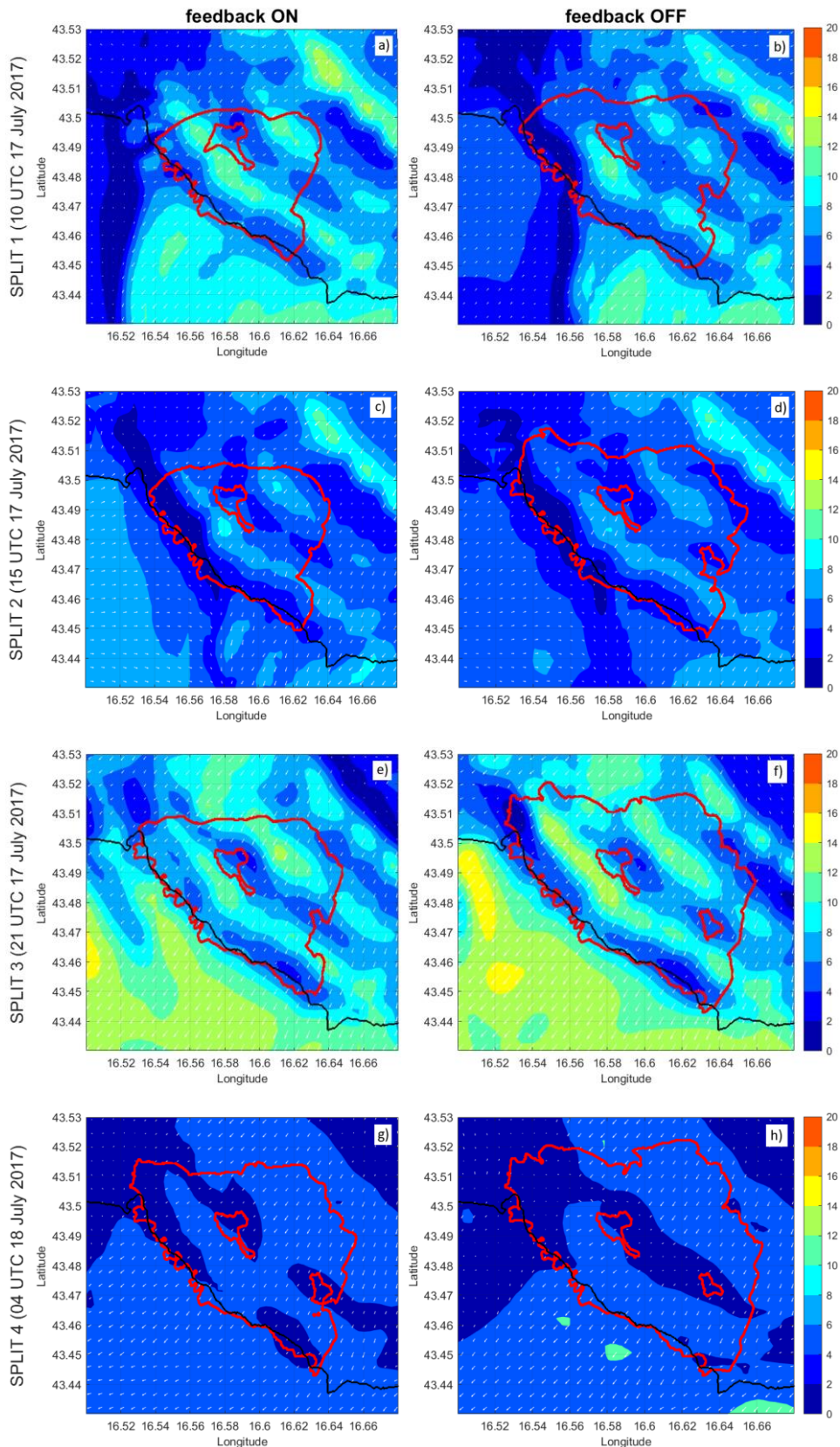


Figure 9.5. Fire perimeter (red line) and wind speed ( $\text{m s}^{-1}$ ; colored and array) at 6.1 m elevation at the end of SPLIT 1 to SPLIT 4 periods for feedback ‘on’ (left panels) and feedback ‘off’ (right panels) simulations with one ignition point (wind vector at every 15<sup>th</sup> grid or at every 500 m).

By the end of the SPLIT 3 period (Figure 9.5e, f) *bura* reinforced its speed and this time was stronger in the feedback ‘off’ simulation (up to 16–20 m s<sup>-1</sup>). Stronger *bura* constrained the fire spread towards north and enhanced fire growth in the southeast section. This part of simulation revealed that if there was a flank of the fire and spotting in the northwest, along the hill C, strong *bura* would push the fire downslope towards the city of Split, which did occur in real fire. Although the downslope fire run was not simulated by the WRF SFIRE model due to the coarse vegetation spatial distribution and topography input data it did to some extent reproduced the fire perimeters and outline the complex local environmental winds in the area.

The approach on including and excluding the feedback between the fire and the atmosphere in Split wildfire simulation follows the recent meteorological analyses of fire case studies from Australia. The advantage of this approach is that WRF SFIRE outputs can show how fire perimeter is affected by the coupling processes and can be used to assess how fire can modify the local atmosphere (Peace at al., 2015). However, some studies warn that the feedback ‘off’ simulation should be interpreted with caution since it can present an inaccurate physical representation of fire propagation (Coen at al., 2013). Previous studies showed that simulated fire wind fields (mid-flame height at 6.1 m) are comparable with 10 m wind (Cao and Fovell, 2018). Therefore, the most prominent fire induced effect on the surrounding atmosphere at the end of the SPLIT 1 period that was found in comparison of feedback ‘on’ and ‘off’ simulations is additionally confirmed with the WRF output of 500 m resolution (Figure 9.6a, b).

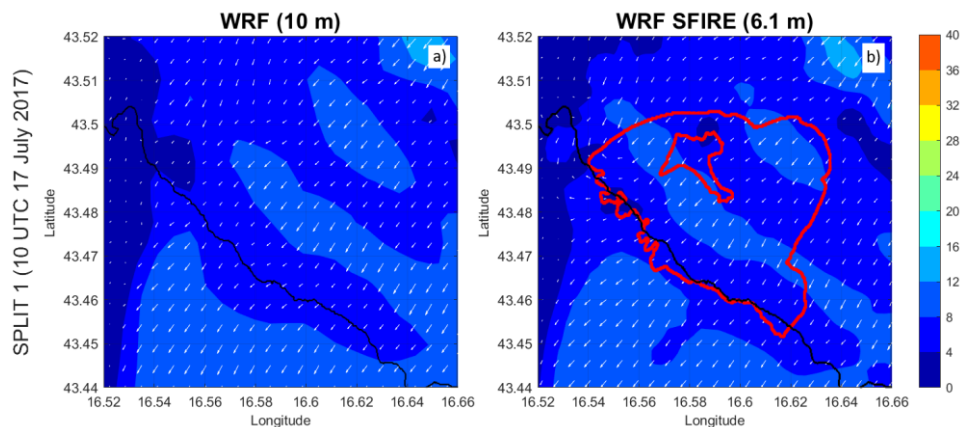


Figure 9.6. Comparison of wind speed (m s<sup>-1</sup>; colored and array) in a) WRF simulation (from 500 m grid spacing) at 10 m and b) WRF SFIRE feedback ‘on’ simulation (33.3 m resolution with wind vector at every 15<sup>th</sup> grid or at every 500 m) at 6.1 m and fire perimeter (red line), both at 10 UTC on 17 July 2017 (end of SPLIT 1 period). Note: wind speed scale here is up to 40 m s<sup>-1</sup>.

More detailed insight into the northwestern flank of the fire reveals the evident shift of wind vectors inside the fire perimeter (Figure 9.7). This shift occurred approximately 2.5 km downstream of the strongest part of *bura* flow, which lies along the Adriatic Sea coastline. *Bura* flow here turned to east and further to southeast, following the direction of the fire progression and pushing the head fire forward. The unmodified background *bura* inflow had speed of between 8 and 12 m s<sup>-1</sup> (Figure 9.6a), which in the vicinity of the fire accelerated to between 12 and 16 m s<sup>-1</sup> (Figure 9.6b and 9.7).

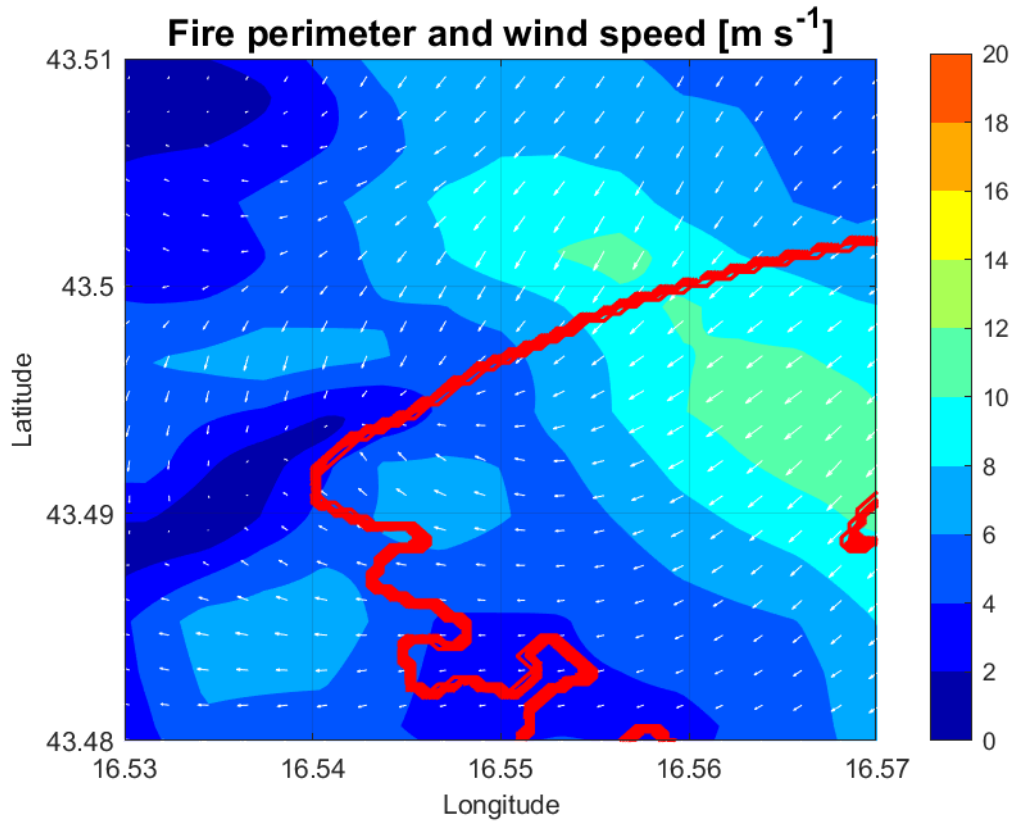


Figure 9.7. WRF SFIRE feedback 'on' simulation of NW flank of the Split wildfire at 10 UTC on 17 July 2017 (end of the SPLIT 1 period): fire perimeter (red line) and wind speed (m s<sup>-1</sup>; colored and array). Fire wind fields are at 6.1 m mid-flame height (with wind vector at every 5<sup>th</sup> grid or at every 166.5 m).

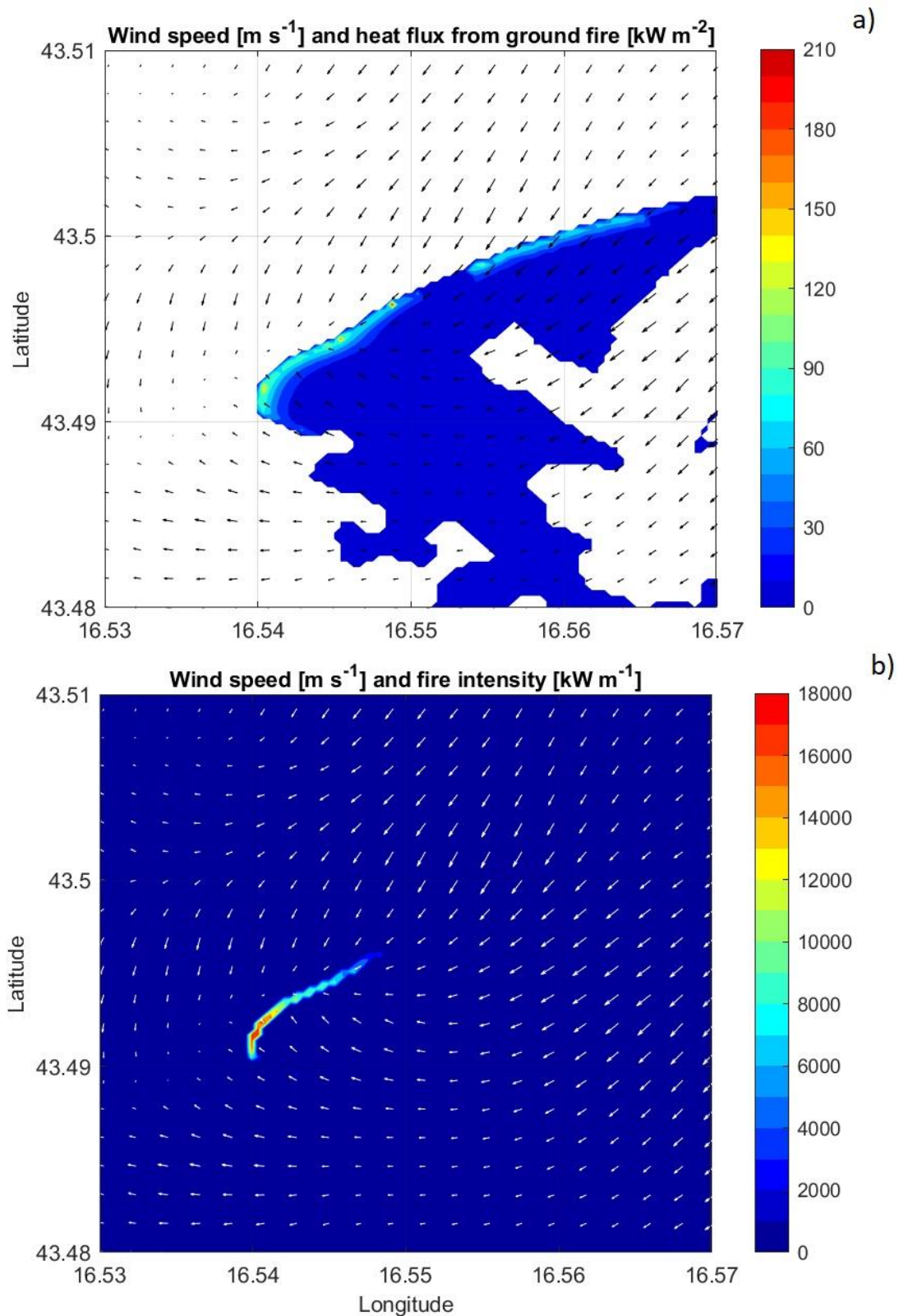


Figure 9.8. WRF SFIRE feedback 'on' simulation of NW flank of the Split wildfire at 10 UTC on 17 July 2017 (end of the SPLIT 1 period): a) heat flux ( $\text{W m}^{-2}$ ; contoured) from ground fire and wind speed ( $\text{m s}^{-1}$ ; array) and b) fire intensity ( $\text{kW m}^{-1}$ ; contoured). Fire wind fields are at 6.1 m mid-flame height (with wind vector at every 5<sup>th</sup> grid point or at every 166.5 m).

Fire progression in the WRF SFIRE model is calculated by a level-set method (Mandel et al., 2011) using the Rothermel (1972) equations. At each time step heat and moisture fluxes are calculated based on the amount and type of fuel consumed at each grid cell. The heat fluxes ( $\text{W m}^{-2}$ ) are further converted into potential temperature and water vapor forcing terms and inserted into differential equations of the atmospheric model. The calculated values are inserted into a layer above surface, further using an exponential decay with altitude. At the next time step the energy released by the fire affects the atmospheric (wind) fields. In the feedback ‘off’ option no fluxes are inserted into the lowest atmospheric layer and the atmosphere is unaware of the fire burning beneath (Peace, 2014). Heat flux from the ground fire at the end of the SPLIT 1 period was the highest at the northwestern flank. In the area of the fire modified winds heat flux reached  $206 \text{ kW m}^{-2}$  (Figure 9.8a).

Fire intensity refers to the amount of energy emitted by a fire or the features of fire behavior, such as flame height and spread rate (Keeley, 2008). Quantity of fire intensity is fire-line intensity, which describes the radiant energy per unit length of the fire line. It is useful in fire management as it gives an insight on how likely a fire is to further propagate and how difficult it will be to extinguish. Fire-line intensity ( $\text{W m}^{-1}$ ) is calculated according to Byram (Byram, 1959) and it is equal to the product of the fuel low heat of combustion (defined in WRF SFIRE simulation as a constant of  $17.433 \times 10^6 \text{ kJ kg}^{-1}$ ), quantity of fuel consumed in the flaming front (constant for 13 fuel categories of Anderson;  $\text{kg m}^{-2}$ ), and the linear rate of fire spread (computed from the WRF SFIRE model;  $\text{m s}^{-1}$ ). Fire-line intensity values can range from 10 - 100,000  $\text{kW m}^{-1}$ . Low values describe slow progression of a fire, while the highest values denote fast-spreading fire in heavy fuel. Some studies suggest simpler scale of wildland fire intensity for the purpose of easier communication with the public – to convert intensities from 10 to 100,000  $\text{kW m}^{-1}$  to the logarithmic scale in range from 1 to 5. The highest fire-line intensity at the northwestern flank of the Split wildfire that coincides with the wind field deformation (Figure 9.8b) is estimated at 18,118  $\text{kW m}^{-1}$  or at 4.26 of logarithmic scale. This intensity is found at the particular fire grid point along the fire front at the end of the SPLIT 1 period. This, however, does not exclude the possibility of even higher fire intensities in this case that could be found in between denoted burn periods. The maximum rate of fire spread in aforementioned time slot was  $0.95 \text{ m s}^{-1}$ .

#### 9.4. Validation of the WRF SFIRE Simulations over Croatia

The results demonstrated that the WRF SFIRE model has the ability to work with real data from Croatia and produce adequate results for forecasting fire spread. Successful

simulations provide the first numerical evidence that a wildfire from the Adriatic coast region can modify the dynamical structure of the surrounding atmosphere, which agrees with observations from fire grounds.

The in-depth reconstruction of the real fire event near the city of Split in July 2017 allowed the verification of WRF SFIRE model simulations. Simulated fire does reproduce the real fire to some extent, at times overestimating the rate of spread, but overall underestimating the final burnt area. There are three most probable explanations for the discrepancy between the simulation and actual outcomes. The first is neglecting the firefighting suppression, which was in the case of the Split wildfire heavily applied throughout the event both from the air and ground. The second is due to coarse resolution of initial fuel and topography data, which are additionally interpolated from 100 m to finer fire mesh grid of 33.3 m. While high resolution fuel datasets are unavailable for Croatia, there are accessible high resolution topography data. However, those were not assimilated for presented WRF SFIRE simulations. The third and final explanation lies in the fact that WRF SFIRE model capabilities are limited to simulating surface fires that spread through fuels lying on the ground, grass, shrubs and litter (Mandel et al, 2011; Coen et al., 2013). WRF SFIRE does not yet incorporate algorithms needed to treat possible crown fires, spreading through the canopies of trees. This is most probable reason why the total burnt area in simulated fire is smaller than in real fire, despite of the model neglecting firefighting suppression.

The preliminary simulations here are designed to guide further WRF SFIRE model usage for investigating future real cases while resolving the assimilation of high-resolution input data. Also, preliminary WRF SFIRE simulations were not optimized for speed. Therefore, in order to incorporate predictive coupled atmosphere-fire simulations for operational fire weather forecasting and fire management in Croatia, the future scope should be to find an appropriate model setting, which would demonstrate the model's ability to provide the near real time results. The WRF SFIRE model has the potential for operational application in Croatia with more accurate fire predictions in the future, which could be accomplished by inserting the higher resolution input data into the model. Possible uses for fire management in Croatia includes prediction of fire spread and intensity that may vary under changing weather conditions, available fuels and topography, planning effective and safe deployment of ground and aerial firefighting forces, preventing wildland-urban interface fires, effective planning of evacuation routes etc. The WRF SFIRE model results from this research demonstrate that the model is important for fire weather research and education purposes in order to better understand this hazardous phenomenon that occurs in Croatia.



## CHAPTER 10

### CONCLUSIONS

#### *10.1. Summary and Conclusions*

The primary aim of this study was to investigate the fire weather of two catastrophic wildfires that occurred in Croatia and Tasmania (southeast Australia). Before the meteorological analysis of these wildfires, a comprehensive literature review of fire weather meteorology was undertaken together with past and future climate influencing fire risk along the Adriatic coast in Croatia and in southeastern Australia. The two case studies provided an opportunity to study some of the most extreme fire weather recorded to date in Croatia and Tasmania and, while occurring in different hemispheres, the chosen cases share similarities in latitude, coastal setting and topography. The Croatian case study was based on the Split wildfire in July 2017 – the most severe wildfire in Croatia’s history given the size and unexpected fire behavior, which produced downslope fire runs into densely populated areas. The Australian case study was based on the Forcett-Dunalley wildfire in January 2013, which caused vast destruction, rapid fire spread and generated firestorm in the form of a pyrocumulonimbus – the first on record in Tasmania. Meteorological analyses of wildfires were preceded by their reconstruction and definition of the most severe burn periods in order to associate atmospheric conditions and fire behavior in detail. The second aim of this study was to draw similarities between dynamic atmospheric processes and mechanisms that occurred in these wildfire cases. The final aim was to implement a coupled fire-atmosphere model for the first time in Croatia and to investigate the effects that wildfire occurring along the Adriatic coast has on the surrounding atmosphere.

This research confirmed fire weather patterns previously found in multiple cases to date to coincide with the most catastrophic wildfires. In the case of Split, the ignition of the wildfire coincided with an episode of a strong downslope bura windstorm, while in Dunalley case, the wildfire occurred at the peak of a heatwave and immediately before a cold front passage. The research also confirmed that analyzed wildfires from opposite sides of the world share some similarities in fire weather. The antecedent conditions in both cases included the drier and warmer than average periods months prior to the wildfires. While it would be expected that warm and dry periods are more extreme in Tasmania than in Croatia, the hottest January on record in 2013 with extensive heatwave in terms of spatial coverage and duration was exceptional even for Australia. Extreme weather conditions in both cases consequently

contributed to continued drying out fuels in the area of each wildfire and had an impact on fire danger rating. In particular, the FWI reached its annual maximum exactly on the day of the Split wildfire, while in the case of Dunalley FFDI reached ‘catastrophic’ category and got close to the all-time state record. In both instances, fire danger rating pointed to extreme fire behavior, which eventually did occur in both cases. According to the wildfire chronology, the fire behaviour included rapid fire spread, multiple fire fronts, crown fire and in the case of Dunalley, generation of violent firestorm in form of pyroCb.

The research has showed that both wildfires were wind driven from the ignition due to wildfires’ locations situated in the area of tight pressure gradient, which resulted in strong gusty surface wind. The synoptic pattern caused a tight pressure gradient in the case of Split, which included the combination of the Azores anticyclone stretching towards central Europe and low pressure area over the southeastern Balkans. In the case of Dunalley, an anticyclone was situated in the Tasman Sea that coincided with a cold front approaching from the west. While northeast bura wind in the case of Split brought cool and dry air in the wildfire’s area, the northwest wind in the case of Dunalley brought hot and dry air from the central Australian mainland. For that reason and the fact that the Split wildfire was ignited during the night and Dunalley during the day, other meteorological properties differed. Initial surface conditions were more severe in the case of Dunalley with highest on record air temperature being recorded (highest air temperature in 120 years and highest minimum air temperature in January for Hobart station). However, higher surface air temperatures and low relative humidity did favor the fire spread in the Split case as well.

Important findings on atmospheric dynamics associated with the wildfires were revealed using the operational model, reanalysis and high resolution numerical atmospheric model. In the case of Split, important meteorological features coinciding with the wildfire included long amplitude and shortwave upper-level trough extending over the study area at the time of the wildfire’s ignition. The Split wildfire was exactly on the western or rear edge of the upper-level cyclone, which caused the cool and dry air outbreak from the north of the continent. At the same time, the synchronization of the low surface pressure area with the upper tropospheric trough produced a deep northeasterly bura flow over the Adriatic Sea. Deep bura flow, in contrast to shallow bura, extends throughout the troposphere and is rare for summer months (Grisogono and Belušić, 2009). In this case, deep bura coincided with the wildfire ignition and dominated the fire ground turning it into a large conflagration.

Upper-level features that accompanied deep bura flow during the Split wildfire included a hydraulic jump, low-level jet (LLJ) and the absence of the tropopause. Hydraulic jumps are

frequent features of strong bura flow over the Adriatic and was also identified in this case as well. A hydraulic jump is marked by a wave-breaking aloft, accelerated downward wind on the lee slopes and strong turbulence immediately above (Smith, 1985; Jurčec and Visković, 1989; Whiteman, 2000; Sharples, 2009). Hydraulic jump flow culminated right at the time of the ignition and was accompanied by a significant drop in relative humidity. The drop in relative humidity was potentially caused by the complete absence of the tropopause, which led to larger vertical motion and dry air subsidence from the stratosphere (stratospheric intrusion) towards the lower levels of the troposphere and subsequently, to the surface. The dry air is found to descend sharply towards the wildfire's region right at the time of the ignition. A significant reduction in relative humidity also coincided with the downslope fire runs into the city of Split. The relevance of dry air subsidence is previously documented to coincide with severe fire weather conditions during other catastrophic wildfires, particularly in Australia (e.g., Mills, 2008a; Mills, 2008b).

The present research appears to be the first research to investigate spatial distribution of LLJ. The spatial extent of LLJ revealed that the strongest jet occurred over the highest coastal mountains right before the Split wildfire ignition, with parts of the flow stretching over the Adriatic Sea accompanied by wakes in between. LLJ is found to have an effect on fire behavior. It is associated with higher turbulent kinetic energy that can be mixed down to fireground and cause rapid fire spread (Charney et al., 2003). Also, LLJ is especially dangerous in the mountainous area due to intersection of its core and the active fire edge in the elevated forested terrain. LLJ also has negative effect on firefighting aircraft operations. Therefore, forecasts of LLJ appearance and strength might be useful as predictor of possible extreme fire behavior.

The investigation on fire weather features during the Dunalley wildfire revealed that the area stood out with absolute maximum temperature values, lowest relative humidity and strong and gusty northwesterly wind that influenced fire grounds from the ignition time. The major findings in the Dunalley case are related to pyroconvection and escalation of fire activity that occurred on the second day of the wildfire. Violent firestorm development from Dunalley wildfire was associated with highly unstable atmosphere, which was triggered by the approaching line of convergence in the hours prior to the cold front passage. Although the strong and gusty northwesterly airflow was persistent in the Dunalley area, pyroCb formed in the lower wind zone situated along the line of convergence, which extended immediately downwind of the wildfire location. Favorable upper-level conditions supporting the pyroconvection included a deep well-mixed boundary layer and moist unstable middle troposphere, which is known to support the moist convective plume (Tory et al., 2016). A

classic inverted-V sounding found in the case of Dunalley has been reported in literature to illustrate conditions favorable for pyroconvection and intense fire activity (e.g., [Rosenfeld et al., 2007](#); [Cunningham and Reeder, 2009](#); [Fromm et al., 2012](#); [Johnson et al., 2014](#); [Tory and Kepert, 2021](#)). The inverted-V profile also points to possible downburst development, which can significantly influence fire ground and pose a great threat to firefighters (e.g., [Kaplan et al., 2021](#)). Possible downbursts in this case provided an explanation for escalation in fire activity and size of burnt area. Downbursts can be also confirmed by the lack of precipitation in this case, which is a common feature of strongly polluted pyroCbs ([Tory et al., 2016](#)).

While most meteorological conditions found at the location of the pyroCb aligned to support the fire storm, conditions in the upper troposphere were not that favorable to support further convection due to a strong jet stream aloft. However, the cloud's injection up to the 12 km height did last for a few minutes. Explosive vertical pyroCb development was supported by the combination of the convergence of the surface wind field and the strongest area of upward motion found immediately downwind of Dunalley. Also, combustion processes within the escalated wildfire further enhanced instability and contributed to already severe conditions favorable for the blow-up fire. Heat source from the fire burning through dry eucalyptus vegetation was sufficiently large and intense and the energy release must have been enormous so that vertical injection could reach the tropopause height. Therefore, the combination of the heat from the wildfire, ease in the wind and atmospheric instability ahead of the cold front triggered the explosive pyroCb development in the case of the Dunalley wildfire, while the cold front passage brought the change in weather conditions in terms of the advection of cool and moist air and subsequent ease in fire activity.

Enhanced fuel consumption together with complex local topography also played an important role in the total fire escalation in the Split case. Extreme fire activity which included the downslope run into the city of Split occurred during relatively benign fire weather conditions. However, the wildfire at the time burned into abundant dry fuels in the elevated terrain which was aligned with the bura flow. As bura was still moderate to strong in this elevated area, it contributed to a channeling effect and pushed the fire downslope, towards the city of Split. Such dynamic fire channeling is considered impossible to control due to high fire spread rate and intensity ([Sharples, 2009](#)), as was the case in this event.

The catastrophic wildfire events provided an opportunity to investigate the most severe fire weather patterns and reveal the mechanisms that contribute in their generation. The analysis of these two wildfires that occurred in such widely separated locations revealed that, while the individual circumstances of each individual fire varied, they exhibited similar characteristics of

interaction with the atmosphere, fuels and topography. This highlights the value of such comparative studies, in that understanding of fire interactions with its environment can be applied globally. This new understanding may provide a useful early indicator of future severe events and therefore help to improve predictions on fire risk and behaviour and contribute to fire management.

Additional contribution of this research to Croatian fire weather research and knowledge is the application of coupled fire-atmosphere model, which was used for the first time for a Croatian wildfire event. Preliminary results of coupled model confirmed fire-atmosphere interactions in the case of the Split wildfire, which is the first numerical evidence of such interaction between wildfire and atmosphere occurring along the Adriatic coast. Although coupled simulations over Croatia should be improved with input vegetation and topography data of higher resolution, the present study lays the groundwork for future improvement and research.

Future research might explore low level jet occurrence and influence of fire behaviour in the Dunalley case in more detail. Also, it would be interesting to assess the atmospheric potential for pyroCb by calculating pyroCb firepower threshold (PFT). PFT, or the minimum firepower required to generate pyroCb for a given atmospheric environment, is an analytic solution that provides an insight into possible plume behaviour and pyroCb formation and has recently been implemented in operational fire weather forecasts in Australia ([Tory and Kepert, 2021](#)). Previous studies have suggested that wildfires can blow up into a pyroCb, even if the relatively low atmosphere's instability as a result (e.g., [Tory et al., 2018](#); [Tory and Kepert, 2021](#)), it would be interesting to ascertain whether or not the atmospheric conditions during the Split wildfire were close to blow-up conditions – similar to that of the Dunalley case.

## *10.2. Recommendations for the Improvement of Fire Management in Croatia*

This Cotutelle PhD provided a unique opportunity for collaboration between Croatian and Australian fire weather experts. Exchange of knowledge and an open dialog with firefighters and aerial firefighting pilots from both countries have opened questions on how Croatian fire management can benefit from a series of recommendations already implemented in Tasmania and Australia as a whole. Suggestions on new or improving existing practices are presented in the following set of recommendations. Professional fire management in Croatia should consider establishing and/or improving the following:

- a) Urgently establish public fire weather forecasts and warnings.
- b) Ensure a full-time fire weather meteorologists support (at the main firefighting centre during the fire season).
- c) Greater efforts are needed to ensure better collaboration between meteorologists and firefighters in order to better interpret and understand meteorological information prior to adverse events.
- d) Establish regular fire weather training for professional firefighters and aerial firefighting pilots. The training course should include introduction to meteorological data, observations, indices and model products together with findings of the most relevant and latest fire weather research and knowledge on the critical fire weather patterns in Croatia.
- e) Establish a main communication centre during the fire season that would secure a single source of reliable source of information and regularly inform the public about on-going fire incidents, fire management and fire weather forecasts.
- f) Financially support fire weather and fire behaviour research. Establish fire weather and fire behaviour research centre that would ensure collaboration between meteorologists and fire behaviour analysts. This is essential in order to analyse past fire incidents, establish controlled fire experiments, test and/or adopt fire behaviour models and FWI model on major Croatian vegetation types and prepare validations of fire behaviour models.

Improvement of fire weather forecasts:

- a) Provide specialized fire weather detailed spot forecasts for individual wildfire events.
- b) Introduce fire smoke forecasts and low air quality forecasts and warnings due to wildfires.
- c) Introduce total fire ban outside a fire season in collaboration with meteorologists.

Scientific research:

- a) Collaborate with European and other fire weather scientists in order to share knowledge, especially in fire weather and fire behaviour modelling.
- b) Collaborate with international experts and test the possibility of introducing fuel reduction burns outside a fire season (with close collaboration with meteorologists).
- c) Provide training for fire behaviour analysts.
- d) Provide regular meteorological reports on large wildfire incidents that caused large material and/or natural destruction, deaths or produced specific fire behaviour phenomena and make it publicly available.
- e) Incorporate high resolution vegetation and topography data into WRF SFIRE model.
- f) Test the rapid deployment of WRF SFIRE model and incorporate it into operational use.
- g) Further adopt and extend FWI forecast using already available operational NWP model and provide spatial distribution of FWI.
- h) Extend the automatic meteorological stations network for the purpose of fire protection and acquire mobile meteorological station for the purpose of the standardised collection of meteorological measurements for on-going incidents.
- i) Regularly provide climatological analysis for the purpose of fire risk assessment.
- j) Explore Hot Dry Windy Index for operational use.

Public fire risk awareness and fire risk reduction could be accomplished and improved by:

- a) Continuous public education on fire watch and fire risk (and outside the fire season).
- b) Educating tourists on fire risk and total fire ban (during the summer season) in Croatia upon their arrival.
- c) Introducing fire risk awareness and reduction into children's school program.
- d) Continuous education of journalists on fire management, fire risk and its reduction, fire behaviour, fire weather and climate change influencing fires and fire regime.
- e) Educating farmers on composting vegetation leftovers and avoiding vegetation burn-offs, especially in spring and autumn.
- f) Education of the general public on how to react and act when the wildfire starts.
- g) Basic firefighting training for general public available on demand.
- h) Raise awareness on maintaining fuel free area around residential houses and in agriculture plantations.

Other:

- a) Regular cleaning and maintenance of firefighting trails within forests and other natural areas.

b) Implement more strict obligations on fuel free area and fuel type around new constructions and residential houses in Croatian law.

c) Future afforestation plans regarding the area and type of vegetation in accordance with forest management plans together with the construction of access forest protection roads.

Implementation of suggested steps would lead to improved fire management operations of on-going fires, improvement of fire weather forecasts which would meet fire management needs, ensure accurate and fast fire weather forecast delivery to fire management and public, increase public fire risk awareness, rise knowledge on fire weather among firefighters and, as a whole, enhance resilience to fire and reduce fire risk in Croatia in the on-going transition to a more fire-prone climate.



## PROŠIRENI SAŽETAK

### POGLAVLJE 1

#### UVOD

Šumski požari su dio globalnog ekosustava i kao sastavni dio prirodnog ciklusa igraju ključnu ulogu u bioraznolikosti flore faune te oblikuju mozaika krajolika (Flannigan i sur., 2000; Keeley, 2012; Keeley i Syphard, 2016). Ako se šumski požar brzo i nekontrolirano širi, može uzrokovati ogromna razaranja i uzrokovati prirodnu katastrofu (Meng i sur., 2015). Na globalnoj razini izvješća govore o „najgorim“, „najvećim“, „najduljim“, „najskupljim“ i „rekordnim“ šumskim požarima i požarnim sezonama (IAWF, 2019).

U 21. stoljeću već svjedočimo o novoj alarmantnoj kategoriji šumskih požara – tzv. megapožarima (Williams, 2013). Izraz megapožar korišten je za opisivanje velikih i intenzivnih šumskih požara u svijetu (Dimitrakopoulos i sur., 2011; Coen i sur., 2018; de la Barrera i sur., 2018), obično većih od 10 000 ha (Stephens i sur., 2014). Iako su izuzetno rijetki (samo 1% od ukupnog broja požara), megapožari mogu biti odgovorni za više od 90% spaljene površine u jednoj požarnoj sezoni (Bartlett i sur., 2007; Strauss i sur., 1989). S meteorološkog kuta gledanja megapožari su šumski požari koji jako djeluju na okolnu atmosferu. U tim uvjetima megapožari mogu generirati dovoljno energije za modificiranje prevladavajućih meteoroloških uvjeta i stvaranje vlastitih vremenskih uvjeta – požarnih oluja (Vines, 1981). Požarne oluje, u ekstremnim slučajevima mogu generirati pirokonvekciju, odnosno duboki konvektivni stup, koji se očituje kao posebna vrsta oblaka – pirokumululus (pyroCu) ili pirokumulonimbus (pyroCb; Sharples i sur., 2016). Konvektivna uzlazna i silazna strujanja unutar pyroCu ili pyroCb utječu na ponašanje požara zbog velikih i brzih promjenama brzine i smjera vjetra (Potter, 2012a, 2012b). U Australiji je do danas zabilježen veliki broj požara koji su generirali pyroCb, ali i ekstremne popratne pojave poput požarnih pijavica i tornada (Fromm i sur., 2006; Cruz i sur., 2012; McRae i sur., 2013; Field i sur., 2016; Ndalila i sur., 2019).

Šumski požari takvih razmjera još nisu zabilježeni u Hrvatskoj, no do pirokonvekcije je sigurno došlo (slika 1.2b), iako do danas nije potvrđen slučaj razvoja oblaka pyroCb. Unatoč tome, bilo je izvješća o neuobičajeno razornim, nekontroliranim i vjetrom nošenim šumskim požarima koji su gorjeli tijekom noći bez znakova usporavanja, s nezaustavljivim napredovanjem vatre, napredujući nizbrdo i dosežući prigradska područja koja se obično smatraju zaštićenima od takvih požara. Sve to zabilježeno je još 2017. godine, najgore požarne sezone u Hrvatskoj posljednjih 60-setak godina. Posljednjih godina hrvatski vatrogasci i piloti

protupožarnih zrakoplova često opisuju požare kao previše intenzivne za gašenje ili čak nemogućnost da im se približe, što nije sigurno zbog nestalnosti vjetra, ostavljajući im jedinu mogućnost uklanjanja goriva ispred vatre. Stoga je Hrvatska, kao i Australija, zabilježila dosad neviđene šumske požare i ponašanje požara što je meteorološki povezano s pojačanom dinamikom između požara i atmosfere. Ti događaji zahtijevaju posebnu pozornost i naglašavaju potrebu da znanstvenici trebaju bolje razumjeti mehanizme koji ih uzrokuju i pokreću.

Hoće li šumski požar pokazati ekstremno ponašanje i postati velika prijetnja uvelike ovisi o vremenu, točnije određenoj kombinaciji meteoroloških uvjeta (Bradstock i sur., 2009). Stoga je pravodobno i važno znati cijeli skup meteoroloških uvjeta koji izazivaju šumske požare kako bi se što točnije prognozirali i što ranije najavili spasilačkim i vatrogasnim službama. Sveobuhvatna meteorološka istraživanja šumskih požara mogu poboljšati naše znanje o toj razarajućoj i katastrofalnoj pojavi i doprinijeti znanosti o požarnoj meteorologiji i učinkovitijim vatrogasnim operacijama.

Glavni cilj ovog dvojnog doktorata je istražiti meteorološke prilike za vrijeme ekstremnih šumskih požara – iz Hrvatske i jugoistočne Australije. Izabrani slučajevi ekstremnih požara raslinja uključuje Splitski požar iz srpnja 2017. iz Hrvatske te požar Forcett-Dunalley iz siječnja 2013. iz Tasmanije. Drugi cilj ovog istraživanja je pronalaženje sličnosti između dinamičkih atmosferskih procesa i mehanizama koji su se dogodili u tijekom analiziranih požara. Također, pitanje na koje ovo istraživanje želi dobiti odgovor je da li su šumski požari duž Jadranske obale dovoljno intenzivni da utječu i mijenjaju meteorološke uvjete u okolnoj atmosferi, kao onima koji se javljaju u Australiji. U tu svrhu u Hrvatskoj je po prvi puta primijenjen združeni model koji simulira odnose između požara i atmosfere.

## **POGLAVLJE 2**

### **PREGLED LITERATURE**

Znatan utjecaj na vremenske uvjete povoljne za požare raslinja duž Jadrana ima položaj Azorske anticiklone nad zapadnom Europom. Dugotrajni ili blokirajući anticiklonalni uvjeti udaljavaju ciklonalne poremećaje od jadranske obale te uzrokuju dugotrajno razdoblje toplog, suhog i mirnog vremena, s uglavnom slabom obalnom cirkulacijom poput zmorca ili kopnenjaka. Očito je da su ti uvjeti povoljni za šumske požare, ali ono što se čini ključnim za pojavu velikih šumskih požara na jadranskom području je pomicanje Azorske anticiklone prema sjeveru. To omogućuje hladnoj fronti da zahvati područje Jadrana, poništi lokalnu obalnu cirkulaciju te promijeni smjer i brzinu vjetra. Ljetne hladne fronte obično su suhe, ili donose

malu količinu oborine, nedovoljnu za već suhu vegetaciju ili za gašenje već nastalih šumskih požara.

Najčešći tip šumskih požara duž jadranske obale su požari nošeni vjetro, a u manjem obimu požari uzrokovani ekstremnom vrućinom. Istraživanja prošlih katastrofalnih požara u Hrvatskoj otkrila su, između ostalog, specifični vertikalni profil – signifikantni maksimum brzine vjetra u prvih 250 do 900 m visine (sa specifičnim smanjenjem brzine do 3 km visine; [Vučetić i Vučetić, 1999](#)). Takvi vertikalni profili pronađeni su u različitim sinoptičkim situacijama i tijekom različitih prevladavajućih smjerova vjetra – juga, bure i maestrala. Prijašnje istraživanje iz SAD-a definiralo je takvu vrstu vertikalnog profila brzine vjetra kao nisku mlaznu struju (engl. *low-level jet*, LLJ) i otkrilo da je takav profil vjetra među najopasnijim s obzirom na ponašanje požara u prirodi kojima dominira jak vjetar. Vrlo je vjerojatno da će uzrokovati pojavu velikih vrtloga što je vrlo opasno za gradove i sela ispred vatrene fronte ([Byram, 1954](#)). Isti takav vertikalni profil brzine vjetra potvrđen je i prvi put u hrvatskoj literaturi definiran kao LLJ u opsežnom meteorološkom istraživanju najtragičnijeg požara u hrvatskoj povijesti – Kornatskog požara iz 2007, kada je smrtno stradalo 12 vatrogasaca te je jedan teško ozlijeđen ([Vučetić i sur., 2007](#)). Kasnije studije potvrdile su prolaz hladne fronte i LLJ kao ključne meteorološke uvjete za vrijeme velikih šumskih požara na jadranskoj obali, a također su ponovno potvrdile važnost analize vertikalne strukture atmosfere. Na primjer, taj tipični sinoptički obrazac i vertikalni profil vjetra pojavio se u slučajevima svih šumskih požara većih od 500 ha u razdoblju 2001–2010. ([Tomašević, 2012](#)). Zanimljivo je da je sve velike šumske požare u tom razdoblju potaknula jaka bura.

Požari u Hrvatskoj ne događaju se samo duž jadranske obale. U drugom desetljeću 21. stoljeća bilo je velikih šumskih požara i u unutrašnjosti kontinenta ([Kuraži, 2015](#)), što je u skladu s rezultatima indeksa opasnosti od požara raslinja koji su otkrili znatno povećanje meteorološke opasnosti u ovim područjima koja su se nekoć smatrale sigurnima od tih katastrofalnih događaja ([Barešić, 2011](#)). Više detalja u [Tomašević i sur. \(2022\)](#).

Istraživanja velikih šumskih požara u Australiji pronašla su dva glavna tipa najčešće prisutnih meteoroloških uvjeta. Prvi uključuje bilo koji obrazac koji donosi suhi zrak od središta kontinenta do periferije gdje je više gorivog materijala, a drugi obrazac odgovara frontalnim poremećajima nakon anticiklone i najčešći je u jugoistočnoj Australiji. Područje, gdje se vruća kontinentalna zračna masa iz unutrašnjosti susreće s hladnim morskim zrakom iznad Južnog oceana, je sjecište zračnih masa koje pojačava hladne fronte kako se približavaju obali i dolaze u interakciju s obalnim temperaturnim gradijentom ([Luke i McArthur, 1978](#); [Mills, 2002](#)). Frontama obično prethodi jaka anticiklona, koja usmjerava suhi zrak iz zagrijane unutrašnjosti

kontinenta prema jugoistoku (Reeder i Smith, 1992; Reeder i Smith, 1998). Takva sinoptička situacija dogodila se za vrijeme katastrofalnog šumskog požara u jugoistočnoj Australiji poznatim kao Crna subota (engl. *Black Saturday*) 2009., kada je smrtno stradalo 173 osobe (VBRC, 2009).

Ostali ključni meteorološki uvjeti za vrijeme velikih požara uključuje međudjelovanje strujanja s topografijom. Na primjer, neki slučajevi iznenadnih povećanja indeksa opasnosti od požara u jugoistočnoj Australiji povezani su s pojavom fena (engl. *foehn*, Sharples i sur., 2010) i atmosferskih planinskih valova. Mnogo godina upozorava se i na opasnost od spuštanja suhog zraka s visine što uzrokuje rapidno smanjenje relativne vlažnosti zraka pri tlu i tako utječe na vlagu gorivog materijala i povećava rizik od požara. Vrijeme pogodno za nastanak požara uključuje i konvektivne procese koji mogu uzrokovati tzv. požare dominirane uzlaznim gibanjima (više nego horizontalnim vjetrom).

Istraživanja iz obje države pokazuju porast indeksa meteorološke opasnosti od požara raslinja kao posljedicu promijenjene klime. Klimatske projekcije u budućnost pokazuju da u obje regije postoji prilično velika vjerojatnost za izmijenjeni i opasniji požarni režim s produljenjem požarne sezone, te ako požar nastane, postoji velika vjerojatnost da preraste u požar velikih razmjera i ekstremnog ponašanja.

### **POGLAVLJE 3**

#### **METODE**

Kako bi se atmosferski uvjeti povezali s ekstremnim ponašanjem požara, prije meteoroloških analiza izrađena je detaljne rekonstrukcije požara. Za slučaj požara kod Splita koristile su se digitalne vremenski referencirane fotografije sa službenih vatrogasnih kamera smještenih na tornju Zahod na jugoistočnom vrhu brda Perun (slika 4.2). Širenje požara većinom je rekonstruirano iz 3 208 radijskih zapisa i 1 124 hitnih poziva ustupljenih od Javne vatrogasne postrojbe Split (JVP Split). Dodatne informacije o širenju i ponašanju požara dobivene su iz izjava svjedoka, intervjua s vatrogascima i pilotima i fotografija s požarišta. Sve informacije su georeferencirane i korištene za približno definiranje izokrona požara. Rekonstrukcija širenja požara i izokrone požara ucrtane su na izokronu ukupne spaljene površine koju je ustupila JVP Split. Rekonstrukcija šumskog požara Forcett-Dunalley uglavnom je preuzeta iz gotovih izvješća Australskog ureda za meteorologiju (engl. *Bureau of Meteorology*, BoM). Kako bi se detaljnije povezalo ponašanje požara i meteorološki uvjeti, oba

šumska požara podijeljena su u nekoliko razdoblja gorenja od početka požara do znatnijeg smanjenja aktivnosti požara.

Pomoću meteoroloških podataka s postaja, koje su najbliže požaru, analizirani su prizemni vremenski uvjeti. Za Splitski požar korišteni su podaci s meteorološke postaje Split-Marjan (slika 4.2), a za požar Dunalley postaje Dunalley, Hobart, zračna luka Hobart i Campania (slika 5.1b). Za određivanje visine oblaka pyroCb upotrijebljeni su radarski podaci s planine Koonya (Soderholm i sur., 2019). Vremenska zona u analizi Splitskog požara je univerzalno koordinirano vrijeme (UTC) što je srednjoeuropsko ljetno vrijeme (CEST) – 2 h. Za slučaj Dunalley vremena su iskazana prema australskom istočnom ljetnom vremenu (AEDT) što je UTC + 11 h. Sva su mjerenja preračunata u skladu s tim.

Meteorološka opasnost od požara raslinja analizirana je pomoću kanadskog indeksa opasnosti od požara FWI (engl. *Fire Weather Index*) za slučaj Splitskog požara (Van Wagner i Pickett, 1985; Stocks i sur., 1989). FWI se sastoji od podindeksa koji pokazuju vlažnost mrtvog gorivog materijala i moguće ponašanje požara (tablice 3.1 i 3.2). Za slučaj požara Dunalley primijenjen je australski indeks opasnosti od požara (tablica 3.3; Luke i McArthur, 1978). Oba indeksa izračunata su iz mjerenja s automatskih meteoroloških postaja.

Sinoptička analiza za splitski požar uključivala je podatke njemačke meteorološke službe (njem. *Deutsche Wetterdienst*, DWD, [www1.wetter3.de/Archiv/](http://www1.wetter3.de/Archiv/)), a sinoptička analiza požara Dunalley temeljila se na analizi Nacionalnog meteorološkog i oceanografskog centra (engl. *National Meteorological and Oceanographic Centre*, NMOC; <http://www.bom.gov.au/australia/charts/archive/>).

Numeričke simulacije za studiju slučaja Split provedene operativnim modelom za numeričku prognozu vremena ograničenog područja modelom ALADIN/HR (ALADIN International Team, 1997) koji se koristi u Državnom hidrometeorološkom zavodu (DHMZ). Model ALADIN/HR je inicijaliziran u 00 UTC za svaki dan požara u Splitu, sa satnim izlaznim podacima. Korištena je i dinamička adaptacija polja vjetra (ALADIN-HRDA) za splitsko područje s horizontalnim razlučivanjem od 2 km. Vertikalna struktura atmosfere analizirana je pomoću vertikalnih presjeka koji su prikazani na slici 4.1a.

Za potrebe ovog istraživanja uveden je novi produkt modela ALADIN, prostorna raspodjela niske mlazne struje (engl. *low level jet* LLJ) koja je u točki mreže definirana prema Bonneru (1968) uz dodatni najniži kriterij od 10 m/s. Razlog tome je što su prethodna istraživanja pokazala da model ALADIN može podcijeniti maksimalnu brzinu vjetra u donjoj troposferi (npr. Vučetić i sur., 2007). Prema našim saznanjima prostorna raspodjela maksimalne brzine i visine LLJ nikada nije primijenjena u istraživanju vremena požara do danas.

BoM-ova regionalna reanaliza visoke razlučivosti za Australiju (BARRA) primijenjena je u analizi požara Dunalley (Su i sur., 2019). Najniža domena BARRA reanalize oko Tasmanije (BARRA-TA) ima horizontalnu razlučivost od 1.5 km (slika 3.2).

Detaljnije numeričke simulacije napravljene su numeričkim modelom WRF (engl. *The Weather Research Forecasting Model*; Skamarock i sur., 2008) verzije 4.1.5. Simulacije su inicijalizirane pomoću ERA-Interim reanalize od Europskog centra za srednjoročnu prognozu vremena (engl. *European Centre for Medium-Range Weather Forecasts*, ECMWF; Dee i sur., 2011). Simulacija za hrvatski požar uključila je razdoblje od 60 sati, od 16. srpnja 2017. u 12 UTC do 19. srpnja 2017. u 00 UTC, a za australski požar 72 sata, od 3. siječnja 2013. u 00 UTC do 6. siječnja 2013. u 00 UTC. Izabrane domene (slika 3.3. i 3.4.) imaju horizontalnu rezoluciju od 9 (d01), 4.5 (d02), 1.5 (d03) i 0.5 km (d04) (tablica 3.4) te 66 vertikalnih razina (koji prate topografiju). Za detaljniju analizu utjecaja požara na okolnu atmosferu primijenjen je model WRF SFIRE 4.2.2. (engl. *Spread FIRE*) koji omogućuje simuliranom požaru da "stvori svoje vlastite vremenske uvjete" (Coen i sur., 2013). Opis modela može se naći u Mandel i sur. (2011).

Numerička simulacija Splitskog požara trajala je 48 sati, od 16. srpnja 2017. u 12 UTC, što je 10 sati prije izbijanja šumskog požara (kako bi se omogućilo filtriranje početnih odstupanja u modelu tzv., *spin-up time*) do 18. srpnja 2017. u 12 UTC. Početni rubni uvjeti su jednaki kao i za simulacije modelom WRF primjenom ERA-Interim reanalize. Simulacije su pokrenute u tri ugniježdene domene u jednakom početnom položaju kao u simulacijama WRF (slika 3.3) i jednakom razlučivosti, tj. jednakim brojem točaka horizontalne mreže i vertikalnih slojeva razlučivanja (tablica 3.4). Model požara pokrenut je u unutarnjoj domeni (d04) kojoj je dodatno povećana razlučivost na 33.3 m (tablica 3.5). Izlazni podaci modela za unutarnju domenu bili su dostupni u 10-minutnom intervalu.

Model WRF SFIRE zahtijeva topografske podatke visoke razlučivosti i podatke o pokrivenosti gorivog materijala. Jedini dostupni topografski podaci za Hrvatsku koji su pretvoreni u oblik prikladan za model WRF bili su u razlučivosti od 100 m što je dodatno interpolirano na razlučivost od 33.3 m. Budući da za Hrvatsku ne postoje besplatno dostupni podaci o gorivom materijalu visoke razlučivosti, za ovu su svrhu korišteni podaci iz baze CORINE *Land Cover* (CLC), također dostupni u razlučivosti od 100 m i naknadno interpolirani na 33.3 m. Sljedeće metode su iz Kartsios i sur. (2021), rasterski podaci CLC podijeljeni u 13 kategorija različite vegetacije prema Andersonu (1982), a kategorija 14 dodijeljena je "bez gorivog materijala" (tablica 3.6).

## POGLAVLJE 4

### SPLITSKI POŽAR – REKONSTRUKCIJA

Područje koje je najviše ugroženo požarima u Hrvatskoj je obala Jadranskog mora (slika 4.1a), zajedno s okolnim zaobaljem i otocima, kojih ima više od tisuću. Velika opasnost od požara izražena je tijekom ljetnih mjeseci, od lipnja do kolovoza, kada dugotrajna sušna razdoblja i velike vrućine pogoduju nastanku, razbuktavanju i širenju požara zbog lako zapaljive sredozemne vegetacije – različite kserofilne šume; makije i garizi vazdazelenih listača i šume četinjača (Španjol i sur., 2011). Prosječna godišnja spaljena površina na Jadranu iznosi približno 18 400 ha u oko 2500 šumskih požara (DUZS, 2018). Veličina spaljene površine bila je najveća 2017. s oko 87 000 ha u više od 4100 šumskih požara na Jadranu što je značilo najgoru požarnu sezonu u Hrvatskoj. Najkatastrofalniji požar sezone i u povijesti Hrvatske bio je požar u Splitu koji se dogodio u srpnju 2017. godine.

Požar je izbio 15 km jugoistočno od grada, u dolini između brežuljaka paralelnih s jadranskom obalom i orijentiranih od sjeverozapada do jugoistoka (slike 4.2, 4.3a i A1). Reljef terena je karakteriziran strmim gorskim lancem vrlo blizu obale koji može znatno utjecati na strujanje zraka i rezultirati složenom atmosferskom dinamikom u tom području. Splitski požar trajao je devet dana, od 16. do 25. srpnja 2017., a spaljeno je 5122 ha (Jovanović i Župan, 2017, od čega većina u prvih 30 sati od početka požara.

Splitski požar može se podijeliti u četiri vrlo aktivna požarna razdoblja u prvih 30 sati od nastanka (slika 4.2) koja su definirana kao SPLIT 1 do SPLIT 4. SPLIT 1 odnosi se na prvih 11 sati šumskog požara, odnosno na razdoblje od kasnonoćnog zapaljenja do jutarnjih sati sljedećeg dana kada se aktivnost požara malo smanjila. U tom razdoblju protupožarni zrakoplovi nisu mogli sudjelovati u intervenciji zbog turbulencija u zraku. Razdoblje SPLIT 2 odnosi se na reaktiviranje požara tijekom ranih poslijepodnevni sati i daljnje širenje požara s mozaičkom požarnom frontom. SPLIT 3 odnosi se na kasno poslijepodnevno razbuktavanje požara uzduž cijelog područja fronte požara s najjačim silaznim (niz brdo) napredovanjem požara prema Splitu. Četvrto i posljednje razdoblje SPLIT 4 obuhvaća još jedno širenje požara niz brdo tijekom noćnih sati u istočno predgrađe Splita.

Meteorološka analiza u sljedećem 5. poglavlju ima za cilj odgovoriti na pitanja o ulozi koju su meteorološki uvjeti odigrali u najvažnijim razdobljima požara:

1. Koji meteorološki uvjeti su bili prije i neposredno nakon izbijanja požara u Splitu u kasnim noćnim satima 16. srpnja 2017.?

2. Koji su uvjeti spriječili protupožarni zrakoplov da se uključi u intervenciju od ranog jutra do kasnog poslijepodneva 17. srpnja (razdoblje SPLIT 1)?

3. Koji su uvjeti doprinijeli iznenadnoj reaktiviranju požara oko podneva 17. srpnja (prijelaz između razdoblja SPLIT 1 i SPLIT 2)?

4. Kakvi su meteorološki uvjeti pratili razbuktavanje požara u svim zonama i napredovanje požara niz brdo u područje grada Splita u kasnim poslijepodnevrim satima 17. srpnja (razdoblje SPLIT 3)?

5. Koji su se meteorološki uvjeti bili tijekom drugog napredovanja požara niz brdo prema istočnim prigradskim naseljima tijekom noći između 17. i 18. srpnja 2017. (razdoblje SPLIT 4)?

## **POGLAVLJE 5**

### **SPLITSKI POŽAR – METEOROLOŠKA ANALIZA**

U mjesecima koji su prethodili požaru u Splitu, produženo razdoblje ekstremno toplih i suhih uvjeta uzrokovalo je kontinuirano sušenje goriva na tom području i povećanje opasnosti od požara koja je kulminirala upravo na dan požara. Godišnji maksimum FWI-a 16. srpnja 2017. na postaji Split-Marjan pokazao je stanje gorivog materijala kao vrlo suho i zapaljivo s mogućnošću brzog širenja požara, višestrukih požarnih fronti i požara krošnji, a sve se to dogodilo tijekom požara u Splitu.

Povoljni sinoptički uvjeti u ovom slučaju uključivali su: 1) jak prizemni gradijent tlaka uzrokovan Azorskom anticiklonom koja se protezala prema središnjoj Europi i području niskog tlaka iznad jugoistočnog Balkana i 2) visinsku dolinu velike amplitude koja se protezala od Baltičkog do Jonskog mora uz popratnu visinsku ciklonu iznad jugoistočnog Balkana. Povezivanje područja niskog prizemnog tlaka s visinskom dolinom proizvela je duboko sjeveroistočno strujanje bure nad Jadranskim morem. Duboka bura, za razliku od plitke bure, proteže se cijelom troposferom i tipična je za hladnije mjesece ([Grisogono i Belušić, 2009](#)), a u ovom se slučaju poklopila s razbuktavanjem požara i znatno pridonijela njegovom prerastanju u veliki požar.

Istraživanje je pokazalo da je došlo do spuštanja suhog zraka iz donjih slojeva stratosfere koje se dogodilo u kombinaciji s visinskom dolinom i dinamikom mlazne struje iznad područja Jadrana. Proces supsidencije počeo je 24 sata prije šumskog požara, pri čemu se suhi zrak naglo spuštao prema Splitu točno u trenutku nastanka požara te tijekom prvih 30 sati požara.



Prethodna istraživanja pokazala su da LLJ ima znatan utjecaj na ponašanje požara i djelovanje protupožarnog zrakoplovstva. LLJ je bila povezana s turbulentnom kinetičkom energijom koja može uzrokovati brzo širenje požara (Charney i sur., 2003). LLJ u atmosferi je posebno opasna u planinskim područjima (Byram, 1954). Razlog tome leži u podudaranju LLJ i uzdignutog šumskog terena što pri nastanku požara može dovesti do razbuktavanja i ekstremnog ponašanja požara. LLJ je uočena prije početka i tijekom Splitskog požara.

Na osnovi meteorološke analize u ovom istraživanju najvažnija razdoblja širenja požara mogu se obrazložiti na sljedeći način: 1) Jak prizemni gradijent tlaka zraka s izvorom suhog zraka iz donje stratosfere koji se zahvaljujući buri spustio do tla te je doveo do brzog širenja požara odmah nakon njegova nastanka (razdoblje SPLIT 1). U prvih nekoliko sati jaka bura nosila je požar nizbrdo na južnim padinama brda Makirine (slika 4.2) prema dolini, gdje su vatrogasci zaustavili požar. Šumski požar se istovremeno širio uzbrdo iz dva razloga. Prvi je zbog učinka uzgona na plamen i dim između udara bure, a drugi je potencijalno posljedica vrtloga i rotora u zavjetrini ispod jezgre LLJ.

2) Složenost strujanja zraka na požarištu posebno je bilo izraženo tijekom razdoblja SPLIT 2 (slika 4.3d). Iznenadno reaktiviranje požara i njegovo ponovno širenje nizbrdo (slika 4.4) po drugi je puta nakon izbijanja ugrozio naselja u dolini koja su se tada već smatrala sigurnima od požara jer je on bio iznad njih na većoj nadmorskoj visini. Mogući razlog zbog kojeg se fronta požara vratila u dolinu je najvjerojatnije zbog smanjenja brzine i spuštanja LLJ. Smanjenjem visine LLJ došlo je do poklapanja maksimalne brzine vjetra u donjoj troposferi s frontom požara. Slabljenjem vjetra i smanjenjem turbulencije uz padine brda ponovno je uzrokovalo spuštanje požarne fronte niz brdo Makirina.

3) Potpuno razbuktavanje požara dogodilo se tijekom relativno mirnijih meteoroloških uvjeta. Bura je oslabila početkom razdoblja SPLIT 3 (slika 5.7c) te su se u intervenciju mogli uključiti i protupožarni zrakoplovi. Međutim, položaj požarišta je u tom trenutku, zbog reljefa terena, zajedno s lokalnim vremenskim uvjetima vjerojatno bio presudan za brzo širenje vatre nizbrdo u gradsko područje. Požar je do tada napredovao do rubnih dijelova grada na padinama Mosora. Mjesto požara bilo je prekriveno gustom borovom šumom i obilnim suhim gorivim materijalom. Pored toga taj uzdignuti teren bio je pod utjecajem od umjereno do jake bure i zbog kanalnog učinka bura je usmjeravala požar niz jugozapadne padine, odnosno prema gradu Splitu. Smatra se da je takvo dinamičko usmjeravanje vatre nizbrdo nemoguće kontrolirati zbog velike brzine širenja i intenziteta vatre (Sharples, 2009).

4) Drugo napredovanje požara nizbrdo tijekom razdoblja SPLIT 4 može se objasniti umjerenom burom na tom području (slika 5.7d) koja je prebacila požar preko vrha brda Perun

prema njegovoj južnoj strani (slika 4.2). Širenje požara nizbrdo bilo je stoga pojačano burom, a dodatno je pogodovalo i smanjenje relativne vlažnosti zraka tijekom noći, zbog spuštanja suhog zraka iz više troposfere. Također, požar je tijekom spuštanja niz brdo Perun zapalio hrastovu šumu. To je uzrokovalo najgori oblik požara tzv. požar krošnje prije nego što je zahvatio urbano područje u podnožju Peruna (slika 4.8a i b). Takvo ponašanje požara i njegovo širenje nizbrdo iznimno je opasno za vatrogasce, ljude i imovinu.

## **POGLAVLJE 6**

### **FORCETT-DUNALLEY POŽAR – REKONSTRUKCIJA**

Tasmanija, australska otočna država, s kopnom dijeli povijest čestih šumskih požara. Vrhunac požarne sezone u Tasmaniji je u kasno ljeto i ranu jesen (Luke i McArthur 1978), no nedavna istraživanja također su otkrile porast opasnosti od požara u proljeće (Fox-Hughes, 2008). Područje koje je najviše izloženo požarima je jugoistok države. Prosječna spaljena površina u razdoblju 2002–2011. bila je 51 920 ha u godišnje 65 šumskih požara. Najveće spaljeno područje zabilježeno je u požarnoj sezoni 2012/13. kada je u 128 šumskih požara spaljeno 119 267 ha. Najkatastrofalniji šumski požar te sezone, ali i u posljednjih pet desetljeća, bio je šumski požar Forcett-Dunalley u siječnju 2013. (Marsden-Smedley, 2014).

Požar Forcett-Dunalley trajao je 16 dana, od 3. do 18. siječnja 2013., ali je proglašen potpuno ugašenim tek 20. ožujka 2013. Započeo je slučajnim paljenjem u ruralnom naselju Forcett, 35 km sjeveroistočno od Hobarta, glavnog grada države. Požar je zaprijetio ljudskim životima i gotovo potpuno uništio općinu Dunalley. Činjenica da je u tom šumskom požaru spaljeno 25 950 ha i to većinu u samo 6 sati (Marsden-Smedley, 2014; Ndalila i sur., 2018) te proizveo pirokumulonimbus (pyroCb), prvi zabilježen u Tasmaniji (Ndalila i sur., 2019) govori o povoljnim vremenskim uvjetima za ekstremno širenje i ponašanje požara. Požar je uništio je ili ošteti 431 kuću, uništio osnovnu školu i policijsku postaju u Dunalleyu i prisilio ljude da skaču u more kako bi izbjegli smrt. Jedan vatrogasac koji je sudjelovao u intervenciji je izgubio život, ali ne izravno od požara. U šumskom požaru spaljeno je 25 950 ha autohtonih šuma, poljoprivrednog zemljišta, šumskih plantaža, više od 660 km komercijalnih ograda te 10 000 grla stoke, uglavnom ovaca.

U svrhu ovog istraživanja su prva 82 sata šumskog požara Forcett-Dunalley označena kao DUNALLEY 1 do DUNALLEY 3. DUNALLEY 1 odnosi se na prva 23 sata požara ili razdoblje od nastanka 3. siječnja do podneva 4. siječnja, neposredno prije razbuktavanja požara. Razdoblje DUNALLEY 2 je jaka vatrena oluja koja se dogodila u poslijepodnevnim satima

4. siječnja. Treće i posljednje razdoblje DUNALLEY 3 odnosi se na promjenu smjera požara
5. siječnja i retrogradnog širenja
6. siječnja.

Meteorološka analiza u poglavlju 7 ima za cilj odgovoriti na sljedeća pitanja:

1. Koji su prethodni vremenski uvjeti doprinijeli šumskom požaru Forcett-Dunalley?
2. Koji su se vremenski uvjeti požara poklopili s izbijanjem šumskog požara?
3. Koji su vremenski uvjeti pratili smanjenje aktivnosti požara tijekom noći između 3. i 4. siječnja te koji su uvjeti pridonijeli promjeni ponašanja požara tijekom jutra 4. siječnja (razdoblje DUNALLEY 1)?
4. Koji su vremenski uvjeti omogućili siloviti razvoj vatrene oluje i dopustili da dođe do pirokonvekcije tijekom poslijepodneva 4. siječnja (razdoblje DUNALLEY 2)?
5. Koji su vremenski uvjeti uzrokovali promjenu smjera fronte požara i retrogradno gorenje 5. i 6. siječnja (razdoblje DUNALLEY 3)?

## **POGLAVLJE 7**

### **POŽAR FORCETT-DUNALLEY – REKONSTRUKCIJA**

Požar Forcett-Dunalley dogodio se tijekom vrlo povoljnih vremenskih uvjeta za požare i u okruženju koje pogoduje ekstremnom ponašanju požara. Izbijanje požara poklopio se s vrhuncem dugotrajnog toplinskog vala koji je bio neuobičajen prema veličini zahvaćenog teritorija Australije i dugom trajanju. Toplinski val doveo je do rekordne temperature zraka u južnoj Tasmaniji. Na postaji Hobart je 4. siječnja 2013. izmjereno 41.8°C što je najviša temperatura zraka u 120 godina. Rekordnu vrućinu u Tasmaniji uzrokovalo je jako sjeverozapadno strujanje zraka koje je donijelo vruć i suh zrak iz središnje unutrašnjosti australskog kopna. Jak sjeverozapadni vjetar uzrokovan je velikim gradijentom tlaka zraka između anticiklone nad Tasmanskim morem, sjeveroistočno od Tasmanije, i duboke ciklone jugozapadno od Tasmanije. Hladna fronta se približavala sa zapada.

Sjeverozapadni vjetar utjecao je na aktivnost požara tijekom razdoblja DUNALLEY 1. Napredovanje vatre se usporilo i gotovo zaustavilo tijekom noći između 3. i 4. siječnja samo zbog kratkotrajnog smanjenja brzine vjetra. Međutim, temperatura zraka je ostala visoka (iznad 20°C na plohi od 850 hPa), a relativna vlažnost zraka niska (ispod 30%) što je onemogućilo proces hlađenja i povećanja vlage u gorivom materijalu preko noći. Ponovna aktiviranje i razbuktavanje požara ujutro 4. siječnja pa do kraja razdoblja DUNALLEY 1 poklopilo se s LLJ i sjeverozapadnim vjetrom kroz cijelu troposferu.

U poslijepodnevnim satima 4. siječnja 2013., tijekom razdoblja DUNALLEY 2, požarna aktivnost je bila najveća i požar je prerastao u oluju pyroCb, jedinu dosad zabilježenu u Tasmaniji. Kako je meteorološka analiza pokazala, pyroCb je bio povezan s vrlo nestabilnom atmosferom i približavanjem linije konvergencije nad područje požara. PyroCb se formirao u zoni slabijeg vjetra smještenoj duž linije konvergencije, koja se protezala odmah niz vjetar i jugoistočno od mjesta požara. Uz izvor energije potpuno razbuktanog požara uz sjeverozapadni vjetar i izvor vlage iznad Tasmanskog mora na jugoistoku, preko kojeg se širio oblak, pyroCb je dobio potrebnu energiju za eksplozivan vertikalni razvoj. Iako se pyroCb formirao u razdoblju od nekoliko sati, eksplozivni razvoj oblaka trajao je samo nekoliko minuta. Dok su meteorološki uvjeti pri tlu pogodovali vatrenoj oluji, uvjeti u višoj troposferi nisu bili toliko povoljni zbog olujnog vjetra i mlazne struje na tropopauzi. Međutim, izvor topline od požara gdje je gorjela suha šuma eukaliptusa bio je dovoljno velik i intenzivan, a oslobađanje energije je moralo biti ogromno da bi pyroCb mogao dosegnuti tropopauzu, što se i dogodilo u ovom slučaju.

PyroCb proizveo je dva udara groma, koji u ovom slučaju nisu zapalili dodatne požare jer se pyroCb gibao nad Tasmanskim morem. Radiosondažni podaci potvrdili su povoljne meteorološke uvjete za elektrifikaciju oblaka. Radiosondaža je također pokazala da je vrlo moguće došlo do olujnih silaznih strujanja unutar pyroCb-a. Takva silazna strujanja mogu utjecati na povećanje brzine i promjenu smjera okolnog vjetra, a time požar može postati vrlo nepredvidljiv i biti velika prijetnja vatrogascima (npr. [Fromm i sur., 2006](#); [Trentmann i sur., 2006](#); [Fromm i sur., 2012](#)). To objašnjava razbuktavanje požara i enormno povećanje spaljene površine do kraja razdoblja DUNALLEY 2.

Prolaz hladne fronte u prvim satima 5. siječnja 2013., označenim kao DUNALLEY 3 razdoblje, uzrokovao je smanjenje brzine vjetra i advekciju hladnog i vlažnog zraka s jugozapada. Ovi vremenski uvjeti zaustavili su napredovanje požara prema jugoistoku i uzrokovali širenje šumskog požara retrogradno, odnosno sjeveroistočno od mjesta izbijanja požara, dalje u unutrašnjost kopna.

## **POGLAVLJE 8**

### **METEOROLOŠKI UVJETI TIJEKOM POŽARA U HRVATSKOJ I AUSTRALIJI – STUDIJA USPOREDBE**

Dva katastrofalna šumska požara sa suprotnih strana svijeta i s različitih polutki povezuju ih neki zajednički meteorološki uvjeti. Uvjeti koji su prethodili požarima bili su nedvojbeno podjednaki: veliki manjak oborine i iznadprosječna temperatura zraka u mjesecima prije oba požara. Takvi vremenski uvjeti posljedično su utjecali na opasnost od požara raslinja koja je u oba slučaja bila ekstremna. Vrlo velika opasnost od požara pokazuje moguće ekstremno ponašanje požara koje uključuje brzo širenje vatre, višestruke vatrene fronte i požar krošnji. Prema rekonstrukciji katastrofalnih požara, takvo ponašanje požara dogodilo se u oba slučaja.

Prizemni vremenski uvjeti tijekom nastanka požara razlikovali su se u temperaturi zraka i relativnoj vlažnosti zraka, ali su bili podjednaki prema jačini vjetra. Osnovni razlog razlike u temperaturi zraka i relativnoj vlažnosti zraka je zbog toga što se požar kod Splita dogodio u kasnim večernjim satima i nakon znatne promjene vremenskih uvjeta, a požar Dunalley počeo je u ranim poslijepodnevnim satima, dan prije vrhunca toplinskog vala u Tasmaniji. Ipak, prizemni uvjeti u slučaju Splita su također bili povoljni za širenje vatre. Oba požara je od samog nastanka raspirivao jak prizemni vjetar.

Visinski atmosferski uvjeti u analiziranim su slučajevima bili različiti zbog različite sinoptičke situacije. Katastrofalni šumski požar u Splitu bio je povezan s visinskom dolinom i praćen epizodom duboke i jake bure koja je pogodovala poniranju suhog zraka s visine, a ekstremno ponašanje požara u slučaju Dunalley dogodilo se na vrhuncu toplinskog vala i neposredno prije prolaza hladne fronte. Ekstremno ponašanje požara uključivalo je širenje požara nizbrdo u slučaju Splita i pirokonvekciju u slučaju Dunalley. Dakle, požar u Splitu može se definirati kao požar nošen jakim vjetrom, a požar Forcett-Dunalley bio je kombinacija požara zbog jakog vjetra i uzgona.

## POGLAVLJE 9

### PRELIMINARNE SIMULACIJE ZA PODRUČJE HRVATSKE WRF SFIRE MODELOM

Preliminarni rezultati WRF SFIRE modela za područje Hrvatske pokazali su mogućnost da se simulira širenje požara i međudjelovanja požara i atmosfere. Uspješne simulacije daju prve numeričke dokaze da šumski požar s područja jadranske obale može promijeniti dinamičku strukturu okolne atmosfere, što se slaže s opažanjima s požarišta.

Detaljna rekonstrukcija katastrofalnog požara kod Splita u srpnju 2017. omogućila je verifikaciju simulacija WRF SFIRE modelom. Simulirani požar do neke je mjere reproducirao stvarni požar, ponekad precjenjujući brzinu širenja, ali općenito podcjenjujući konačnu spaljenu površinu. Dva su najvjerojatnija objašnjenja za odstupanje između simulacije i stvarnih rezultata. Prvi je zanemarivanje vatrogasnih intervencija u modelu, a koje je bilo intenzivno tijekom cijelog trajanja požara i iz zraka i sa zemlje. Drugi je zbog grube razlučivosti početnih podataka koji se odnose na gorivi materijal i topografiju. Dostupni podaci na razlučivost od 100 m naknadno su interpolirani na finiju mrežu požara od 33.3 m. Podaci o gorivom materijalu visoke razlučivosti za Hrvatsku nisu javno dostupni, ali dostupni su topografski podaci visoke razlučivosti. Međutim, oni nisu asimilirani u ovim preliminarnim simulacijama.

Preliminarne simulacije osmišljene su kao smjernice za daljnju upotrebu modela WRF SFIRE za istraživanje budućih stvarnih požara raslinja dok se rješava asimilacija ulaznih podataka visoke razlučivosti. Također, preliminarne simulacije WRF SFIRE nisu bile optimizirane na brzinu. Stoga, kako bi se takve simulacije širenja požara i međudjelovanje atmosfere i požara koristile za operativno prognoziranje požara i njihovu suzbijanju u Hrvatskoj, u budućim istraživanjima treba pronaći odgovarajuću postavku modela kojom bi se dobivali rezultati gotovo u stvarnom vremenu. Model WRF SFIRE pokazao se vrlo važnim u upravljanju požarima diljem svijeta (npr. [Peace i sur., 2015](#); [Peace i sur., 2016](#); [Coen i sur., 2013](#)). S točnijim prognozama požara u budućnosti, što bi se moglo postići ulaznim podacima finije razlučivosti, taj model ima potencijal za operativnu primjenu i u Hrvatskoj. Moguća primjena za upravljanje požarima kod nas uključuje prognozu širenja i intenziteta požara koji ovisi o promjenjivim vremenskim uvjetima, dostupnom gorivom materijalu i topografiji, planiranje učinkovitog i sigurnog raspoređivanja vatrogasnih snaga za gašenje požara na zemlji i iz zraka, sprječavanje požara na području između prirodnih i urbanih područja, učinkovito planiranje evakuacijskih ruta itd. Rezultati modela WRF SFIRE u ovom istraživanju pokazuju

da je model važan za istraživanje vremenskih uvjeta tijekom požara raslinja kako bi se bolje razumjele ove opasne prirodne pojave te spriječile njihove negativne posljedice.

## **POGLAVLJE 10**

### **ZAKLJUČAK**

#### *10.1. Zaključci i rasprava*

Ovo je istraživanje potvrdilo takve meteorološke uvjete koji su se u više slučajeva do danas podudarali s katastrofalnim šumskim požarima. Splitski požar bio je povezan s jakim burom i spuštanjem hladnog i suhog zraka iz donjih slojeva stratosfere, a požar Dunalley dogodio se na vrhuncu toplinskog vala i neposredno prije prolaska hladne fronte. Istraživanje je također potvrdilo da analizirani šumski požari sa suprotnih strana svijeta imaju neke zajedničke vremenske značajke koje su prethodile požaru i za vrijeme njihova trajanja. U mjesecima prije nastanka oba požara bilo je vrlo sušno i vruće. Tako su ekstremni vremenski uvjeti u oba slučaja pridonijeli jakim isušivanju gorivog materijala na područjima gdje su nastali. To je uzrokovalo vrlo veliku opasnost od požara raslinja koja je upozoravala na ekstremno ponašanje požara što se dogodilo u oba slučaja.

Istraživanje je pokazalo da su oba šumska požara bila nošena vjetrom od trenutka nastanka jer su se oba požara nalazila u području velikog gradijenta tlaka zraka što je rezultiralo jakim prizemnim vjetrom. Kod Splitskog požara hladan zrak u područje požara donio je sjeveroistočni vjetar, bura, a u slučaju Dunalleyj-a pritjecanje vrućeg i suhog zraka iz središnjeg australskog kopna uzrokovao je sjeverozapadni vjetar.

Važna otkrića o atmosferskoj dinamici povezana sa Splitskim požarom bilo je duboko sjeveroistočno strujanje bure nad Jadranskim morem koje je uključivalo hidraulički skok, nisku mlaznu struju (LLJ) i odsutnost tropopauze što je dovelo do spuštanja suhog i hladnog zraka s visine. Ovo je prva analiza koja istražuje prostornu raspodjelu LLJ. Produkti LLJ, prostorna raspodjela maksimalne brzine vjetra u donjoj troposferi i njezine visine, mogu poslužiti kao predkazatelj mogućeg ekstremnog ponašanja požara u budućnosti.

Najvažniji vremenski uvjeti kod požara Dunalley su povezani s pirokonvekcijom i razbuktavanjem požara u požarnu oluju. Jak i brz razvoj vatrene oluje bio je povezan s vrlo nestabilnom atmosferom i potaknut približavanjem linije konvergencije u satima prije prolaska hladne fronte. PyroCb se formirao u zoni slabijeg vjetra smještenoj duž linije konvergencije koja se protezala odmah niz vjetar od položaja požara. Moguća silazna strujanja unutar pyroCb-a su u slučaju tog požara objasnili razbuktavanje požara i veličinu spaljene površine.

Katastrofalni šumski požari analizirani u ovom radu pružili su priliku za istraživanje meteoroloških uvjeta tijekom najvećih požara raslinja i otkrivanje mehanizama koji doprinose njihovom stvaranju i brzom širenju. Iako su pojedinačne okolnosti promatranih požara varirale, istraživanje šumskih požara na tako međusobno dalekim područjima pokazalo je neke zajedničke značajke međudjelovanja između atmosfere, vegetacije i topografije. Vrijednost takvih usporednih istraživanja međudjelovanje požara s okolicom je što se njihovi rezultati mogu primijeniti globalno. Te nove spoznaje mogu biti dodatni rani pokazatelj povoljnih vremenskih uvjeta za nastanak požara raslinja pa tako poboljšavaju predviđanje opasnosti od njihove pojave i ekstremnog ponašanja te doprinose njihovom sprječavanju.

Dodatni doprinos ovog rada hrvatskim istraživanjima i poznavanju vremenskih uvjeta povezanih s požarima je primjena združenog modela požar–atmosfera, koji je prvi put primijenjen za požar raslinja na području Hrvatske. Preliminarni rezultati združenog modela potvrdili su međudjelovanje između požara i atmosfere kod Splitskog požara. To je prvi numerički dokaz takvog međudjelovanja koji se dogodilo duž jadranske obale. Iako bi se združene simulacije nad Hrvatskom trebale poboljšati ulaznim podacima vegetacije i topografije finijom razlučivosti, ovo istraživanje je postavilo temelje za buduća poboljšanja i istraživanja.

#### *10.2. Preporuke za unapređenje vatrogasnih intervencija na požarima raslinja u Hrvatskoj*

Ovaj dvojni doktorat pružio je jedinstvenu priliku za suradnju između hrvatskih i australskih znanstvenika koji se bave istraživanjem vremenskih prilika tijekom požara raslinja. Razmjena znanja i otvoreni dijalog s vatrogascima i pilotima protupožarnih zrakoplova iz obje zemlje otvorili su pitanja o tome kako hrvatsko vatrogastvo može imati koristi od niza preporuka koje su već primijenjene u Tasmaniji i ostatku Australije. Kod profesionalnog upravljanja vatrom u Hrvatskoj treba razmotriti uspostavljanje i/ili poboljšanje sljedećeg:

- a) Hitno uspostaviti upozorenja javnosti na opasnosti na požara raslinja.
- b) Osigurati stalnu meteorološku podršku u glavnom vatrogasnom zapovjedništvu tijekom požarne sezone.
- c) Poboljšati suradnju između meteorologa i vatrogasaca kako bi se bolje interpretirali i razumjeli stvarni i prognostički meteorološki produkti.
- d) Uspostaviti redovitu meteorološku obuku za profesionalne vatrogasce i pilote protupožarnih zrakoplova. Obuka iz meteorologije povezana s požarima raslinja trebala bi uključivati osnove o meteorološkim motrenjima i podacima, indekse meteorološke opasnosti od požara, kritičnim vremenskim prilikama pogodnim za požare u Hrvatskoj te izobrazba o



prognostičkim produktima numeričkih modela zajedno s prikazivanjem rezultata najnovijih meteoroloških istraživanja povezani s požarima.

e) Uspostaviti glavni komunikacijski centar tijekom požarne sezone koji bi osigurao jedan pouzdani izvor informacija i redovito informirao javnost o trenutnim požarima, upravljanju požarima i vremenskoj prognozi relevantnoj za požare koji su u tijeku.

f) Financijski podržati istraživanja iz meteorologije povezane s požarima uključujući istraživanja ponašanja požara. Uspostaviti centar za istraživanje vremenskih prilika i ponašanja požara koji bi osigurao suradnju između meteorologa i požarnih analitičara. To je neophodno kako bi se analizirali prijašnji požari, provodili kontrolirani požarni eksperimenti, testirali i/ili usvojili modeli ponašanja požara te testirao model FWI na osnovnim tipovima vegetacije u Hrvatskoj te pripremile validacije modela ponašanja požara.

Poboljšanje vremenske prognoze požara:

a) Osigurati specijalizirane detaljne vremenske prognoze za pojedinačne požare raslinja.

b) Uvesti prognozu širenja dima od požara te prognozu i upozorenja na nisku kvalitetu zraka nastalu uslijed požara raslinja.

c) Uvesti potpunu zabranu paljenja vatre na otvorenom izvan požarne sezone u suradnji s meteorolozima kada postoje povoljne vremenske prilike za nastanak požara.

Znanstvena istraživanja:

a) Suradivati s europskim i drugim znanstvenicima koji se bave vremenskim uvjetima tijekom požara u svrhu razmjene znanja, posebno u modeliranju vremenskih uvjeta i ponašanja požara.

b) Suradivati s međunarodnim stručnjacima i testirati mogućnosti uvođenja smanjenja gorivog materijala izvan požarne sezone (uz blisku suradnju s meteorolozima).

c) Osigurati obuku za analitičare koji se bave ponašanjem požara.

d) Osigurati redovita meteorološka izvješća o velikim šumskim požarima koji su prouzročili velika materijalna i/ili prirodna razaranja, smrt ili uzrokovali specifično ponašanja požara i učiniti ih javno dostupnima.

e) Uključiti podatke vegetacije i topografije visoke razlučivosti u model WRF SFIRE.

f) Testirati model WRF SFIRE na brzinu širenja požara i uključiti ga u operativnu uporabu.

g) Vremenski i prostorno proširiti prognozu FWI koristeći već raspoloživi operativni model.

h) Proširiti mrežu automatskih meteoroloških postaja u svrhu zaštite šuma i drugog raslinja od požara i nabaviti mobilnu meteorološku postaju u svrhu meteoroloških mjerenja na samom požaru.

i) Redovito davati klimatsku analizu u svrhu procjene opasnosti od požara.

j) Razmotriti operativno uvođenje *Hot Dry Windy* indeksa meteorološke opasnosti od požara.

Podizanje javne svijesti o opasnosti od požara raslinja i smanjenje njihove opasnosti mogu se postići i poboljšati sljedećim:

a) Stalno educirati javnost o opasnosti od požara raslinja (i izvan požarne sezone).

b) Educirati turiste o opasnosti od požara raslinja i potpunoj zabraniti paljenja vatre na otvorenom tijekom ljetne sezone za vrijeme njihova boravka u Hrvatsku.

c) Uključiti izobrazbu o opasnosti od požara raslinja i načinu smanjenja te opasnosti u školski program.

d) Stalno educirati novinare o upravljanju požarima, opasnosti od požara i njegovom smanjenju, ponašanju požara, vremenskim uvjetima tijekom požara raslinja te klimatskim promjenama koje utječu na požare i požarni režim.

e) Educirati poljoprivrednike o kompostiranju biljnih ostataka i izbjegavati njihovo spaljivanje, posebno u proljeće i jesen.

f) Educirati javnosti kako reagirati i postupiti kada izbije požar raslinja.

g) Održavati osnovnu vatrogasna obuka za javnost koja je dostupna na zahtjev.

h) Podići svijest o održavanju čistog pojasa bez gorivog materijala oko stambenih zgrada i kuća te na poljoprivrednim površinama.

Ostalo:

a) Redovito čistiti protupožarne puteve unutar šuma i drugih prirodnih područja.

b) Uvesti strože propise o održavanju područja čistim od gorivog materijala te o vrsti vegetacije planirane oko novogradnja i stambenih kuća u hrvatski zakon.

c) Planirati pošumljavanje (površinu i izbor vrste vegetacije) sukladno šumsko-gospodarskim planovima s izradom pristupnih šumskih-protupožarnih cesta.

Provedba predloženih koraka dovela bi do poboljšanja vatrogasnog upravljanja požarima raslinja, poboljšanja vremenske prognoze za potrebe požara koja bi osigurala točniju i pravodobnu meteorološku informaciju vatrogascima i javnosti, povećala svijest javnosti o opasnosti od požara, povećala znanje o vremenskim uvjetima povoljnim za požare među vatrogascima te, u cjelini, povećala otpornost na požare i smanjila opasnost od požara raslinja u Hrvatskoj uslijed klimatskih promjena.

## REFERENCES

- Abatzoglou, J.T., Hatchett, B.J., Fox-Hughes, P., Gershunov, A., Nauslar, N.J., 2020. Global climatology of synoptically-forced downslope winds. *Intl. J. Climatol.* 41, 1–20. <https://doi.org/10.1002/joc.6607>.
- Abram, N.J., Henley, B.J., Gupta, A.S., Lippmann, T.J., Clarke, H., Dowdy, A.J., Sharples, J.J., Nolan, R.H., Zhang, T., Wooster, M.J., Wurtzel, J.B., 2021. Connections of climate change and variability to large and extreme forest fires in southeast Australia. *Commun. Earth Environ.* 2, 1–17. <https://doi.org/10.1038/s43247-020-00065-8>.
- ALADIN International Team, 1997. The ALADIN project: Mesoscale modelling seen as a basic tool for weather forecasting and atmospheric research. *WMO Bull.* 46, 317–324.
- Albini, F. A., 1976. Estimating wildfire behavior and effects. USDA Forest Service General Tech. Rep. INT-30, 92 pp.
- Amatulli, G., Camia, A., San-Miguel-Ayanz, J., 2013. Estimating future burned areas under changing climate in the EU-Mediterranean countries. *Sci. Total Environ.* 450–451, 209–222. <https://doi.org/10.1016/j.scitotenv.2013.02.014>.
- Andela, N., Morton, D.C., Giglio, L., Chen, Y., van der Werf, G.F., Kasibhatla, P.S., DeFries, R.S., Collatz, R.J., Hantson, S., Kloster, S., Bachelet, D., Forrest, M., Lasslop, G., Li, F., Mangeon, S., Melton, J.R., Yue, C., Randerson, J.T., 2017. A human-driven decline in global burned area. *Science.* 356, 1356–1362. <https://doi.org/10.1126/science.aal4108>.
- Anderson, H. E., 1982. Aids to determining fuel models for estimating fire behavior. USDA Forest Service, Intermountain Forest and Range Experiment Station General Tech. Rep. INT-122, 22 pp. [Available online at [http://www.fs.fed.us/rm/pubs\\_int/int\\_gtr122.pdf](http://www.fs.fed.us/rm/pubs_int/int_gtr122.pdf).]
- Bakšić, N., Vučetić, M., Španjol, Ž., 2015. A potential risk of fire on open space in the Republic of Croatia. *Firefighting and management.* 5, 30–40 (in Croatian).
- Bally, J., 1995. The Haines Index as a predictor of fire activity in Tasmania. In *Proceedings of Bushfire '95, Australian Bushfire Conference, 27–30 September, Hobart, Tasmania, Australia.*
- Barešić, D., 2011. The Impact of Climate Change on the Potential Risk of Forest Fires in Croatia, Master Thesis, Faculty of science, University of Zagreb, Zagreb, Croatia (in Croatian).
- Barlow, J., Berenguer, E., Carmenta, R., França, F., 2019. Clarifying Amazonia's burning crisis. *Glob. Chang. Biol.* 26, 319–321. <https://doi.org/10.1111/gcb.14872>.

- Bartlett, T., Leonard, M., Morgan, G., 2007. The megafire phenomenon: some Australian perspectives. In *The 2007 Institute of Foresters of Australia and New Zealand Institute of Forestry Conference: Programme, Abstracts and Papers*, Institute of Foresters of Australia, Canberra, ACT, Australia. Available at <http://www.forestry.org.au/pdf/pdf-public/conference2007/papers/Bartlett%20Megafire-final%20Draft27%2003.pdf>.
- Baughman, R.G., Albini, F.A., 1980. Estimating midflame windspeeds. In: *Sixth Conference on Fire and Forest Meteorology*, Seattle, WA, USA. 88–92.
- Beals, E.A., 1914. The value of weather forecasts in the problem of protecting forests from fire. *Mon. Wea. Rev.*, **42**, 111–119. [https://doi.org/10.1175/1520-0493\(1914\)42](https://doi.org/10.1175/1520-0493(1914)42).
- Bedia, J., Herrera, S., Camia, A., Moreno, J.M., Gutiérrez, J.M., 2014. Forest fire danger projections in the Mediterranean using ENSEMBLES regional climate change scenarios. *Clim. Change*. 122, 185–199. <https://doi.org/10.1007/s10584-013-1005-z>.
- Belušić, A., Telišman Prtenjak, M., Güttler, I., Ban, N., Leutwyler, D., Schär, C., 2018. Near-surface wind variability over the broader Adriatic region: insights from an ensemble of regional climate models. *Clim. Dyn.* 50, 4455–4480, doi:/10.1007/s00382-017-3885-5.
- Bento-Gançalves, A., Vieira, A., 2019. Wildfires in the wildland-urban interface: Key concepts and evaluation methodologies. *Sci. Tot. Environ.* 707, 135592. <https://doi.org/10.1016/j.scitotenv.2019.135592>.
- Boegelsack, N., Withey, J., O’Sullivan, G., McMartin, D., 2018. A critical examination of the relationship between wildfires and climate change with consideration of the human impact. *J. Environ. Prot. Sci.* 9, 461–467. <https://doi.org/10.4236/jep.2018.95028>.
- BoM (Bureau of Meteorology), 2008a. *Fire Weather Directive – Tasmania and Antarctic Regional Office*, Bureau of Meteorology, Hobart, Tasmania. 53 pp.
- BoM (Bureau of Meteorology), 2009. *Meteorological Aspects of the 7 February 2009 Victorian Fires, An Overview*. Bureau of Meteorology Report for the 2009 Victorian Bushfires Royal Commission, Bureau of Meteorology, Melbourne, Australia.
- BoM (Bureau of Meteorology) 2013a. *Tasmanian Bushfires Inquiry*, Bureau of Meteorology, Hobart, Tasmania, Australia.
- Bureau of Meteorology (BoM), 2013b. *Special Climate Statement 43 – extreme heat in January 2013*, Melbourne, Australia, 2013.
- Bureau of Meteorology (BoM), 2018. *2007-2016 atmospheric reanalysis over Tasmania: Product specification*, Bureau of Meteorology, Hobart, Australia, 2018.

- Bond, H.G., Mackinnon, K., Noar, P.F., 1967. Report on the Meteorological Aspects of the Catastrophic Bushfires in the South-eastern Tasmania on 7 February 1967, Bureau of Meteorology, Melbourne, Australia.
- Bonner, W.D., 1968. Climatology of the low-level jet. *Mon. Wea. Rev.* 96, 833–850, doi:/10.1175/1520-0493(1968)096<0833:COTLLJ>2.0.CO;2.
- Borchers Arriagada, N., Palmer, A.J., Bowman, D., Morgan, G.G., Jalaludin, B.B., Johnston, F.H., 2020. Unprecedented smoke-related health burden associated with the 2019-2020 bushfires in eastern Australia. *Med. J. Aust.* 213, 282–283. <https://doi.org/10.5694/mja2.50545>.
- Bowman, D.M.J., Balch, J.K., Artaxo, P., Bond, W.J., Carlson, J.M., Cochrane, M.A., D’Antonio, C.M., DeFries, R.S., Doyle, J.C., Harrison, S.P., Johnston, F.H., Keeley, J.E., Krawchuk, M.A., Kull, C.A., Marston, J.B., Moritz, M.A., Colin Prentice, I., Roos, C.I., Scott, A.C., Swetnam, T.W., Van der Werf, G.R., Pyne, S.J., 2009. Fire in the Earth System. *Science*. 324, 481–484. <https://doi.org/10.1126/science.1163886>.
- Bradstock, R.A., Cohn, J.S., Gill, A.M., Bedward, M., Lucas, C., 2009. Prediction of the probability of large fires in the Sydney region of south-eastern Australia using fire weather. *Intl. J. Wildland Fire*. 18, 932–943. <https://doi.org/10.1071/WF08133>.
- Brey, S.J., Barnes, E.A., Pierce, J.R., Swann, A.L.S., Fischer, E.V., 2021. Past variance and future projections of the environmental conditions driving western U.S. summertime wildfire burn area. *Earth’s Future*. 9. <https://doi.org/10.1029/2020EF001645>.
- Brewer, M.J., Clements, C.B., 2020. The 2018 Camp Fire: Meteorological analysis using in situ observations and numerical simulations. 11, 47, doi:10.3390/atmos11010047.
- Brinkmann, W.A.R., 1971. What is a foehn? *Weather*. 26, 230–239.
- Brotak, E.A., 1976. A Synoptic Study of the Meteorological Conditions Associated with Major Wildland Fires, PhD dissertation, Yale University, New Haven, CT, U.S.
- Brotak, A.E., Reifsnyder, W.E., 1977. An investigation of the synoptic situations associated with major wildland fires. *Fire Manag. Today*. 38, 867–870, doi:/10.1175/1520-0450(1977)016<0867:AIOTSS>2.0.CO;2.
- Brotak, E.A., Reifsnyder, W.E., 2003. Predicting major wildland fire occurrence. *Fire Manag. Today*. 63, 20–24.
- Brown, T., Leach, S., Wachter, B., Gardunio, B., 2020. The northern California 2018 extreme fire season. In ‘Explaining extremes of 2018 from a climate perspective’. *Bull. Amer. Meteor. Soc.* 101, S1-S4. <https://doi.org/10.1175/BAMS-D-19-0275.1>.

- Buckland, M.K., 2019. What is a Megafire? Defining the Social and Physical Dimensions of Extreme U.S. Wildfires (1988-2014), Master thesis, Department of Geography, Faculty of the Graduate School, University of Colorado, Boulder, Colorado, United States.
- Burgess, T. Burgmann, JR. Hall, S. Holmes, D., Turner, E., 2020. Black Summer: Australian newspaper reporting on the nation's worst bushfire season, Monash Climate Change Communication Research Hub, Monash University, Melbourne, pp. 30.
- Byram, G.M., 1940. Sun and wind and fuel moisture. *J. For.* 38, 639–640.
- Byram, G.M., Jemison, G.M., 1943. Solar radiation and forest fuel moisture. *J. Agricultural Res.* 67, 149–176.
- Byram, G.M., 1954. Atmospheric conditions related to blowup fires, Station Paper SE-SP-35, USDA-Forest Service, Southeastern Forest Experiment Station, Asheville.
- Byram, G.M., 1959. Combustion of forest fuels. In *Forest Fire Control and Use*; Davis, K.P., Ed.; McGraw-Hill: New York, NY, USA, 1959; 61–89.
- Camia, A., Amatulli, G., San-Miguel-Ayanz, J., 2008. Past and future trends of forest fire danger in Europe, JRC Scientific and Technical Reports No. 6., European Commission, Joint Research Centre, Ispra.
- Canadell, J.G., Meyer, C.P., Cook, G.D., Dowdy, A., Briggs, P.R., Knauer, J., Pepler, A., Haverd, V. Multi-decadal increase of forest burned area in Australia is linked to climate change. *Nat. Commun.* 12, 6921 (2021). <https://doi.org/10.1038/s41467-021-27225-4>.
- Cao, Y., Fovell, R.G., 2018. Downslope Windstorms of San Diego County. Part II: Physics Ensemble Analyses and Gust Forecasting. *Weather Forecast.* 33, 539–559.
- Carmona-Moreno, C., Belward, A., Malingreau, J.P., Hartley, A., Garcia-Alegre, A., Antonovs, M.L., Buchshtaber, V., Pivovarov, V., 2005. Characterizing interannual variations in global fire calendar using data from Earth observing satellites. *Glob. Chang. Biol.* 11, 1537–1555. <https://doi.org/10.1111/j.1365-2486.2005.001003>.
- Cardil, A., Salis, M., Spano, D., Delogu, G., Molina, T.D., 2014. Large wildland fires and extreme temperatures in Sardinia (Italy). *Iforest.* 7, 161–168.
- Cardil, A., Eastaugh, C.S., Molina, D.M., 2015. Extreme temperature conditions and wildland fires in Spain. *Theor. Appl. Climatol.* 122, 219–228. <https://doi.org/10.1007/s00704-014-1295-8>.
- Cary, G.J., 2002. Importance of a changing climate for fire regimes in Australia, in: Bradstock, R.A., Williams, J.E., Gill, A.M. (Eds.), *Flammable Australia: The Fire Regimes and Biodiversity of a Continent*. Cambridge University Press, Cambridge, U.K.

- Chen, B., Jin, Y., Scaduto, E., Moritz, M.A., Goulden, M.L., Randerson, J.T., 2021. Climate, fuel, and land use shaped the spatial pattern of wildfire in California's Sierra Nevada. *J. Geophys. Res. Biogeosci.* 126. <https://doi.org/10.1111/doi:10.1029/2020JG005786>.
- Cheney, N.P., 1976. Bushfire Disasters in Australia, 1945–1975. *Aust. For.* 39, 245–268. <https://doi.org/10.1080/00049158.1976.10675654>.
- Cesini, D., Morelli, S., Parmiggiani, F., 2004. Analysis of an intense bora event in the Adriatic area. *Nat. Hazards Earth Syst. Sci.* 4, 323–337, doi:/10.5194/nhess-4-323-2004.
- Charney, J.J., Bian, X., Potter, B., Heilman, W.E.: The role of a stratospheric intrusion in the evolution of the Double Trouble State Park wildfire. In: 5<sup>th</sup> Symposium on fire and forest meteorology joint with 2<sup>nd</sup> International wildland fire ecology and fire management congress, Orlando, 16–20 November 2003.
- Cindrić, K., Telišman-Prtenjak, M., Herceg-Bulić, I., Mihajlović, D., Pasarić, Z., 2016. Analysis of the extraordinary 2011/2012 drought in Croatia. *Theor. Appl. Climatol.* 123. 3, 503–522. doi:10.1007/s00704-014-1368-8.
- Clarke, H.G., Evans, J.P., 2019. Exploring the future change space for fire weather in southeast Australia. *Theor. Appl. Climatol.* 136, 513–527. <https://doi.org/10.1007/s00704-018-2507-4>.
- Clarke, H.G., Lucas, C., Smith, P.L., 2013. Changes in Australian fire weather between 1973 and 2010. *Intl. J. Climatol.* 33, 931–944. <https://doi.org/10.1002/joc.3480>.
- Clarke, H.G., Smith, P.L., Pitman, A.J., 2011. Regional signatures of future fire weather over eastern Australia from global climate models. *Intl. J. Wildland Fire.* 20, 550–562, <https://doi.org/10.1071/WF10070>.
- Clarke, H., Evans, J.P., 2019. Exploring the future change space for fire weather in southeast Australia. *Theor. Appl. Climatol.* 136, 513–527. <https://doi.org/10.1007/s00704-018-2507-4>.
- Coen, J.L., Stavros, E.N., Fites-Kaufman, J.A., 2018. Deconstructing the King megafire. *Ecol. Appl.* 28, 1565–1580. <https://doi.org/10.1002/eap.1752>.
- Collins, L., Bradstock, R.A., Clarke, H., Clarke, M.F., Nolan, R.H. and Penman, T.D., 2021. The 2019/2020 mega-fires exposed Australian ecosystems to an unprecedented extent of high-severity fire. *Environ. Res. Lett.* 16, p.044029. <https://doi.org/10.1088/1748-9326/abeb9e>.
- Conedera, M., Marxer P., Hoffmann, C., Tinner, W., Amman, B., 1996. Forest fire research in Switzerland. Part 1: Fire ecology and history research in the Southern part of Switzerland. *Int. For. Fire News.* 15, 13–21.

- Cruz, M.G., Sullivan, A.L., Gould, J.S., Sims, N.C., Bannister, A.J., Hollis, J.J. and Hurley, R.J., 2012. Anatomy of a catastrophic wildfire: The Black Saturday Kilmore East fire in Victoria, Australia. *Forest Ecol. Manage.* 284, 269–285. <http://doi.org/10.1016/j.foreco.2012.02.035>.
- Cunningham, P., Reeder, M.J., 2009. Severe convective storms initiated by intense wildfires: Numerical simulations of pyro-convection and pyro-tornadogenesis. *Geophys. Res. Lett.* 36, L12812. <http://doi.org/10.1029/2009GL039262>.
- Čavlina Tomašević, I., Cheung, K. K. W., Vučetić, V., Fox-Hughes, P., Horvath, K., Telišman Prtenjak, M., Beggs, P. J., Malečić, B., Milić, V., 2022. The 2017 Split wildfire in Croatia: Evolution and the role of meteorological conditions. *Nat. Hazards Earth Syst. Sci. Discuss.* 22, 3143–3165. <https://doi.org/10.5194/nhess-2022-116>.
- De la Barrera, F., Barraza, F., Favier, P., Ruiz, V., Quense, J., 2018. Megafires in Chile 2017: Monitoring multiscale environmental impacts of burned ecosystems. *Sci. Tot. Environ.* 637–638, 1526–153. <http://doi.org/10.1016/j.scitotenv.2018.05.119>.
- Dee, D., Uppala, S.M., Simmons, A., Berrisford, P., Poli, P., Kobayashi, S., Andrae, U., Balmaseda, M.A., Balsamo, G., Bauer, P., Bechtold, P., Beljaars, A.C., Berg, L.V., Bidlot, J., Bormann, N., Delsol, C., Dragani, R., Fuentes, M., Geer, A.J., Haimberger, L., Healy, S.B., Hersbach, H., Holm, E.V., Isaksen, L., Kållberg, P.W., Köhler, M., Matricardi, M., McNally, A.P., Monge-Sanz, B., Morcrette, J.J., Park, B., Peubey, C., Rosnay, P.D., Tavolato, C., Thepaut, J., & Vitart, F., 2011. The ERA-Interim reanalysis: configuration and performance of the data assimilation system. *Quart. J. Roy. Meteorol. Soc.* 137, 553–597. <https://doi.org/10.1002/QJ.828>.
- Di Virgilio, G., Evans, J.P., Blake, S.A.P., Armstrong, M., Dowdy, A.J., Sharples, J., McRae, R., 2019. Climate change increases the potential for extreme wildfires. *Geophys. Res. Lett.* 46, 8517–8526. <https://doi.org/10.1029/2019GL083699>.
- Di Virgilio, G., Evans, J.P., Clarke, H., Sharples, J., Hirsch, A.L., Hart, M.A., 2020. Climate change significantly alters future wildfire mitigation opportunities in Southeastern Australia. *Geophys. Res. Lett.* 47. <https://doi.org/10.1029/2020GL088893>.
- Dimitrakopoulos, A., Gogi, C., Stamatelos, G., Mitsopoulos, I., 2011. Statistical analysis of the fire environment of large forest fires (>1000 ha) in Greece. *Pol. J. Environ. Stud.* 20, 327–332.
- Dimitrov, T., 1982. Forest fires and forest fire danger assessment, in: Bertović, S. (Ed.), *Osnovne zaštite šuma od požara*. Centar za informacije i publicitet, Zagreb, pp. 181–256. (in Croatian).



- Doerr, S.H., Santín C., 2016. Global trends in wildfire and its impacts: perceptions versus realities in a changing world. *Phil. Trans. R. Soc. B371*, 20150345. <http://dx.doi.org/10.1098/rstb.2015.0345>.
- Dowdy, A.J., 2018. Climatological Variability of Fire Weather in Australia. *J. Appl. Meteor. Climatol.* 57, 221–234. <https://doi.org/10.1175/JAMC-D-17-0167.1>.
- Dowdy, A.J., Mills, G.A., Finkele, K., de Groot, W., 2009. Australian Fire Weather as Represented by the McArthur Forest Fire Danger Index and the Canadian Forest Fire Weather Index. CAWCR Technical Report No. 10, Centre for Australian Weather and Climate Research, Melbourne, Australia.
- Dowdy, A.J., Fromm, M.D., McCarthy, N., 2017. Pyrocumulonimbus lightning and fire ignition on Black Saturday in southeast Australia. *J. Geophys. Res. Atmos.* 122, 7342–7354. <https://doi.org/10.1002/2017JD026577>.
- Dowdy, A.J., Pepler, A., 2018. Pyroconvection risk in Australia: Climatological changes in atmospheric stability and surface fire weather conditions. *Geophys. Res. Lett.* 45, 2005–2013. <https://doi.org/10.1002/2017GL076654>.
- Dowdy, A. J., Ye, H., Pepler, A., Thatcher, M., Osbrough, S. L., Evans, J. P., 2019. Future changes in extreme weather and pyroconvection risk factors for Australian wildfires. *Sci. Rep.* 9(1), 10073. <https://doi.org/10.1038/s41598-019-46362-x>.
- Dudhia, J., 1989. Numerical study of convection observed during the Winter Monsoon Experiment using a mesoscale two-dimensional model. *J. Atmos. Sci.* 46, 3077–3107. [https://doi.org/10.1175/1520-0469\(1989\)046<3077:CO;2](https://doi.org/10.1175/1520-0469(1989)046<3077:CO;2).
- Dupuy, J.L., Fargeon, H., Martin-St Paul, N., Pimont, F., Ruffault, J., Guijarro, M., Hernando, C., Madrigal, J., Fernandes, P., 2020. Climate change impact on future wildfire danger and activity in southern Europe: a review. *Ann. For. Sci.* 77. <https://doi.org/10.1007/s13595-020-00933-5>.
- DUSZ (National Protection and Rescue Directorate), 2018. Report on the realization of the program of activities in the implementation of special measures of protection from forest fires in Republic of Croatia in 2017, National protection and rescue directorate, Zagreb. (in Croatian)
- Efimov, V.V., Stanichnyi, S.V., Shokurov, M.V., Yarovaya, D.A., 2008. Observations of a quasi-tropical cyclone over the Black Sea. *Russ. Meteor. Hydrol.* 33. 233239, <https://doi.org/10.3103/S1068373908040067>.

- Ellis, S., Kanowski, P., Whelan, R., 2004. National Inquiry on Bushfire Mitigation and Management, Council of Australian Governments (COAG), Canberra, Australia.
- Ellis, T.M., Bowman, D.M., Jain, P., Flannigan, M.D., Williamson, G.J. 2022. Global increase in wildfire risk due to climate driven declines in fuel moisture. *Glob. Change Biol.* 28(4), 1544–1559. <https://doi.org/10.1111/gcb.16006>.
- Engel, C.B., Lane, T.P., Reeder, M.J., Rezný, M., 2013. The meteorology of Black Saturday. *Q. J. R. Meteorol. Soc.* 139, 585–599. <https://doi.org/10.1002/qj.1986>.
- Enright, N.J., Fontaine, J.B., 2013. Climate Change and the Management of Fire-Prone Vegetation in Southwest and Southeast Australia. *Geog. Res.* 52, 34–44. <https://doi.org/10.1111/1745-5871.12026>.
- Fargeon, H., Pimont, F., Martin-St Paul, N., de Caceres, M., Ruffault, J., Barbero, R., Dupuy, J.L., 2020. Projections of fire danger under climate change over France: where do the greatest uncertainties lie? *Clim. Change.* 160, 479–493. <https://doi.org/10.1007/s10584-019-02629-w>.
- Ferina, J., Vučetić, V., 2018. Rating the fire season 2017. Croatian Meteorological and Hydrological Service, Zagreb, Croatia (in Croatian).
- Field, R.D., Luo, M., Fromm, M., Voulgarakis, A., Mangeon, S., Worden, J., 2016. Simulating the Black Saturday 2009 smoke plume with an interactive composition-climate model: Sensitivity to emissions amount, timing, and injection height. *J. Geophys. Res. Atmos.* 121, 4296–4316. <https://doi.org/10.1002/2015JD024343>.
- Fink, A.H., Brücher, T., Krüger, A., Leckebusch, G.C., Pinto, J.G., Ulbrich, U., 2004. The 2003 European summer heatwaves and drought – synoptic diagnosis and impacts. *Weather.* 59, 209–216. <https://doi.org/10.1256/wea.73.04>.
- Finkele, K., Mills, G.A., Beard, G., Jones, D. 2006. National daily gridded soil moisture deficit and drought factors for use in prediction of Forest Fire Danger Index in Australia. *Aust. Met. Mag.* 55, 183-97.
- Finney, M.A., Cohen, J.D., Forthofer, J.M., McAllister, S.S., Gollner, M.J., Gorham, D.J., Saito, K., Akafuah, N.K., Adam, B.A. and English, J.D., 2015. Role of buoyant flame dynamics in wildfire spread. *Proc. Natl. Acad. Sci. U.S.A.* 112, 9833–9838. <https://doi.org/10.1073/pnas.1504498112>.
- Flannigan, M.D., Cantin, A.S., de Groot, W.J., Wotton, M., Newbery, A., Gowman, L.M., 2013. Global wildland fire season severity in the 21st century. *Forest Ecol. Manag.* 294, 54–61. <https://doi.org/10.1016/j.foreco.2012.10.022>.

- Flannigan, M.D., Harrington, J.B., 1988. A study of the relation of meteorological variables to monthly provincial area burned by wildfire in Canada 1953–80. *J. Appl. Meteor.* 27, 441–452. [https://doi.org/10.1175/1520-0450\(1988\)027<0441: ASOTRO>2.0.CO;2](https://doi.org/10.1175/1520-0450(1988)027<0441: ASOTRO>2.0.CO;2).
- Flannigan, M.D., Krawchuk, M.A., de Groot, W.J., Wotton, B.M., Gowman, L.M., 2009. Implications of changing climate for global wildland fire. *Intl. J. Wildland Fire.* 18, 483–507. <https://doi.org/10.1071/WF08187>.
- Flannigan, M.D., Logan, K.A., Amiro, B.D., Skinner, W.R., Stocks, B.J., 2005. Future Area Burned in Canada. *Clim. Change.* 72, 1–16. <https://doi.org/10.1007/s10584-005-5935-y>.
- Flannigan, M.D., Stocks, B.J., Wotton, B.M., 2000. Climate change and forest fires. *Sci. Tot. Environ.* 262, 221–229.
- Foley, J.C., 1947. A Study of Meteorological Conditions associated with Bush and Grass Fires and Fire Protection Strategy in Australia, Bulletin Number 38, Bureau of Meteorology, Melbourne, Commonwealth of Australia.
- Fox-Hughes, P., 2008. A fire danger climatology for Tasmania. *Aust. Met. Mag.* 57, 109–120.
- Fox-Hughes, P., 2011. Impact of More Frequent Observations on the Understanding of Tasmanian Fire Danger. *J. Appl. Meteor. Climatol.* 50, 1617–1626. <https://doi.org/10.1175/JAMC-D-10-05001.1>.
- Fox-Hughes, P., 2012. Springtime fire weather in Tasmania, Australia: two case studies. *Wea. Forecasting.* 27, 379–395. <https://doi.org/10.1175/WAF-D-11-00020.1>.
- Fox-Hughes, P., Harris, R.M.B., Lee, G., Grose, M.R., Bindoff, N.L., 2014. Future fire danger climatology for Tasmania, Australia, using a dynamically downscaled regional climate model. *Intl. J. Wildland Fire.* 23, 309–321. <https://doi.org/10.1071/WF13126>.
- Francetić, N., 2017. We can learn from the Split wildfire. *Vatrogasni vjesnik.* 8/2017, 14–17, 2017 (in Croatian).
- French, B.J., Prior, L.D., Williamson, G.J., Bowman, D.M., 2016. Cause and effects of a megafire in sedge-heathland in the Tasmanian temperate wilderness. *Aust. J. Bot.* 64, 513–525.
- Fromm, M., Tupper, A., Rosenfeld, D., Servranck, R., McRae, R., 2006. Violent pyroconvective storm devastates Australia’s capital and pollutes the stratosphere. *Geophys. Res. Lett.* 33, L05815. <https://doi.org/10.1029/2005GL025161>.
- Fromm, M.D., R. H. D. McRae, J. J. Sharples, and G. P. Kablick III, 2012. Pyrocumulonimbus pair in Wollemi and Blue Mountains national parks, 22 November 2006. *Aust. Meteor. Oceanogr. J.* 62, 117–126. <https://doi.org/10.22499/2.6203.001>.

- Giorgi, F., 2006. Climate change hot-spots. *Geophys. Res. Lett.* 33, L08707, <https://doi.org/10.1029/2006GL025734>.
- Gisborne, H.T., 1928. *Measuring Forest Fire Danger in Northern Idaho*. USDA Miscellaneous Publication 64, Washington DC, U.S.
- Griffiths, D., 1999. Improved formula for the drought factor in McArthur's Forest Fire Danger Meter. *Aust. For.* 62, 202-6.
- Grisogono, B., Belušić, D., 2009. A review of recent advances in understanding the meso- and micro-scale properties of the severe Bora wind. *Tellus A: Dyn. Meteorol. Oceanogr.* 61, 1–16. <https://doi.org/10.1111/j.1600-0870.2008.00369.x>.
- Gohm, A., Mayr, G.J., 2005. Numerical and observational case-study of a deep Adriatic bora. *Q. J. R. Meteorol. Soc.* 131, 1363–1392, doi:/10.1256/qj.04.82.
- Gohm, A., Mayr, G.J., Fix, A., Giez, A., 2008. On the onset of bora and the formation of rotors and jumps near a mountain gap. *Q. J. R. Meteorol. Soc.* 134, 21–46, doi:/10.1002/qj.206.
- Grisogono, B., Belušić, D., 2009. A review of recent advances in understanding the meso- and micro-scale properties of the severe Bora wind. *Tellus A: Dyn. Meteorol. Oceanogr.* 61, 1–16, doi:/10.1111/j.1600-0870.2008.00369.x.
- Grose, M.R., Fox-Hughes, P., Harris, R.M.B., Bindoff, N.L., 2014. Changes to the drivers of fire weather with a warming climate – a case study of southeast Tasmania. *Clim. Change.* 124, 255–269. <https://doi.org/10.1007/s10584-014-1070-y>.
- Grubišić, V., 2004. Bora-driven potential vorticity banners over the Adriatic. *Q. J. R. Meteorol. Soc.* 130, 2571–2603, doi:/10.1256/qj.03.71.
- Haines, D.A., 1988. A lower atmosphere severity index for wildlife fires. *Natl. Weather Dig.* 13, 23–27.
- Harris, S., Mills, G., Brown, T., 2017. Variability and drivers of extreme fire weather in fire-prone areas of south-eastern Australia. *Intl. J. Wildland Fire.* 26, 177–190. <https://doi.org/10.1071/WF16118>.
- Hasson, A.E.A., Mills, G.A., Timbal, B., Walsh, K., 2009. Assessing the impact of climate change on extreme fire weather events over southeastern Australia. *Clim. Res.* 39, 159–172. <https://doi.org/10.3354/cr00817>.
- Hennessy, K., Lucas, C., Nicholls, N., Bathols, J., Suppiah, R., Ricketts, J., 2005. *Climate Change Impacts on Fire Weather in Southeast Australia*. CSIRO Marine and Atmospheric Research Report, CSIRO Marine and Atmospheric Research, Aspendale, Victoria, Australia.

- Hernandez, C., Drobinski, P., Turquety S., 2015. How much does weather control fire size and intensity in the Mediterranean region? *Ann. Geophys.* 33, 931–939, doi:/10.5194/angeo-33-931-2015.
- Hoinka, K.P., De Castro, M., 2003. The Iberian Peninsula thermal low. *Quart. J. Roy. Meteorol. Soc.* 129, 1491–1511. <https://doi.org/10.1256/qj.01.189>.
- Holbrook, S., 1944. The Peshtigo fire. *Am. Scholar.* 13, 201–209.
- Horvath, K., Ivatek-Šahdan, S., Ivančan-Picek, B., Grubišić, V., 2009. Evolution and Structure of Two Severe Cyclonic Bora Events: Contrast between the Northern and Southern Adriatic. *Weather. Forecast.* 24, 946–964, doi:/10.1175/2009WAF2222174.1.
- Hrastinski, M., Horvath, K., Odak Plenković, I., Ivatek-Šahdan, S., Bajić A., 2015. Verification of the operational 10 m wind forecast obtained with the ALADIN mesoscale numerical weather prediction model. *Croat. Meteorol. J.* 50, 105–120.
- Huang, C., Lin, Y.L., Kaplan, M.L., Charney, J.J., 2009. Synoptic-scale and mesoscale environments conducive to forest fires during the October 2003 extreme fire event in Southern California. *J. Appl. Meteor. Climatol.* 48, 553–579, <https://doi.org/10.1175/2008JAMC1818.1>.
- IAWF, 2019. International Association of Wildland Fire Statement. Climate Change Week at the United Nations, 23–29 September, New York, U.S.
- IPCC, 2021. Climate Change 2021: The Physical Science Basis, in: Masson-Delmotte, V., P. Zhai, A. Pirani, S. L. Connors, C. Péan, S. Berger, N. Caud, Y. Chen, L. Goldfarb, M. I. Gomis, M. Huang, K. Leitzell, E. Lonnoy, J. B. R. Matthews, T. K. Maycock, T. Waterfield, O. Yelekçi, R. Yu and B. Zhou (Eds.), Contribution of Working Group I to the Sixth Assessment Report of the Intergovernmental Panel on Climate Change, Cambridge University Press., U.K.
- Ivančan-Picek, B., Tudor, M., Horvath, K., Stanešić, A., Ivatek-Šahdan, S., 2016. Overview of the first HyMeX special observation period over Croatia. *Nat. Hazards Earth Syst. Sci.* 16, 2657–2682. <https://doi.org/10.5194/nhess-16-2657-2016>.
- Jain, P., Castellanos-Acuna, D., Coogan, S.C.P. Abatzoglou, J.T., Flannigan, M.D., 2022. Observed increases in extreme fire weather driven by atmospheric humidity and temperature. *Nat. Clim. Change.* 12, 63–70. <https://doi.org/10.1038/s41558-021-01224-1>.

- Jézéquel, A., Cattiaux, J., Naveau, P., Radanovics, S., Ribes, A., Vautard, R., Vrac, M., Yiou, P., 2018. Trends of atmospheric circulation during singular hot days in Europe. *Env. Res. Lett.* 13, 54007. <https://doi.org/10.1088/1748-9326/aab5da>.
- Johnson, E.A., Wowchuk, D.R., 1993. Wildfires in the southern Canadian Rocky Mountains and their relationship to mid-tropospheric anomalies. *Canadian J. Forest Res.* 23, 1213–1222. <https://doi.org/10.1139/X93-153>.
- Jolly, W. M., Cochrane, M. A., Freeborn, P. H., Holden, Z. A., Brown, T. J., Williamson, G. J., Bowman, D. M. J. S., 2015. Climate-induced variations in global wildfire danger from 1979 to 2013. *Nature Comm.* 6(1). <https://doi.org/10.1038/ncomms8537>.
- Jones, M.W., Abatzoglou, J.T., Veraverbeke, S., Andela, N., Lasslop, G., Forkel, M., Smith, A.J., Burton, C., Betts, R.A., van der Werf, G.R., Sitch, S., 2022. Global and regional trends and drivers of fire under climate change. *Rev. Geophys.* 2020RG000726.
- Jovanović, N., Župan, R., 2017. Analysis of vegetation conditions before and after forest fires in Dalmatia using Sentinel-2 satellite images. *Geodetski list.* 71, 233-248.
- Juliano, T.W., Parish, T.R., Rahn, D.A., Leon, D.C., 2017. An atmospheric hydraulic jump in the Santa Barbara Channel. *J. Appl. Meteor. Climatol.* 56, 2981-2998. <https://doi.org/10.1175/JAMC-D-16-0396.1>.
- Jurčec, V., 1989. Severe Adriatic bora storms in relation to synoptic developments. *Rasprave.* 24, 11–20.
- Jurčec, V., 1992. Low-level jet stream over the Adriatic area. *Vijesti.* 1991, 36–41.
- Jurčec, V., Visković, S., 1989. Causes of bora in Split. *Vijesti.* 1989, 20–26.
- Kain, J.S., Kain, J., 2004. The Kain - Fritsch convective parameterization: an update. *J. Appl. Meteorol.* 43, 170–181. [https://doi.org/10.1175/1520-0450\(2004\)0432.0.CO;2](https://doi.org/10.1175/1520-0450(2004)0432.0.CO;2).
- Kaplan, M.L., James, C.N., Ising, J., Sinclair, M.R., Lin, Y.L., Taylor, A., Riley, J., Karim, S.M. and Wiles, J., 2021. The Multi-Scale Dynamics Organizing a Favorable Environment for Convective Density Currents That Redirected the Yarnell Hill Fire. *Climate*, 9(12), p.170.
- Kapusta, A., Wiluś, R., 2017. Geography of Tourism in Croatia, in: Widawski, K., Wyrzykowski, J. (Eds.), *The Geography of Tourism of Central and Eastern European Countries*. Springer, Cham, pp. 109–147, doi:/10.1007/978-3-319-42205-3\_4.
- Kartsios, S., Karacostas, T., Pytharoulis, I., Dimitrakopoulos, A.P., 2021. Numerical investigation of atmosphere-fire interactions during high-impact wildland fire events in Greece. *Atmos. Res.* 247, 105253. <https://doi.org/10.1016/j.atmosres.2020.105253>.

- Kassomenos, P., 2010. Synoptic circulation control on wild fire occurrence. *Phys. Chem. Earth.* 35, 544–552.
- Keegan, K.M., Albert, M.R., McConnell, J.R., Baker, I., 2014. Climate change and forest fires synergistically drive widespread melt events of the Greenland Ice Sheet. *Proc. Nat. Acad. Sci.* 111, 7964–7967. <https://doi.org/10.1073/pnas.1405397111>.
- Keeley, J.E., 2008. Fire, in: Sven Erik Jørgensen, Brian D. Fath, (Ed.), *Encyclopedia of Ecology*, Academic Press, 1557–1564, 2008.
- Keeley, J.E., 2012. Fire in Mediterranean climate ecosystems – a comparative overview. *Isr. J. Ecol. Evol.* 58, 123–135. <https://doi.org/10.1560/IJEE.58.2-3.123>.
- Keeley, J.E., Syphard, A.D., 2016. Climate change and future fire regimes: examples from California. *Geosci. J.* 6. <https://doi.org/10.3390/geosciences6030037>.
- Keetch, J.J., Byram, G.M., 1968. A drought index for forest fire control, USDA Forest Service Research Paper, Asheville, NC, USA.
- Kirkpatrick, J.B., Styger, J.K., Marsden-Smedley, J.B., 2018. Impact of changes in lightning fire incidence on the values of the Tasmanian wilderness world heritage area. *Pap. proc. R. Soc. Tasmania.* 152, 27–32. <https://doi.org/10.26749/rstpp.152.27>.
- Klaić, Z.B., Pasarić, Z., Tudor, M. 2009. On the interplay between sea-land breezes and Etesian winds over the Adriatic. *J. Mar. Syst.* 78, S101-S118.
- Kochanski, A. K., Jenkins, M. A., Mandel, J., Beezley, J. D., Clements, C. B., and Krueger, S., 2013. Evaluation of WRF-SFIRE performance with field observations from the FireFlux experiment, *Geosci. Model Dev.*, 6, 1109–1126, <https://doi.org/10.5194/gmd-6-1109-2013>.
- Kondo, J., Kuwagata, T., 1992. Enhancement of forest fires over northeastern Japan due to atypical strong dry wind. *J. Appl. Meteor.* 31, 386–396, doi:/10.1175/1520-0450.
- Kozarić, T., Mokorić, M., 2012. Kvarner fire 23rd and 24th July 2012 - weather analysis. *Firefighting and Management.* 2, 53–66 (in Croatian).
- Krawchuk, M.A., Moritz, M.A., Parisien, M.-A., Van Dorn, J., Hayhoe, K., 2009. Global Pyrogeography: The Current and Future Distribution of Wildfire. *Plos. One.* 4, e5102. <https://doi.org/10.1371/journal.pone.0005102>.
- Kuraži, D., Vučetić, V., 2015. Weather analysis of a large forest fire on Mount Strahinjčica in March 2012. *Firefighting and Management.* 5, 5–16 (in Croatian).
- Lagouvardos, K., Kotroni, V., Giannaros, T.M., Dafis, S., 2019. Meteorological conditions conducive to the rapid spread of the deadly wildfire in Eastern Attica, Greece. *Bull. Am. Meteorol. Soc.* 100, 2137–2145. <https://doi.org/10.1175/BAMS-D-18-0231.1>.

- Laureau, N.P., Nauslar, N.J., Abatzoglou, J.T., 2019. The Carr fire vortex: A case of pyrotornadogenesis? *Geophys. Res. Lett.* 45, 107–13. <https://doi.org/10.1029/2018GL080667>.
- Lepri, P., Večenaj, Ž., Kozmar, H., Grisogono, B., 2015. Near-ground turbulence of the Bora wind in summertime. *J. Wind Eng. Ind. Aerodyn.* 147, 345–357, doi:/10.12989/was.2014.19.5.505.
- Levin, N., Saaroni, H., 1999 Fire weather in Israel – synoptic climatological analysis. *GeoJournal.* 47, 523–538.
- Lionello, P., Malanotte-Rizzoli, P., Boscolo, R., Alpert, P., Artale, V., Li, L., Luterbacher, J., May, W., Trigo, R.M., Tsimplis, M., Ulbrich, U., Xoplaki, E., 2006. The Mediterranean climate: an overview of the main characteristics and issues, in: Lionello, P., Malanotte-Rizzoli, P., Boscolo, R. (Eds.), *Mediterranean, Developments in Earth and Environmental Sciences*, Elsevier, pp. 1–26. [https://doi.org/10.1016/S1571-9197\(06\)80003-0](https://doi.org/10.1016/S1571-9197(06)80003-0).
- Long, M., 2006. A climatology of extreme fire weather days in Victoria. *Aust. Met. Mag.* 55, 3–18.
- Long, R.R., 1953. Some aspects of the flow of stratified fluids. I. A theoretical investigation. *Tellus.* 5, 42–58.
- Lucas, C., 2010. On developing a historical fire weather data-set for Australia. *Aust. Meteorol. Oceanogr. J.* 60, 1–14.
- Lucas, C., Hennessy, K., Mills, G., Bathols, J., 2007. *Bushfire Weather in Southeast Australia: Recent Trends and Projected Climate Change Impacts*, Consultancy Report prepared for The Climate Institute of Australia, Bureau of Meteorology Research Centre, Melbourne, Australia.
- Luderer, G., J. Trentmann, and M. O. Andreae, 2009: A new look at the role of fire-released moisture on the dynamics of atmospheric pyro-convection. *Int. J. Wildland Fire*, 18, 554–562. <https://doi.org/10.1071/WF07035>.
- Luke, R., McArthur, A., 1978. *Bushfires in Australia*, Australian Government Publishing Service, Canberra, Australia.
- Lydersen, J.M., North, M.P., Collins, B.M., 2014. Severity of an uncharacteristically large wildfire, the Rim Fire, in forests with relatively restored frequent fire regimes. *Forest Ecol. Manage.* 328, 326–334, doi:/10.1016/j.foreco.2014.06.005.
- Mamut, M., 2011. Ties between the geographical and social geographical features of Dalmatia with the endangerment of forest fires. *Croat. J. For. Eng.* 1–2/2011, 37–50 (in Croatian).



- Marsden-Smedley, J., 2014. *Tasmanian Wildfires January-February 2013: Forcett-Dunalley, Repulse, Bicheno, Giblin River, Montumana, Molesworth and Gretna*, Bushfire Cooperative Research Centre, East Melbourne, Australia, 2014.
- Marsh, L., 1987. *Fire weather forecasting in Tasmania*, Meteorological Note 171, Bureau of Meteorology, Melbourne, Australia, 47 pp.
- Mass, C.F., Ovens, D., 2019. The Northern California Wildfires of 8–9 October 2017: The Role of a Major Downslope Wind Event. *Bull. Amer. Meteor. Soc.* 100, 235–256, <https://doi.org/10.1175/BAMS-D-18-0037.1>.
- Mass, C.F., Ovens, D., 2021. The synoptic and mesoscale evolution accompanying the 2018 camp fire of Northern California. *Bull. Amer. Meteor. Soc.* 102, E168–E192.
- McAneney, J., Sandercock, B., Crompton, R., Mortlock, T., Musulin, R., Pielke, R., Gissing, A., 2019. Normalised insurance losses from Australian natural disasters: 1966–2017. *Environ. Hazards*. 18, 414–433. <https://doi.org/10.1080/17477891.2019.1609406>.
- McArthur, A.G., 1967. *Fire behaviour in eucalypt forests*, Leaflet Number 107, Commonwealth of Australia Department of National Development, Forestry and Timber Bureau, Canberra, ACT, Australia.
- McCarthy, E.F., 1923. Forest fire weather in the southern Appalachians. *Mon. Weather Rev.* 51, 182–185, doi:/doi:10.1175/1520-0493.
- McRae, R., Sharples, J.J., Wilkes, S.R., Walker, A., 2013. An Australian pyro-tornadogenesis event. *Nat. Hazards*. 65, 1801–1811. <https://doi.org/10.1007/s11069-012-0443-7>.
- Meng, Y., Deng, Y., Shi, P., 2015. Mapping forest wildfire risk of the world, in Shi, P., Kaspersen, R. (Eds.), *World Atlas of Natural Disaster Risk*, Springer-Verlag Berlin Heidelberg and Beijing Normal University Press, pp. 261–275.
- Mifka, B., Vučetić, V., 2012. Weather analysis during extreme forest fire on island of Brač from 14 to 17 July 2011. *Firefighting and management*. 1, 13–25 (in Croatian).
- Millán, M.M., Estrela, M.J., Badenas, C., 1998. Meteorological processes relevant to forest fire dynamics on the Spanish Mediterranean coast. *J. Appl. Meteor.* 37, 83–100.
- Mills, G.A., 2002. A case of coastal interaction with a cool change. *Aust. Meteorol. Mag.* 51, 203–211.
- Mills, G.H., 2005a. A re-examination of the synoptic and mesoscale meteorology of Ash Wednesday 1983. *Aust. Met. Mag.* 54, 35–55. <https://doi.org/10.1175/1522-6679>.
- Mills, G.H., 2005b. On the sub-synoptic scale meteorology of two extreme fire weather days during the Eastern Australian fires of January 2003, Bureau of Meteorology Research Centre, 55 pp.

- Mills, G.A., 2008a. Abrupt surface drying and fire weather Part 1: overview and case study of the South Australian fires of 11 January 2005. *Aust. Meteorol. Mag.* 57, 299–309.
- Mills, G.A., 2008b. Abrupt surface drying and fire weather Part 2: a preliminary synoptic climatology in the forested areas of southern Australia. *Aust. Meteorol. Mag.* 57, 311–328.
- Mills, G.A., Pendlebury, S., 2003. Processes leading to a severe windshear incident at Hobart Airport. *Aust. Meteorol. Mag.* 52, 171–188.
- Mills, G.A., McCaw, L., 2010. Atmospheric Stability Environments and Fire Weather in Australia – Extending the Haines Index, CAWCR Technical Report No. 20, Centre for Australian Weather and Climate Research, Australia.
- Ministry of Tourism, 2018. Tourism in numbers 2017, Republic of Croatia, Zagreb ([https://www.htz.hr/sites/default/files/2018-08/HTZ%20TUB%20HR\\_%202017%20FINAL.pdf](https://www.htz.hr/sites/default/files/2018-08/HTZ%20TUB%20HR_%202017%20FINAL.pdf)).
- Mlawer, E.J., Taubman, S.J., Brown, P.D., Iacono, M.J., Clough, S.A., 1997. Radiative transfer for inhomogeneous atmospheres: RRTM, a validated correlated-k model for the longwave. *J. Geophys. Res. Atmos.* 102, 16663–16682.
- Moreira, F., Viedma, O., Arianoutsou, M., Curt, T., Koutsias, N., Rigolot, E., Barbati, A., Corona, P., Vaz, P., Xanthopoulos, G., Mouillot, F., Bilgilir, E., 2011. Landscape–wildfire interactions in southern Europe: implications for landscape management. *J. Environ. Manage.* 92, 2389–2402, doi:10.1016/J.JENVMAN.2011.06.028.
- Moriondo, M., Good, P., Durao, R., Bindi, M., Giannakopoulos, C., Corte-Real, J., 2006. Potential impact of climate change on fire risk in the Mediterranean area. *Clim. Res.* 31, 85–95.
- Moritz, M.A., Parisien, M.A., Batllori, E., Krawchuk, M.A., Van Dorn, J., Ganz, D.J., Hayhoe, K., 2012. Climate change and disruptions to global fire activity. *Ecosphere*. 3, 49.
- Morrison, H., Thompson, G., Tatarskii, V., 2009. Impact of cloud microphysics on the development of trailing stratiform precipitation in a simulated squall line: comparison of one- and two-moment schemes. *Mon. Weather Rev.* 137, 991–1007. <https://doi.org/10.1175/2008MWR2556.1>.
- Mouillot, F., Field, C.B., 2005. Fire history and the global carbon budget: a 1°× 1° fire history reconstruction for the 20th century. *Glob. Change Biol. Bioenergy*. 11, 398–420. <https://doi.org/10.1111/J.1365-2486.2005.00920.X>.

- Nakanishi, M., Niino, H., 2006. An improved Mellor-Yamada Level-3 model: its numerical stability and application to a regional prediction of advection fog. *Boundary-Layer Meteorol.* 119, 397–407. <https://doi.org/10.1007/s10546-005-9030-8>.
- Nampak, H., Love, P., Fox-Hughes, P., Watson, C., Aryal, J., Harris, R.M.B., 2021. Characterizing Spatial and Temporal Variability of Lightning Activity Associated with Wildfire over Tasmania, Australia. *Fire*. 2021, 4. <https://doi.org/10.3390/fire4010010>.
- Nauslar, N., Abatzoglou, J., Marsh, P., 2018. The 2017 North Bay and Southern California fires: a case study. *Fire*. 1, 18. <https://doi.org/10.3390/fire1010018>.
- Ndalila, M.N., Williamson, G.J., Bowman, D., 2018. Geographic Patterns of Fire Severity Following an Extreme Eucalyptus Forest Fire in Southern Australia: 2013 Forcett-Dunalley Fire. *Fire*. 2018, 1. <https://doi.org/10.3390/fire1030040>.
- Ndalila, M.N., Williamson, G.J., Fox-Hughes, P., Sharples, J., Bowman, D.M.J.S., 2019. Evolution of an extreme pyrocumulonimbus-driven wildfire event in Tasmania, Australia. *Nat. Haz. Earth Syst. Sci.* 20, 1497–1511. <https://doi.org/10.5194/nhess-2019-354>.
- Newark, M.J., 1975. The relationship between forest fire occurrence and 500-mb longwave ridging. *Atmosphere*. 13, 26–33.
- Nicholls, N., 2004. The changing nature of Australian droughts. *Clim. Chan.* 63, 323–336.
- Nimchuk, N., 1983. Wildfire Behavior associated with Upper Ridge Breakdown, Report Number T/50, Alberta Energy and Natural Resources Forest Service, Edmonton, AB, Canada.
- Nolan, R.H., Boer, M.M., Collins, L., Resco de Dios, V., Clarke, H.G., Jenkins, M., Kenny, B., Bradstock, R.A., 2020. Causes and consequences of eastern Australia's 2019-20 season of mega-fires. *Glob. Change Bio.* <https://doi.org/10.1111/gcb.14987>.
- Omazić, B., Vučetić, V., 2017. Weather condition analysis during wildfires on the Pelješac Peninsula in July 2015. *Firefighting and Management*. 7, 6–23 (in Croatian).
- Papadopoulos, A., Paschalidou, A.K., Kassomenos, P.A., McGregor, G., 2013. Investigating the relationship of meteorological/climatological conditions and wildfires in Greece. *Theor. Appl. Climatol.* 112, 113–126.
- Pausas, J.G., Llovet J., Rodrigo A., Vallejo, R., 2008. Are wildfires a disaster in the Mediterranean basin? – A review. *Int. J. Wildland Fire*. 17, 713–723. <https://doi.org/10.1071/WF07151>.
- Peace, M., 2014. Coupled fire-atmosphere simulations of three Australian fire where unusual fire behaviour occurred. Doctor of Philosophy Thesis, Faculty of Engineering, Computer

and Mathematical Sciences, School of Mathematical Sciences, The University of Adelaide.

- Peace, M., Mattner, T., Mills, G., Kepert, J., McCaw, L., 2015. Fire-modified meteorology in a coupled fire-atmosphere model. *J. Appl. Meteor. Climatol.* 54, 704–720. <https://doi.org/10.1175/JAMC-D-14-0063.1>.
- Peace, M., Mattner, T., Mills, G., Kepert, J., McCaw, L., 2016. Coupled fire-atmosphere simulations of the Rocky River fire using WRF-SFIRE. *J. Appl. Meteor. Climatol.* 55, 1151–1168. <https://doi.org/10.1175/JAMC-D-15-0157.1>.
- Peace, M., Hanstrum, B., Greenslade, J., Zovko-Rajak, D., Santra, A., Kepert, J., Fox-Hughes, P., Ye, H., Shermin, T., Jones, J., 2021. Coupled fire-atmosphere simulations of five Black Summer fires using the ACCESS-Fire model - Black Summer final report, Bushfire and Natural Hazards CRC, Melbourne, Australia.
- Pereira, M.G., Trigo, R.M., Da Camara, C.C., Pereira, J.M.C., Leite, S.M., 2005. Synoptic patterns associated with large summer forest fires in Portugal. *Agrl. Forest Meteorol.* 129, 11–25. <https://doi.org/10.1016/j.agrformet.2004.12.007>.
- Peterson, D.A., Campbell, J.R., Hyer, E.J., Fromm, M.D., Kablick III, P., Cossuth, J.H., Deland, M.T., 2018. Wildfire-driven thunderstorms cause a volcano-like stratospheric injection of smoke. *Npj. Clim. Atmos. Sci.* 1, 30. <https://doi.org/10.1038/s41612-018-0039-3>.
- Peterson, D.A., Fromm, M.D., McRae, R.H., Campbell, J.R., Hyer, E.J., Taha, G., Camacho, C.P., Kablick, G.P., Schmidt, C.C. and DeLand, M.T., 2021. Australia’s Black Summer pyrocumulonimbus super outbreak reveals potential for increasingly extreme stratospheric smoke events. *Npj. Clim. Atmos. Sci.* 4, 1–16.
- Pitman, A.J., Narisma, G.T., McAneney, J., 2007. The impact of climate change on the risk of forest and grassland fires in Australia. *Clim. Chan.* 84, 383–401. <https://doi.org/10.1007/s10584-007-9243-6>.
- Potter, B.E., 1996. Atmospheric Properties Associated with Large Wildfires. *Intl. J. Wildland Fire.* 6, 71–76.
- Potter, B.E., 2012a. Atmospheric interactions with wildland fire behaviour – I. Basic surface interactions, vertical profiles and synoptic structures. *Intl. J. Wildland Fire.* 21, 779–801. <https://doi.org/10.1071/WF11128>.
- Potter, B.E., 2012b. Atmospheric interactions with wildland fire behaviour – II. Plume and vortex dynamics. *Intl. J. Wildland Fire.* 21, 802–817. <https://doi.org/10.1071/WF11129>.

- Pretorius, I., Sturman, A., Strand, T., Katurji, M., Pearce, G., 2020. A meteorological study of the Port Hills fire, Christchurch, New Zealand. *J. Appl. Meteorol. Climatol.* 59, 263–280. <https://doi.org/10.1175/jamc-d-19-0223.1>.
- Price, C., Rind, D., 1994. The impact of a 2×CO<sub>2</sub> climate on lightning-caused fires. *J. Clim.* 7(10), 1484–1494.
- Pyne, S.J., Andrews, P.L., Laven, R.D., 1996. *Introduction to Wildland Fire*, second ed. John Wiley & Sons Inc, New York.
- Rasilla, D.F., García-Codron, J.C., Carracedo, V., Diego, C., 2010. Circulation patterns, wildfire risk and wildfire occurrence at continental Spain. *Phys. Chem. Earth.* 35, 553–560.
- Reeder, M.J., Smith, R.K., 1992. Australian spring and summer cold fronts. *Aust. Meteorol. Mag.* 41, 101–124.
- Reeder, M.J., Smith, R.K., 1998. Mesoscale meteorology, in: Vincent, D., Karoly, D.J. (Eds.), *Meteorology of the Southern Hemisphere*, American Meteorological Society, Boston, Massachusetts, U.S., pp. 201–241.
- Reeder, M.J., Spengler, T., Musgrave, R., 2015. Rossby waves, extreme fronts, and wildfires in southeastern Australia. *Geophys. Res. Lett.* 42, 2015–2023.
- Robin, A.G., Wilson, G.U., 1958. The effect of meteorological conditions on major fires in the Riverina (New South Wales) district. *Aust. Meteorol. Mag.* 21, 49–75.
- Rodriguesa, M., Trigod, R.M., Vega-García, C., Cardil, A., 2020. Identifying large fire weather typologies in the Iberian Peninsula. *Agric. For. Meteorol.* 280, 107789. <https://doi.org/10.1016/j.agrformet.2019.107789>.
- Romanić, D., 2019. Local winds of Balkan Peninsula. *Intl. J. Climatol.* 39, 117. <https://doi.org/10.1002/joc.5743>.
- Romps, D.M., Seeley, J.T., Vollaro, D. and Molinari, J., 2014. Projected increase in lightning strikes in the United States due to global warming. *Science.* 346(6211), 851–854.
- Rosenfeld, D., M. D. Fromm, J. Trentmann, G. Luderer, M. O. Andreae, and R. Servranckx, 2007. The Chisolm firestorm: Observed microstructure, precipitation and lightning activity of a pyro-cumulonimbus. *Atmos. Chem. Phys.*, 7, 645–659. <https://doi.org/10.5194/acp-7-645-2007>.
- Rothermel, R., 1972. *A mathematical model for predicting fire spread in wildland fires*, USDA Forest Service Research Paper INT-115, Ogden, Utah, USA.
- Ruffault, J., Curt, T., Moron, V., Trigo, R.M., Mouillot, F., Koutsias, N., Pimont, F., Martin-St Paul, N., Barbero, R., Dupuy, J.L., Russo, A., Belhadj-Khedher, C., 2020. Increased

- likelihood of heat-induced large wildfires in the Mediterranean basin. *Sci. Rep.* 10. <https://doi.org/10.1038/s41598-020-70069-z>.
- Ruffault, J., Moron, V., Trigoc R.M., Curta T., 2017. Short Communication: Daily synoptic conditions associated with large fire occurrence in Mediterranean France: evidence for a wind-driven fire regime. *Int. J. Climatol.* 37: 524–533. <https://doi.org/10.1002/joc.4680>.
- Rundel, P.W., Arroyo M.T.K., Cowling R.M., Keeley J.E., Lamont B.B., Pausas J.G., Vargas P., 2018. Fire and plant diversification in Mediterranean-climate regions. *Front. Plant. Sci.* 9:851. <https://doi.org/10.3389/fpls.2018.00851>.
- San-Miguel-Ayanz, J., Moreno, J.M., Camia, A., 2013. Analysis of large fires in European Mediterranean landscapes: Lessons learned and perspectives. *For. Eco. Man.* 294, 11–22. <https://doi.org/10.1016/j.foreco.2012.10.050>.
- Sanchez-Benítez, A., Garcia-Herrera, R., Barriopedro, D., Sousa, P. M., Trigo, R. M., 2018. June 2017: The Earliest European Summer Mega-heatwave of Reanalysis Period. *Geophys. Res. Lett.* 45, 1955–1962. <https://doi.org/10.1002/2018GL077253>.
- Schroeder, M.J., 1950. The Hudson Bay High and the spring fire season in the Lake States. *Fire Control Notes.* 11, 1–8.
- Schroeder, M.J., Glovinsky, M., Hendricks, V.F., Hood, F.C., Hull, M.K., Jacobson, H.L., Kirkpatrick, R., Krueger, D.W., Mallory, L.P., Oertel A.G., Reese, R.H., Sergius, L.A., Syverson, C.E., 1964. Synoptic weather types associated with critical fire weather, Forest Service, US Department of Agriculture, Berkeley.
- Scorer, R.S., 1952. Mountain-gap winds: A study of surface winds at Gibraltar. *Quart. J. Roy. Meteor. Soc.* 78, 53–61.
- Sharples, J.J., 2009. An overview of mountain meteorological effects relevant to fire behaviour and bushfire risk. *Int. J. Wildland Fire.* 18, 737–754. <https://doi.org/10.1071/WF08041>
- Sharples, J.J., Cary, G.J., Fox-Hughes, P., Mooney, S., Evans, J.P., Fletcher, M.S., Fromm, M., Grierson, P.F., McRae, R., Baker, P., 2016. Natural hazards in Australia: extreme bushfire. *Clim. Change.* 139, 85–99. <https://doi.org/10.1007/s10584-016-1811-1>.
- Sharples, J.J., McRae, R.H.D., Wilkes, S.R., 2012. Wind-terrain effects on the propagation of wildfires in rugged terrain: fire channelling. *Int. J. Wildland Fire.* 21, 282–296. <https://doi.org/10.1071/WF10055>.
- Sharples, J.J., Mills, G.A., McRae, R.H.D., Weber, R.O., 2010. Foehn-Like winds and elevated fire danger conditions in southeastern Australia. *J. Appl. Meteorol. Climatol.* 49, 1067–1095. <https://doi.org/10.1175/2010JAMC2219.1>.

- Simpson, C. C., Sharples, J. J., Evans, J. P., and McCabe, M. F., 2013. Large eddy simulation of atypical wildland fire spread on leeward slopes, *Int. J. Wildland Fire*, 22, 599–614, doi:10.1071/WF12072.
- Simpson, C. C., Sharples, J. J., Evans, 2015. WRF-Fire Simulation of Lateral Fire Spread in the Bendora Fire on 18 January 2003. 21st International Congress on Modelling and Simulation, Gold Coast, Australia.
- Skinner, W.R., Stocks, B.J., Martell, D.L., Bonsal, B., Shabbar, A., 1999. The association between circulation anomalies in the mid-troposphere and area burned by wildland fire in Canada. *Theor. Appl. Climatol.* 63, 89–105. <https://doi.org/10.1007/S007040050095>.
- Smith, R. B., 1985. On severe downslope winds. *J. Atmos. Sci.* 42, 2597–2603.
- Soderholm, J., Protat, A., Jakob, C., 2019. Australian Operational Weather Radar Dataset. Electronic dataset, National Computing Infrastructure. <https://doi.org/10.25914/5cb686a8d9450>, 2019.
- Sousa, P.M., Trigo, R.M., Barriopedro, D., Soares, P.M.M., Santos, J.A., 2018. European temperature responses to blocking and ridge regional patterns. *Clim. Dyn.* 50, 457–477. <https://doi.org/10.1007/s00382-017-3620-2>.
- Stanešić, A., Horvath, K., Keresturi, E., 2019. Comparison of NMC and Ensemble-Based Climatological Background-Error Covariances in an Operational Limited-Area Data Assimilation System. *Atmosphere*. 10, 570. <https://doi.org/10.3390/atmos10100570>.
- Stephens, S.L., Burrows, N., Buyantuyev, A., Gray, R.W., Keane, R.E., Kubian, R., Liu, S., Seijo, F., Shu, L., Tolhurst, K.G., van Wagendonk, J.W., 2014. Temperate and boreal forest mega-fires: characteristics and challenges. *Front. Ecol. Environ.* 12, 115–122. <https://doi.org/10.1890/120332>.
- Stephenson, C., Handmer, J., Betts, R., 2012. Estimating the economic, social and environmental impacts of wildfires in Australia. *Environ. Hazards*. 12, 93–111. <https://doi.org/10.1080/17477891.2012.703490>.
- Stocks, B.J., Lawson, B.D., Alexander, M.E., Van Wagner, C.E., McAlpine, R.S., Lynham, T.J., Dube, D.E., 1989. The Canadian Forest Fire Danger Rating System: an overview. *Forestry Chronicle* 65, 450–457.
- Storey, M.A., Price, O.F., Sharples, J.J., Bradstock, R.A., 2020. Drivers of long-distance spotting during wildfires in south-eastern Australia. *Int. J. Wildland Fire*. 29, 459–472.
- Strauss, D., Bednar, L., Mees, R., 1989. Do one percent of forest fires cause ninety-nine percent of the damage? *For. Sci.* 35, 319–328.
- Struzik, E., 2017. *Firestorm: How Wildfire Will Shape Our Future*. Island Press, Washington.

- Su, C.-H., Eizenberg, N., Steinle, P., Jakob, D., Fox-Hughes, P., White, C. J., Rennie, S., Franklin, C., Dharssi, I., Zhu, H., 2019. BARRA v1.0: the Bureau of Meteorology Atmospheric high-resolution Regional Reanalysis for Australia. *Geosci. Model Dev.* 12, 2049–2068. <https://doi.org/10.5194/gmd-12-2049-2019>.
- Swetnam, T.W., 1993. Fire history and climate change in giant sequoia groves. *Science*. 262, 885–889. <https://doi.org/10.1126/science.262.5135.885>.
- Šoljan, V., Belušić, A., Šarović, K., Nimac, I., Brzaj, S., Suhin, J., Belavić, M., Večenaj, Ž., Grisogono, B., 2018. Micro-Scale Properties of Different Bora Types. *Atmosphere*. 9, 116. <https://doi.org/10.3390/atmos9040116>.
- Španjol, Ž., Barčić, D., Vučetić, M., 2001. Ecological factors in the occurrence and restoration of forest fires. In *Fire Protection, Anti-burglary and Video Surveillance*, 22–24. March 2001, Šibenik, Croatia.
- Teague, B., McLeod, R., Pascoe, S., 2010. 2009 Final Report Summary, Victorian Bushfires Royal Commission, Parliament of Victoria, Melbourne, Australia.
- Telišman Prtenjak, M., Belušić, D., 2009. Formation of reversed lee flow over the north-eastern Adriatic during bora. *Geofizika*. 26, 2; 145-155.
- Telišman Prtenjak, M., Horvat, I., Tomažić, I., Kvakić, M., Viher, M., Grisogono, B., 2015. Impact of mesoscale meteorological processes on anomalous radar propagation conditions over the northern Adriatic area. *J. Geophys. Res. Atmos.* 120, 8759–8782. <https://doi.org/10.1002/2014JD022626>.
- Telišman Prtenjak, M., Viher, M., Jurković J., 2010. Sea-land breeze development during a summer bora event along the north-eastern Adriatic coast. *Q. J. R. Meteorol. Soc.* 136, 1554–1571. [doi.org/10.1002/qj.649](https://doi.org/10.1002/qj.649).
- Telišman Prtenjak, M., Grisogono, B., Nitis, T., 2006. Shallow mesoscale flows at the north-eastern Adriatic coast. *Q. J. R. Meteorol. Soc.* 132. 620; 2191–2216.
- Telitsyn, G.P., 1965. Dependence of rate of spread of surface fires on weather conditions. *Sbornik Trudov*. 1965, 390–405 (in Russian).
- The Guardian, 2013. Firestorm: The story of the bushfire at Dunalley, The Guardian, 23 May 2013. Available online: <https://www.theguardian.com/world/interactive/2013/may/26/firestorm-bushfire-dunalley-holmes-family> (accessed on 26 November 2021).
- Tomašević, I., 2012. Vertical Atmospheric Profiles during the Large Wild-land Fires, Master thesis, Faculty of science, University of Zagreb, Zagreb, Croatia (in Croatian).



- Tomašević, I., Vučetić, V., 2014. Rating the fire season 2013 and comparison with the fire season 2012. *Firefighting and Management*. 4, 19–35 (in Croatian).
- Tomašević, I.Č., Cheung, K.K.W., Vučetić, V., Fox-Hughes, P., 2022. Comparison of Wildfire Meteorology and Climate at the Adriatic Coast and Southeast Australia. *Atmosphere*. 13, 755. <https://doi.org/10.3390/atmos13050755>.
- Tory, K.J., Kepert, J.D., 2021. Pyrocumulonimbus Firepower Threshold: Assessing the atmospheric potential for pyroCb. *Weather Forecast*. 36, 439-456. <https://doi.org/10.1175/WAF-D-20-0027.1>.
- Tory, K. J., Peace, M., Thurston, W., 2016. Pyrocumulonimbus forecasting: Needs and issues. Report no 239.2016. Bushfire and Natural Hazards CRC, Melbourne, Australia.
- Tory, K. J., Thurston, W., Kepert, J. D., 2018. Thermodynamics of Pyrocumulus: A Conceptual Study, *Mon. Weather Rev.* 146(8), 2579–2598. [doi.org/10.1175/MWR-D-17-0377.1](https://doi.org/10.1175/MWR-D-17-0377.1).
- Trentmann, J., G., Luderer, T., Winterrath, M. D., Fromm, R., Servranckx, M., Herzog, H. F., Graf, M. O., Andreae, 2006. Modeling of biomass smoke injection into the lower stratosphere by a large forest fire (Part I): Reference simulation. *Atmos. Chem. Phys.* 6, 5247–5260. <https://doi.org/10.5194/acp-6-5247-2006>.
- Trigo, R.M., Pereira, J.M.C., Pereira, M.G., Mota, B., Calado, T.J., Dacamara, C.C., Santo, F.E., 2006. Atmospheric conditions associated with the exceptional fire season of 2003 in Portugal. *Intl. J. Climatol.* 26, 1741–1757. <https://doi.org/10.1002/joc.1333>.
- Trigo, R.M., Sousa, P.M., Pereira, M.G., Rasilla, D., Gouveia, C.M., 2013. Modelling wildfire activity in Iberia with different atmospheric circulation weather types. *Intl. J. Climatol.* 36, 2761–2778. <https://doi.org/10.1002/joc.3749>.
- Trigo, R.M., Sousa, P.M., Pereira, M.G., Rasilla, D., Gouveia, C.M., 2016. Modelling wildfire activity in Iberia with different atmospheric circulation weather types. *Int. J. Climatol.* 36, 2761–2778. <https://doi.org/10.1002/joc.3749>.
- Tudor, M., Ivatek-Šahdan, S., Stanešić, A., Horvath, K., Bajić A., 2013. Forecasting weather in Croatia using ALADIN numerical weather prediction model in: Zhang, Y., Ray, P. (Eds.), *Climate Change and Regional/Local Responses*. IntechOpen, Rijeka, pp. 59–88. <https://doi.org/10.5772/55698>.
- Tudor, M., Stanešić, A., Ivatek-Šahdan, S., Hrastinski, M., Odak Plenković, I., Horvath, K., Bajić A., Kovačić, T., 2015. Operational validation and verification of ALADIN forecast in Meteorological and hydrological service of Croatia. *Croat. Meteorol. J.* 50, 47–70.

- Turco, M., Jerez, S., Augusto, S., Tarín-Carrasco, P., Ratola, N., Jiménez-Guerrero, P., Trigo, R.M., 2019. Climate drivers of the 2017 devastating fires in Portugal. *Sci. Rep.* 9:13886. <https://doi.org/10.1038/s41598-019-50281-2>.
- Turco, M., Llasat, M.C., Von Hardenberg, J., Provenzale, A., 2014. Climate change impacts on wildfires in a Mediterranean environment. *Clim. Change.* 125, 369–380. <https://doi.org/10.1007/s10584-014-1183-3>.
- Turco, M., Rosa-Cánovas, J.J., Bedia, J., Jerez, S., Montávez, J.P., Llasat, M.C., Provenzale, A., 2018. Exacerbated fires in Mediterranean Europe due to anthropogenic warming projected with nonstationary climate-fire models. *Nature Comm.* 9, 3821. <https://doi.org/10.1038/s41467-018-06358-z>.
- Turco, M., Von Hardenberg, J., AghaKouchak, A., Llasat, M.C., Provenzale, A., Trigo, R.M., 2017. On the key role of droughts in the dynamics of summer fires in Mediterranean Europe. *Sci. Rep.* 7:81. <https://doi.org/10.1038/s41598-017-00116-9>.
- Uccellini, L.W., 1980. On the Role of Upper Tropospheric Jet Streaks and Leaside Cyclogenesis in the Development of Low-Level Jets in the Great Plains. *Mon. Weather. Rev.* 108, 1689–1696. [https://doi.org/10.1175/1520-0493\(1980\)108<1689:OTROUT>2.0.CO;2](https://doi.org/10.1175/1520-0493(1980)108<1689:OTROUT>2.0.CO;2).
- Van Oldenborgh, G. J., Krikken, F., Lewis, S., Leach, N. J., Lehner, F., Saunders, K. R., van Weele, M., Haustein, K., Li, S., Wallom, D., Sparrow, S., Arrighi, J., Singh, R. K., van Aalst, M. K., Philip, S. Y., Vautard, R., and Otto, F. E. L.: Attribution of the Australian bushfire risk to anthropogenic climate change. *Nat. Hazards Earth Syst. Sci.* 21, 941–960. <https://doi.org/10.5194/nhess-21-941-2021>.
- Van Wagner, C.E., 1976. Conditions for the start and spread of crown fire. *Can. J. For. Res.* 7, 23–34.
- Van Wagner, C.E., 1979. A laboratory study of weather effects on the drying rate of jack pine litter. *Can. J. For. Res.* 9, 267–275. <https://doi.org/10.1139/X79-044>.
- Van Wagner, C.E., Pickett, T.L., 1985. Equations and Fortran Program for the Canadian Forest Fire Weather Index System, Forestry Technical Report 33, Canadian Forestry Service, Government of Canada, Ontario.
- VBRC (Victorian Bushfire Royal Commission), 2009. Final report. Volume 1. The Fires and the Fire-related Deaths.
- Vines, R.G., 1981. Physics and chemistry of rural fires, in: Gill, A.M., Groves, R.H., Noble, I.R. (Eds.), *Fire and the Australian Biota*, Australian Academy of Sciences, Canberra, Australia, pp. 129–149.

- Vitolo, C., Di Giuseppe, F., Barnard, C., Coughlan, R., San-Miguel-Ayanz, J., Libertá, G., Krzeminski, B., 2020. ERA5-based global meteorological wildfire danger maps. *Sci. Rep.* 7, 216. <https://doi.org/10.1038/s41597-020-0554-z>.
- Vercoe, T., 2003. Whoever owns the fuel owns the fire. Fire management for forest growers, AFG Special Liftout. 65, 26(3). Available from: [http://www.coagbushfireenquiry.gov.au/subs\\_pdf/57\\_2\\_ragg\\_afg.pdf](http://www.coagbushfireenquiry.gov.au/subs_pdf/57_2_ragg_afg.pdf).
- Von Platen, J., Kirkpatrick, J.B., Allen, K.J., 2011. Fire frequency variation in south-eastern Tasmanian dry eucalypt forest 1740–2004 from fire scars. *Aust. For.* 74, 180–189. <https://doi.org/10.1080/00049158.2011.10676361>.
- Vučetić, M., 1987. Meteorological conditions of a catastrophic forest fire on Korčula in 1985. *Croat. Meteorol. J. (Rasprave)*. 22, 67–72 (in Croatian).
- Vučetić, M., 1992. Weather phenomena during the 13–31 July 1990 Forest fire on the island of Hvar. *Croat. Meteorol. J.* 27, 69–76 (in Croatian).
- Vučetić, M., 1998. The influence of weather condition on forest fire on the island of Hvar, 28 July–4 August 1997. In *International Conference on Forest Fire Research and 14<sup>th</sup> Conference on Fire and Forest Meteorology*, 16–20 November 1998, Luso, Portugal. 1295–1303.
- Vučetić, M., 2001. Weather conditions and forest fires on the coastal area of Croatia during 2000. *J. Forestry*. 7-8, 367–378 (in Croatian).
- Vučetić, M., 2002. Weather conditions and a comparison of the forest fire season 2001 with long-term mean values. *J. Forestry*. 11-12, 563–574 (in Croatian).
- Vučetić, M., Vučetić, V., Španjol, Ž., Barčić, D., Rosavec, R., Mandić, A., 2006. Secular variations of monthly severity rating on the Croatian Adriatic coast during the forest fire season. In *5<sup>th</sup> International Conference on Forest Fire Research*, Portugal, 27–30 November 2006, and abstract in *For. Ecol. Manag.* 234, supplement 1, 251.
- Vučetić, M., Vučetić, V., 1999. Different types of the forest fires on the Croatian coast. In *Forest fires: needs & innovations*, Athens, Greece, pp 365–369.
- Vučetić, M., Vučetić, V., 2011. Fire risk analysis during the Kornat fire on 30 August 2007. *Firefighting and management*. 1, 12–25 (in Croatian).
- Vučetić, M., Vučetić, V., 2013. *Adriatic Weather – Meteorology for Sailors*, Fabra Press, Zagreb.
- Vučetić, M., Vučetić, V., 2019. Wildfire risk in Croatia using the Canadian Forest Fire Weather Index System. In *6<sup>th</sup> International Fire Behavior and Fuels Conference*, 29 April–3 May 2019, Marseille, France, International Association of Wildland Fire.

- Vučetić, V., 1988. Bora on the northern Adriatic, 12 – 16 April 1982. *Croat. Meteorol. J. (Rasprave)*. 23, 27–44.
- Vučetić, V., 1991. Statistical analysis of severe Adriatic bora. *Croat. Meteorol. J.* 26, 41–51.
- Vučetić, V., 1993. Severe bora on the mid-Adriatic. *Croat. Meteorol. J.* 28, 19–36.
- Vučetić, V., Čavlina Tomašević, I., Mifka, B., 2019. Low level jet and large wildfires in Croatia. In 6<sup>th</sup> International Fire Behavior and Fuels Conference, 29 April–3 May 2019, Marseille, France, International Association of Wildland Fire.
- Vučetić, V., Ivatek Šahdan, S., Tudor, M., Kraljević, L., Ivančan-Picek, B., Strelec-Mahović, N., 2007. Weather analysis during the Kornat fire on 30 August 2007. *Croat. Meteorol. J.* 42, 41–65 (in Croatian).
- Wang, H.H., 2011. Analysis on downwind distribution of firebrands sourced from a wildland fire. *Fire Technol.* 47, 321–340. <https://doi.org/10.1007/s10694-009-0134>.
- Wang, X., Parisien, M., Flannigan, M.D., Parks, S.A., Anderson, K.R., Little, J.M., Taylor, S.W., 2014. The potential and realized spread of wildfires across Canada. *Glob. Change Biol.* 20, 2518–2530.
- Werth, P.A., 2017. Critical fire weather patterns. *Fire Management Today*. 1, 28–32.
- Werth, P.A., Potter, B.E., Clements, C.B., Finney, M.A., Forthofer, J.A., McAllister, S.S., Goodrick, S.L., Alexander, M.E., Cruz, M.G., 2011. Synthesis of Knowledge of Extreme Fire Behavior: Volume I for Fire Managers, JFSP Synthesis Reports, Department of Agriculture, Forest Service, Portland, Oregon, U.S.
- Westerling, A.L., Cayan, D.R., Brown, T.J., Hall, B.L., Riddle, L.G., 2004. Climate, Santa Ana winds and autumn wildfires in southern California. *Eos Trans. AGU.* 85, 289–296.
- Whiteman, C.D., 2000. In *Mountain Meteorology: Fundamentals and Applications*, Oxford University Press, New York.
- Williams, J., 2013. Exploring the onset of high-impact mega-fires through a forest land management prism. *For. Ecol. Manag.* 294, 4–10. <http://doi.org/10.1016/j.foreco.2012.06.030>.
- Williams, A.A.J., Karoly, D.J., Tapper, N., 2001. The sensitivity of Australian fire danger to climate change. *Clim. Change.* 49, 171–191.
- Yospin, G.I., Wood, S.W., Holz, A., Bowman, D.M., Keane, R.E. and Whitlock, C., 2015. Modeling vegetation mosaics in sub-alpine Tasmania under various fire regimes. *Model. Earth Syst. Environ.* 1, 1–10. <https://doi.org/10.1007/s40808-015-0019-0>.

- You, C., Yao, T., Xu, C., 2018. Recent increases in wildfires in the Himalayas and surrounding regions detected in central Tibetan ice core records. *J. Geophys. Res. Atmos.* 123, 3285–3291. <https://doi.org/10.1002/2017JD027929>.
- Zimet, T., Martin, J.E., Potter, B.E., 2007. The influence of an upper-level frontal zone on the Mack Lake Wildfire environment. *Meteorol. Appl.* 14, 131–147. <https://doi.org/10.1002/met.14>.
- Zscheischler, J., Westra, S., Van Den Hurk, B.J.J.M., Seneviratne, S.I., Ward, P.J., Pitman, A., Aghakouchak, A., Bresch, D.N., Leonard, M., Wahl, T., Zhang, X., 2018. Future climate risk from compound events. *Nat. Clim. Change.* 8, 469–477.
- Zylstra, P.J., 2018. Flammability dynamics in the Australian Alps. *Austral. Ecology* 43, 578–591. <https://doi.org/10.1111/aec.12594>.

## APPENDICES

### APPENDIX A:

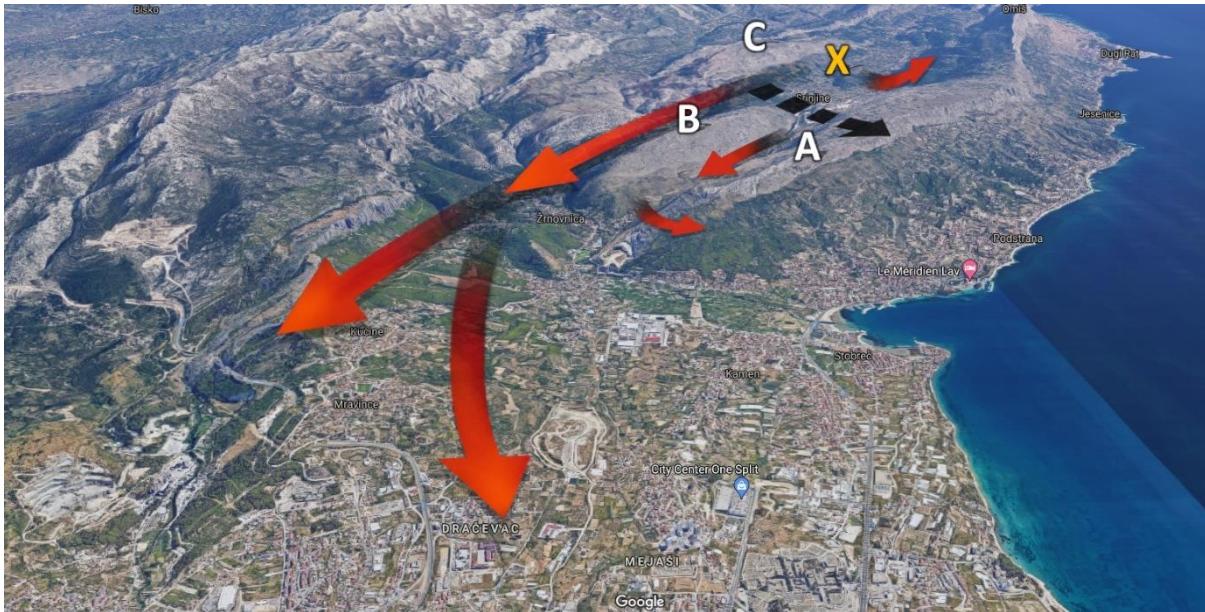


Figure A1. Overview of the wildfire's path viewed from the Split city peninsula. Letters note hills Perun (A), Sridivica (B), Makirina (C) and ignition location (X).



Figure A2. a) Fire escalation with burning smoke during the SPLIT 4 period (photographed by Damira Kalajzić) and b) flame in the shape of a fire man (photographed by Zvonimir Barišin).

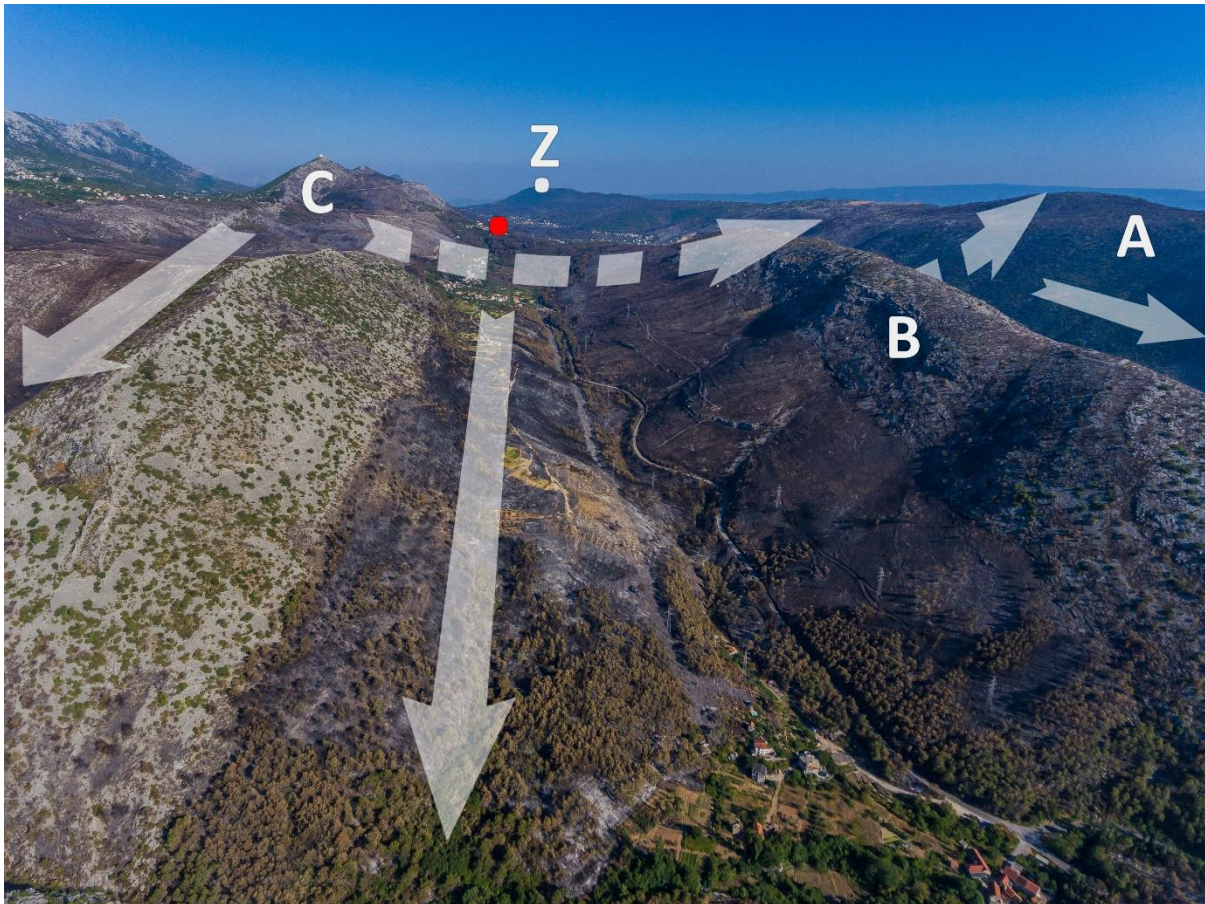


Figure A3. Aerial photograph of fire scar with noted wildfire path within coastal outback. Arrows show direction of wildfire spread. Full arrows indicate spread towards Split in the NW and dashed arrows towards the Adriatic Sea in the SW direction during SPLIT 1 and SPLIT 2 period. Ignition location is noted as X, camera at Zahod location as Z and hills Perun, Sridivica and Makirina with letters A, B and C (photographed by Zvonimir Barišin on 23 July 2017).



Figure A4. Aerial photograph of fire scar viewed from the Makirina hill (C) towards the city of Split and hills Sridivica (B) and Perun (A). Arrow indicates direction of wildfire spread towards Split during the SPLIT 3 period (photographed by Zvonimir Barišin on 23 July 2017).



Figure A5. a) Aerial photograph of fire scar within V shaped valley between hills Sridivica (B) and Perun (A). Dashed arrow indicates fire spread in SW direction, downhill of Sridivica and uphill of Perun, while full arrow indicates fire spread towards Split in NW direction, both during SPLIT 2 period and b) aerial view of fire scar within urban suburbs with arrow indicating downslope fire run during SPLIT 3 period (photographed by Zvonimir Barišin on 23 July (a) and 19 July 2017 (b)).

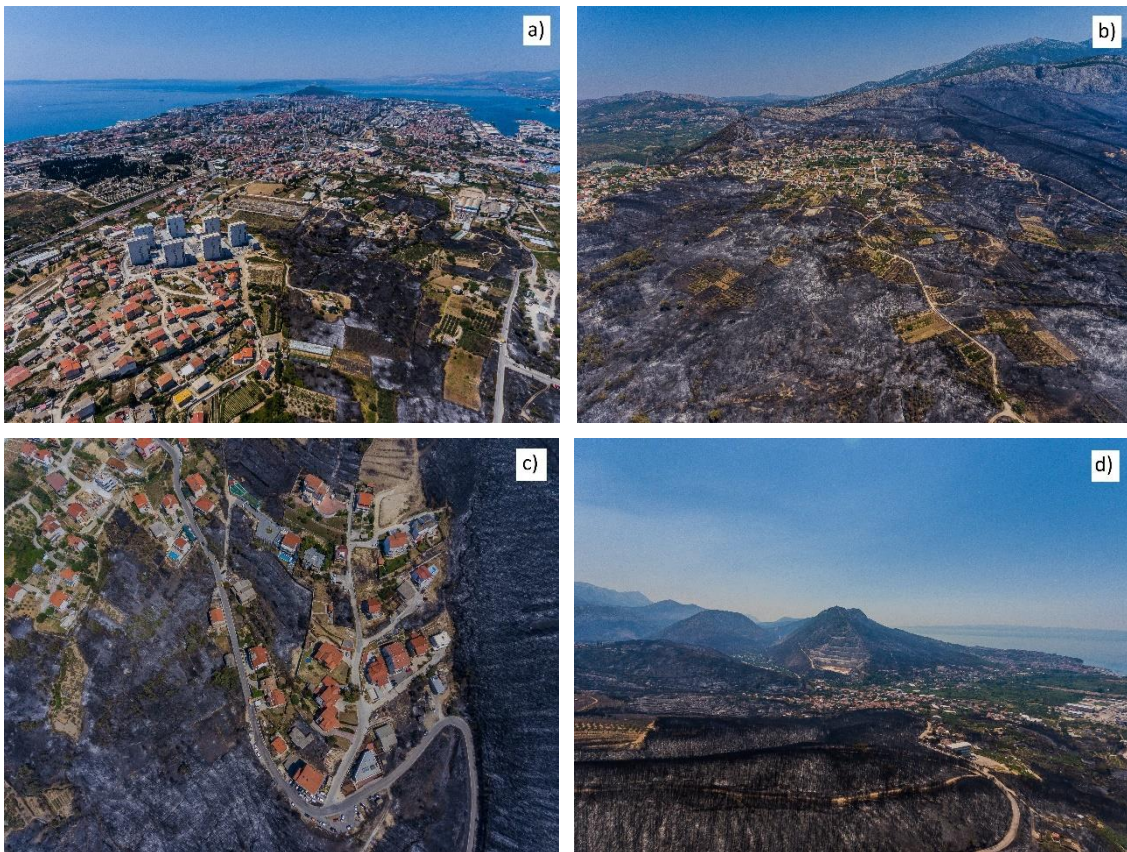


Figure A6. Aerial photograph of fire scar within the city of Split (photographed by Zvonimir Barišin on 19 July 2017).



**APPENDIX B:**

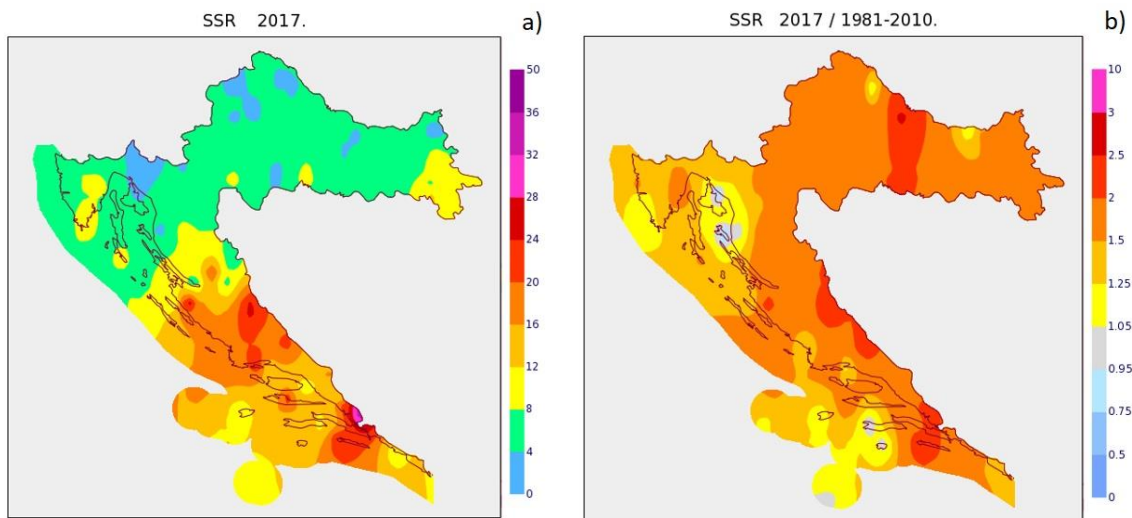


Figure B1. a) Seasonal Severity Rating (SSR) index for 2017 and b) SSR of 2017 in comparison with SSR in 30-year period (1981–2010).

Table B1. Monthly Severity Rating (MSR) for July 2017 and Seasonal Severity Rating (SSR) in 2017 together with mean value for July and SSR: at Split-Marjan meteorological station in the period 1949–2020 and at Split airport station in the period 1981–2020.

Meteorological station	MSR July 2017	SSR 2017	Mean July	Mean SSR
Split-Marjan (1949–2020)	20.7	13.4	15.1	11.7
Split airport (1981–2020)	<b>37.7</b>	25.1	20.4	14.3

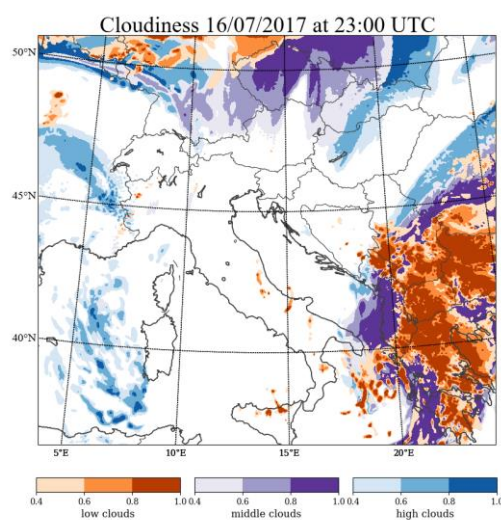


Figure B2. ALADIN model cloudiness valid for 16 July 2017 at 23:00 UTC. Colour patterns represent cloud type (low clouds are in brown scale, middle in purple scale and high in blue scale).

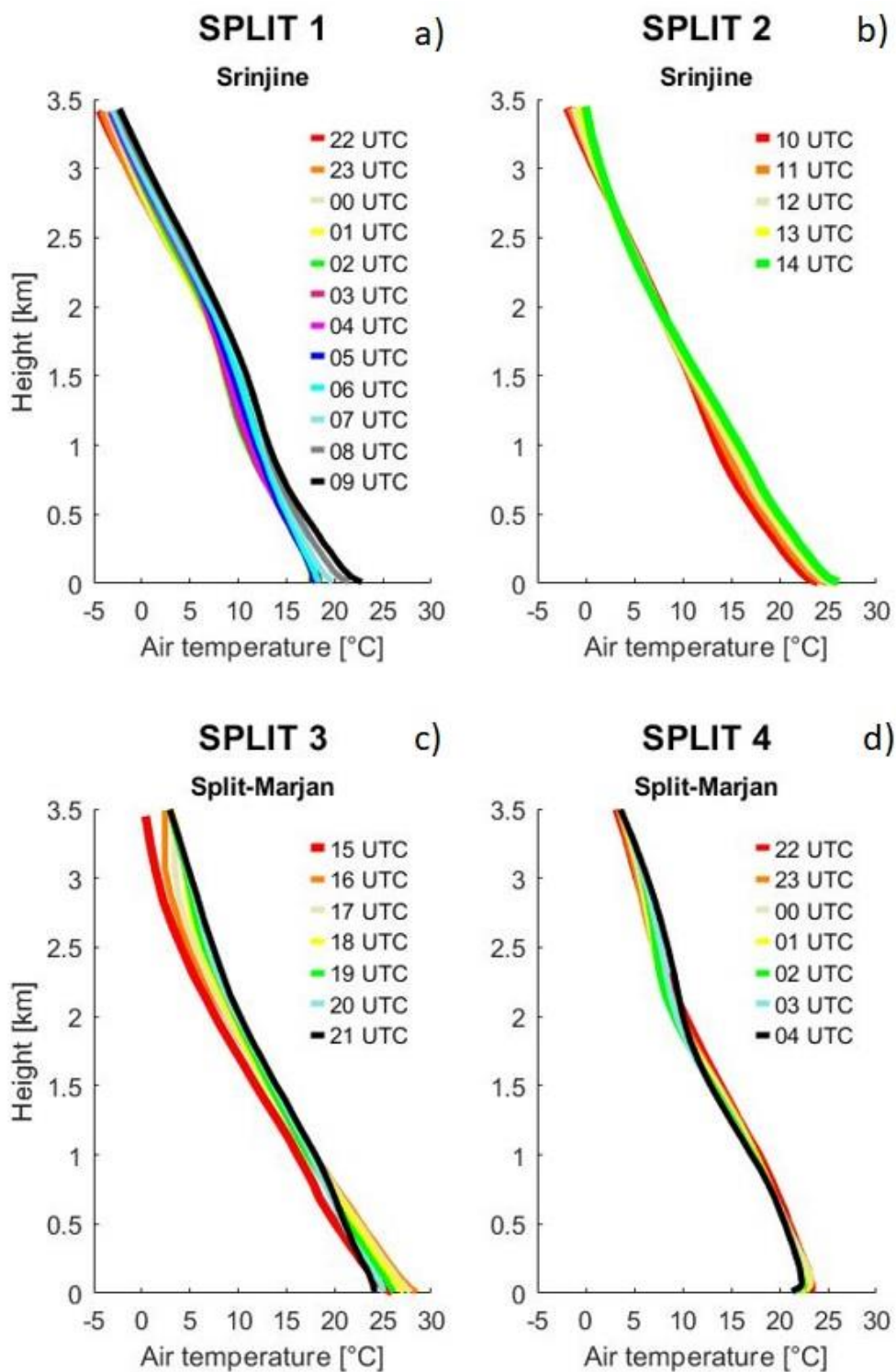


Figure B3. Vertical profiles of air temperature ( $^{\circ}\text{C}$ ) at Srinjine and Split-Marjan locations for periods SPLIT 1 (from 22:00 UTC on 16 July to 09:00 UTC on 17 July), SPLIT 2 (from 10:00 UTC to 15:00 UTC on 17 July), SPLIT 3 (from 16:00 UTC to 21:00 UTC on 17 July) and SPLIT 4 (from 22:00 UTC on 17 July to 04:00 UTC on 18 July) from ALADIN model. See Fig. 2 for location of Split-Marjan and Srinjine (noted as S).

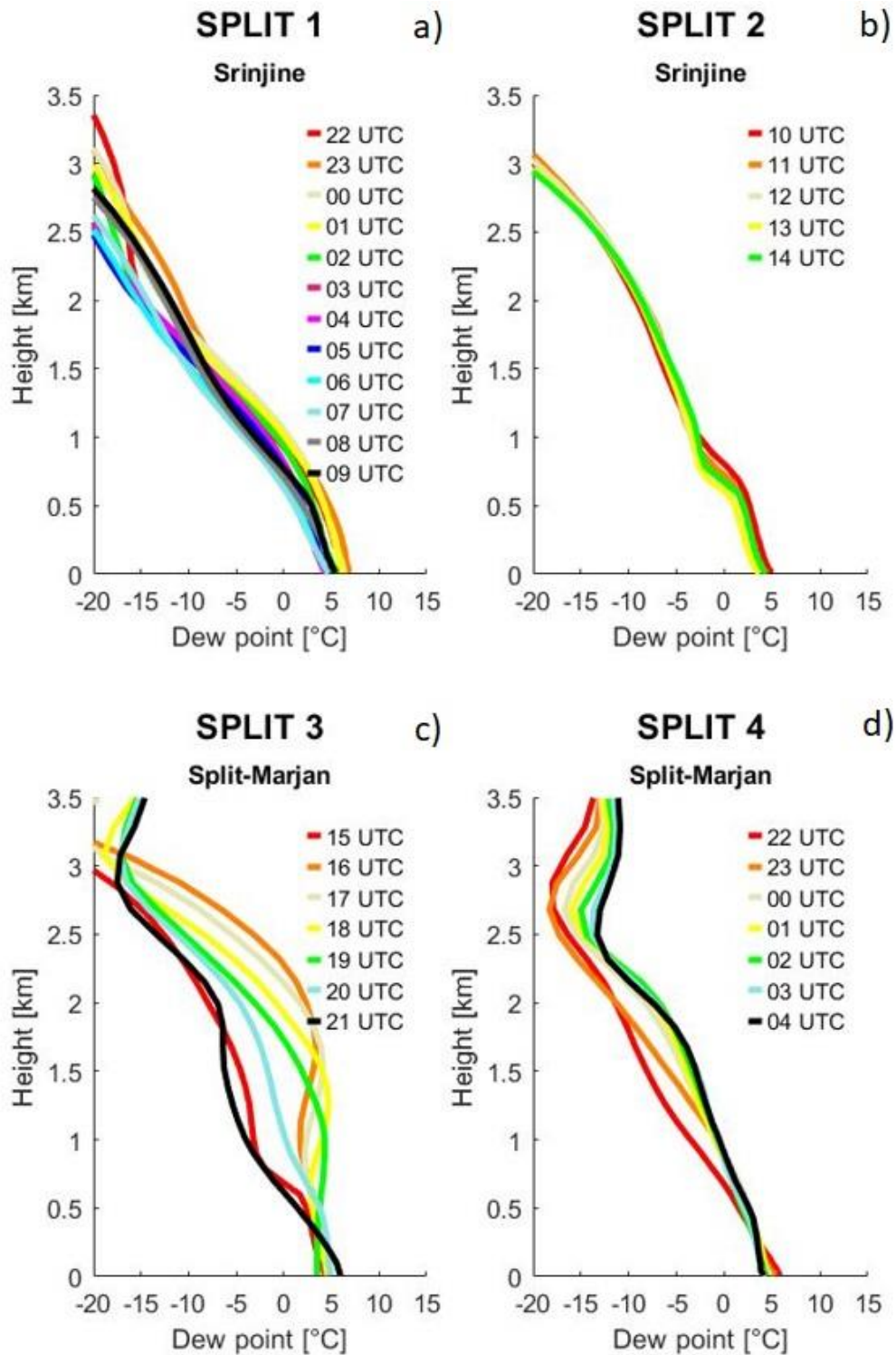


Figure B4. Vertical profiles of dew point (°C) at Srinjine and Split-Marjan locations for periods SPLIT 1 (from 22:00 UTC on 16 July to 09:00 UTC on 17 July), SPLIT 2 (from 10:00 UTC to 15:00 UTC on 17 July), SPLIT 3 (from 16:00 UTC to 21:00 UTC on 17 July) and SPLIT 4 (from 22:00 UTC on 17 July to 04:00 UTC on 18 July) from ALADIN model. See Fig. 2 for location of Split-Marjan and Srinjine (noted as S).

## APPENDIX C:

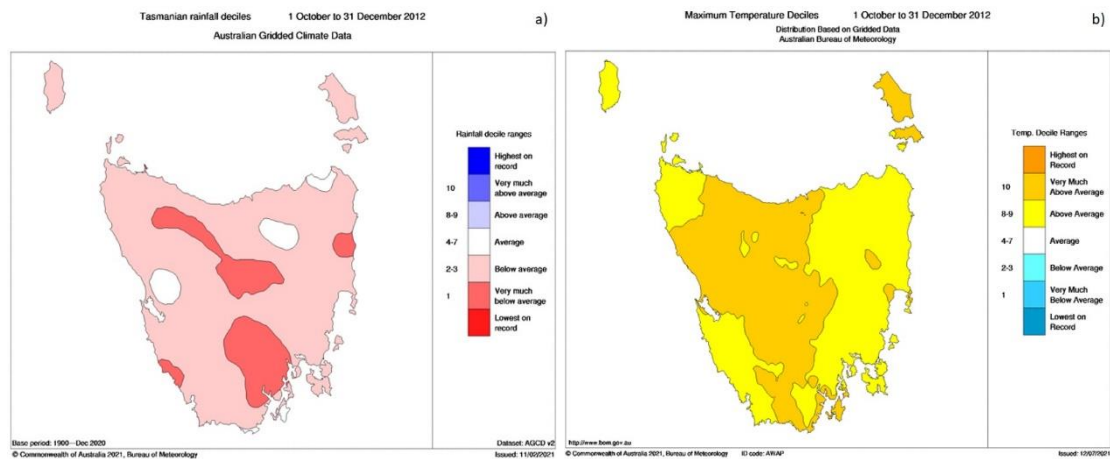


Figure C1. a) Rainfall decile and b) maximum temperature decile for Tasmania from 1 October to 31 December 2012 comparing to period 1900–2020 (BoM).

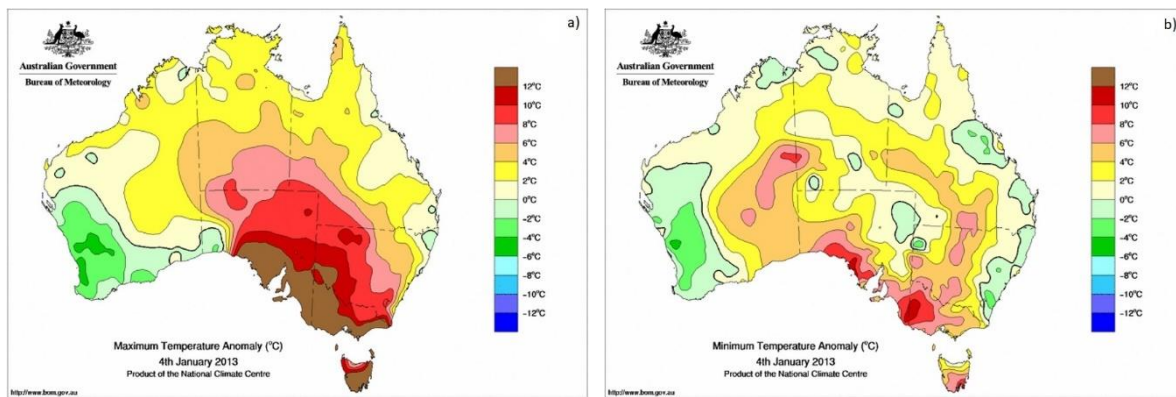


Figure C2. a) Maximum air temperature anomaly and b) minimum air temperature anomaly for 4 January 2013 (National Climate Centre, BoM).

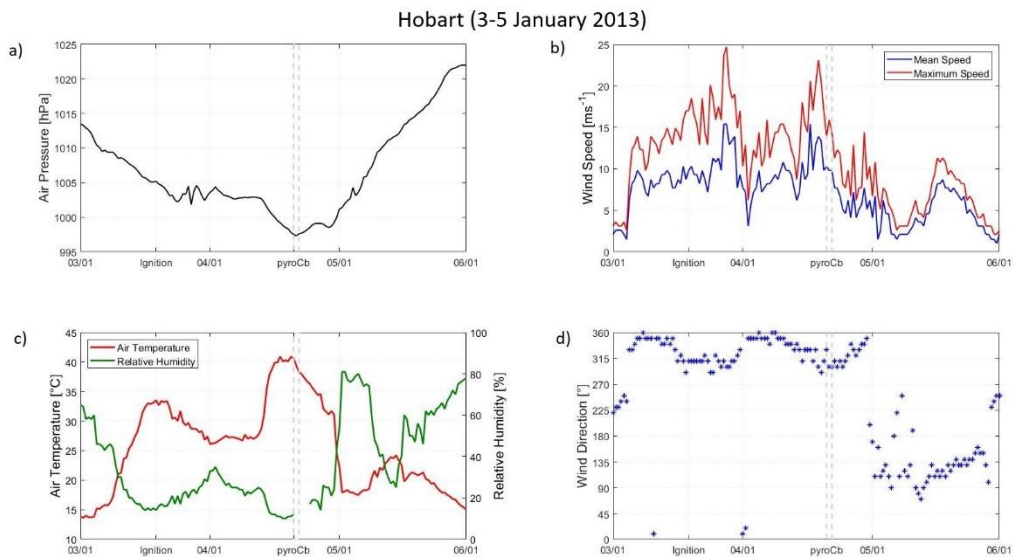


Figure C3. Hobart automatic weather station 30-minute observations of a) air pressure (hPa), b) mean and maximum wind speed ( $\text{ms}^{-1}$ ), c) air temperature ( $^{\circ}\text{C}$ ) and relative humidity (%) and d) mean wind speed direction ( $^{\circ}$ ) from 3 to 5 January 2013. Mean and maximum wind speeds are 10-minute values available every half hour. Missing values between 16:35 AEST to 17:58 AEST of relative humidity are due to corrupted measurements when the wet bulb reservoir dried out. Dashed grey lines indicate the peak activity of the pyroCb, between 15:30 AEST and 16:00 AEST on 4 January 2013 (the DUNALLEY 2 period).

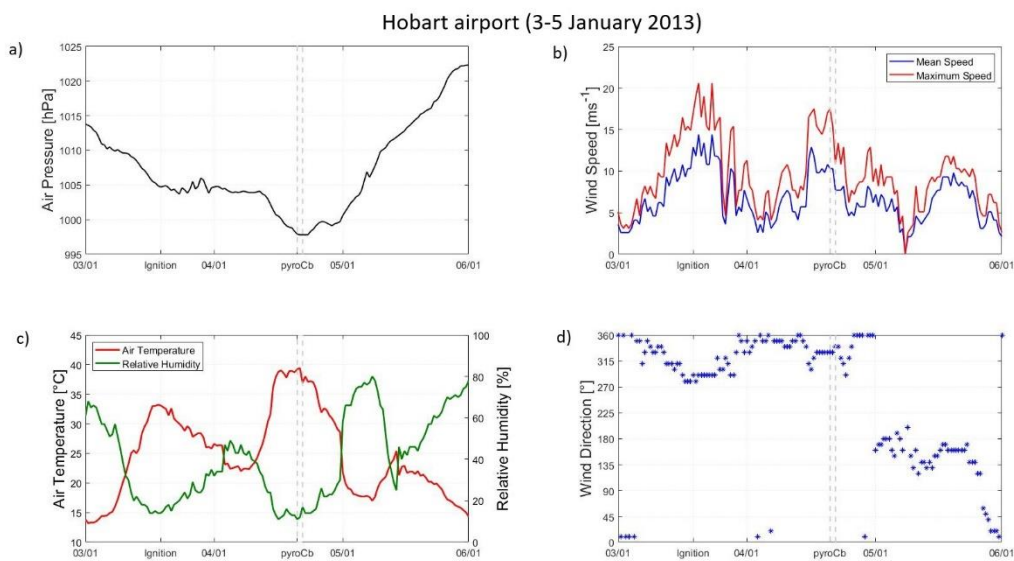


Figure C4. Hobart airport automatic weather station 30-minute observations of a) air pressure (hPa), b) mean and maximum wind speed ( $\text{ms}^{-1}$ ), c) air temperature ( $^{\circ}\text{C}$ ) and relative humidity (%) and d) mean wind speed direction ( $^{\circ}$ ) from 3 to 5 January 2013. Mean and maximum wind speeds are 10-minute values available every half hour. Dashed grey lines indicate the peak activity of the pyroCb, between 15:30 AEST and 16:00 AEST on 4 January 2013 (the DUNALLEY 2 period).

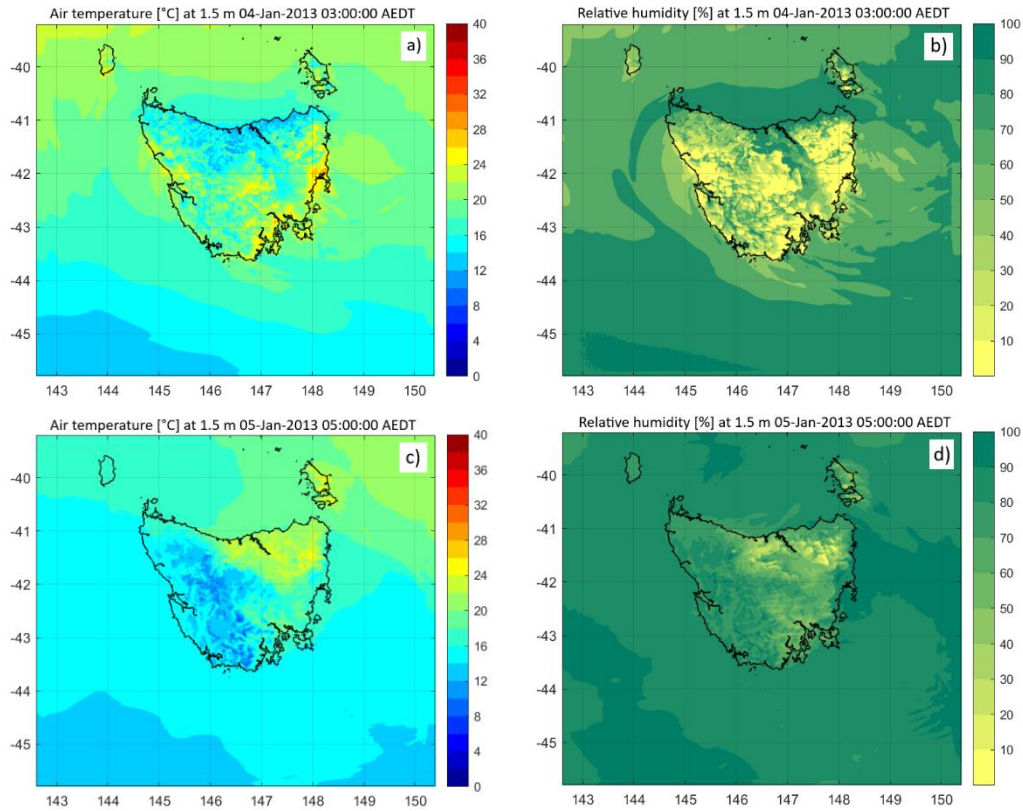


Figure C5. Air temperature ( $^{\circ}\text{C}$ ) and relative humidity (%) at 1.5 m at a) and b) 03 AEDT on 4 January, c) and d) 05 AEDT on 5 January from BARRA reanalysis.

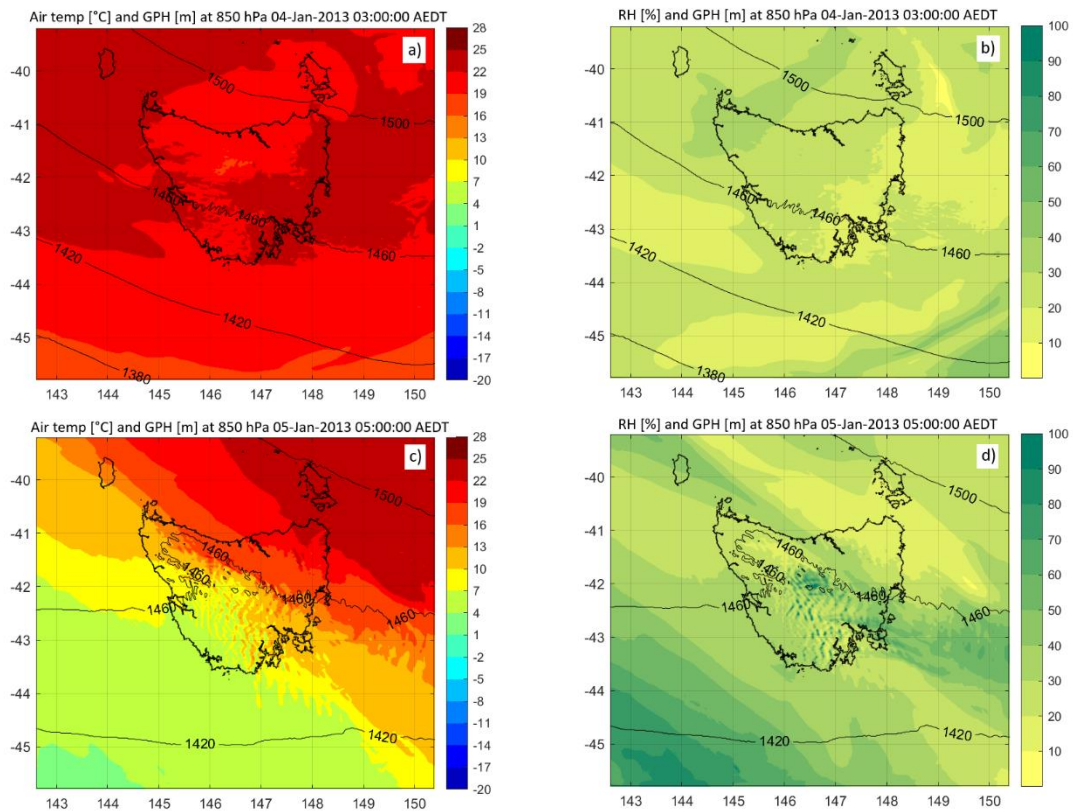


Figure C6. Air temperature ( $^{\circ}\text{C}$ ) and relative humidity (%) at 850 hPa at a) and b) 03 AEDT on 4 January, c) and d) 05 AEDT on 5 January 2013 from BARRA reanalysis.

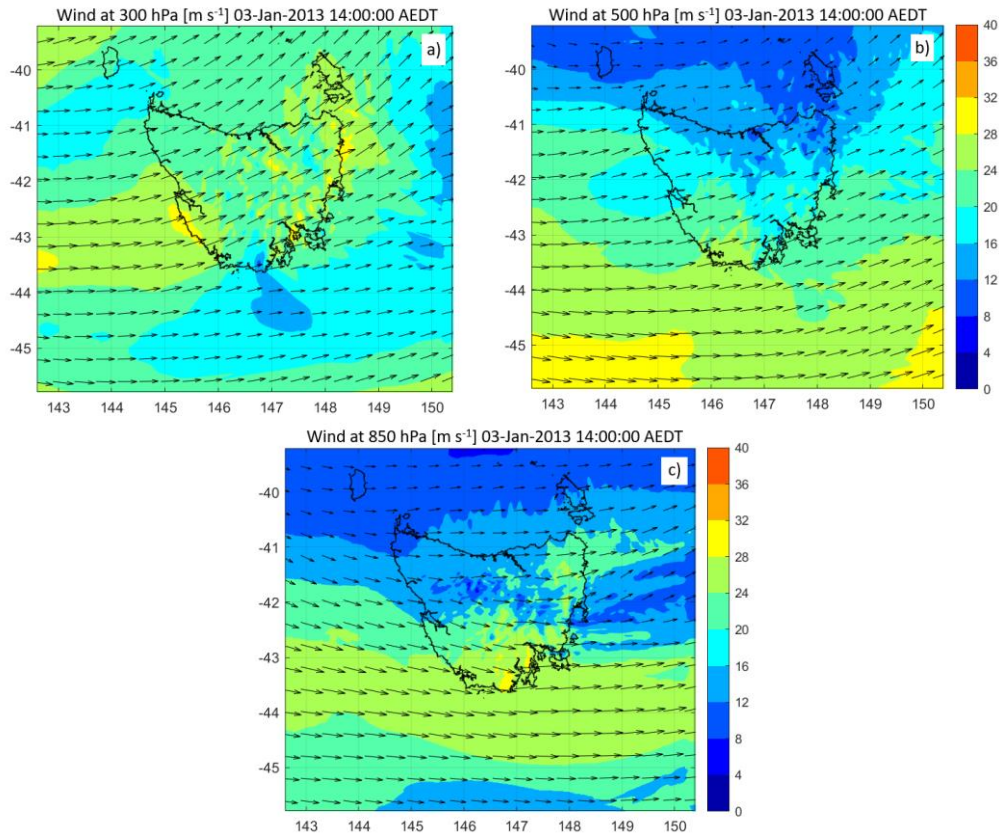


Figure C7. Wind speed ( $\text{m s}^{-1}$ ; coloured) and direction (array) at a) 300 hPa, b) 500 hPa and c) 850 hPa all at 14 AEDT on 3 January 2013 from BARRA reanalysis.

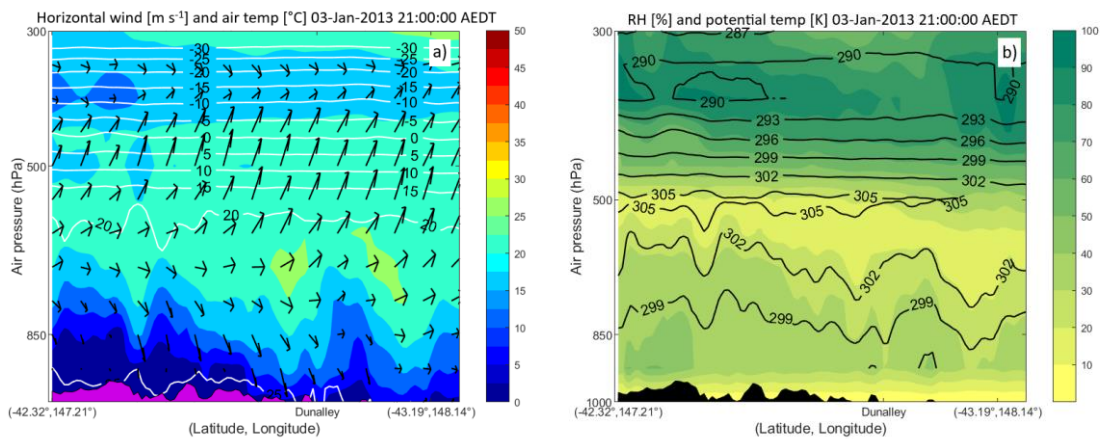


Figure C8. Vertical cross sections of a) wind speed ( $\text{m s}^{-1}$ ) and direction and air temperature ( $^{\circ}\text{C}$ ) and b) relative humidity (%) and potential temperature (K) both at 21 AEDT on 3 January 2013 from BARRA reanalysis. The bottom violet and black area depict the terrain. Air flow in each panel is from left to right.

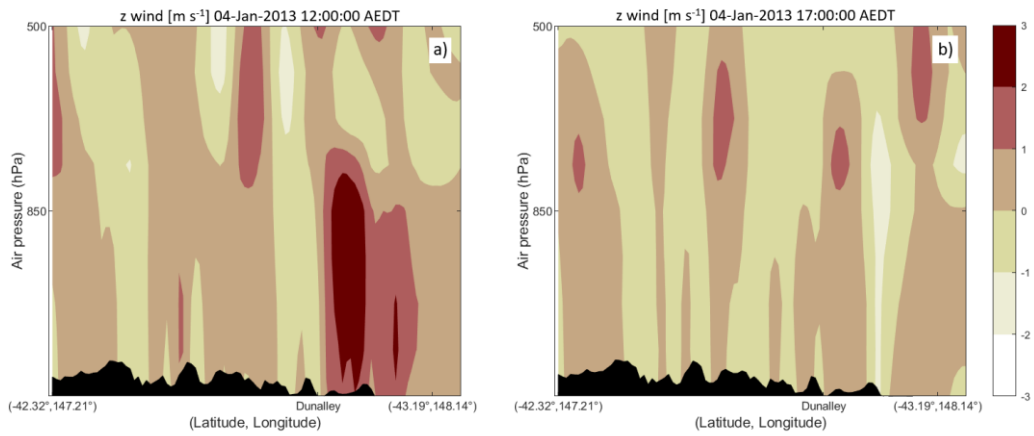


Figure C9. Vertical cross sections of z wind ( $\text{m s}^{-1}$ ) at a) 12 AEDT and b) 17 AEDT on 4 January 2013 from BARRA reanalysis. The bottom black area depicts the terrain. Air flow in each panel is from left to right.



## APPENDIX D:



Figure D1. Ignition location at the foothill of Sridivica (hill C in [Figure 4.2](#)) with the view towards a) east and b) west (photographed by Ivana Čavlina Tomašević on 21 June 2021). Fuel models at this location correspond to fuel model 1 and 6 in WRF SFIRE input data (by definition of [Anderson, 1982](#)).



Figure D2. View of a) south slopes of hill Makirina (hill C in [Figure 4.2](#)) and the astronomical observatory at the top and b) north slopes of hill Perun (hill A; photographed by Ivana Čavlina Tomašević on 21 June 2021). Fuel models at the location of hill Makirina correspond to fuel model 1 (at the top) and 6 (bottom), while fuel model at the location of hill Perun corresponds to fuel model 4 in WRF SFIRE input data (by definition of [Anderson, 1982](#)).



Figure D3. a) View of south slopes of hill Sridivica (hill B in [Figure 4.2](#)) and b) downy oak on south slopes of hill Perun (hill A; photographed by Ivana Čavlina Tomašević on 21 June 2021). Fuel models at the location of hill Sridivica correspond to fuel model 1, while downy oak fuels at the southwestern side of hill Perun are classified as the fuel model 10 in WRF SFIRE input data (by definition of [Anderson, 1982](#)).



Figure D4. View from the top of hill Makirina (hill C in [Figure 4.2](#)) towards west (with hill Sridivica, B on the left) where the northwestern flank of the wildfire was located between burn periods SPLIT 2 and SPLIT 3 (photographed by Ivana Čavlina Tomašević on 21 June 2021). Fuel models at this location are mixture of fuel models 1, 2, 6 and 10 in WRF SFIRE input data (by definition of [Anderson, 1982](#)).

## **CURRICULUM VITAE**

Ivana Čavlina Tomašević was born on 29th March 1985 in Osijek, Croatia where she finished elementary school Antun Mihanović in 1999 and III. Gymnasium in 2003. She graduated at the Department of Geophysics, Faculty of Science, University of Zagreb on 20th January 2012 with the research topic ‘Vertical profiles of the atmosphere during the large wildfires in Croatia’. In September 2013 she started working at the Croatian Meteorological and Hydrological Service (DHMZ). In November 2015 she enrolled postgraduate doctoral program in geophysics at Faculty of Science, University of Zagreb. In September 2017 she was granted a scholarship from the Macquarie University, Australia to enroll Cotutelle PhD program per agreement between the University of Zagreb and Macquarie University. She spent one year, from May 2018 until May 2019 on campus at Macquarie University in Sydney. In January 2018 she became the Head of the Agrometeorological Research Unit and since January 2021 she has been the Head of the Agrometeorological Information Unit at DHMZ.

Since 2013 she has attended more than 30 conferences and workshops on agrometeorology and forest meteorology. She gave dozen lectures to farmers and firefighters on agrometeorology and fire weather and actively promoted meteorology since college. She gave dozen media interviews and regularly presents agrometeorological forecast for Croatian television. At the 6th Fire Behaviour and Fuels Conference in Sydney in May 2019 she received the Best Student Poster Award with the ‘Meteorology of the Split fire in Croatia, 16 July 2017’.

#### LIST OF PUBLICATIONS:

- Čavlina Tomašević, I., Cheung, K. K. W., Vučetić, V., Fox-Hughes, P., Horvath, K., Telišman Prtenjak, M., Beggs, P. J., Malečić, B., Milić, V., 2022. The 2017 Split wildfire in Croatia: Evolution and the role of meteorological conditions. *Nat. Hazards Earth Syst. Sci. Discuss.* 22, 3143–3165. <https://doi.org/10.5194/nhess-2022-116>.
- Tomašević, I.Č., Cheung, K.K.W., Vučetić, V., Fox-Hughes, P., 2022. Comparison of Wildfire Meteorology and Climate at the Adriatic Coast and Southeast Australia. *Atmosphere.* 13, 755. <https://doi.org/10.3390/atmos13050755>.
- Tomašević, I., Vučetić, V., 2014. Rating the Fire Season 2013 and Comparison with the Fire Season 2012. *Firefighting and Management.* 4, 19–35 (in Croatian).

#### CONFERENCE PAPERS:

- Čavlina Tomašević, I., Cheung, K., Vučetić, V., Horvath, K., Telišman Prtenjak, M., 2019. Meteorology of the Split fire in Croatia, 16 July 2017. In 6<sup>th</sup> International Fire Behaviour and Fuels Conference, 29 April–3 May 2019, Sydney, Australia, International Association of Wildland Fire.
- Vučetić, V., Čavlina Tomašević, I., Mifka, B., 2019. Low level jet and large wildfires in Croatia. In 6<sup>th</sup> International Fire Behaviour and Fuels Conference, 29 April–3 May 2019, Marseille, France, International Association of Wildland Fire.
- Vučetić, V., Tomašević, I., 2014. Analysis of vertical profiles of the atmosphere during large wildfires in Croatia. In 3<sup>rd</sup> Agrometeorological Workshop – Agrometeorology in the Service to the Users: Environmental Protection and Forest Fires, 24 March 2014, Dubrovnik, Croatia, Croatian Agrometeorological Society.

## **SUPERVISOR'S CURRICULUM VITAE**

Maja Telišman Prtenjak graduated from the Faculty of Science in Zagreb (1995), she holds a master's degree 2001, and received her doctorate in 2006 at the University of Zagreb. Since 1996, she has been working at Geophysics at the Faculty of Science department of the University of Zagreb, currently in the title of associate professor and scientific advisor. She won the Scientific Excellence Award of the Ministry of Education and Culture in 2009. She studied abroad and participated in a series of international conferences/workshops. Maja Telišman Prtenjak is or was a member of three journal editorial boards (Geofizika, Meteorology and Atmospheric Physics and Croatian Meteorological Journal) and was a member of ten organizational/scientific committees of international scientific and scientific-expert meetings and workshops. She participated in the work of several scientific and professional international and domestic projects, as an associate (11 of them) and as a manager (4 of them). So far, she is a co-author in more than 40 scientific papers and around 110 conference announcements in cooperation with domestic and foreign colleagues. She reviewed several international and domestic projects and about 60 papers for more renowned international and domestic journals. So far, she has been a mentor in 22 graduate theses and 2 doctorate. The focus of the work is on mesoscale meteorological phenomena (with special reference to dangerous weather conditions such as hail, lightning, frost, strong wind, forest fires, etc.) over complex topography in current and future climatic conditions using measurements and mesoscale numerical (prognostic and climate) models.

Associate Professor Paul Beggs works in the School of Natural Sciences, Faculty of Science and Engineering, Macquarie University, in Sydney, Australia. He is a climate scientist and an environmental health scientist. His research interests include impacts of climate change on human health, with a particular focus on allergens and allergic diseases. It is for this research that he won the 2009 Eureka Prize for Medical Research. Paul was also a contributing author of the Intergovernmental Panel on Climate Change's (IPCC's) Fourth Assessment Report published in 2007, the same year the IPCC won the Nobel Peace Prize. Paul is a Past President of the International Society of Biometeorology (having served as President from 2008-2011) and is current Vice President of the International Association for Aerobiology. He has 127 research outputs, including 72 journal articles, and has 2332 citations and an h-index of 26. He is Editor of the award-winning book titled "Impacts of climate change on allergens and allergic diseases" published by Cambridge University Press in 2016.